

Design and Synthesis of Multifunctional Biomimetic Metal Complexes: Some Having Application as Chemotherapeutic Agents, Some as Radio-protective Agents

A Thesis Submitted for the Degree of

Doctor of Philosophy

by

Priyanga Deb

Index Number: 140/15/Chem./24

To the

DEPARTMENT OF CHEMISTRY

JADAVPUR UNIVERSITY

KOLKATA 700032, INDIA

August, 2023



যাদবপুর বিশ্ববিদ্যালয়
কলকাতা-৭০০ ০৩২, ভারত



*JADAVPUR UNIVERSITY
KOLKATA-700032, INDIA

FACULTY OF SCIENCE : DEPARTMENT OF CHEMISTRY : INORGANIC SECTION

CERTIFICATE FROM THE SUPERVISOR

This is to certify that the thesis entitled “**Design and Synthesis of Multifunctional Biomimetic Metal Complexes: Some Having Application as Chemotherapeutic Agents, Some as Radio-protective Agents**” submitted by **PRIYANGANA DEB** (Index No. 140/15/Chem./24) who got her name registered on 24-08-2015 for the award of **Ph. D. (Science)** degree of **Jadavpur University**, is based upon her own work performed under the supervision of Prof. Kalyan K. Mukherjea in the Department of Chemistry at Jadavpur University, Kolkata, India. However, owing to Prof. Mukherjea's retirement from the University and myself being the other supervisor following Prof. Mukherjea's retirement, the thesis is being submitted under my monitoring and guidance.

Neither this thesis nor any part of it has been submitted for any degree / diploma or any other academic award anywhere before.

.....
Saurabh Das 04/08/2023
.....

(Signature of the Supervisor date with official seal)

Dr. Saurabh Das
Professor
Department of Chemistry
Jadavpur University
Kolkata - 700 032

*Established on and from 24th December, 1955 vide Notification No. 10986-Edn/IU-42/55 dated 6th December, 1955 under Jadavpur University Act, 1955 (West Bengal Act XXXIII of 1955) followed by Jadavpur University Act, 1981 (West Bengal Act XXIV of 1981)

দুরভাব : ২৪১৪-৬৬৬৬/৬১২৪/৬৬৪০/৬৪২৪/৬৪৪০ প্রসারণ : ২৪৬৯

Website : www.jadavpur.edu

Phone : 2414-6666/6194/6643/6495/6443 Extn. 2469

দুরবার্তা : (৯১)-৩৩-২৪১৪-৬৪১৪/২৪১০-৭১২১/২৪১৪-৬২১০

E-mail : registrar@admin.jdpu.ac.in

Fax : (91)-033-2414-6414/2413-7121/2414-6210



JADAVPUR UNIVERSITY
KOLKATA-700 032
MARK SHEET

NO. PHCW/1701/

(For Ph.D Course Work)

Results of the	PH.D. COURSE WORK EXAMINATION, 2016
In	SCIENCE held in NOVEMBER, 2016
Name	PRIYANGANA DEB
Examination Roll No.	PHDCHEM16224

Course Name / Subject	Credit Hr.(c)	Marks	Grade
COMPULSORY UNITS :: EX/CHEM/PHD/A & B RESEARCH METHODOLOGY & REVIEW OF RESEARCH WORK	4	76	A
ELECTIVE UNITS :: EX/CHEM/PHD/I-1 :: APPLICATION OF SPECTROSCOPIC STUDIES IN CHEMICAL RESEARCH EX/CHEM/PHD/I-2 :: MATERIALS, CATELYSES & ELECTROCHEMICAL STUDIES EX/CHEM/PHD/I-3 :: METALS IN LIFE & REACTION DYNAMICS EX/CHEM/PHD/I-4 :: SINGLE CRYSTAL X-RAY STR. SUPRAMOLECULAR CHEM.& DFT COMPUTN.	4	78	A

Total Marks : 154 (out of 200)

SGPA: 10.00

Remarks: P

Prepared by :

Checked by :

Date of issue : 07-02-2017

Controller of Examinations

DECLARATION

I do hereby declare that the work embodied in this thesis entitled "*Design and Synthesis of Multifunctional Biomimetic Metal Complexes: Some Having Application as Chemotherapeutic Agents, Some as Radio-protective Agents*" submitted for an award of **Doctor of Philosophy (Ph.D.)** in Science is the completion of studies carried out by me under the supervision of Prof. Kalyan K. Mukherjea in the Department of Chemistry at Jadavpur University, Kolkata, India. However, owing to Prof. Mukherjea's retirement from the said University, the thesis is being submitted under the generous monitoring and guidance of Prof. Saurabh Das of the Department of Chemistry, Jadavpur University.

In keeping with the general practice of reporting scientific observations, due acknowledgements have been made wherever the work described was done taking an active assistance from a laboratory that has an expertise in that particular field of investigation.

Priyanshona Deb
04-08-2023

(Priyanagna Deb)

Research Fellow

Department of Chemistry

Jadavpur University

Kolkata- 700032

India

Dedicated to



"We must fight if we want to live."

-Subhas Chandra Bose

Acknowledgements

*I would like to start by expressing my sincere gratitude to **Prof. Saurabh Das**, whose unhesitating support and guidance have been pivotal in helping me to reach this milestone. His expertise and mentorship have been instrumental in shaping my Ph.D. journey. His belief in my abilities and dedication to my success has been invaluable and I am truly grateful for his inspiration and insightful input.*

*Furthermore, I would like to extend my appreciation to **Prof. Kalyan K. Mukherjee** for his guidance and support throughout my research work which helped me to learn so many important lessons in life.*

*I am sincerely grateful to **Prof. Subenoy Chakraborty**, The Dean of Science, for his constant support and invaluable contributions, which have significantly impacted my academic growth. I express my heartfelt appreciation for his unwavering support to complete my Ph.D. journey.*

***Prof. Suranjan Das**, the Vice Chancellor, **Prof. Subenoy Chakraborty**, the Dean of Science, **Prof. Subratanath Konar**, the Head of the department (Chemistry) and **Prof. Saurabh Das** have played an indispensable role in my academic growth, and I am truly indebted to them for their mentorship and encouragement. I sincerely regard and extend my heartfelt thanks to them for their instrumental contributions to my research journey.*

*I would like to extend my sincere gratitude to **Dr. Abhijit Saha**, former Director of UGC-DAE CSR Kolkata and **Prof. Prasanta K. Nandi** of IEST Shibpur, for their support and for allowing me to perform research work with them at their respective Institutes.*

*I also express my sincere thanks to Jadavpur University for its instrumental facilities. I am thankful to WB-DST for the fellowship during my research period. Here it is mandatory to mention the name of The Senior Scientific Officer of WB-DST **Dr. Amiya K. Kalidaha** for his constant support throughout the period of my research. I would as well take a moment to thank staff members of the Research Section and Dean (Science) office of Jadavpur University for their help during my research.*

*To my dedicated teachers **Prof. Achintya Sarkar**, **Prof. Dipak K. Mandal**, **Prof. Gandhi K. Kar**, **Prof. Samragee Dutta**, and **Prof. Ashish K. Nag** — thank you for imparting knowledge, nurturing my intellectual curiosity, and challenging me to reach new heights. Your guidance and mentorship have shaped my academic foundation and equipped me with the tools to succeed. **Bisakha Deb**, **Samarendranath Panja**, **Subrata Chatterjee**, **Subhrajit Senapati** and **Chinmoyee Chatterjee** — your patience, dedication and passion for education have had a profound impact on my development as a scholar. I am forever grateful for your relentless support and belief in my potential.*

I extend my sincere appreciation to my dear friends, **Satyabarata, Moumita, Sreejita, Chandramouli, Abhijit, Debjit, Soumi, Uditadi and Sreetama**, who have stood by my side and provided unwavering support and encouragement throughout this challenging endeavor. I am thankful to **Sagar, Sushobhan, Shamik and Ranita** your kind words, uplifting gestures, and understanding and support during those moments of doubt have played a crucial role in keeping me focused and determined. All your presence in my life has been a constant source of inspiration and I am grateful for the cherished memories we have created together.

To my seniors and colleagues **Swarup da, Debalina di, Sourav, Subha and Nayim** — thank you for your collaboration, stimulating discussions and the camaraderie we have shared.

The successful culmination of my Ph.D. thesis would not have been possible without **Dr. Sanjit Pal's** unwavering support and encouragement. I would like to express my sincere gratitude to **Mr. Utpal Mondal, Smt. Supriya Ghosal, and Smt. Aloka Roy** who have been a constant source of encouragement throughout the journey of completing this thesis.

Smt. Sudha Sarkar and Smt. Monobina Deb, though you are no longer physically with me, your spirit and the values that you instilled in me remain etched in my heart, guiding me through every step of my academic journey. **Sri Ranajit Kumar Sarkar, Sri Byomkesh Sarkar, Smt. Eva Sarkar, Smt. Minati Mitra and Sri Dipak Mitra** I wish you were here to witness this momentous achievement. In this moment of triumph, I honor your memory and express my deepest gratitude for the love, guidance and blessings you bestowed on me.

To my parents, **Swapna Deb Sarkar (Maa) and Sangit Deb (Babai)** your untiring support and sacrifices have been the bedrock of my success. Your belief in my abilities and your constant encouragement has propelled me forward, even during the most challenging times. I am eternally grateful for everything you have together done for me. Thank you, for being my guiding light and for shaping me into the person I am today. This thesis is a testament to your love and I hope it serves as a tribute to your profound impact on my life and academic pursuits.

First and foremost, I express my deepest gratitude to my family members, **Ratna Sarkar, Swapan Sarkar, Debashis Sarkar, Shila Sarkar, Rina Sarkar** and of course **Subhasis Sarkar** for their unconditional love, patience, and constant belief in me throughout this arduous undertaking. I am also grateful to **Gargi Deb, Sandip Deb and Durba Bhattacharya** for their constant support and encouragement since my childhood. I am truly grateful for the love, and encouragement that my sister **Tirna Deb** has provided me. Here it is worth mentioning the tireless efforts and unforgettable contributions of **Smt. Arati Patra and Smt. Sipra Das** who actually paved the way to the goal.

I would like to express my deepest appreciation to my parents-in-law, **Mrs. Bulbul Hazra** and **Mr. Joydev Hazra**, for their support and understanding. Their nurturing environment has played a pivotal role in enabling me to pursue my academic aspirations. Furthermore, in times of need I found solace and guidance through meaningful discussions with **Smt. Ramala Konar**, **Utpal Konar**, **Biswajit Konar**, **Sima Konar** and **Moumita Bhattacharya** that were proven to be invaluable in helping me navigate numerous challenging situations.

I am thankful to **Mrs. Rita Kundu** and **Mr. Indra Nath Kundu** for their presence in my life, and I will be grateful to them for helping me to come out of some serious crisis in our life.

To my beloved husband, **Bidhan Hazra** — your dependable presence and firm belief in me have driven my perseverance. Your unconditional love, understanding and constant encouragement provided me with the strength and motivation to overcome obstacles along this journey. Your constant motivation has given me the courage to pursue my dreams and for that, I am forever grateful. This accomplishment is as much yours as it is mine.

I am profoundly grateful to my an year and nine months old son, **Panchajanya**, who, despite his young age has been an incredible invisible problem solver in my Ph.D. journey. His tiny presence and joyful spirit have brought immense comfort and inspiration during challenging times, reminding me of the greater purpose behind my academic pursuits. In this thesis, I acknowledge the silent contributions of my son, whose presence has been a guiding light, reminding me of the importance of the balance of love and duty in the journey itself.

Whenever I found myself in a state of distress, I would turn to the comforting embrace of a song, “আমি অকৃতি অধম বলেও তো কিছু কম করে মোরে দাওনি..” by the legendary **Rajanikanta Sen**, sung in the mesmerizing voice of renowned artist **Mrs. Jayati Chakraborty** which became my personal form of meditation, carrying me to a place of solace and serenity. Once when I got a chance to meet Jayati Madam in person, her inspirational words resonated deeply within me, igniting a powerful surge of motivation and hope which was much needed at that moment.

I am also grateful to my Gurudev **Mr. Shribendu Lahiri Mahasaya** — his presence became an invaluable lifeline, pulling me out from the depths of despair and propelling me towards a brighter tomorrow.

Last, but certainly not the least, this achievement would not have been possible without the collective efforts of many others; I express my deepest gratitude to all the individuals who have contributed to my academic and personal growth.

List of Abbreviations used

UV: Ultraviolet

IR: Infrared

NMR: Nuclear Magnetic Resonance

EPR: Electron Paramagnetic Resonance

DNA: Deoxyribonucleic acid

CT- DNA: calf thymus DNA

pUC19 DNA: The designation "pUC" is derived from the classical "p" prefix (denoting "*plasmid*") and the abbreviation for the *University of California*, where early work on the plasmid series had been conducted.

BHAN: β -hydroxy- α -naphthaldehyde

OV: ortho-vanilline

DPPH: α, α -diphenyl- β -picrylhydrazyl

VHPO: Vanadium Haloperoxidases

HPO: Haloperoxidases

Br-PO: Bromoperoxidases

Contents

Chapter 1 <i>Introduction</i>	1-7
Chapter 2 <i>Transitional metal complexes as anti-cancer agents</i>	8-21
Chapter 3 <i>Biophysical and biochemical interactions of several complexes with DNA</i>	22-33
Chapter 4 <i>Review on radioprotectors</i>	34-43
Chapter 5 <i>A review on Haloperoxidase Mimicking</i>	44-51
Chapter 6 <i>Genesis and Scope of the research</i>	52-59
Chapter 7 <i>General experimental methods</i>	60-77
Chapter 8 <i>Synthesis, characterisation, theoretical simulation and DNA nuclease activity of a newly synthesized Mn-based chemotherapeutic agent</i>	78-109
Chapter 9 <i>Synthesis and characterization of a Dioxomolybdenum complex [cis-MoO₂(BHAN)₂] using β-hydroxy-α-naphthaldehyde (BHAN) as ligand</i>	110-123
Chapter 10 <i>cis-MoO₂(BHAN)₂ complex: their role in the protection of radiation-induced DNA damage</i>	124-145
Chapter 11 <i>The role of cis-MoO₂(BHAN)₂ complex in the Haloperoxidase mimicking oxidative bromination</i>	146-154
Chapter 12 <i>Synthesis and characterization of a dioxomolybdenum complex [cis-MoO₂(OV)₂] using ortho-vanilline (OV) as a ligand</i>	155-172
Chapter 13 <i>Application of complex cis-MoO₂(OV)₂ in radiation-induced DNA damage protection</i>	173-193

Chapter 14 *Application of complex cis-MoO₂(OV)₂ in Haloperoxidase mimicking oxidative bromination*.....**194-203**

Summary and Conclusions.....**204-207**

Appendix – I List of Publications

Appendix – II Reprint of publication

Chapter 1

Introduction

“We must not forget that when radium was discovered no one knew that it would prove useful in hospitals. The work was one of pure science. And this is a proof that scientific work must not be considered from the point of view of the direct usefulness of it. It must be done for itself, for the beauty of science, and then there is always the chance that a scientific discovery may become like the radium, a benefit for mankind.”

- MARIE CURIE

This thesis honors and draws heavily from not only the life and works of Marie Curie, but also her approach towards scientific discovery. Her work with Radium proved to be indispensable in the treatment of cancer. However, the tragic irony is in the fact that Curie herself died of cancer, despite contributing significantly to cancer research.

Cancer is probably the oldest malady that exists on earth since the inception of the animal kingdom and remains pertinent as an “unsolved mystery”. It is one of the most terrifying threats to human civilization. However, the disease existed before human evolution. Evidence suggests that cancer may have been recognized and documented in various forms throughout history, possibly dating thousands of years. According to a recent report in *The Lancet Oncology*, researchers claim that the first confirmation of a cancer diagnosis was that in dinosaurs at the cellular level.¹ Approximately 5,000 years ago, cancer was first documented in Egypt.² Since then, people all over the world from different countries and cultures have written about the disease and its potential treatment. Studies on cancer called ‘*ONCOLOGY*’ includes the research of countless doctors and scientists worldwide whose discoveries in anatomy, physiology, chemistry, epidemiology and other fields have enriched the subject to what it is today. Technological advances and advancements in scientific instrumentation

Introduction

further augmented our understanding of the disease, making this field one of modern medicine's most rapidly evolving areas. Scientists have obtained more details on cancer in the last 2 decades than ever before. Starting in the mid-1990s, emphasis on clinical cancer research shifted towards therapies derived from biotechnology like cancer immunotherapy, gene therapy etc. By analyzing the history of cancer, we witness the progress made and also the development of knowledge regarding underlying causes and possible treatments. While **Hippocrates** is often credited as the first person to use the term "*cancer*," he actually used the Greek word "*karkinos*" and "*karkinoma*" to describe tumors, which were derived from the Greek word for "*crab*" because he believed tumors looked like crabs inside.³ The Roman physician **Celsus** was the one who translated the word into its Latin term "*cancer*."

In the 20th century, modern methods not only allowed a better understanding of the treatment of cancer but also aided the development of cancer surgery. In this century, the ability to examine body tissues removed during surgery led to some of the most significant discoveries in medical history. Japanese professor **Takeshi Hirayama** published the first research linking lung cancer to direct or passive smoking.⁴ **Baruch S. Blumberg** helped develop a vaccine against hepatitis B, which can cause liver cancer.⁵ The first gene therapy cancer treatments began to evolve.⁶ Scientists discovered the BRCA1 gene, which was the first of its kind found in a person with symptoms of developing breast or ovarian cancer.⁷ **Jan Walboomers** and **Michele Manos** found evidence that human papillomavirus (HPV) is the cause of cervical cancer in most cases.⁸

Today, in the 21st century, we are still in the process of learning about cancer. Over the years, significant progress has been made in prevention, treatment and even cure of some forms of cancer. Thanks to clinical trials, scientists have been able to explore and test innovative methods to detect and manage cancer. The first vaccine against HPV was

Introduction

approved in the United States in 2006.⁹ Researchers found that immunotherapy improves cure rates in children with neuroblastoma.¹⁰ Low-dose computed tomography (CT) scans help reduce lung cancer deaths by finding early-stage cancer in high-risk people¹¹ The OncoKB, a genetic variant database, was recognized as a tool for predicting drug responses in people with cancer.¹² This is helping oncologists find the best individual treatments for people with specific types of cancer. **Precision medicine** has become an increasingly important approach to cancer treatment that involves using genetic and molecular information to tailor treatment to specific characteristics of a person's cancer. This can help improve treatment effectiveness while reducing the risk of side effects. Advancement in technology have also played a significant role in cancer research and treatment. For example, **artificial intelligence (AI)** is used to analyze large amounts of data to identify new cancer treatments¹³ and develop predictive models to determine which treatments are most likely to be effective for individual patients. A growing body of scientific evidence also links air **pollution** and **global warming** to an increased risk of cancer. According to the **International Agency for Research on Cancer (IARC)**¹⁴, a specialized agency of the **World Health Organization (WHO)**¹⁵, outdoor air pollution and some specific air pollutants are carcinogenic to humans. Exposure to these pollutants can lead to lung cancer and other respiratory cancers. In addition to outdoor air pollution, indoor air pollution has also been linked to an increased risk of cancer. For example, exposure to second hand smoke has been shown to cause lung cancer in non-smokers, and exposure to radon gas has also been linked to lung cancer. **Climate change** is also expected to have an impact on cancer rates. The *American Cancer Society* notes global warming could lead to an increase in air pollution, which in turn could increase the risk of cancer.¹⁶ Additionally, climate change may lead to changes in the distribution of infectious diseases. The probability of developing specific types of cancer can be elevated by the aforementioned factors. Climate change due to global warming and increase in pollution is a

major concern of the 21st century that may lead to changes in the distribution of infectious diseases and also increase the risk of certain types of cancer. Hence, despite advancement in clinical research and technology, cancer remains a complex disease and there is still much work to be done to improve cancer prevention, detection, and treatment. Research efforts continue to focus on understanding the underlying mechanisms of the progress of cancer and in the process identify new targets for treatment. Collaboration among researchers, healthcare providers and patients is very essential to be able to continue the fight against cancer in the 21st century.

References:

- (1) Ekhtiari, S.; Chiba, K.; Popovic, S.; Crowther, R.; Wohl, G.; Kin On Wong, A.; Tanke, D. H.; Dufault, D. M.; Geen, O. D.; Parasu, N.; Crowther, M. A.; Evans, D. C. First Case of Osteosarcoma in a Dinosaur: A Multimodal Diagnosis. *Lancet. Oncol.* **2020**, *21* (8), 1021–1022.
- (2) What, U.; Is, C.; Times, A.; Understanding, P.; Causes, C.; Times, A.; History, P.; Epidemiology, C.; History, P.; Screening, C.; Detection, E.; History, P.; Treatments, C.; History, S.; Treatments, C.; Treatments, C.; History, R. T.; Treatments, C.; History, C.; Treatments, C.; History, I.; Treatments, C.; Advancement, T. T.; Survivorship, C. The History of Cancer Understanding What Cancer Is : Ancient Times to Present. *Am. cancer society* **2017**, 1–35.
- (3) Faguet, G. B. A Brief History of Cancer: Age-Old Milestones Underlying Our Current Knowledge Database. *Int. J. cancer* **2015**, *136* (9), 2022–2036.
- (4) Iida, K.; Proctor, R. N. ‘The Industry Must Be Inconspicuous’: Japan Tobacco’s Corruption of Science and Health Policy via the Smoking Research Foundation. *Tob.*

- Control* **2018**, 27 (e1), e3–e11.
- (5) Gerlich, W. H. Medical Virology of Hepatitis B: How It Began and Where We Are Now. *Viol. J.* **2013**, 10.
 - (6) Rosenberg, S. A.; Aebersold, P.; Cornetta, K.; Kasid, A.; Morgan, R. A.; Moen, R.; Karson, E. M.; Lotze, M. T.; Yang, J. C.; Topalian, S. L.; Merino, M. J.; Culver, K.; Miller, A. D.; Blaese, R. M.; Anderson, W. F. Gene Transfer into Humans — Immunotherapy of Patients with Advanced Melanoma, Using Tumor-Infiltrating Lymphocytes Modified by Retroviral Gene Transduction. *N. Engl. J. Med.* **1990**, 323 (9), 570–578.
 - (7) Takaoka, M.; Miki, Y. BRCA1 Gene: Function and Deficiency. *Int. J. Clin. Oncol.* **2018**, 23 (1), 36–44.
 - (8) Okunade, K. S. Human Papillomavirus and Cervical Cancer. *J. Obstet. Gynaecol. (Lahore)*. **2019**, 40 (5), 602–608.
 - (9) Dehlendorff, C.; Baandrup, L.; Kjaer, S. K. Real-World Effectiveness of Human Papillomavirus Vaccination Against Vulvovaginal High-Grade Precancerous Lesions and Cancers. *J. Natl. Cancer Inst.* **2021**, 113 (7), 869–874.
 - (10) *Discovery – Ch14.18 Immunotherapy to Treat Neuroblastoma - NCI.*
<https://www.cancer.gov/research/progress/discovery/neuroblastoma>
 - (11) *Discovery – Lung Cancer Screening Saves Lives: The NLST - NCI.*
<https://www.cancer.gov/research/progress/discovery/nlst>
 - (12) *FDA recognizes Memorial Sloan-Kettering database of molecular tumor marker information | FDA.* <https://www.fda.gov/drugs/resources-information-approved-drugs/fda-recognizes-memorial-sloan-kettering-database-molecular-tumor-marker-information>

- (13) Elemento, O.; Leslie, C.; Lundin, J.; Tourassi, G. Artificial Intelligence in Cancer Research, Diagnosis and Therapy. *Nat. Rev. Cancer* **2021**, *21* (12), 747–752.
- (14) *IARC: Outdoor air pollution a leading environmental cause of cancer deaths – IARC.* <https://www.iarc.who.int/news-events/iarc-outdoor-air-pollution-a-leading-environmental-cause-of-cancer-deaths/>
- (15) *Household air pollution.* <https://www.who.int/news-room/fact-sheets/detail/household-air-pollution-and-health>
- (16) Nogueira, L. M.; Yabroff, K. R.; Bernstein, A. Climate Change and Cancer. *CA. Cancer J. Clin.* **2020**, *70* (4), 239–244.

Chapter 2

Transitional Metal Complexes as Anti-Cancer Agents

Transitional metal complexes as anti-cancer agents

Metal-based compounds have been recognized for their therapeutic benefits since ancient times. Civilizations like the Assyrians, Egyptians and the Chinese understood the significance of utilizing such compounds for treating various diseases. For instance, they employed cinnabar, a compound containing mercury sulfide, to address ailments.¹ Nature has inherently recognized the significance of metals as crucial constituents within cells. These elements are commonly present in the catalytic domain of enzymes and play vital roles in numerous biological processes, encompassing electron exchange, catalysis, and structural functions.^{2,3} Their utilization extends extensively across cellular activities. Notably, metals like Gallium, Zinc, Cobalt, Silver, Vanadium, Strontium, Manganese, and Copper are indispensable in minute quantities to initiate catalytic processes in biological organisms.⁴ The emergence of molecular biology and combinatorial chemistry has opened the doors for a systematic creation of chemical compounds tailored to interact with particular molecules.⁵ In recent times, the demand for metal-based compounds in cancer treatment has experienced an upsurge. This is attributed to the alarming prevalence of cancer and more so, notable cytotoxic effects demonstrated by recently synthesized metal-based compounds *in vitro*.⁶ Moreover, by employing ligand substitution and modifying existing chemical structures, a diverse range of metal-based compounds has been successfully synthesized, some exhibiting improved cytotoxicity and pharmacokinetic profiles. Additionally, a novel approach in cytotoxic drug design has emerged, involving the conjugation of metallic compounds with bile acid, steroid, peptide or sugar. This strategy facilitates direct drug delivery to cancer cells, thereby overcoming certain pharmacokinetic challenges. Despite their undeniable therapeutic potential, metal-based compounds, particularly transition metals possess distinct characteristics like their ability to engage in redox reactions. Consequently, activities of metals and their redox processes are carefully controlled to uphold overall health and well-being.⁷⁻⁹ As chemotherapeutic drugs continue to be developed and improved with researchers

Transitional metal complexes as anti-cancer agents

focusing on personalized medicine, immunotherapy and other innovative approaches to cancer treatment has profoundly impacted medicines, providing an effective treatment for a range of diseases, improving the quality of life for millions of patients worldwide. The intriguing therapeutic potential of metal complexes in cancer therapy has garnered significant attention primarily due to the distinctive attributes displayed by metals. These include their redox activity, versatile coordination modes and reactivity towards organic substrates.² These characteristics serve as enticing factors in the development of metal complexes that possess the ability to selectively bind to bio molecular targets, leading to subsequent modifications in cellular proliferation mechanisms.

A well-known example of a transition metal complex used in chemotherapy is *cisplatin*, a platinum-containing compound used to treat a variety of solid tumors, including testicular, ovarian and lung cancer.¹⁰ Cisplatin works by forming DNA adducts that inhibit DNA replication leading to cell death. This has been used as a very efficient chemotherapeutic agent for decades. The emergence of resistance to cisplatin served as a fundamental catalyst for the exploration of alternative metallic compounds that exhibit enhanced anticancer and pharmacokinetic properties. In recent times, there has been a surge in the synthesis of additional platinum complexes that are being assessed for their anticancer effects on tumor cell lines. This process entails modifying the original platinum compound by conjugating it with various ligands to attain desired outcomes. Conjugating carbohydrates (sugars) with the platinum compound can induce both biological and physicochemical alterations.¹¹

Thereafter, scientists and oncologists explored the potential of transition metal complexes as anticancer agents, owing to their ability to interact with different biological molecules and demonstrate selective cytotoxicity towards cancer cells. The complexes typically contain transition metal ions like copper, silver, gold, ruthenium and manganese coordinated to ligands in a manner that influences biological activity. For example, ruthenium-based

Transitional metal complexes as anti-cancer agents

compounds have shown activity against a variety of cancer cell lines¹². Ruthenium compounds have gained recognition for their ability to induce fewer and less severe side effects compared to other compounds. This is attributed to octahedral complexes formed by ruthenium, which allow for the exploration of a wider range of ligands in contrast to platinum(II) complexes that primarily form square planar complexes. Innovation in the field of ruthenium drug design is centered around creation of a ruthenium organic directing molecule (RODM)¹³. In this approach, an organic molecule binds to active sites on an enzyme, while the attached ruthenium ion binds to nearby residues of the same enzyme. This strategy offers the advantage of having a known biological target, enabling enzymological studies such as investigations into the rate of enzyme inhibition. In addition to the aforementioned approaches, directed therapy and multinuclear approach have been investigated in ruthenium drug design. Ruthenium's capability to form multinuclear and supramolecular architecture has also been explored, leading to development of ruthenium cluster complexes, ruthenium DNA intercalators and ruthenium-platinum-mixed metal compounds. In directed therapy, ruthenium is chemically bonded to an organic compound that possesses a known biological target.¹⁴ This attachment enables the drug to be directed specifically to cells, thereby enhancing the potency of the compound.

Copper complexes display cytotoxic properties, operating through a distinct mechanism of action compared to the widely used platinum compound, cisplatin.¹⁵ The effectiveness of these compounds varies depending on a specific ligand attached to the basic copper complex. Research into the cytotoxic effects of copper-based complexes has been driven by the hypothesis that endogenous copper may be less harmful to normal cells compared to cancer cells.¹⁶ However, in reality it is different, as copper exhibits redox activity and competes for binding sites that could otherwise be occupied by other metals.

Transitional metal complexes as anti-cancer agents

The primary goal of drug design in this context is to develop highly effective compounds that possess reduced toxicity and selectively bind to active sites of enzymes. Gold-based complexes have also been shown to have anticancer activity¹⁷ with some compounds exhibiting selectivity towards cancer cells over healthy cells. Gold(III) complexes have shown promising potential for selectivity towards thiol-containing enzymes like thioredoxin reductase (TrxR), making them attractive candidates for designing compounds that can specifically bind to residues within the enzyme's active site.¹⁸ Numerous types of gold(III) complexes have been synthesized and evaluated for their anticancer activity against various cancer cell lines.

In the past, silver complexes did not receive much attention compared to other metals, despite demonstrating promising cytotoxic activity on different cancer cell lines. However, there has been a recent surge of interest in the cytotoxic properties of silver(I) complexes. Researchers discovered that most silver(I) complexes exhibit even greater cytotoxic activity than cisplatin. Moreover, these silver(I) complexes demonstrate relatively low toxicity and display a higher level of selectivity toward cancer cells. A recent *in vitro* study aimed to assess cytotoxic properties of silver(I) complexes against B16 (murine melanoma), a cancerous cell line and 10T1/2 (murine fibroblast), a noncancerous cell line found that silver complexes containing the hydroxymethylene group displays significantly higher cytotoxic activity on B16 cells compared to AgNO₃ and cisplatin. These complexes exhibit relatively low toxicity when tested on noncancerous 10T1/2 cells.¹⁹ This discovery highlights the potential of silver(I) complexes as effective and selective agents against cancer. A study investigating anti-cancer properties of gold(I) and silver(I) N-heterocyclic carbene complexes also examined their effects on H460 lung cancer cell line.²⁰ Results indicate that complexes like cisplatin, displayed comparable anticancer activity. These findings suggest gold(I) and silver(I) N-

Transitional metal complexes as anti-cancer agents

heterocyclic carbene complexes hold promise as potential alternatives or complementary treatments to cisplatin for lung cancer.

In addition, manganese complexes were explored for their potential use in medical applications. Some studies show certain manganese complexes have anti-tumor activity and can act as artificial nuclease to induce death in cancer cells.²¹⁻²³ In 1987, Eric Fouquet *et al* discovered oxidative cleavage of DNA achieved by combining potassium hydrogen persulphate, an oxygen donor with a water-soluble manganese porphyrin.²⁴ Even at low concentrations of manganese porphyrin and potassium hydrogen persulphate, nuclease activity was observed. Interestingly, potassium hydrogen persulphate is more effective than hydrogen peroxide in promoting metalloporphyrin-mediated DNA cleavage. According to a report by Jean Bernadou *et al.* (1989), there is a correlation between potassium mono persulphate and a water-soluble manganese porphyrin complex producing a potent reagent for oxidative fragmentation of DNA.²⁵ P-31 NMR was employed to characterize terminal phosphates found in fragments of calf thymus DNA that were induced by artificial nuclease cationic manganese porphyrin meso-tetrakis (4-Nmethylpyridiniumyl)porphyrinato manganese pentaacetate (MnTMPyP), associated to potassium monopersulphate (KHSO₅). Findings show oxidative damage to deoxyribose resulting in the formation of two monophosphate esters, located at 3' and 5' ends on both sides of the cleavage site.²⁶ This method shows great promise for a way to visualize phosphate termini produced during DNA or RNA cleavage by cytotoxic drugs or chemical nucleases. Additionally, it provides new insights into molecular mechanisms in action. Later in 1998, Cathy Drexler *et al* synthesized a manganese(III) porphyrin complex bearing two acridine moieties to try and explore cleaving activity of an abiotic nuclease in presence of oxygen donor atoms.²⁷ The cleavage mechanism between complexes and plasmid DNA is likely to involve hydroxyl radicals as the reactive oxygen species. In another study, *in vitro* tests of the manganese(II) complex of

Transitional metal complexes as anti-cancer agents

6,7-dicyanodipyridoquinoxaline on four different cell lines (HL-60, KB, HeLa, and BGC-823) revealed that it exhibits considerable antitumor properties. 50% inhibition concentrations (IC_{50}) of the complex were found to be within millimolar range, comparable to those of 5-fluorouracil suggesting that this manganese(II) complex could be a promising candidate for further investigations as an antitumor agent.²⁸ DNA cleavage studies of two new mononuclear Mn(II) complexes, $Mn(dmbpy)_2(OCN)_2$ and $Mn(dmbpy)_2(dca)_2$ ($dmbpy$ = 4,4'-dimethyl-2,2'-bipyridine, dca = dicyanamide) promote plasmid DNA cleavage in presence of H_2O_2 under physiological conditions. Their cleavage activities are both pH dependent and also dependent on the concentration of the complex.²⁹ In 2008, Dipanjan Pan *et al* developed nanobialys, a novel theranostic agent having the potential of site-specific MR T1-weighted molecular imaging with manganese (as opposed to gadolinium) along with local delivery of potent chemotherapy agents. This unique combination makes nanobialys a highly attractive option for further exploration both from a diagnostic and therapeutic standpoint.³⁰ A trinuclear Mn complex $\{[MnCl(bpma)]_2-[Mn(\mu-Cl)_4(H_2O)_2]\} \cdot CH_3CN$ [$bpma$ = N,N-bis(2-pyridyl methyl)methylamine], resembling a linear sandwich was originally designed and analyzed as a potential nuclease mimic. Surprisingly, it was discovered that it existed as a dinuclear cation in solution. Ability of the dinuclear cation to promote DNA cleavage was demonstrated via a hydrolytic mechanism under anaerobic conditions. This was further confirmed through a T4 ligase experiment.³¹ Another study demonstrates when long and flexible cationic substituents are added to the periphery of a porphyrin macrocycle, it hindered interaction with the minor groove resulting in low DNA affinity. Conversely, addition of phenylpyridiniumyl substituents onto a porphyrin macrocycle unexpectedly resulted in tight binding of the new porphyrin derivative within the minor groove of a sequence containing six consecutive AT base pairs.³² These findings shed light on the structural requirements for a minor groove DNA binder that can aid in the deliberate design

Transitional metal complexes as anti-cancer agents

of porphyrin derivatives for the targeted binding of quadruplex DNA rather than double-stranded DNA. Jun-Teng Huang and colleagues reported in 2013 the ability of a water-soluble sulphonated manganese(III) corrole to bind to DNA and exhibit nuclease activity. These findings provide valuable insights into DNA binding properties of corroles and their potential applications as nuclease mimics.³³ In another study, a novel water-soluble carboxyl manganese(III) corrole was characterized. Studies on inhibition showed that oxidative cleavage that was observed in case of DNA was not caused by hydroxyl radicals or singlet oxygen but rather due to the formation of (oxo) manganese corrole. This points to a new category of synthetic restriction enzymes related to nucleic acids. In 2017, Jingjing Liu and colleagues created a novel type of biodegradable theranostic nanoplatform by developing Nanoscale-Coordination-Polymer-Shelled manganese dioxide composite nanoparticles.³⁴ This demonstrated the response to both reductive and acidic tumor microenvironment making it a promising candidate for augmenting cancer combination therapy through multiple mechanisms that act in synergy. Over the past decade, significant interest has been in theranostic nanoplatforms that combine diagnostic and therapeutic functions. Hollow manganese (Mn)-based nanoplatforms are particularly noteworthy owing to their ability to integrate the benefits of hollow structures with intrinsic theranostic properties of Mn^{2+} . The hollow interior of these nanoplatforms can encapsulate various small-molecule drugs, including chemotherapeutic agents, photothermal agents and photosensitizers for chemotherapy, photodynamic therapy (PDT) and photothermal therapy (PTT) respectively.³⁵ Upon degradation in tumor microenvironment (TME), Mn^{2+} is released, which acts both as a magnetic resonance (MR) imaging contrast agent and a Fenton-like agent for chemodynamic therapy (CDT). Importantly, the synergistic effects of these therapies can be optimized through rational design of hollow nanosystems.

Transitional metal complexes as anti-cancer agents

Hence, transition metal complexes show promise as potential anticancer agents in chemotherapy.^{36,37} While cisplatin is the most widely used transition metal complex in clinical practice, ongoing research focuses on developing new and improved complexes that may show greater selectivity and efficacy against cancer cells. Since the discovery of cisplatin, extensive research has been conducted to explore the therapeutic potential of metal-based complexes in cancer treatment. Despite challenges associated with the clinical use of platinum compounds, there is a growing demand for metal-based compounds in cancer therapy. Excitement among researchers in this field stems from the possibility of directly targeting cancer cells through innovative drug design strategies, as exemplified in the mentioned study. This advancement alleviates concerns about the toxicity often associated with organometallic compounds, as the drugs can be delivered specifically to cancer cells, sparing healthy cells from harm. Although the pharmacokinetic profile of these drugs in the human system is yet to be fully understood, development of designing metal-based compounds that selectively target cancer cells represents a significant breakthrough in this area of research. Another promising approach in anticancer drug design involves utilizing nanoparticles (NPs) to target specific biomolecules, ensuring precise drug delivery to cancer cells. With the concept of selective targeting, there is great hope for future development of therapeutics that can effectively and selectively target cancer cells while preserving the well-being of healthy cells.

References:

- (1) Norn, S.; Permin, H.; Kruse, E.; Kruse, P. Mercury--a Major Agent in the History of Medicine and Alchemy. *Dan. Medicinhist. Arbog* **2008**.
- (2) Frezza, M.; Hindo, S.; Chen, D.; Davenport, A.; Schmitt, S.; Tomco, D.; Ping Dou, Q. Novel Metals and Metal Complexes as Platforms for Cancer Therapy. *Curr. Pharm.*

- Des.* **2010**, *16* (16), 1813–1825.
- (3) Bruijninx, P. C.; Sadler, P. J. New Trends for Metal Complexes with Anticancer Activity. *Curr. Opin. Chem. Biol.* **2008**, *12* (2), 197–206.
 - (4) Mouriño, V.; Cattalini, J. P.; Boccaccini, A. R. Metallic Ions as Therapeutic Agents in Tissue Engineering Scaffolds: An Overview of Their Biological Applications and Strategies for New Developments. *J. R. Soc. Interface* **2012**, *9* (68), 401.
 - (5) Ji, H. F.; Li, X. J.; Zhang, H. Y. Natural Products and Drug Discovery. Can Thousands of Years of Ancient Medical Knowledge Lead Us to New and Powerful Drug Combinations in the Fight against Cancer and Dementia? *EMBO Rep.* **2009**, *10* (3), 194.
 - (6) Gasser, G.; Ott, I.; Metzler-Nolte, N. Organometallic Anticancer Compounds. *J. Med. Chem.* **2011**, *54* (1), 3–25.
 - (7) Jungwirth, U.; Kowol, C. R.; Keppler, B. K.; Hartinger, C. G.; Berger, W.; Heffeter, P. Anticancer Activity of Metal Complexes: Involvement of Redox Processes. *Antioxid Redox Signal* **2011**, *15* (4), 1085–1127.
 - (8) Hentze, M. W.; Muckenthaler, M. U.; Andrews, N. C. Balancing Acts: Molecular Control of Mammalian Iron Metabolism. *Cell* **2004**, *117* (3), 285–297.
 - (9) Gupte, A.; Mumper, R. J. Elevated Copper and Oxidative Stress in Cancer Cells as a Target for Cancer Treatment. *Cancer Treat. Rev.* **2009**, *35* (1), 32–46.
 - (10) Dasari, S.; Bernard Tchounwou, P. Cisplatin in Cancer Therapy: Molecular Mechanisms of Action. *Eur. J. Pharmacol.* **2014**, *740*, 364–378.
 - (11) Yano, S.; Ohi, H.; Ashizaki, M.; Obata, M.; Mikata, Y.; Tanaka, R.; Nishioka, T.; Kinoshita, I.; Sugai, Y.; Okura, I.; Ogura, S. I.; Czaplewska, J. A.; Gottschaldt, M.; Schubert, U. S.; Funabiki, T.; Morimoto, K.; Nakai, M. Syntheses, Characterization, and Antitumor Activities of Platinum(II) and Palladium(II) Complexes with Sugar-

- Conjugated Triazole Ligands. *Chem. Biodivers.* **2012**, *9* (9), 1903–1915.
- (12) Lee, S. Y.; Kim, C. Y.; Nam, T. G. Ruthenium Complexes as Anticancer Agents: A Brief History and Perspectives. *Drug Des. Devel. Ther.* **2020**, *14*, 5375–5392.
- (13) Page, S. M.; Boss, S. R.; Barker, P. D. Tuning Heavy Metal Compounds for Anti-Tumor Activity: Is Diversity the Key to Rutheniums Success? *Future Med. Chem.* **2009**, *1* (3), 541–559.
- (14) Lee, S. Y.; Kim, C. Y.; Nam, T.-G. Ruthenium Complexes as Anticancer Agents: A Brief History and Perspectives. **2020**.
- (15) Palma, G.; D’Aiuto, M.; Rea, D.; Bimonte, S.; Lappano, R.; Sinicropi, M. S.; Maggiolini, M.; Longo, P.; Arra, C.; Saturnino, C. Organo-Metallic Compounds: Novel Molecules in Cancer Therapy. *Biochem. Pharmacol. Open Access* **2014**, *3* (6), 1–12.
- (16) Santini, C.; Pellei, M.; Gandin, V.; Porchia, M.; Tisato, F.; Marzano, C. Advances in Copper Complexes as Anticancer Agents. *Chem. Rev.* **2014**, *114* (1), 815–862.
- (17) Yeo, C. I.; Ooi, K. K.; Tiekink, E. R. T. Gold-Based Medicine: A Paradigm Shift in Anti-Cancer Therapy? *Molecules* **2018**, *23* (6), 1410.
- (18) Zou, T.; Lum, C. T.; Lok, C. N.; Zhang, J. J.; Che, C. M. Chemical Biology of Anticancer Gold(III) and Gold(I) Complexes. *Chem. Soc. Rev.* **2015**, *44* (24), 8786–8801.
- (19) Kalinowska-Lis, U.; Felczak, A.; Chęcińska, L.; Szabłowska-Gadomska, I.; Patyna, E.; Małecki, M.; Lisowska, K.; Ochocki, J. Antibacterial Activity and Cytotoxicity of Silver(I) Complexes of Pyridine and (Benz)Imidazole Derivatives. X-Ray Crystal Structure of [Ag(2,6-Di(CH₂OH)Py)₂]NO₃. *Molecules* **2016**, *21* (2).
- (20) Siciliano, T. J.; Deblock, M. C.; Hindi, K. M.; Durmus, S.; Panzner, M. J.; Tessier, C. A.; Youngs, W. J. Synthesis and Anticancer Properties of Gold(I) and Silver(I) N-

- Heterocyclic Carbene Complexes. *J. Organomet. Chem.* **2011**, 696 (5), 1066–1071.
- (21) Qian, J.; Yu, S.; Wang, W.; Wang, L.; Tian, J.; Yan, S. Efficient Single-Strand Cleavage of DNA Mediated by a Mn^{III}Mn^{IV}-Based Artificial Nuclease. *Dalt. Trans.* **2014**, 43 (6), 2646–2655.
- (22) Wu, H.; Zhang, Y.; Wang, H.; Bai, Y.; Shi, F.; Wang, X.; Yang, Z. Manganese(II) and Silver(I) Complexes Based on the V-Shaped Ligand, Bis(2-Benzimidazolylmethyl)Amine: Synthesis, Crystal Structures, DNA-Binding Properties, and Antioxidant Activities. *J. Coord. Chem.* **2014**, 67 (10), 1771–1781.
- (23) Yigider, E.; Taspinar, M. S.; Sigmaz, B.; Aydin, M.; Agar, G. Humic Acids Protective Activity against Manganese Induced LTR (Long Terminal Repeat) Retrotransposon Polymorphism and Genomic Instability Effects in Zea Mays. *Plant Gene* **2016**, 6, 13–17.
- (24) Fouquet, E.; Pratviel, G.; Bernadou, J.; Meunier, B. Nuclease Activity of a Water-Soluble Manganese Porphyrin Associated with Potassium Hydrogen Persulphate: Oxidative Cleavage of DNA. *J. Chem. Soc. Chem. Commun.* **1987**, No. 15, 1169–1171.
- (25) Bernadou, J.; Pratviel, G.; Bennis, F.; Girardet, M.; Meunier, B. Potassium Monopersulfate and a Water-Soluble Manganese Porphyrin Complex, [Mn(TMPyP)](OAc)₅, as an Efficient Reagent for the Oxidative Cleavage of DNA. *Biochemistry* **1989**, 28 (18), 7268–7275..
- (26) Gasmi, G.; Padeloup, M.; Pratviel, G.; Pitie, M.; Bernadou, J.; Meunier, B. Characterization of Terminal Phosphates Induced on DNA by the Artificial Nuclease “Mn-TMPyP/KHSO₅” in Comparison with DNases I and II. *Nucleic Acids Res.* **1991**, 19 (11), 2835–2839.
- (27) Drexler, C.; Hosseini, M. W.; Pratviel, G.; Meunier, B. Design, Synthesis and

- Cleaving Activity of an Abiotic Nuclease Based on a Manganese(III) Porphyrin Complex Bearing Two Acridine Moieties. *Chem. Commun.* **1998**, 0 (13), 1343–1344.
- (28) Xu, Z. D.; Liu, H.; Xiao, S. L.; Yang, M.; Bu, X. H. Synthesis, Crystal Structure, Antitumor Activity and DNA-Binding Study on the Mn(II) Complex of 2H-5-Hydroxy-1,2,5-Oxadiazolo[3,4-f]1,10-Phenanthroline. *J. Inorg. Biochem.* **2002**, 90 (3–4), 79–84.
- (29) Zhu, L.-N.; Jin, Y.-W.; Li, X.-Z.; Wang, J.; Kong, D.-M.; Mi, H.-F.; Liao, D.-Z.; Shen, H.-X. Synthesis, Structure and DNA Cleavage Activity of Two 4,4'-O-Dimethyl-2,2'-Bipyridyl Manganese(II) Complexes. *Inorganica Chim. Acta* **2008**, 361 (1), 29–35.
- (30) Pan, D.; Caruthers, S. D.; Hu, G.; Senpan, A.; Scott, M. J.; Gaffney, P. J.; Wickline, S. A.; Lanza, G. M. Ligand-Directed Nanobialys as Theranostic Agent for Drug Delivery and Manganese-Based Magnetic Resonance Imaging of Vascular Targets. *J. Am. Chem. Soc.* **2008**, 130 (29), 9186–9187.
- (31) Qian, J.; Ma, X. F.; Xu, H. Z.; Tian, J. L.; Shang, J.; Zhang, Y.; Yan, S. P. Synthesis, Crystal Structure, DNA Binding, and Hydrolytic Cleavage Activity of a Manganese(II) Complex. *Eur. J. Inorg. Chem.* **2010**, 2010 (20), 3109–3116.
- (32) Romera, C.; Sabater, L.; Garofalo, A.; M. Dixon, I.; Pratviel, G. Interaction of Cationic Nickel and Manganese Porphyrins with the Minor Groove of DNA. *Inorg. Chem.* **2010**, 49 (18), 8558–8567.
- (33) Huang, J. T.; Wang, X. L.; Zhang, Y.; Mahmood, M. H.; Huang, Y. Y.; Ying, X.; Ji, L. N.; Liu, H. Y. DNA Binding and Nuclease Activity of a Water-Soluble Sulfonated Manganese(III) Corrole. *Transit. Met. Chem.* **2013**, 38 (3), 283–289.
- (34) Liu, J.; Chen, Q.; Zhu, W.; Yi, X.; Yang, Y.; Dong, Z.; Liu, Z. Nanoscale-Coordination-Polymer-Shelled Manganese Dioxide Composite Nanoparticles: A Multistage Redox/PH/H₂O₂-Responsive Cancer Theranostic Nanoplatfrom. *Adv.*

- Funct. Mater.* **2017**, 27 (10), 1605926.
- (35) Liang, S.; Liao, G.; Zhu, W.; Zhang, L. Manganese-Based Hollow Nanoplatfoms for MR Imaging-Guided Cancer Therapies. *Biomater. Res.* **2022**, 26 (1), 1–21.
- (36) Wu, H.; Yang, Z.; Wang, F.; Peng, H.; Zhang, H.; Wang, C.; Wang, K. V-Shaped Ligand 1,3-Bis(1-Ethylbenzimidazol-2-Yl)-2-Thiapropane and Manganese(II), Cobalt(II) and Copper(II) Complexes: Synthesis, Crystal Structure, DNA-Binding Properties and Antioxidant Activities. *J. Photochem. Photobiol. B Biol.* **2015**, 148, 252–261.
- (37) Gao, E.; Xing, J.; Qu, Y.; Qiu, X.; Zhu, M. Synthesis, Characterization, DNA Binding, Cytotoxicity and Molecular Docking Properties of Cu (II) and Mn (II) Complexes with 1,4-Bis (Pyrazol-1-Yl) Terephthalic Acid. *Appl. Organomet. Chem.* **2018**, 32 (10), e4469.

Chapter 3

Biophysical and Biochemical Interactions of Several Complexes with DNA

Advancements were made in the field of metal complexes, offering a highly effective class of biological agents for the treatment of cancer. However, the compounds have notable drawbacks, such as limited solubility and side effects like nausea, neurotoxicity, and nephrotoxicity¹⁻³. Additionally, certain cancer types exhibit inherent or acquired resistance to compounds. Therefore, it becomes imperative to develop new anticancer strategies to combat the challenges associated with chemotherapy. One such approach focuses on the development of compounds that can disrupt cancerous cellular machinery through unconventional interactions with nucleic acids. Medicinal chemists have dedicated their efforts to this area⁴⁻⁶, recognizing the value of small molecules capable of inducing or suppressing cellular interactions involving the DNA. These molecules can manipulate cellular function to achieve desired outcomes, enabling the diagnosis and treatment of diseases^{7,8}. Transition metals are particularly well-suited for this purpose due to their unique properties, which allow for specific interactions with DNA and other biomolecules⁹. Moreover, their spectroscopic characteristics make them valuable tools for biophysical studies that can continuously monitor changes within a biological system^{10,11}. Consequently, there is significant interest in developing transition metal complexes due to the wide range of available ligands for coordination, diverse geometries, coordination numbers, redox potentials, kinetic properties and thermodynamic characteristics that is offered by these metals¹². Platinum, Ruthenium, Titanium, Rhodium, Copper, Palladium, Gold, and Iron are among the transition metals extensively utilized in medicinal chemistry. In this chapter, I tried to explore biophysical and biochemical interactions of transition metal complexes with DNA encompassing binding modes and structural motifs.

DNA serves as a crucial target for therapeutic interventions, playing a central role in a wide range of intracellular interactions¹³. The stability of DNA relies on hydrogen bonding

between specific nucleic acid pairs, namely adenine and thymine (A-T) and guanine and cytosine (G-C). In its native form, DNA strands are arranged in an anti-parallel double helix, with bases stacked in parallel orientations¹⁴. This helical structure gives rise to major and minor grooves, which serve as binding sites for small molecules¹⁵. It's worth noting here that these grooves exhibit distinct characteristics, including differences in size, shape, hydration, electrostatic potential and positioning of hydrogen bonding sites¹⁶. Exploiting these unique conformations of DNA presents opportunities for small molecules to selectively bind and modulate DNA function.

The structural complexity and polymorphic nature of DNA offer numerous opportunities for intermolecular interactions, which includes irreversible *covalent binding*, reversible *groove association or intercalation*¹⁷. Dwyer's insight into the potential of coordination metal complexes to elucidate biomolecular structures remains relevant¹⁸⁻²⁰. By varying properties like size, charge distribution, stereochemistry and redox potential during chemical synthesis, metal chelates can serve as valuable pharmacological tools for investigating cellular functional systems. Metal complex-DNA interactions highlight the influence of the metal's coordination geometry and ligand disposition on binding activity. In contrast, square planar complexes offer greater capacity for intercalator insertion compared to geometries such as octahedral or tetrahedral arrangements¹⁸. However, in octahedral complexes like $[\text{Co}(\text{phen})_3]^{2+}$ or $[\text{Ru}(\text{phen})_3]^{2+}$ arrangement of phenanthroline (phen) ligands can impede complete insertion. Steric hindrance caused by DNA phosphate backbone can impede covalent binding in specific complexes like $[\text{Ru}(\text{phen})_2\text{Cl}_2]^{2+}$ ²¹. Furthermore, a comparative study involving zinc (tetrahedral) and cobalt (octahedral) complexes featuring a porphyrin ligand revealed that the cobalt complex exhibit DNA binding through intercalation, whereas presence of an axial water ligand hindered binding of the zinc complex²². These examples

highlight the diverse binding interactions different transition metal complexes can undergo with DNA. There are several significant types of biophysical and biochemical interactions between metal complexes and DNA. These interactions include *covalent binding*, *intercalation*, *bimodal interactions involving both covalent binding and intercalation and covalent binding* and *groove binding*, as well as only *groove binding*. Each of these interactions play a crucial role in understanding the intricate relationship between metal complexes and DNA.

Covalent binding is a widely employed mechanism through which anticancer drugs interact with DNA. Among these drugs, cisplatin emerged as the most successful DNA covalent binder in clinical applications²³. Binding of cisplatin relies on hydrolysis of its labile chloride ligands. The cis configuration of cisplatin is crucial for its effective activity in the body. In contrast, the trans isomer, transplatin, undergoes more rapid degradation in vivo and is unable to form the most potent 1,2-intrastrand adducts. Moreover, the 1,3-intrastrand adducts formed by *trans* platin are rapidly repaired compared to cisplatin²⁴. By utilizing metals with diverse coordination geometries to platinum(II) and a broader range of ligands, researchers have generated a new collection of complexes exhibiting distinct cellular behaviors and demonstrating higher efficacy *in vitro* than currently utilized clinical compounds²⁴⁻²⁶. The biological effects of ruthenium(II) and (III) complexes are gaining recognition due to their stable and well-characterized structures, which can be achieved by selecting appropriate ligands²⁷. Through further development, the first and only ruthenium(III) complexes to undergo clinical trials were produced. These complexes include NAMI-A (imidazolium *trans*-[tetrachlorido(imidazole)(dimethylsulfoxide) ruthenate(III)] and KP1019 (indazolium *trans*-[tetrachloridobis(1*H*-indazole)ruthenate(III)]). These complexes have demonstrated the ability to inhibit the formation of metastasis and suppress the growth of advanced tumors

with relatively low toxicity^{28,29}. The complex of the type $[\text{Ru}(\eta^6\text{-arene})\text{-(en)(Cl)}]^+$ has been found to form monofunctional adducts with guanine bases of DNA leading to anticancer activity^{30,31}. Interestingly, anticancer activity of these complexes increase with the size of the arene, with larger arenes (such as biphenyl and tetrahydroanthracene) exhibiting greater effectiveness compared to smaller ones (such as benzene and p-cymene). NMR studies have indicated that these complexes can covalently bind to DNA although the arene moiety can also intercalate from the minor groove of the DNA helix^{32,33}.

Intercalation refers to the process in which a positively charged planar polycyclic aromatic molecule inserts itself between adjacent base pairs of DNA³⁴. This insertion is facilitated by π - π stacking interactions between aromatic ring system and base pairs, resulting in elongation, rigidity and unwinding of the DNA helix^{35,36}. The extent of this effect, however, depends on the depth of insertion into the DNA. Intercalation is a reversible process, and its stability is influenced by a combination of electrostatic, hydrogen bonding, entropic, van der Waals, and hydrophobic interactions^{36,37}. Various organic compounds like phenanthrolines, phenanthridines, acridines, anthraquinones, anthracenes, and ellipticines, are commonly known as intercalators to DNA. Ruthenium(II) polypyridyl complexes have been widely recognized as effective DNA intercalators, offering advantageous spectroscopic properties and low toxicity³⁸. These complexes have shown the potential as a diagnostic agent. Studies have indicated each complex binds to DNA through intercalation, although there are notable differences in the binding affinities observed when the metal ion is different. It was proposed that the Ni complex exhibits highest binding affinity due to its square planar coordination geometry, allowing it to deeply insert between base pairs of DNA³⁹. In contrast, Cu and Zn complexes with their octahedral geometries may have a relatively lower ability to penetrate deeply between DNA base pairs. A notable example is [chlorido(2,2':6',2''-

terpyridine)platinum(II)]([Pt(terpy)Cl]⁺). Studies on the binding behavior of this complex reveals it initially intercalates with DNA and then forms covalent bonds with the base pairs upon detachment of the labile chloride ligand⁴⁰⁻⁴².

Groove binding involves reversible intermolecular associations between the complex and DNA. This type of binding is characterized by crescent-shaped complexes that complement either the major or minor groove of DNA⁴³. These grooves possess distinct characteristics in terms of size, shape and properties allowing an association under different circumstances. For instance, binding to the major groove is driven by enthalpy, while interactions at the minor groove are primarily influenced by entropic effects⁴⁴. Groove binding relies on intermolecular interactions like electrostatic and van der Waals. However, it does not involve direct stacking between base pairs and the resulting structural changes in the DNA double helix are relatively minor¹⁶.

A distinctive example of intermolecular force-driven binding that deviates from typical interactions between base pairs or along the grooves of DNA is the association along the phosphate backbone. This type of interaction was observed in a study involving an analogue of the multinuclear complex $[\{trans\text{-Pt}(\text{NH}_3)_2(\text{NH}_2(\text{CH}_2)_6\text{-(NH}_3^+))\}_2\text{-}\mu\text{-}\{trans\text{-Pt}(\text{NH}_3)_2(\text{NH}_2(\text{CH}_2)_6\text{NH}_2)_2\}]^{8+}$ (referred to as TriplatinNC). The complex was found to associate with DNA minor groove but also displayed binding along the phosphate backbone. In this complex, the amine protons form hydrogen bonds with oxygen atoms along the DNA chain.⁴⁵

In this chapter, a review of some examples showcasing how transition metal complexes can interact with DNA in its various structural forms was provided, that employs diverse binding modes. It is evident that combinations of these interaction modes can be employed to enhance

binding affinity and selectivity of metal complexes. However, it should be noted that this review is not exhaustive and that numerous other examples exist. The design and flexibility offered by transition metals, owing to their diverse physicochemical properties and the vast array of ligands available for coordination, allows for the development of potent therapeutic and diagnostic agents in the form of metal complexes. These complexes can effectively explore the structural diversity of DNA, further emphasizing their potential in the field.

References:

- (1) Qu, Y.; Rauter, H.; Fontes, A. P. S.; Bandarage, R.; Kelland, L. R.; Farrell, N. Synthesis, Characterization, and Cytotoxicity of Trifunctional Dinuclear Platinum Complexes: Comparison of Effects of Geometry and Polyfunctionality on Biological Activity. *J. Med. Chem.* **2000**, *43* (16), 3189–3192.
- (2) Loehrer, P. J.; Einhorn, L. H. Cisplatin. *Ann. Intern. Med.* **1984**, *100* (5), 704–713.
- (3) Wang, Y.; Zhou, J.; Qiu, L.; Wang, X.; Chen, L.; Liu, T.; Di, W. Cisplatin–Alginate Conjugate Liposomes for Targeted Delivery to EGFR-Positive Ovarian Cancer Cells. *Biomaterials* **2014**, *35* (14), 4297–4309.
- (4) Klein, A. V.; Hambley, T. W. Platinum Drug Distribution in Cancer Cells and Tumors. *Chem. Rev.* **2009**, *109* (10), 4911–4920.
- (5) Benjamin Garbutcheon-Singh, K.; J Harper, B. W.; Myers bc, S.; Aldrich-Wright, J. R. Combination Studies of Platinum(II)-Based Metallointercalators with Buthionine-S,R-Sulfoximine, 3-Bromopyruvate, Cisplatin or Carboplatin . *Met.* **2014**, *6*, 126.
- (6) Song, Y.; Suntharalingam, K.; Yeung, J. S.; Royzen, M.; Lippard, S. J. Synthesis and Characterization of Pt(IV) Fluorescein Conjugates to Investigate Pt(IV) Intracellular Transformations. *Bioconjug. Chem.* **2013**, *24* (10), 1733–1740.
- (7) PEI, X.; ZHANG, J.; LIU, J. Clinical Applications of Nucleic Acid Aptamers in

- Cancer. *Mol. Clin. Oncol.* **2014**, 2 (3), 341.
- (8) Mjos, K. D.; Orvig, C. Metallodrugs in Medicinal Inorganic Chemistry. *Chem. Rev.* **2014**, 114, 4540–4563.
- (9) Meggers, E. Exploring Biologically Relevant Chemical Space with Metal Complexes. *Curr. Opin. Chem. Biol.* **2007**, 11 (3), 287–292.
- (10) Nial J. Wheate; Craig R. Brodie; J. Grant Collins; Sharon Kemp; Janice R. Aldrich-Wright. DNA Intercalators in Cancer Therapy: Organic and Inorganic Drugs and Their Spectroscopic Tools of Analysis. *Mini-Reviews Med. Chem.* **2007**, 7 (6), 627–648.
- (11) Krause-Heuer, A. M.; Price, W. S.; Aldrich-Wright, J. R. Spectroscopic Investigations on the Interactions of Potent Platinum(II) Anticancer Agents with Bovine Serum Albumin. *J. Chem. Biol.* **2012**, 5 (3), 105–113.
- (12) Bruijninx, P. C.; Sadler, P. J. New Trends for Metal Complexes with Anticancer Activity. *Curr. Opin. Chem. Biol.* **2008**, 12 (2), 197–206.
- (13) Quin, J. E.; Devlin, J. R.; Cameron, D.; Hannan, K. M.; Pearson, R. B.; Hannan, R. D. Targeting the Nucleolus for Cancer Intervention. *Biochim. Biophys. Acta - Mol. Basis Dis.* **2014**, 1842 (6), 802–816.
- (14) Watson, J. D.; Crick, F. H. C. Molecular Structure of Nucleic Acids: A Structure for Deoxyribose Nucleic Acid. *Nature* **1953**, 171 (4356), 737–738.
- (15) Arnott, S. Major Groove or Minor Groove? *Nature* **1986**, 320 (6060), 313–313.
- (16) Oguey, C.; Foloppe, N.; Hartmann, B. Understanding the Sequence-Dependence of DNA Groove Dimensions: Implications for DNA Interactions. *PLoS One* **2010**, 5 (12), e15931.
- (17) Jamieson, E. R.; Lippard, S. J. Structure, Recognition, and Processing of Cisplatin–DNA Adducts. **1999**.

- (18) Pages, B. J.; Ang, D. L.; Wright, E. P.; Aldrich-Wright, J. R. Metal Complex Interactions with DNA. *Dalt. Trans.* **2015**, *44* (8), 3505–3526.
- (19) Dwyer, F. P.; Gyarfas, E. C.; O'Dwyer, M. F. Configurational Activity. *Nature* **1951**, *167* (4260), 1036–1036.
- (20) Dwyer, F. P.; Gyarfas, E. C.; Rogers, W. P.; Koch, J. H. Biological Activity of Complex Ions. *Nature* **1952**, *170* (4318), 190–191.
- (21) Barton, J. K.; Lolis, E. Chiral Discrimination in the Covalent Binding of Bis(Phenanthroline)Dichlororuthenium(II) to B-DNA. *J. Am. Chem. Soc.* **1985**, *107* (3), 708–709.
- (22) Asadi, M.; Safaei, E.; Ranjbar, B.; Hasani, L. Thermodynamic and Spectroscopic Study on the Binding of Cationic Zn(II) and Co(II) Tetrapyridinoporphyrazines to Calf Thymus DNA: The Role of the Central Metal in Binding Parameters. *New J. Chem.* **2004**, *28* (10), 1227–1234.
- (23) Ishida, S.; Lee, J.; Thiele, D. J.; Herskowitz, I. Uptake of the Anticancer Drug Cisplatin Mediated by the Copper Transporter Ctr1 in Yeast and Mammals. *Proc. Natl. Acad. Sci. U. S. A.* **2002**, *99* (22), 14298–14302.
- (24) Alderden, R. A.; Hall, M. D.; Hambley, T. W. The Discovery and Development of Cisplatin. *J. Chem. Educ.* **2006**, *83* (5), 728–734.
- (25) Wang, D.; Lippard, S. J. Cellular Processing of Platinum Anticancer Drugs. *Nat. Rev. Drug Discov.* **2005**, *4* (4), 307–320.
- (26) Dhar, S.; Kolishetti, N.; Lippard, S. J.; Farokhzad, O. C. Targeted Delivery of a Cisplatin Prodrug for Safer and More Effective Prostate Cancer Therapy in Vivo. *Proc. Natl. Acad. Sci. U. S. A.* **2011**, *108* (5), 1850–1855.
- (27) Bergamo, A.; Gaiddon, C.; Schellens, J. H. M.; Beijnen, J. H.; Sava, G. Approaching

- Tumour Therapy beyond Platinum Drugs: Status of the Art and Perspectives of Ruthenium Drug Candidates. *J. Inorg. Biochem.* **2012**, *106* (1), 90–99.
- (28) Sava, G.; Clerici, K.; Capozzi, I.; Cocchietto, M.; Gagliardi, R.; Alessio, E.; Mestroni, G.; Perbellini, A. Reduction of Lung Metastasis by ImH[Trans-RuCl₄(DMSO)Im]: Mechanism of the Selective Action Investigated on Mouse Tumors. *Anticancer. Drugs* **1999**, *10* (1), 129–138.
- (29) Hartinger, C. G.; Zorbas-Seifried, S.; Jakupec, M. A.; Kynast, B.; Zorbas, H.; Keppler, B. K. From Bench to Bedside – Preclinical and Early Clinical Development of the Anticancer Agent Indazolium Trans-[Tetrachlorobis(1H-Indazole)Ruthenate(III)] (KP1019 or FFC14A). *J. Inorg. Biochem.* **2006**, *100* (5–6), 891–904.
- (30) Yan, Y. K.; Melchart, M.; Habtemariam, A.; Sadler, P. J. Organometallic Chemistry, Biology and Medicine: Ruthenium Arene Anticancer Complexes. *Chem. Commun.* **2005**, No. 38, 4764–4776.
- (31) Chen, H.; Parkinson, J. A.; Parsons, S.; Coxall, R. A.; Gould, R. O.; Sadler, P. J. Organometallic Ruthenium(II) Diamine Anticancer Complexes: Arene-Nucleobase Stacking and Stereospecific Hydrogen-Bonding in Guanine Adducts. *J. Am. Chem. Soc.* **2002**, *124* (12), 3064–3082.
- (32) Aird, R. E.; Cummings, J.; Ritchie, A. A.; Muir, M.; Jodrell, D. I.; Morris, R. E.; Chen, H.; Sadler, P. J. In Vitro and in Vivo Activity and Cross Resistance Profiles of Novel Ruthenium (II) Organometallic Arene Complexes in Human Ovarian Cancer. *Br. J. Cancer* **2002**, *86* (10), 1652–1657.
- (33) Dougan, S. J.; Melchart, M.; Habtemariam, A.; Parsons, S.; Sadler, P. J. Phenylazo-Pyridine and Phenylazo-Pyrazole Chlorido Ruthenium(II) Arene Complexes: Arene Loss, Aquation, and Cancer Cell Cytotoxicity. *Inorg. Chem.* **2006**, *45* (26), 10882–

- 10894.
- (34) Lerman, L. S. Structural Considerations in the Interaction of DNA and Acridines. *J. Mol. Biol.* **1961**, 3 (1), 18-14.
- (35) Arena, G.; Scolaro, L. M.; Pasternack, R. F.; Romeo, R. Synthesis, Characterization, and Interaction with DNA of the Novel Metallointercalator Cationic Complex (2,2':6',2''-Terpyridine)Methylplatinum(II). *Inorg. Chem.* **1995**, 34 (11), 2994–3002.
- (36) Monaco, R. R. Capture of a Transition State Using Molecular Dynamics: Creation of an Intercalation Site in DsDNA with Ethidium Cation. *J. Nucleic Acids* **2010**, 2010.
- (37) Intercalation_DNA_Kinking_and_the_Contro.Pdf. *Science* (80-.). **1996**, 271, 778–784.
- (38) Johann, T. W.; Barton, J. K. Recognition of DNA by Octahedral Coordination Complexes. *Philos. Trans. R. Soc. London. Ser. A Math. Phys. Eng. Sci.* **1996**, 354 (1706), 299–324.
- (39) Lauria, A.; Bonsignore, R.; Terenzi, A.; Spinello, A.; Giannici, F.; Longo, A.; Almerico, A. M.; Barone, G. Nickel(II), Copper(II) and Zinc(II) Metallo-Intercalators: Structural Details of the DNA-Binding by a Combined Experimental and Computational Investigation. *Dalt. Trans.* **2014**, 43 (16), 6108–6119.
- (40) Jennette, K. W.; Gill, J. T.; Sadownik, J. A.; Lippard, S. J. Metallointercalation Reagents. Synthesis, Characterization, and Structural Properties of Thiolato(2,2',2''-Terpyridine)Platinum(II) Complexes. *J. Am. Chem. Soc.* **1976**, 98 (20), 6159–6168.
- (41) Yu, C.; Hoi-Yiu Chan, K.; Man-Chung Wong, K.; Wing-Wah Yam, V. Single-Stranded Nucleic Acid-Induced Helical Self-Assembly of Alkynylplatinum(II) Terpyridyl Complexes. *PNAS* **1965**, 103, 19652–19657.
- (42) David Mcfadyen, W.; Wakelin, L. P. G.; Roos, I. A. G.; Hillcoat, B. L. Binuclear

Platinum (11-Terpyridine Complexes A New Class of Bifunctional DNA-Intercalating Agent. *Biochem. J* **1986**, 238, 757–763.

- (43) Kim, S. K.; Nordén, B. Methyl Green. A DNA Major-Groove Binding Drug. *FEBS Lett.* **1993**, 315 (1), 61–64.
- (44) Privalov, P. L.; Dragan, A. I.; Crane-Robinson, C.; Breslauer, K. J.; Remeta, D. P.; Minetti, C. A. S. A. What Drives Proteins into the Major or Minor Grooves of DNA? *J. Mol. Biol.* **2007**, 365 (1), 1–9.
- (45) Komeda, S.; Moulaei, T.; Woods, K. K.; Chikuma, M.; Farrell, N. P.; Williams, L. D. A Third Mode of DNA Binding: Phosphate Clamps by a Polynuclear Platinum Complex. *J. Am. Chem. Soc.* **2006**, 128 (50), 16092–16103.

Chapter 4

Review on Radioprotectors

Radiation therapy is a cancer treatment option in medicine for over a century, with its origin dating back to Wilhelm Röntgen's discovery of X-rays in 1895.¹ It is a common treatment for more than half of cancer patients. The field of radiation therapy experienced significant growth in the early 1900s largely due to the pioneering research of Marie Curie and her husband Pierre Curie who successfully isolated radium in 1898 from pitchblende. Researchers realized that atoms were not the fundamental building blocks of matter, as they could disintegrate into still smaller subatomic particles. Upon release, these particles generate a powerful impact on tissues in their trajectory causing burns. It was not too long before scientists harnessed the imperceptible rays of radium for the treatment of cancer. This ground breaking work marked the beginning of a new era in medical treatment and research. However, during 1920s, the dangers of radiation exposure were not fully understood and therefore protective measures were not taken. Radium was believed to have extensive curative properties leading to application of radiotherapy for the treatment of numerous diseases. Radiation therapy using radium and low-voltage diagnostic machines began with some of these early discoveries.

It is now well established that radiation functions by harming the DNA within cells (Figure 1). Radiation has both direct and indirect effects on DNA. When exposed to ionizing radiation, DNA can directly experience damage such as strand breaks, base alteration, crosslinking and dimer formation. In addition to direct effects, radiation can also indirectly affect DNA by acting on water molecules and producing free radicals. These free radicals can cause damage to DNA or form harmful compounds like the peroxides and superoxides leading to structural changes in cells that ultimately results in cell death.

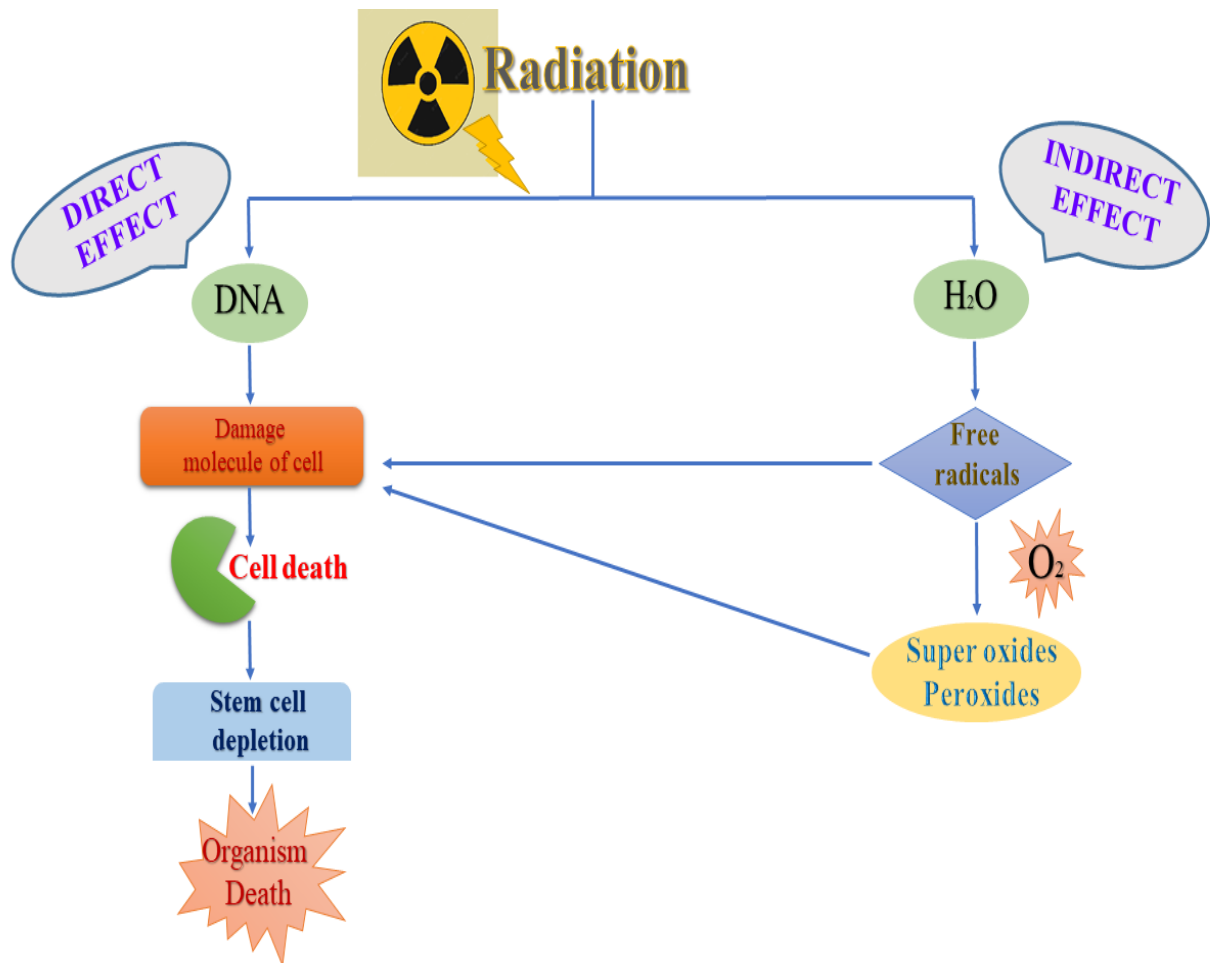


Figure 1: Schematic diagram showing influence of ionizing radiation on biological targets.

Cancer cells are less capable of repairing DNA damage in comparison to healthy cells, rendering them more vulnerable to death. Before elucidation of its mechanism of action, individuals who worked with radiation were unaware of the importance of taking safety precautions resulting in severe consequences. The fundamental problem with radiation-induced damage was due to a lack of knowledge about radiation, inadequate instrumentation to measure radiation dose and an undefined unit of measurement in those days. Radiation can damage healthy tissues and organs surrounding the area being treated, resulting in short-term and long-term side effects like skin irritation, fatigue, and permanent organ damage or cancer in severe cases. When exposed to ionizing radiation (IR), living tissues are damaged through a series of molecular events, including photoelectric, Compton, and Auger effects, which

depend on the radiation energy. As human tissues consist of 80% water, the primary radiation damage is caused by aqueous free radicals generated by the radiation's action on water.² The most significant free radicals resulting from aqueous radiolysis include OH, H, e_{aq}^- , HO₂, H₃O⁺, and more.^{3,4} These free radicals react with cellular macromolecules like DNA, RNA, proteins, and membranes, leading to cell dysfunction and mortality. In order to effectively inhibit further proliferation of cancer cells, a more potent dosage of radiation may be employed. However, it is also crucial to protect healthy tissues from radiation-induced damage. This necessitates the utilization of radioprotective compounds to safeguard normal tissues during the treatment process. Hence, these compounds play a vital role in clinical radiotherapy. However, this review will only focus on clinically relevant agents and their mechanisms of radioprotection, given the vast amount of literature on this topic.

A unique type of radioprotective compound exhibits multiple functions, encompassing antioxidant and adaptogen properties. It serves as both a mitigator and a therapeutic agent, or alternatively as a radioprotector and an adsorbent. Consequently, it defies conventional categorizations and deviates from established classifications. As a result, any substance capable of visibly diminishing the impact of ionizing radiation can be classified as a radioprotective drug or substance.⁵ These substances work by scavenging free radicals that are generated by ionizing radiation, which can cause DNA damage and other harmful effects in the body. Healthcare professionals therefore try to minimize the risk of side effects and long-term complications in patients by using radioprotectors during radiotherapy. Hence, it is crucial to ensure radioprotectors are effective and meet certain criteria like that of protecting normal cells without interfering with the radiation's ability to target and destroy cancer cells.⁶ Proper use of radioprotectors can improve overall success of radiation therapy and enhance the patient's quality of life during and after treatment. In 1942, Dale used the term "*radioprotection*" in his articles in which he suggested inactivity of enzymes and proteins

induced by X-rays was the cause of cell death resulting from radiation injury.⁷ However, in 1960s, the concept of radioprotection based on prevention of ‘DNA damage’ replaced Dale's earlier hypothesis. Starting in 1970s, numerous investigators began reporting on radioprotectors. Despite this, only *amifostine* was approved by Food and Drug Administration (FDA) in 1995 as a co-therapy agent for reducing normal tissue damage during radiation therapy.⁸ Therefore, it is important to consider the use of radioprotectors as part of a treatment plan for patients undergoing radiotherapy. However, it is essential to note that use of radioprotectors should be carefully evaluated on a case-by-case basis and should only be used under the guidance of a trained healthcare professional. Research on radioprotective chemicals began more than half a century ago in the United States, specifically during the Manhattan Project. Various types of radioprotectors were investigated in experimental studies thus far.⁹ Enzymes like superoxide dismutase, glutathione peroxidase and catalase are crucial in protecting mammalian cells from oxidative radiation damage.¹⁰ Melatonin has been recognized for over two decades for its radioprotective properties, primarily through *in vitro* studies.^{11,12} A considerable number of *in vivo* and *in vitro* experiments have been conducted to explore its potential protective effects on various cells and organs. Melatonin has been shown to alleviate several cytotoxic effects of ionizing radiation, including inflammation, cataracts, DNA damage, apoptosis, infertility, and fibrosis¹³. Numerous studies have validated that melatonin can offer radiation protection without inducing any cytotoxic effects on the regular operations of other organs. It accomplishes radioprotection through multiple mechanisms, such as enhancing the response to DNA damage, neutralizing free radicals, and ameliorating inflammatory responses by regulating the signaling pathways involved in the process. Around 60 years ago, an article was published in *Science* by Patt et al., which showcased the effectiveness of sulfhydryl compounds as radioprotectors.¹⁴ Their experiments involved exposing laboratory animals to

ionizing radiation and demonstrating how cysteine, in particular, exhibited robust protective properties. This study proved to be a source of inspiration for radiobiology researchers, who began conducting their investigations into the synthesis of sulfhydryl compounds, specifically aminothiols, and phosphorothioates. In 1968, Weil et al. published in *Nature* that highlighted the antioxidant qualities of stable synthetic nitroxides, and their possible use as radioprotective agents.¹⁵ This marked a crucial breakthrough in this field of research. Recent experiments conducted *in vitro* and *in vivo* using water-soluble nitroxides have indicated that administering these compounds before exposure to ionizing radiation is imperative for their radioprotective properties to be effective.¹⁶ Presently, a diverse array of synthetic antioxidants can safeguard mammals against the detrimental consequences of ionizing radiation exposure. Among this group of pharmaceuticals are thiophane, probucol, succinobucol, fridox, olifen, N-acyldihydroalanine, and various others, totaling several such compounds.¹⁷ Multiple studies have proven that administering ‘*immunomodulators*’ as an early therapeutic or preventive measure can considerably mitigate the harm caused by radiation exposure. Lipopolysaccharides, a type of bacterial endotoxin, were among the initial ‘*immunomodulators*’ to undergo investigation, and have been studied for over fifty years. These compounds have demonstrated a protective effect when given before, or even after, exposure to ionizing radiation.¹⁸ Studies have demonstrated that prostaglandins have radioprotective qualities in different tissues, including the gastrointestinal tract, bone marrow, and hair follicles. Prostaglandins achieve this effect primarily by enhancing cell resistance and regulating local biological processes. Nevertheless, prostaglandins’ clinical use is restricted because they tend to serve as mediators of inflammatory processes, leading to several undesirable side effects.¹⁹ Experimental evidence has shown that specific metal salts and metallothioneins can provide defense against radiation-induced death in test animals, as long as they are given at low, non-toxic doses.²⁰ Recent research suggests that specific

nanomaterials, also known as nano-radioprotectors, possess inherent radioprotective characteristics that enable them to eliminate excessive reactive oxygen species (ROS) generated by ionizing radiation. Furthermore, these nano-radioprotectors have a prolonged blood circulation time and are less effectively cleared by the reticuloendothelial system (RES) when compared to small-molecule radioprotectors.²¹ Some studies focus on exploring the impact of molybdenum nanoparticles (Mo-NPs) in radiation protection properties of polyvinyl alcohol (PVA) for shielding gamma rays and applications thereof. Results of another study indicates PVA/Mo nanocomposite films containing varying percentages of Mo-NPs can be used as radiation shielding material.²² In yet another study molybdenum-based polyoxometalate nanoclusters (Mo-POM NCs) were developed as potent radioprotectants with impressive free radical scavenging capabilities for protection against ionizing radiation. These nanoclusters were effective in shielding ionizing radiation-induced DNA damage and disruption of the radiation-sensitive hematopoietic system due to their antioxidant properties resulting in a valence shift of molybdenum ions. Unlike toxic chemotherapeutic drug candidates, Mo-POM NCs showed effective shielding capacity without causing much harm. Radioprotectants with exceptional ROS-scavenging capabilities like nanomaterials are a desirable substitute for conventional molecular drugs in achieving an efficient radiation protection.²³ This has resulted in high demand for such materials. In comparison to the clinically used radioprotectant amifostine (AM), Mo-POM NCs demonstrated superior radioprotective effects. Additionally, ultra-small-sized Mo-POM NCs that were prepared using mimetic Folin-Ciocalteu assay could be readily eliminated from the body via the renal-urinary pathway and the hepato-enteral excretory system after fulfilling their mission of radiation protection, thus having no long-term retention issues. This innovative approach expands the potential application of polyoxometalate (POM) based chemotherapeutic drugs to serve as new radioprotectants.²⁴

References:

- (1) *History - Radiation Oncology / UAB.*
<https://www.uab.edu/medicine/radonc/about/history>
- (2) Scholes, G. Radiation Effects on DNA. The Silvanus Thompson Memorial Lecture, April 1982. *Br. J. Radiol.* **2014**, *56* (664), 221–231.
- (3) Pradhan, D. S.; Nair, C. K. K.; Sreenivasan, A. Radiation Injury Repair and Sensitisation of Micro-Organisms. *Proc. Indian Natl. Sci. Acad., Part B* **1973**, *39* (4), 516–527.
- (4) IVAN G. DRAGANIĆ - ZORICA D. DRAGANIĆ. *The Radiation Chemistry of Water*; 1971; Vol. 26.
- (5) Citrin, D.; Cotrim, A. P.; Hyodo, F.; Baum, B. J.; Krishna, M. C.; Mitchell, J. B. Radioprotectors and Mitigators of Radiation-Induced Normal Tissue Injury. *Oncologist* **2010**, *15* (4), 360–371.
- (6) Mishra, K.; Alsbeih, G. Appraisal of Biochemical Classes of Radioprotectors: Evidence, Current Status and Guidelines for Future Development. *3 Biotech* **2017**, *7* (5), 292.
- (7) Dale, W. M. The Effect of X-Rays on the Conjugated Protein d-Amino-Acid Oxidase. *Biochem. J.* **1942**, *36* (1–2), 80–85.
- (8) Bourhis, J.; Rosine, D. Radioprotective Effect of Amifostine in Patients with Head and Neck Squamous Cell Carcinoma. *Semin. Oncol.* **2002**, *29* (6 Suppl 19), 61–62.
- (9) Farhood, B.; Goradel, N. H.; Mortezaee, K.; Khanlarkhani, N.; Salehi, E.; Nashtaei, M. S.; Mirtavoos-mahyari, H.; Motevaseli, E.; Shabeeb, D.; Musa, A. E.; Najafi, M.

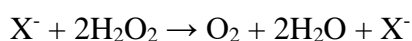
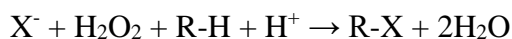
- Melatonin as an Adjuvant in Radiotherapy for Radioprotection and Radiosensitization. *Clin. Transl. Oncol.* **2019**, *21* (3), 268–279.
- (10) Fridovich, I. The Biology of Oxygen Radicals. *Science* (80-.). **1978**, *201* (4359), 875–880.
- (11) Vijayalaxmi; Reiter, R. J.; Herman, T. S.; Meltz, M. L. Melatonin Reduces Gamma Radiation-Induced Primary DNA Damage in Human Blood Lymphocytes. *Mutat. Res. Mol. Mech. Mutagen.* **1998**, *397* (2), 203–208.
- (12) Vijayalaxmi; Reiter, R. J.; Meltz, M. L.; Herman, T. S. Melatonin: Possible Mechanisms Involved in Its ‘Radioprotective’ Effect. *Mutat. Res. Mol. Mech. Mutagen.* **1998**, *404* (1–2), 187–189.
- (13) Vijayalaxmi; Reiter, R. J.; Tan, D. X.; Herman, T. S.; Thomas, C. R. Melatonin as a Radioprotective Agent: A Review. *Int. J. Radiat. Oncol. Biol. Phys.* **2004**, *59* (3), 639–653.
- (14) Patt, H. M.; Tyree, E. B.; Straube, R. L.; Smith, D. E. Cysteine Protection against X Irradiation. *Science* (80-.). **1949**, *110* (2852), 213–214.
- (15) Weil, J. T.; Van Der Veen, J.; Olcott, H. S. Stable Nitroxides as Lipid Antioxidants. *Nature* **1968**, *219*, 168–169. <https://doi.org/10.1038/219168a0>.
- (16) Tabaczar, S.; Talar, M.; Gwoździński, K. Nitroksydy Jako Antyoksydanty – Możliwości Ich Zastosowania w Celach Chemioprewencyjnych Oraz Radioprotekcyjnych * Nitroxides as Antioxidants – Possibilities of Their Application in Chemoprevention and Radioprotection. *Postep. Hig Med Dosw Online* **2011**, *65*, 46–54.

- (17) Halliwell, B. Antioxidant Defence Mechanisms: From the Beginning to the End (of the Beginning). *Free Radic. Res.* **1999**, *31* (4), 261–272.
- (18) Wilson, B. R., & Matsuzawa, T. Germfree Studies of Protection Induced by Bacterial Endotoxin against X-Radiation. *Radiat. Res.* **1963**, *19* (1), 231.
- (19) Hanson, W. R.; Zhen, W.; Geng, L.; Hunter, N.; Milas, L. The Prostaglandin E₁ Analog, Misoprostol, a Normal Tissue Protector, Does Not Protect Four Murine Tumors In Vivo from Radiation Injury. *Radiat. Res.* **1995**, *142* (3), 281–287.
- (20) A N Koterov, I. V. F. The Radiobiology of Metallothioneins. *Radiats Biol Radioecol* **1995**, *35* (2), 162–180.
- (21) Pan, Y.; Tang, W.; Fan, W.; Zhang, J.; Chen, X. Development of Nanotechnology-Mediated Precision Radiotherapy for Anti-Metastasis and Radioprotection. *Chem. Soc. Rev.* **2022**, *51* (23), 9759–9830.
- (22) Abulyazied, D. E.; Saudi, H. A.; Zakaly, H. M. H.; Issa, S. A. M.; Henaish, A. M. A. Novel Nanocomposites Based on Polyvinyl Alcohol and Molybdenum Nanoparticles for Gamma Irradiation Shielding. *Opt. Laser Technol.* **2022**, *156* (January), 108560.
- (23) Colon, J.; Herrera, L.; Smith, J.; Patil, S.; Komanski, C.; Kupelian, P.; Seal, S.; Jenkins, D. W.; Baker, C. H. Protection from Radiation-Induced Pneumonitis Using Cerium Oxide Nanoparticles. *Nanomedicine Nanotechnology, Biol. Med.* **2009**, *5* (2), 225–231.
- (24) Tao, Z.; Wang, J.; Wu, H.; Hu, J.; Li, L.; Zhou, Y.; Zheng, Q.; Zha, L.; Zha, Z. Renal Clearable Mo-Based Polyoxometalate Nanoclusters: A Promising Radioprotectant against Ionizing Irradiation. *ACS Appl. Mater. Interfaces* **2023**, *15* (9), 11474–11484.

Chapter 5

A Review on Haloperoxidase Mimicking

Hydrogen peroxide oxidizes halides (iodide, bromide, and chloride) in the presence of haloperoxidases, which are a specific class of enzymes, to halogens.¹ Such enzyme processes subsequently lead to halogenation of specific organic substrates or halide-assisted disproportionation of hydrogen peroxide, resulting in formation of dioxygen. The reactions can be represented as follows:



For every equivalent of the halogenated substrate produced in the halogenation reaction, hydrogen peroxide and protons are consumed in a stoichiometric manner. It would be important to note that fluoride cannot serve as a substrate in the process because hydrogen peroxide lacks the capacity to oxidize fluorides. There are two distinct classes of haloperoxidases those that contain vanadium and those containing Fe-Heme. Within the vanadium-haloperoxidase class, two subcategories were identified: vanadium bromoperoxidases (V-BrPO) primarily found in marine algae and vanadium chloroperoxidases (V-CIPO) primarily found in terrestrial fungi. Numerous naturally occurring halogenated compounds have been discovered and isolated from marine organisms. Crystal structure analysis of vanadium bromoperoxidase (V-BrPO) derived from *Ascophyllum nodosum* reveal that the central vanadium atom forms a covalent bond with the N of histidine's imidazolyl moiety. Additionally, extensive hydrogen bonding occurs between vanadium and various amino acid side chains like Arg, His, Ser, Lys, as also with interstitial water molecules near the active site.^{2,3} This sheds light on the presence of vanadium in the active sites of biological systems, specifically bromoperoxidases that enhances the interest to explore vanadium complexes with organic ligands to mimic the biological activities observed in natural systems. Identification of vanadium within active sites of bromoperoxidases and an

understanding of the surrounding environment have sparked of interest in exploring vanadium complexes with organic ligands. Such research aims to replicate the biological activity observed in natural systems leading to the development of synthetic compounds that could then mimic the functions of vanadium in biological systems. The study of vanadium bromoperoxidases and other marine haloperoxidases, in relation to biosynthesis of similar compounds is experiencing a growing interest through various forms of investigations. The first functional mimic of vanadium bromoperoxidase, *cis*-dioxovanadium (VO_2^+)^{4,5}, was initially reported in an aqueous acidic solution. The observed reactivity difference may be influenced by speciation of the peroxo-vanadium(V) oxidant. However, it was evident that enzyme catalysis is mediated by a monomeric vanadium(V) center in the presence of a protein ligand leading to significantly faster reaction rates at neutral pH. Unlike the mechanism observed in acid-mediated oxidation of a bromide by $\text{VO}_2^+/\text{H}_2\text{O}_2/\text{Br}^-$, where $(\text{VO})_2(\text{O}_2)_3$ is involved, research revealed that iodide is oxidized by $\text{VO}(\text{O}_2)^+$, $\text{VO}(\text{O}_2)_2^-$, VO_2^+ or by their protonated forms.^{6,7} Several other studies explored vanadium(V)-catalyzed oxidation of bromide by hydrogen peroxide in aqueous or aqueous/organic mixtures, albeit without investigating detailed speciation of vanadium peroxospecies.^{8,9} These reports have primarily focused on substrate bromination and distribution of products under varying conditions. According to a proposal by DiFuria *et al.*, oxidation of bromide by peroxo-V-BrPO is suggested to occur initially within a hydrophilic region of the enzyme.^{8,9} Subsequently, the oxidized bromine (Br) intermediate undergoes migration to a more hydrophobic part of the protein where bromination of the organic substrate occurs and decomposition by hydrogen peroxide is limited.^{8,9} The ability of peroxo-vanadium(V) compounds to oxidize halides raises questions about the reactivity of other peroxo-metal complexes. Notably, molybdenum(VI)¹⁰⁻¹², tungsten(VI)¹², and methyl-rheniumtrioxide^{13,14} have also demonstrated peroxidative halogenation. However, it is worth mentioning that

aqueous titanium(IV) exhibits an opposite effect by stabilizing peroxide and thus preventing the oxidation of iodide.¹⁵

In an acidic solution, with excess hydrogen peroxide, only oxodiperoxo-Mo(VI) and W(VI) species were detected.¹² The rate of the reaction is independent of the concentration of hydrogen peroxide, suggesting H₂O₂ quickly rebinds to Mo(VI) and the rate-limiting step is that of the oxidation of bromide. The general trend for bromide oxidation is WO(O₂)₂ > MoO(O₂)₂ > VO(O₂)₂⁻. The enhanced reactivity of group VI metals compared to vanadium(V) is thought to arise from their higher oxidation state, resulting in increased oxidation potential of the bound peroxide.¹² On the other hand, Ti(IV) which exhibits weaker Lewis acid character, stabilizes peroxide.¹⁵ In acidic solutions, methylrhenium trioxide (CH₃ReO₃) has also been observed to catalytically oxidize halides. Both the monoperoxocomplex CH₃ReO₂(η²-O₂) and the diperoxo-complex (CH₃ReO₂(η²-O₂)₂(H₂O)) exhibit oxidation activity towards bromide and chloride in the presence of HClO₄.¹⁴

Discovery of enzymes that use hydrogen peroxide to oxidize bromide under natural settings has greatly advanced the study of oxidative bromination. Among them, a vanadate (V)-dependent bromoperoxidase that is found in brown algae *Ascophyllum nodosum* was proven useful for catalyzing the oxidation of bromide in hydrogen peroxide, sodium bromide solutions making it very much valuable for bromofunctionalization of donor-substituted arenes. Nature's approach to element cycling highlights the need for sustainable production of organobromine that follows the planetary bromine cycle.¹⁶ In nature, this cycle begins with a bromide and requires effective pathways for bromide oxidation under physiological conditions to perform electrophilic hydrocarbon bromination. The search for the origin of naturally occurring organohalogens¹⁷⁻¹⁹ led to the identification of marine bromoperoxidases^{20,21} that use hydrogen peroxide to oxidize bromide in ocean water.²²⁻²⁴

Since the discovery of bromoperoxidases, research on oxidative bromination has expanded becoming a dynamic field.²⁵ With the selectivity demonstrated by V-BrPO, achieving the biogenesis of chiral halogenated marine natural products and selectively halogenated or oxidized indole marine natural products has become an achievable objective. Additionally, there is an anticipation to design novel functional mimics of V-HPOs to further explore our comprehension of essential structural characteristics of vanadium haloperoxidases and crucial catalytic residues involved in these enzymes.

References:

- (1) Hager, L. P.; Morris, D. R.; Brown, F. S.; Eberwein, H. Chloroperoxidase: II. UTILIZATION OF HALOGEN ANIONS. *J. Biol. Chem.* **1966**, *241* (8), 1769–1777.
- (2) Pohlmann, A.; Nica, S.; Kim, T.; Luong, K.; Plass, W. Dioxovanadium(V V) Complexes with Side Chain Substituted N-Salicylidenehydrazides Modelling Supramolecular Interactions in Vanadium Haloperoxidases. *Inorg. Chem. Comm.* **2005**, *8*, 289–292.
- (3) Rehder, D. The Coordination Chemistry of Vanadium as Related to Its Biological Functions. *Coord. Chem. Rev.* **1999**, *182* (1), 297–322.
- (4) Secco, F. Equilibriums and Kinetics of Reduction by Iodide Ion of the Vanadium(V)-Hydrogen Peroxide System. *Inorg. Chem.* **1980**, *19* (9), 2722–2725.
- (5) Everett, R. R.; Kanofsky, J. R.; Butler, A. A Functional Mimic of Vanadium Bromoperoxidase. *J. Am. Chem. SOC* **1992**, *114* (4), 265.
- (6) Secco, F.; Celsi, S.; Grati, C. A Kinetic Study of the Reaction between Vanadium(V) and Iodide Ions. *J. Chem. Soc. Dalt. Trans.* **1972**, No. 15, 1675–1678.

- (7) Celsi, S.; Secco, F.; Venturini, M. Kinetics of Reaction between Vanadium(V) and Iodide Ions in the Presence of Oxygen. *J. Chem. Soc. Dalt. Trans.* **1974**, No. 8, 793–795.
- (8) Andersson, M.; Conte, V.; Di Furia, F.; Moro, S. Vanadium Bromoperoxidases Mimicking Systems: Bromohydrins Formation as Evidence of the Occurrence of a Hypobromite-like Vanadium Complex. *Tetrahedron Lett.* **1995**, 36 (15), 2675–2678.
- (9) Conte, V.; Di Furia, F.; Moro, S. Synthesis of Brominated Compounds. A Convenient Molybdenum- Catalyzed Procedure Inspired by the Mode of Action of Haloperoxidases. *Tetrahedron Lett.* **1996**, 37 (47), 8609–8612.
- (10) Arias, C.; Mata, F.; Perez-Benito, J. F. Kinetics and Mechanism of Oxidation of Iodide Ion by the Molybdenum (VI)-Hydrogen Peroxide System. *O. Can. J. Chem.* **1990**, 68, 1499.
- (11) Smith, R. H.; Kilford, J. Kinetics of the Molybdate Catalyzed Oxidation of Iodide by Hydrogen Peroxide. *Int. J. Chem. Kinet.* **1976**, 8 (1), 1–10.
- (12) Meister, G. E.; Butler, A. Molybdenum(VI)- and Tungsten(VI)-Mediated Biomimetic Chemistry of Vanadium Bromoperoxidase. *Inorg. Chem.* **1994**, 33 (15), 3269–3275.
- (13) Espenson, J. H.; Pestovsky, O.; Huston, P.; Staudt, S. Organometallic Catalysis in Aqueous Solution: Oxygen Transfer to Bromide. *J. Am. Chem. Soc.* **1994**, 116 (7), 2869–2877.
- (14) Hansen, P. J.; Espenson, J. H. Oxidation of Chloride Ions by Hydrogen Peroxide, Catalyzed by Methylrhenium Trioxide. *Inorg. Chem.* **1995**, 34 (23), 5839–5844.
- (15) Lydon, J. D.; Thompson, R. C. Reduction of Peroxotitanium(IV) by Iodide, Thiodiethanol, Thioxane, and Thiourea in Acidic Solution. *Inorg. Chem.* **1986**, 25

- (20), 3694–3697.
- (16) Clark, J. H.; Deswarte, F. E. I. *Introduction to Chemicals from Biomass. In Wiley Series in Renewable Resources; Wiley-VCH: Chichester; 2008.*
- (17) Raistrick, H.; Smith, G. Studies in the Biochemistry of Micro-Organisms The Metabolic Products of *Aspergillus Terreus* Thom. Part II. Two New Chlorine-Containing Mould Metabolic Products, Geodin and Erdin. *Biochem. J.* **1936**, *30* (8), 1315–1322.
- (18) Franssen, M. C. R. Haloperoxidases: Useful Catalysts for Halogenation and Oxidation Reactions. *Catal. Today* **1994**, *22* (3), 441–457.
- (19) Hager, L. P.; Morris, D. R.; Brown, F. S.; Eberwein, H. Chloroperoxidase. *J. Biol. Chem.* **1966**, *241* (8), 1769–1777.
- (20) Vilter, H. Peroxidases from Phaeophyceae: A Vanadium(V)-Dependent Peroxidase from *Ascophyllum Nodosum*. *Phytochemistry* **1984**, *23* (7), 1387–1390.
- (21) Butler, A.; Walker, J. V. Marine Haloperoxidases. *Chem. Rev.* **1993**, *93* (5), 1937–1944.
- (22) Neidleman, S. L.; Geigert, J. The Enzymatic Synthesis of Heterogeneous Dihalide Derivatives: A Unique Biocatalytic Discovery. *Trends Biotechnol.* **1983**, *1* (1), 21–25.
- (23) Butler, A.; Carter-Franklin, J. N. The Role of Vanadium Bromoperoxidase in the Biosynthesis of Halogenated Marine Natural Products. *Nat. Prod. Rep.* **2004**, *21* (1), 180–188.
- (24) Butler, A.; Clague, M. J.; Meister, G. E. Vanadium Peroxide Complexes. *Chem. Rev.* **1994**, *94* (3), 625–638.

- (25) Podgoršek, A.; Zupan, M.; Iskra, J. Oxidative Halogenation with “Green” Oxidants: Oxygen and Hydrogen Peroxide. *Angew. Chemie Int. Ed.* **2009**, *48* (45), 8424–8450.

Chapter 6

Genesis and Scope of the Research

Chemotherapy and radiotherapy are traditionally important cancer treatment methodologies. Chemotherapy uses drugs that kill cancer cells while radiotherapy uses high-energy radiation to destroy them. Both forms of treatments were designed to target and kill rapidly dividing cells, being a characteristic feature of cancer cells. Chemotherapy and radiotherapy are often used in combination with other treatments like surgery or immunotherapy to increase effectiveness. Chemotherapy is used to shrink tumors before surgery, making it easier to remove them. Radiotherapy on the other hand, in most cases, is used after surgery to kill cancer cells in order to reduce chances of its recurrence. Chemotherapy which is a very common treatment for cancer is associated with significant side effects due to non-specific targeting of healthy cells.¹ Hence, the development of new **chemotherapeutic agents** that selectively target cancer cells, could significantly improve efficacy in cancer treatment and reduce adverse or side effects associated with chemotherapy. Numerous scientific articles exist that describe the role of transition metal complexes of Fe, Cu, Ni, Pt, Ru, Rh, V, Cr, Co, Os, and Pd that mediate DNA cleavage in the presence of oxidants or reductants or even without any assisting agents.²⁻¹¹ **Chapter 2** extensively explores various such transition metal-based anticancer drugs or chemotherapeutic agents, delving into their specific mechanism of action. This comprehensive exploration sheds light on the effectiveness and significance of these agents in combating cancer.

Chapter 3 provides an in-depth analysis of the intricate interactions between metal-based complexes and DNA, elucidating how complexes can be harnessed as potential agents for chemotherapy and radioprotection. With the aid of compelling examples and explanations, this chapter highlights the immense potential of metal-based complexes in the field of medicine.

Radiation therapy can also damage healthy tissues that surround tumors leading to various forms of side effects like irritation of the skin, loss of hair etc. Hence, an important

component of the treatment of cancer using ionizing radiation is that such side effects need to be checked, otherwise the patient might be cured of cancer but might succumb to one or more side effects. Therefore, administration of radiation to cancer patients must make sure that apart from the targeted tumor region surrounding areas are protected from harmful effects of radiation. For this reason, there has been considerable effort to find out ways to protect such surrounding regions from harmful effects of radiation. Radioprotectors are compounds that fit into this requirement having an ability to interact with the consequences of ionizing radiation (i.e. various products formed) much faster than they would interact with a biological target or having the ability to reverse a momentary damage caused on a biological target because of higher affinity of the compound (the Radioprotector) with the products of change on the biological target. Hence, Radioprotectors protect healthy cells from harmful effects of ionizing radiation, permitting a higher dose of radiation to be administered to a tumor minimizing damage to surrounding tissues. *Amifostine* has been the only small-molecule radioprotector approved by FDA, USA for decades.¹² However, serious adverse effects limit its clinical use. To address toxicity issues and yet maintain good potency one needs to focus on the development of new **radioprotective agents** that significantly improve effectiveness of radiation therapy and also reduce side effects. Luciani et. al. reported substantial amount of work on Molybdenum biokinetic and developed a new model for understanding how molybdenum behaves in the human body. The updated model has practical applications for radiation protection and can also aid in the design of future studies to further improve accuracy.¹³ Today, high-energy ionizing radiation like gamma rays are an important component of medical diagnosis and therapy.¹⁴ However, their ability to penetrate and/or damage tissues releasing free radicals raises concerns about harmful effects on the human body.¹⁵ Hence, there is a need for the development of effective shielding materials that are crucial for protecting a patient.¹⁶ **Chapter 4** provides a comprehensive and insightful

examination of various radioprotectors, highlighting their significant role in safeguarding DNA against the detrimental effects of radiation-induced damage. A thorough analysis and discussion in this chapter shed light on diverse mechanisms employed by radioprotectors to effectively shield DNA from harm.

Chapter 5 extensively explores the diverse applications of metal-based complexes, with a particular emphasis on their catalytic role as haloperoxidase (HPO) mimics. **Haloperoxidases**, such as vanadium bromoperoxidase (V-BrPO), play a crucial role in catalyzing the oxidation of halides in the presence of hydrogen peroxide, in various biological processes. By examining the specific example of V-BrPO, which utilizes a vanadate moiety at its active site to selectively oxidize bromide, this chapter highlights significant research efforts dedicated to exploring transition metals as potential mimetics. Notably, molybdenum and tungsten complexes have exhibited promising bromination catalysis when combined with stoichiometric hydrogen peroxide. The ability of haloperoxidases, including V-BrPO, to facilitate oxidation of halides by hydrogen peroxide has garnered substantial interest in recent years, offering the potential for halogenation of diverse organic compounds.

An in-depth analysis of existing literature on metal-based chemotherapeutic agents highlights the importance of further research to fully understand their mechanism of action and potential clinical applications. Promising findings suggest that these agents hold significant potential for revolutionizing chemotherapy in future. Manganese, in particular, offers distinct advantages in cancer treatment due to its unique chemical properties including its ability to interact with biological systems and selectively target cancer cells. Given the challenges posed by drug resistance and severe side effects associated with current chemotherapy drugs, exploring novel alternatives like manganese-based compounds would be important. By attaining a thorough understanding of their effectiveness, safety and underlying mechanisms, we can develop enhanced and personalized cancer treatments effectively addressing an

ongoing demand for more effective therapies in oncology. Currently, DNA-binding studies of oxime-based manganese complexes remain unexplored. Therefore, focusing on synthesizing manganese-oxime based chemotherapeutic agents emerges as a compelling avenue to advance the field and fulfill some of the urgent requirements of cancer patients. In **Chapter 8**, there is a thorough description on a novel class of artificial nuclease based Mn-oxime complex, through a comprehensive analysis using various physicochemical techniques, gel electrophoresis as well as theoretical molecular docking studies. The results obtained from these *in vitro* investigations strongly support the potential of the synthesized Mn-oxime complex as a powerful agent for DNA cleavage, contributing to advancement of opening new avenues for chemotherapeutic applications.

Due to a constant need for the development of effective shielding materials, that are crucial for protecting a cancer patient, from hazardous effects during radiotherapy, an extensive literature search motivated me to explore molybdenum-based radioprotectors as a topic for my research. Literature review revealed molybdenum possesses unique properties that make it a promising candidate for radioprotection. With the goal of minimizing harmful effects of ionizing radiation on normal tissues designing novel molybdenum-based radioprotectors becomes crucial. In **Chapter 9** and **Chapter 12** there are thorough analysis of newly synthesized Mo dioxocomplexes. In **Chapter 10** and **Chapter 13** a discussion on the application of these complexes as potential radioprotectors to protect DNA from radiation induced damage is presented. By delving into the potential of molybdenum-based radioprotectors, I aim to uncover their mechanism of action, evaluate their safety and identify potential clinical applications *in vitro*. By focusing on molybdenum-based radioprotectors, this research contributes to the growing body of knowledge in radioprotection to pave the way for development of improved strategies to safeguard healthy tissues during cancer treatment.

Literature revealed Molybdenum has a promising potential as a catalyst in VHPO mimicking systems, presenting numerous advantages over vanadium including enhanced stability and reduced cost. However, in order to fully grasp the mechanisms underlying catalytic activity and optimize application in industrial settings by Molybdenum, further research is warranted. In this thesis, my objective was to conduct a comprehensive scientific evaluation and advancement of enzymes that mimic VHPO function with a specific focus on Mo-based VHPO enzymes. In **Chapter 11** and **Chapter 13**, application of synthesized Molybdenum dioxocomplexes in bio-mimetic catalysis is examined showcasing their potential utility in this field. By conducting thorough physicochemical and biochemical analyses, this research contributes to advancement in the field. This research endeavor aims to contribute to the expanding knowledge base surrounding remarkable capabilities of molybdenum compounds and their potential for VHPO-like catalysis, thereby opening new avenues for industrial applications in a cost-effective and sustainable manner.

References:

- (1) Gilman, A.; Philips, F. S.; Hedgpeth, J. W. The Biological Actions and Therapeutic Applications of the B-Chloroethyl Amines and Sulfides. *Science* (80-.). **1946**, *103* (2675), 409–436.
- (2) Correia, I.; Roy, S.; Matos, C. P.; Borovic, S.; Butenko, N.; Cavaco, I.; Marques, F.; Lorenzo, J.; Rodríguez, A.; Moreno, V.; Pessoa, J. C. Vanadium(IV) and Copper(II) Complexes of Salicylaldimines and Aromatic Heterocycles: Cytotoxicity, DNA Binding and DNA Cleavage Properties. *J. Inorg. Biochem.* **2015**, *147*, 134–146.
- (3) Becco, L.; Rodríguez, A.; Bravo, M. E.; Prieto, M. J.; Ruiz-Azuara, L.; Garat, B.; Moreno, V.; Gambino, D. New Achievements on Biological Aspects of Copper

- Complexes Casiopeínas®: Interaction with DNA and Proteins and Anti-Trypanosoma Cruzi Activity. *J. Inorg. Biochem.* **2012**, *109*, 49–56.
- (4) Costas, M.; Mehn, M. P.; Jensen, M. P.; Que, L. Dioxygen Activation at Mononuclear Nonheme Iron Active Sites: Enzymes, Models, and Intermediates. *Chem. Rev.* **2004**, *104* (2), 939–986.
- (5) Ghosh, A.; Mandoli, A.; Kumar, D. K.; Yadav, N. S.; Ghosh, T.; Jha, B.; Thomas, J. A.; Das, A. DNA Binding and Cleavage Properties of a Newly Synthesised Ru(II)-Polypyridyl Complex. *Dalt. Trans.* **2009**, No. 42, 9312–9321.
- (6) Wu, A. J.; Penner-Hahn, J. E.; Pecoraro, V. L. Structural, Spectroscopic, and Reactivity Models for the Manganese Catalases. *Chem. Rev.* **2004**, *104* (2), 903–938.
- (7) Bortolini, O.; Conte, V. Vanadium (V) Peroxocomplexes: Structure, Chemistry and Biological Implications. *J. Inorg. Biochem.* **2005**, *99* (8), 1549–1557.
- (8) Parkin, G. Synthetic Analogues Relevant to the Structure and Function of Zinc Enzymes. *Chem. Rev.* **2004**, *104* (2), 699–767.
- (9) Burrows, C. J.; Muller, J. G. Oxidative Nucleobase Modifications Leading to Strand Scission. *Chem. Rev.* **1998**, *98* (3), 1109–1151.
- (10) Mirica, L. M.; Ottenwaelder, X.; Stack, T. D. P. Structure and Spectroscopy of Copper-Dioxygen Complexes. *Chem. Rev.* **2004**, *104* (2), 1013–1045.
- (11) Crans, D. C.; Smee, J. J.; Gaidamauskas, E.; Yang, L. The Chemistry and Biochemistry of Vanadium and the Biological Activities Exerted by Vanadium Compounds. *Chem. Rev.* **2004**, *104* (2), 849–902.
- (12) Goodman, L. S.; Wintrobe, M. M.; Dameshek, W.; Goodman, M. J.; Gilman, A.; McLennan, M. T. NITROGEN MUSTARD THERAPY: Use of Methyl-Bis(Beta-Chloroethyl)Amine Hydrochloride and Tris(Beta-Chloroethyl)Amine Hydrochloride for Hodgkin's Disease, Lymphosarcoma, Leukemia and Certain Allied and

- Miscellaneous Disorders. *J. Am. Med. Assoc.* **1946**, *132* (3), 126–132.
- (13) Luciani, A.; Giussani, A.; Cantone, M. C.; Castellani, C. M. Sensitivity Analysis Techniques Applied to a Revised Model of Molybdenum Biokinetics. *Radiat. Prot. Dosimetry* **2003**, *105* (1–4), 239–242.
- (14) More, C. V.; Alavian, H.; Pawar, P. P. Evaluation of Gamma-Ray Attenuation Characteristics of Some Thermoplastic Polymers: Experimental, WinXCom and MCNPX Studies. *J. Non. Cryst. Solids* **2020**, *546*, 120277.
- (15) Akman, F.; Kaçal, M. R.; Almousa, N.; Sayyed, M. I.; Polat, H. Gamma-Ray Attenuation Parameters for Polymer Composites Reinforced with BaTiO₃ and CaWO₄ Compounds. *Prog. Nucl. Energy* **2020**, *121*, 103257.
- (16) Zakaly, H. M. H.; Saudi, H. A.; Tekin, H. O.; Rashad, M.; Issa, S. A. M.; Rammah, Y. S.; Elazaka, A. I.; Hessien, M. M.; Ene, A. Glass Fabrication Using Ceramic and Porcelain Recycled Waste and Lithium Niobate: Physical, Structural, Optical and Nuclear Radiation Attenuation Properties. *J. Mater. Res. Technol.* **2021**, *15*, 4074–4085.

Chapter 7

General Experimental Methods

1. Techniques to be used for the execution of the work:

1.1. Techniques used for characterization of metal complexes:

To characterize the synthesized Manganese and Molybdenum-based metal complexes, the following tools and techniques have been utilized.

1.1.1. C, H, N analysis:

C, H, N analysis refers to determination of carbon, hydrogen, and nitrogen content of a sample, which is an important analytical technique in many fields, including chemistry, materials science, and environmental science. Here are some of the key reasons why C, H, N analysis is important:

C, H, N analysis provides information about elemental composition of a sample, which can be used to determine molecular formula and identify unknown compounds that are important for understanding the structure.

Elemental analyses were carried out using a Perkin-Elmer 2400 series II CHNS analyzer was used to determine the C, H, and N content of samples. Typically, around 1.5-2.5 mg of sample was placed in the combustion cell, which was heated to approximately 900-980°C. Combustion was carried out using pure oxygen. Pure helium was utilized as a driving gas.

1.1.2. Molar conductance studies:

Molar conductivity is the ratio of the conductivity of a solution to the concentration of ions in solution. This parameter is typically denoted in units of $\text{S}\cdot\text{m}^2\cdot\text{mol}^{-1}\cdot\text{L}^1$, which represents siemens per meter squared per mole per liter. The molar conductivity of a solution can be affected by factors like temperature, pressure and nature of the solvent.

Molar conductivity studies can be used to determine the degree of dissociation of an electrolyte in solution, which is a measure of the extent to which the electrolyte breaks down into ions.

To determine molar conductance values of the isolated complexes at 25°C, a bottle-type cell, and a Systronics (India) Model 335 digital conductivity bridge was used. Measurements were made using a thermostatic arrangement.

1.1.3. Infrared Spectral studies:

Infrared spectroscopy is a technique used to analyze materials based on their interaction with infrared radiation. Upon absorbing infrared radiation molecules undergo resonance pertaining to their vibrational modes that undergo a change. The pattern of absorption of infrared radiation provides information about various functional groups present in the sample depending on stretching and bending modes in such bonds as C=O, C-H, N-H, and O-H.

Infrared spectroscopy involves the interaction of infrared radiation with a sample and measuring intensity of the radiation that is transmitted following absorption by the sample. The resulting spectrum is a plot of the intensity of the absorbed or transmitted radiation as a function of wavelength or frequency (wavenumber) of the radiation. The spectrum is then analyzed to identify the functional groups present in the sample and to determine its chemical composition. Infrared spectroscopy is a non-destructive technique, thus making it very useful for analyzing and characterizing compounds as it is not destroyed as a consequence.

A Perkin-Elmer RFX-I IR spectrophotometer was used to obtain IR spectra of KBr discs at room temperature. The spectra were collected in KBr pellets over a range of 400-4000 cm^{-1} .

1.1.4. Magnetic Susceptibility Measurements:

Magnetic susceptibility measurement is a technique used to determine magnetic properties of a material. It involves measuring the response of a sample to a magnetic field, which can provide information about its electronic structure and bonding. Magnetic susceptibility measurements were conducted by the Gouy method. These measurements commonly used in the fields of chemistry, physics, and material science help in the study of magnetic properties of compounds; of particular utility to an inorganic chemist is in the measurement of the

magnetic moment of the material that enables one to know the coordination geometry based on the spin state of the central metal ion; also to realize orbital contribution if any, in case of some metal ions, since a theoretical estimate of the spin only value can be had.

Magnetic susceptibility of an isolated compound was determined using Gouy method, with mercury (II) tetracyanocobaltate (II) and tris(ethylenediamine)nickel (II) thiosulphate serving as calibrants. The mass susceptibility of the sample is relative to that of a standard calculated using the Gouy method,

$$\chi_g = \frac{\Delta_c - \Delta_{dia}}{\Delta_s - \Delta_{dia}} \times \frac{M_s}{M_c} \times \chi_g$$

where Δ_c = change in weight in mg of the compound after application of magnetic field (+ve when weight increases and -ve when weight decreases).

Δ_s = change in weight in mg of the standard after application of the magnetic field.

Δ_{dia} = loss of weight in mg of empty glass tube in the magnetic field due to diamagnetism of the glass material.

M_s = weight of the standard in g.

M_c = weight of isolated compound in g.

The molar susceptibility χ_m was obtained by multiplying mass susceptibility χ_g by the molecular weight of the complex. Pascal's constant was used to correct for diamagnetic contributions of the constituents to obtain χ_A . The effective magnetic moment value (μ_{eff}) in Bohr Magneton was calculated from the relation,

$$\mu_{\text{eff}} = 2.84 \sqrt{(\chi_A \times T)} \text{ B.M.}$$

T denotes the temperature at which measurements were made.

Magnetic susceptibility measurements were conducted using a Magway MSB MKI Magnetic susceptibility balance (Sherwood Scientific Ltd, Cambridge, England) at a temperature of 298 K. The data was corrected for diamagnetic contributions using Pascal's constants and experimental errors were such that they permitted recording of μ_{eff} up to first place of

decimal. The same equipment was sometimes used to determine diamagnetism of the solid ligand.

1.1.5. pH measurements:

The pH scale is used to determine the acidity or alkalinity of a solution; values ranging from 0 to 14. A pH of 7 is considered neutral at 25°C, while a pH below 7 at the same temperature indicates an acidic solution and that above 7 a basic or alkaline solution. pH measurement was very crucial in studies related to the work reported in this dissertation.

The most common method of pH measurement involves a pH meter, that consists of a glass electrode and a reference electrode. The glass electrode contains a special glass membrane sensitive to hydrogen ions (H^+). The reference electrode provides a stable reference voltage against which the electrode is calibrated to measure a potential difference.

To measure pH with a pH meter, the electrode is immersed in the solution to be measured, and the potential difference between the two electrodes is measured. This potential difference is then converted to a pH value using a calibration curve, which relates the potential difference to pH.

Other methods of pH measurement include using pH indicator papers or solutions known as indicators that change color depending on the pH of the solution being tested. These methods are less precise than using a pH meter but can be useful for quick qualitative measurements.

pH measurements were performed using a Systronics (India) Model-335 digital pH meter.

1.1.6. Thermogravimetric Analysis (TGA):

Thermogravimetric analysis (TGA) is a technique used to analyze thermal stability and composition of materials. It involves the heating of a sample at a controlled rate while monitoring its weight (precisely the loss of it) as a function of temperature. TGA can provide information about decomposition, oxidation and volatilization of materials, as well as their thermal stability, purity and composition.

During a TGA experiment, the sample is placed in a sample holder, which is then placed in a furnace. The temperature of the furnace is ramped up at a controlled rate, and the weight of the sample is continuously monitored by a sensitive balance or microbalance. As temperature increases, the sample may undergo thermal decomposition, loss of water or volatile components, oxidation, or other reactions, resulting in a change in weight. Loss in weight is recorded and plotted as a function of temperature to produce a thermogram which can be analyzed to determine the composition and thermal properties of the sample.

The TGA study was conducted using a Perkin Elmer - Pyris Diamond TG/DTA instrument.

1.1.7. Electronic spectral studies:

The UV-Vis spectra were mostly recorded in the range of 200-800 nm were obtained at room temperature using a Perkin Elmer UV-Vis spectrometer Lambda 25 with a 1 cm quartz cell against an appropriate reagent as blank. Wherever necessary, the UV-Vis spectra in solution were subjected to Gaussian analysis.

1.1.8. Nuclear Magnetic Resonance (NMR) studies:

The study of molecular structure and dynamics is made possible through use of nuclear magnetic resonance (NMR) spectroscopy which is a highly effective analytical technique providing detailed information about the chemical environment, structure and interactions of molecules. By analyzing the NMR spectra of a sample it is possible to determine the types of atoms present in the sample as also the arrangement of atoms in the molecule and nature of the bonds between atoms.

Nuclear magnetic resonance (NMR) spectroscopy operates on the principle that atomic nuclei with an odd number of protons or neutrons possess a magnetic moment, that can be induced to resonate when subjected to radiation in the radiofrequency region in the presence of a magnetic field. NMR spectra are typically represented graphically as a plot of signal intensity (y-axis) as a function of magnetic field strength (x-axis). The position of the signals

in the spectrum, known as chemical shifts, provide information about the chemical environment of the atoms in the sample. The shape, intensity, and splitting of signals provide additional information about the microenvironment around the NMR active atom from where molecular structure and dynamics may be realized

NMR spectroscopy has a wide range of applications in many fields, including chemistry, biochemistry, materials science and medicine. It is used for characterization of organic compounds, determination of purity of chemical samples and for studying the structure and dynamics of proteins, nucleic acids and other biomolecules.

The ^1H and ^{13}C NMR data were obtained at 25°C using a Bruker 300MHz FT spectrometer with CDCl_3 , d_6 -DMSO, or CD_3OD as solvent and tetramethylsilane (TMS) as internal standard. Signals of individual protons were assigned based on chemical shift, spin-spin structure, and substituent effects.

1.1.9. Electron Paramagnetic Resonance (EPR) studies:

Electron paramagnetic resonance (EPR) spectroscopy, also known as electron spin resonance (ESR) spectroscopy is a powerful analytical technique used to study electronic structure and properties of molecules and materials. It is based on the principle that unpaired electrons in a sample have a magnetic moment and can be made to resonate when placed in a magnetic field upon exposure to microwave radiation.

EPR spectroscopy provides detailed information about electronic properties of a sample, including the number and nature of unpaired electrons, their spatial orientation, and strength of the interactions between them with nearby nuclei or other electrons. By analyzing the EPR spectrum of a sample, it is possible to determine the nature of the radicals and paramagnetic species present in the sample, as well as their structural and electronic properties.

EPR spectra are typically represented graphically as a plot of signal intensity (y-axis) as a function of magnetic field strength (x-axis). The position and shape of the signals provide information about electronic structure and properties of the sample.

EPR spectra were recorded on a JEOL-JES FA200 ESR spectrometer in solid-state at 298K. The microwave cavity was constantly flushed with pure and dry nitrogen during measurements. Spectra were calibrated using DPPH (diphenylpicrylhydrazyl) [DPPH, $g = 2.0037$] as reference.

1.1.10. X-Ray Crystallography:

The compounds' single crystal X-ray structures were determined using a Bruker AXS SMART APEX CCD diffractometer with Mo-K α radiation ($\lambda = 0.71073 \text{ \AA}$) at a temperature of 298 K. The crystal was placed 6.03 cm away from the detector and a total of 606 frames were collected with a scan width of 0.3° at different settings of φ . The data were reduced using SAINTPLUS, and empirical absorption correction was applied using SADABS. Direct methods were used to locate metal atoms and the remaining non-hydrogen atoms were obtained from successive Fourier synthesis. The structures were refined using a full matrix least-square procedure on F².

The SHELXTL v.6.14 software was used for calculation and the goodness-of-fit (GOF) was determined using equations (I), (II), and (III) as follows.

$$RI = \frac{\sum ||F_o| - |F_c||}{\sum |F_o|} \quad \text{..... (I)}$$

$$wR2 = \left[\frac{\sum [w (F_o^2 - F_c^2)^2]}{\sum [w (F_o^2)^2]} \right]^{1/2} \quad \text{..... (II)}$$

$$GOF = S = \left[\frac{\sum [w(F_o^2 - F_c^2)^2]}{(n_o - n_p)} \right]^{1/2} \quad \text{..... (III)}$$

n_o =number of reflections

n_p = total number of parameters refined.

1.1.11. Powder X-Ray Diffraction (PXRD):

Powder X-ray diffraction (PXRD) is an analytical technique used to determine the crystal structure of a material by analyzing diffraction patterns produced when a sample is exposed to X-rays. The sample is typically in the form of a fine powder, and X-rays are generated by a specialized instrument known as an X-ray diffractometer.

In PXRD, X-rays are directed onto the sample at various angles and the resulting diffraction pattern is collected by a detector. The diffraction pattern consists of a series of peaks at different angles, corresponding to positions and intensities of diffracted X-rays. The positions and intensities of the peaks are determined by the crystal structure of the material and orientation of crystals in the powder.

By analyzing the diffraction pattern, it is possible to determine the crystal structure of the material, including lattice parameters, unit cell dimensions and positions of atoms within the unit cell. PXRD can also be used to determine purity of a sample, identify unknown materials, and study effects of temperature, pressure and other external factors on the crystal structure and properties of a material. It is a non-destructive and highly informative technique that provides valuable information about the structure and properties of materials at the atomic level.

The Bruker D8 Advance diffractometer was used to collect X-ray powder diffraction patterns, with an operating voltage of 40 kV and a current of 40 mA. The diffractometer was operated using CuK radiation, with an effective wavelength of 1.5418 Å.

1.2. Techniques used to monitor DNA-metal complex interaction:

The following methods are used to explore binding affinity of metal complexes with DNA:

1.2.1. Electronic Absorption Spectra:

Absorption spectroscopy is a technique used to measure the absorption of radiation caused by its interaction with a sample as a function of frequency or wavelength. The sample absorbs

photons from the radiating field, resulting in a variation of absorption intensity across the electromagnetic spectrum, which is known as an absorption spectrum. This method is used in various regions of the electromagnetic spectrum, with the visible region having photon energies ranging from 36 to 72 kcal/mole. The near ultraviolet region extends the energy range up to 143 kcal/mole and reaches 200 nm. However, ultraviolet radiation with wavelengths shorter than 200 nm is rarely used as it is difficult to handle and not commonly used for routine structural analysis.

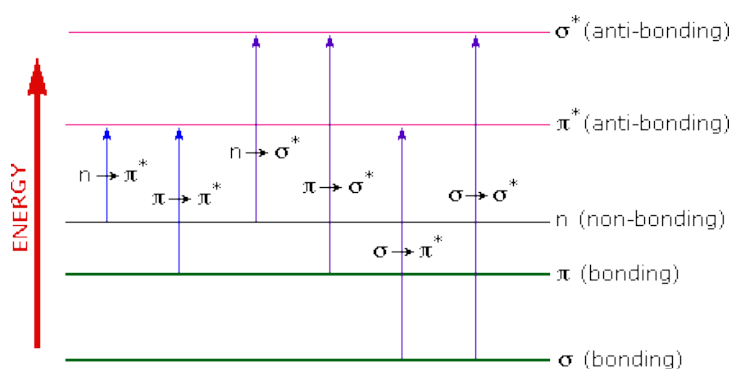


Figure 1: Different types of UV transitions

Absorption spectroscopy is also known as electronic spectroscopy as the energies in this region are sufficient to excite a molecular electron to a higher energy orbital. The above diagram shows the possible electronic excitations that can occur in organic molecules. The two lowest energy transitions (colored blue on the left-most side) can be achieved by the energies available in the 200 to 800 nm spectrum. The energetically favored electron promotion occurs from the highest occupied molecular orbital (HOMO) to the lowest unoccupied molecular orbital (LUMO), resulting in an excited state. Absorption spectroscopy involves exposing molecules in a sample to light that matches a possible electronic transition within the molecule, resulting in the promotion of an electron to a higher energy orbital. An optical spectrometer records the wavelengths and degree of absorption at each wavelength, resulting in a spectrum presented as a graph of absorbance (A) versus wavelength. The absorbance ranges from 0 (no absorption) to 2 (99% absorption) and is corrected for

operational factors to enable comparison of the spectra of different compounds in a meaningful way. Molar absorptivity" is particularly useful in determining the relative strength of light-absorbing functions (chromophores) and comparing spectra of different compounds.

Molar absorptivity (ϵ) is defined as:

Molar Absorptivity, $\epsilon = A / c l$ [according to Lambert- Beer's Law]

(Where A = absorbance, c = sample concentration in moles/liter & l = length of light path through the sample in cm)

1.2.2. Fluorescence Spectra:

Fluorescence is a type of luminescence where a substance emits light following an absorption. In most cases, the emitted light has a longer wavelength and lower energy than that which was absorbed. However, in intense electromagnetic radiation, a single electron can absorb two photons, leading to the emission of radiation with a shorter wavelength than the absorbed radiation. This phenomenon is called two-photon absorption. Alternatively, the emitted radiation may have the same wavelength as the absorbed radiation, which is known as "resonance fluorescence."

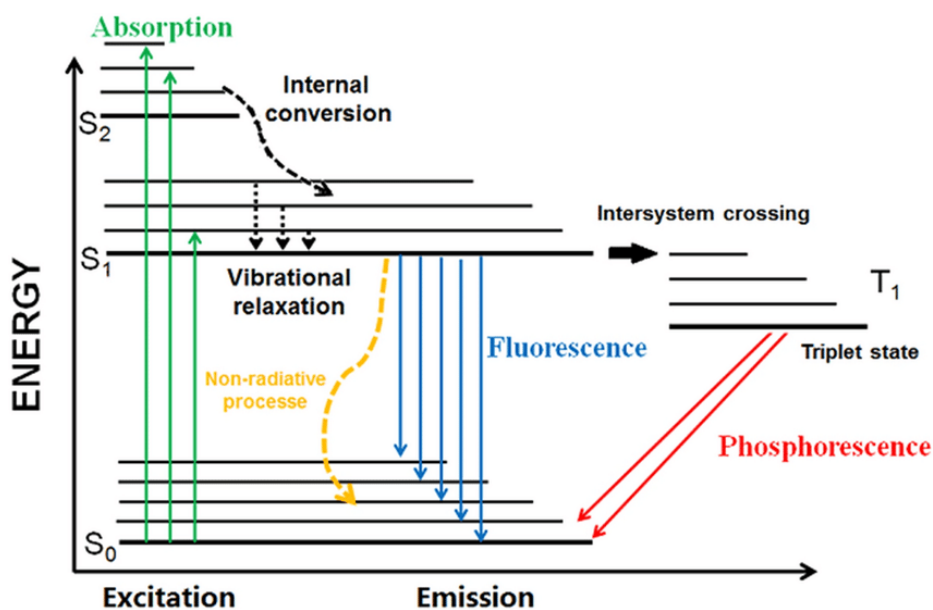


Figure 2: Jablonski Diagram for electronic energy level

The intensity of fluorescence is influenced by several factors, including extinction coefficient, optical path length, solute concentration, fluorescence quantum yield and intensity of the excitation source and fluorescence collection efficiency of the instrument. In dilute solutions or suspensions, fluorescence intensity is linearly related to these parameters. The fluorescence quantum yield is a measure of the efficiency of the fluorescence process and is defined as the ratio of the number of photons emitted to the number of photons absorbed^{2,3}.

$$\Phi = \frac{\text{Number of photons emitted}}{\text{Number of photons absorbed}}$$

A fluorescence quantum yield of 1.0 (100%) represents the maximum efficiency of the fluorescence process, where each absorbed photon results in the emission of a photon. Even compounds with quantum yields as low as 0.10 are still considered relatively fluorescent.

An alternative method of defining the fluorescence quantum yield is by measuring the rate of decay of the excited state:

$$\Phi = \frac{k_f}{\sum_i k_i}$$

Where k_f is the rate of spontaneous emission of radiation $\sum_i k_i$ and is the sum of all rates of excited state decay.

Excited state decay can occur through non-radiative mechanisms that do not involve photon emission. These non-radiative rates can result from dynamic collisional quenching, near-field dipole-dipole interaction (also known as resonance energy transfer), internal conversion, and intersystem crossing. Any changes in the rate of these pathways can affect both the excited state lifetime and fluorescence quantum yield. Fluorescence quantum yields are typically determined by comparing them to a standard.

Ethidium bromide is a dye that is frequently employed in molecular biology laboratories for identifying nucleic acids, such as double-stranded DNA from PCRs and restriction digests, as well as single-stranded RNA that can fold back onto itself and offer local base pairing for the dye to intercalate. When ethidium bromide binds to DNA, it becomes intensely fluorescent. This fluorescence is not due to the rigid stabilization of the phenyl group, which has been shown to project outside the intercalated bases and rotate about its single bond to minimize its interaction with the ring system. Instead, it is believed to be due to the hydrophobic environment found between base pairs. The hydrophobic environment found between the base pairs is responsible for the intense fluorescence of ethidium bromide after binding with DNA. As the ethidium cation enters the hydrophobic environment and moves away from the surrounding solvent, it is compelled to release water molecules that were previously associated with it. This is important because water is a highly efficient fluorescent quencher, meaning that it can inhibit fluorescence. Thus, by shedding these water molecules, ethidium can fluoresce.

1.2.3. Hydrodynamic Methods – Viscosity Measurement:

The viscosity of a polymer solution is influenced by the concentration and size of the dissolved polymer, also known as molecular weight. Utilizing viscosity measurements can provide an approximate understanding of the molecular weight. Although viscosity techniques are relatively simple to conduct, they are not highly accurate, and the resulting molecular weight obtained through viscosity measurements, known as viscosity average molecular weight (M_v), may lack precision. This is because M_v is reliant on a parameter that is affected by the solvent utilized for the viscosity measurement, leading to molecular weight determination being solvent-dependent. Nevertheless, despite these limitations, viscosity techniques remain a valuable tool in polymer analysis.

When a fluid, such as air, moves past a stationary wall, such as a tabletop, the fluid closest to the wall experiences zero movements, while the flow speed increases further away from the wall. This leads to the existence of a velocity gradient, which occurs due to adhesive, cohesive, and frictional forces. The magnitude of this gradient, indicating the rate at which the speed changes concerning the distance, is specific to the fluid and is used to define its coefficient of viscosity, represented by the symbol η .

Poiseuille's equation expresses the relationship between the viscosity coefficient (η) of a fluid, the flow rate, the pressure gradient, and dimensions of the tube or pipe through which the fluid is flowing. It can be represented as follows:

$$\eta = \frac{P\pi r^4 t}{8LV}$$

Where V is the *volume* of liquid delivered in *time* t , through a capillary of *radius* r and *length* L , with a *hydrostatic pressure* P .

In an apparatus designed so that equal volumes of liquid can flow through the same capillary of *length* L and *radius* r , η may be written as,

$$\eta = kh\mathbf{d}gt$$

If \mathbf{g} remains *constant* in any given location and \mathbf{h} , the *height* through which the liquid falls is kept constant, the above equation becomes

$$\eta = \mathbf{k}dt$$

Where \mathbf{k} is the *dimensional constant of the apparatus*.

If two liquids are compared using the same apparatus, it follows that

$$\frac{\eta_1}{\eta_2} = \frac{\mathbf{d}_1 t_1}{\mathbf{d}_2 t_2}$$

If η_2 , the *co-efficient of viscosity of one of the substances*, is known from previous measurements, then η_1 , the viscosity of the other liquid can be calculated from the measured quantities, $\mathbf{d}_1, t_1, \mathbf{d}_2, t_2$.

Viscosity Measurement of a Liquid:

The viscosity of a liquid is a measure of its inability to flow, and this is measured in N s m^{-2} (SI Units) or poise (P), or centipoise (cP).

$$1\text{P} = 0.1 \text{ N s m}^{-2}$$

$$1 \text{ cP} = 0.001 \text{ N s m}^{-2}$$

Currently, viscometers are the preferred tool for measuring viscosity. The viscosity of water is temperature-dependent, meaning that it changes with a variation in temperature. At a temperature of 293 K (20°C), viscosity of water is 1.002 cP. As temperature increases, viscosity decreases.

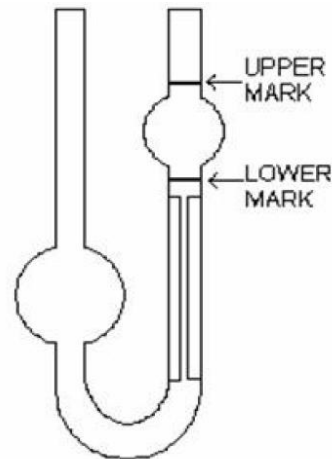


Figure 3: Ostwald Viscometer

1.2.4. Gel Electrophoresis:

Gel electrophoresis is a technique used in molecular biology to separate and analyze DNA, RNA, and protein molecules based on their size and charge. The technique involves placing a sample of the molecules in a gel matrix, typically made of agarose or polyacrylamide, and applying an electric field across the gel. The electric field causes the charged molecules to move through the gel, with smaller molecules moving faster than larger ones.

The plasmid pUC19 DNA is double-stranded and typically exists in a compact, twisted form known as supercoiled (SC). However, when the DNA experiences a break in one or both of its strands, it can take on a different shape. Specifically, a break in one strand will cause SC form to unwind and transform into a nicked circular (NC) form, while a break in both strands will produce a linear form.

To measure the extent of DNA strand breaks, researchers can observe the migration patterns of the different forms of DNA in a gel electrophoresis experiment. The SC form moves quickly through the gel, while the NC form moves more slowly, and the linear form falls somewhere in between the SC and NC forms. By quantifying the amount of NC and linear forms present, researchers can estimate the extent of DNA strand breaks that have occurred.

The separated forms can be visualized by staining the gel with a dye that binds to molecules, such as ethidium bromide for DNA, or by transferring the separated molecules to a membrane for further analysis, such as in case of the Western blot analysis for proteins.

Gel electrophoresis is a widely used technique in molecular biology, with applications in DNA sequencing, gene expression analysis, and protein characterization, among others.

1.2.5. Gamma Radiation:

Gamma radiation is a form of high-energy electromagnetic radiation emitted from the nucleus of an atom. It is a type of ionizing radiation, which means it has enough energy to remove electrons from atoms and molecules, creating charged particles or ions.

Gamma radiation was passed through DNA solution with the help of a GC-900 Gama Chamber, 2 KilloCourie. The GC-900 Gamma Chamber is a device used to generate gamma radiation for various applications, including medical, industrial, and research purposes. The "2 KilloCourie" (kCi) refers to the strength or intensity of the radiation emitted by the chamber. One kilocurie (1 kCi) is equal to 37 terabecquerels (TBq), which is a measure of the number of radioactive decay events that occur in one second.

Therefore, a gamma radiation level of 2 kCi corresponds to a very high level of radiation exposure, and proper precautions must be taken to ensure the safety of individuals working with or near the GC-900 Gamma Chamber. This may include the use of protective clothing, radiation shielding, and monitoring devices to track radiation exposure levels.

1.3. Techniques and soft wares used for the overall research process:

Purpose	Software / Instrument used
Basic Computer Operating System	Windows operating system
Word Processing	MS Word, Adobe Acrobat
Numerical analysis	Origin, MS Excel
Plotting figures	Origin, MS Excel
Web browsing	Sci-Finder for literature, Google Chrome is used as a browser to browse the sites of publication houses
Error analysis	Origin, MS Excel
Curve fitting	Origin, MS Excel
Gel electrophoresis study	UVP Bio Doc-It Imaging System
Analysis of Nicking Percentage in Gel-electrophoresis study	UVP DOC-ItLS software
Optimization of Metal Complexes structures by DFT study	Gaussian09 package
Molecular Docking study	Auto Dock 4.2.0 software package

References:

- (1) G.H. Jeffery, J. Bassett, J. Mendham, R. C. D. A. *Vogel's Text Book of Quantitative Chemical Analysis.*, Wesley Longman Limited, United Kingdom, 5th Ed, (1989).
- (2) Lakowicz, J. R. Principles of Fluorescence Spectroscopy. *Princ. Fluoresc. Spectrosc.* **2006**, 1–954.
- (3) Valeur, B.; Berberan-Santos, M. N. Molecular Fluorescence: Principles and Applications. **2013**, 569.

Chapter 8

**Synthesis, Characterisation, Theoretical Simulation and
DNA Nuclease Activity of a Newly Synthesized Mn-based
Chemotherapeutic Agent**

Synthesis, characterisation, theoretical simulation and DNA nuclease activity of a newly synthesized Mn-based chemotherapeutic agent

1. Introduction:

DNA is the common primary intracellular target of all forms of anticancer drugs as well as chemotherapeutic agents. Interaction between small molecules and DNA may cause DNA damage in cancer cells inhibiting proliferation.¹⁻³ Over the past few decades, studies on the activity of small molecules showing DNA binding and cleavage have generated much interest^{4,5} due to their potential applications as DNA probes and anticancer drugs. Like natural enzymes, artificial nucleases can also hydrolyse DNA and therefore these cleaving agents have found extensive applications as potential chemotherapeutic agents.^{6,7} Although numerous naturally occurring nucleases are known⁸, development of synthetic nucleases would be of great utility and importance to monitor or manipulate desired biological reactions at the molecular level. In recent years, there has been a notable surge in the demand for metal-based compounds in the field of cancer treatment. This increased interest can be attributed to the alarming prevalence of cancer and, particularly, the remarkable cytotoxic effects demonstrated by newly developed metal-based compounds in laboratory studies. Furthermore, through the application of ligand substitution and the modification of existing chemical structures, scientists have successfully synthesized a diverse array of metal-based compounds. Some of these compounds exhibit enhanced cytotoxicity and improved pharmacokinetic profiles, further fueling the enthusiasm surrounding their potential as effective cancer treatments.^{9,10} Transition metal complexes¹¹⁻¹⁵ of Fe, Cu, Ni, Pt, Ru, Rh, V, Cr, Co, Os, and Pd have been reported to mediate DNA cleavage in presence of oxidants, reductants or without any assisting agents.¹⁶⁻²² However, detailed investigation of DNA interaction and nuclease activity exhibited by manganese complexes is scanty. To the best of our knowledge, the field of DNA-binding studies of oxime-based Mn complexes has not been explored. In the present work, we discuss DNA-binding properties and nuclease activity of a

Synthesis, characterisation, theoretical simulation and DNA nuclease activity of a newly synthesized Mn-based chemotherapeutic agent

new oxime-based Mn complex, which could prove to be of biochemical significance in the days to come.

2. Materials and methods:

2.1. Materials and physical methods:

Manganese chloride tetrahydrate, salicylaldehyde and hydroxylamine hydrochloride of extra-pure quality were obtained from Merck (India). All other reagents used were of GR grade and obtained from Merck (India). Analytical grade solvents used for physico-chemical studies were further purified, wherever necessary by standard literature methods before use.²³ Calf thymus DNA and supercoiled plasmid pUC19 DNA were obtained from Sigma Chemical Company, USA and Genei Bangalore, India respectively. All solutions containing DNA were prepared in Tris-HCl buffer at pH 7.4. Other stock solutions were also prepared in Tris-HCl buffer. Millipore water was used throughout the course of investigations.

2.2. Physical Measurements:

IR spectra were taken as KBr discs at room temperature on a Perkin Elmer RFX-I IR spectrophotometer. PXRD data were collected on a Bruker D8 Advance X-ray diffractometer using Cu K α radiation ($\lambda = 1.548 \text{ \AA}$) generated at 40 kV and 40 mA. Elemental analyses were carried out on a Perkin-Elmer 2400 series II CHNS analyzer. UV-vis spectra (200–800 nm) were recorded against an appropriate reagent blank at room temperature using a Shimadzu U-1800 spectrophotometer using a 1 cm quartz cell. EPR spectra were obtained on a JEOL-JES FA200 ESR spectrometer at room temperature. Mass spectral analyses were done on a Waters mass spectrometer (model: XEVO-G2QTOF#YCA351). Gel electrophoresis studies were carried out with UVP Bio Doc-It imaging system and nicking was analyzed by UVP DOC-ItLS software.

Synthesis, characterisation, theoretical simulation and DNA nuclease activity of a newly synthesized Mn-based chemotherapeutic agent

3. Experimental Procedures:

3.1. Preparation of the complex:

The ligand salicylaldehyde-oxime (sal-oxime) was prepared according to a method mentioned in the literature.²⁴ Methanolic solution (5 mL) of Manganese chloride tetrahydrate (2 mmol) was mixed with a methanolic solution (10 mL) of the ligand (salicylaldehyde-oxime, sal-oxime) (4 mmol), dropwise with constant stirring. 20 mL water was then added and stirring was continued for another 12 hours, which on standing produced a light green solid. The solid was collected by filtration, washed with cold water and dried under vacuum. It was purified by recrystallization; yield was 75%. Despite multiple attempts, diffractable grade suitable single crystals were not obtained. IR (KBr, cm^{-1}): 463 [$\nu(\text{Mn-N})$], 539 [$\nu(\text{Mn-O})$]^{25,26}. ESI-MS (+ve) in MeOH: m/z (relative intensity) 363.04 [M^+], 386.03 [$\text{M}^+ + \text{Na}$]. UV-Vis ($\lambda_{\text{max}}/\text{nm}$): 216 and 253. Elemental analysis: found (calc.) C, 46.12% (C, 46.29%); H, 3.99% (H, 4.44%); N, 7.51% (N, 7.71%). The nature of PXRD results (Figure 1) indicate that the complex is crystalline in nature. The compound is soluble in organic solvents like methanol, acetonitrile, chloroform, acetone, N,N-dimethyl formamide (DMF), dimethyl sulfoxide (DMSO) and tetrahydrofuran (THF) and behaves like a non-electrolyte (Molar conductance $2 \text{ ohm}^{-1}\text{cm}^2\text{mole}^{-1}$). Therefore, molecular formula of the compound is $\text{Mn}^{\text{II}}(\text{sal-oxime})_2(\text{H}_2\text{O})_2$ which was supported by a DFT study.

Synthesis, characterisation, theoretical simulation and DNA nuclease activity of a newly synthesized Mn-based chemotherapeutic agent

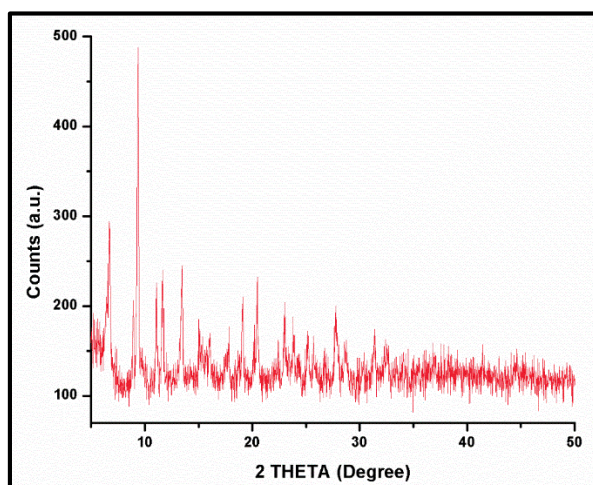


Figure 1: PXRD pattern of the complex

3.2. DFT Calculations:

Molecular geometry of the complex was optimized by Density Functional Theory (DFT), being an established technique to obtain better insights into the geometry, electronic structure and optical properties of systems. Geometry of both the ligand and metal complex was optimized using DFT. All DFT calculations were performed using Gaussian09 package. Ligand geometry was optimized with Becke three parameter hybrid exchange functional and Lee–Yang–Parr correlation functional (B3LYP)²⁷ with 6-31+g (d,p) basis set. Optimization of the complex molecule was done using unrestricted hybrid density functional theory by Becke’s 3 parameter exchange functional^{27,28} with nonlocal Lee-Yang-Parr electron correlation (UB3LYP model)^{27,29} functional. The basis set was augmented to LANL2DZ (ECP)^{30–32} for Mn atom jointly with 6-31G (d,p) basis set for other atoms (C, O,N, and H) using Gaussian09.³³ TD-DFT was performed considering optimized geometry using CAM-B3LYP^{27,28,34} function in combination with LANL2DZ (ECP)^{30–32} for Mn atom and 6-31G (d,p) for other atoms (C,H, N, and O) for the calculation of spectral features of the complex. In order to include solvation effect in TD-DFT calculation, we included the continuum model

Synthesis, characterisation, theoretical simulation and DNA nuclease activity of a newly synthesized Mn-based chemotherapeutic agent

(CPCM)³⁵ (polarizable conductor calculation model along with united-atom topological model having $\epsilon = 78.39$). Geometry of the ligand and the complex was fully optimized without any symmetry constraints. GaussSum 2.1 program³⁶ was used to calculate molecular orbital contributions from groups or atoms.

3.3. DNA binding Studies:

3.3.1. UV-Vis spectral study:

Calf thymus DNA solutions were meticulously prepared in a solution of Tris-HCl / NaCl (50 mM Tris-HCl and 50 mM NaCl, pH 7.2) and stored at 4°C for a maximum of four days to maintain their integrity. To explore the interaction between the complex and DNA, UV-vis spectra were captured using a Shimadzu UV-1800 spectrophotometer. The electronic spectrum of the complex was scrutinized both in the absence and presence of calf thymus DNA. To conduct the titration experiment, a fixed concentration of the complex was progressively titrated with increasing amounts of DNA. By following this approach, we aimed to precisely investigate the changes in the absorption profile and elucidate the potential interaction between the complex and DNA.

3.3.2. Viscometric study:

Viscosity of DNA³⁷ was measured by a fabricated micro viscometer, maintained at 28 (\pm 0.5)⁰C in a thermostatic water bath. Data were presented as $(\eta/\eta_0)^{1/3}$ versus ratio of the concentration of either the ligand or complex to that of CT-DNA, where η_0 is the viscosity of CT-DNA solution alone and η is the viscosity of calf thymus DNA in the presence of the complex. Viscosity values were calculated from observed flow time of calf thymus DNA by the relation; $\eta = t - t_0$, where t and t_0 are values of flow times for solution and buffer respectively.

Synthesis, characterisation, theoretical simulation and DNA nuclease activity of a newly synthesized Mn-based chemotherapeutic agent

3.3.3. Gel electrophoresis study:

DNA cleavage activity of the complex was monitored with the help of gel electrophoresis (Model No. 2101, Genei, Bangalore). The supercoiled pUC19 DNA (0.5 mg per reaction) in Tris-HCl/NaCl buffer (pH 7.2) was treated with increasing amounts of the metal complex over a range of 18–36 μM along with H_2O_2 (16 μM)^{38,39}. After incubation for 45 min at 37⁰C, it was mixed with a sample loading dye. Samples were run on 0.9% agarose in 1 X TAE buffer for 3 hours at 80 mV and then treated with a solution of ethidium bromide. The bands were visualized by UV light and photographed with UVP Bio Doc-It imaging system. Percentage of of supercoiled (SC) pUC19 DNA cleavage, induced by the complex, was determined using UVP BIODOC-ItLS software.

3.3.4. Molecular Docking Study:

The molecular docking study of the Mn complex with calf thymus DNA was carried out using Auto Dock 4.2.0 software. The energy minimized conformation of the complex obtained from DFT calculations were used for docking studies. Docking study was performed with Lamarckian Genetic Algorithm (LGA) inside a 126 \times 126 \times 126 grid box. Discovery studio visualizer 2016 and Chimera 1.10.2 were used to visualize results.

4. Results and Discussions:

4.1. Characterisation of the complex:

4.1.1. IR and UV-vis studies of the complex:

Infrared absorption frequencies of the metal complex were analyzed. The azomethine group frequencies of free Schiff base shifts towards the lower frequency region in the complex from 1618 cm^{-1} to 1587 cm^{-1} (Figure 2 & 3) due to the involvement of the N atom of $-\text{C}=\text{N}-$ group in coordinating the metal centre.⁴⁰ Bands at 463 and 539 cm^{-1} are due to $\nu_{\text{Mn-N1}}$, $\nu_{\text{Mn-N2}}$ and $\nu_{\text{Mn-O1}}$, $\nu_{\text{Mn-O4}}$ vibrations respectively of the coordinated sal-oxime ligand (Figure 3). The

Synthesis, characterisation, theoretical simulation and DNA nuclease activity of a newly synthesized Mn-based chemotherapeutic agent

complex shows a broad absorbance throughout the visible region which may be due to d-d transition of Mn(II) in the complex. The complex shows broad peaks at 253 nm and 216 nm which can be assigned to $n-\pi^*$ and $\pi-\pi^*$ intra-ligand electronic transitions.

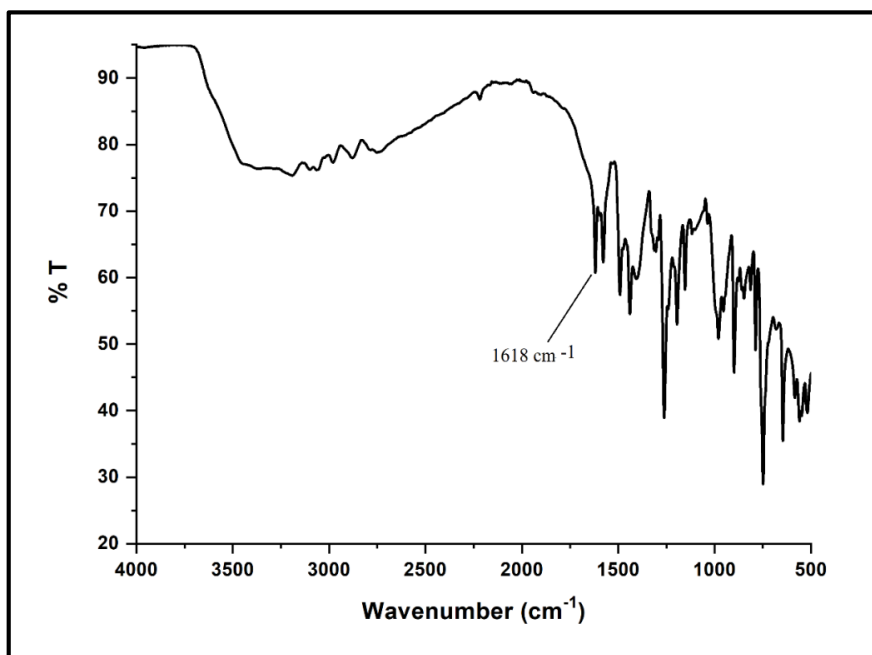


Figure 2: IR spectra of the Ligand

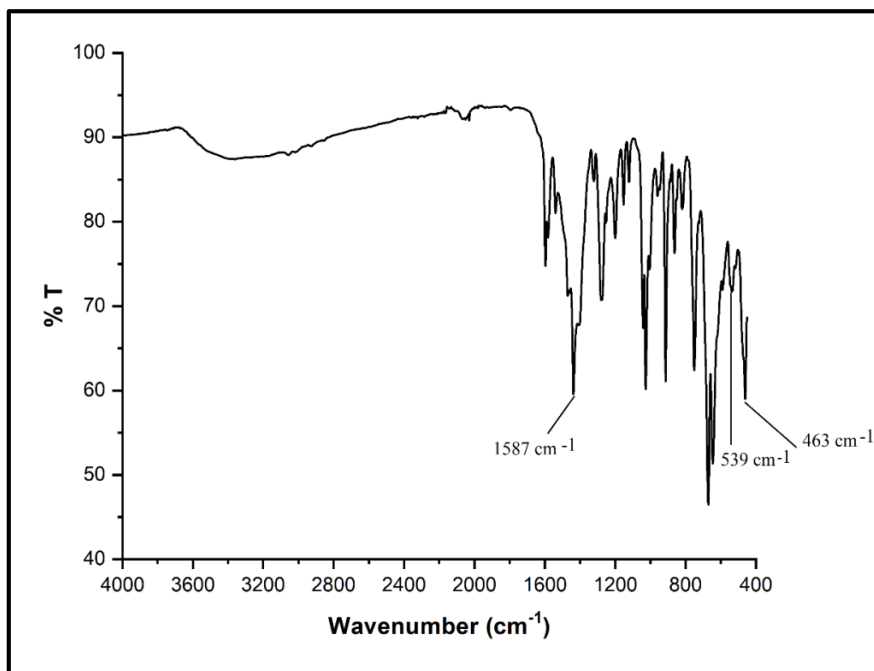


Figure 3: IR spectra of the Complex

Synthesis, characterisation, theoretical simulation and DNA nuclease activity of a newly synthesized Mn-based chemotherapeutic agent

4.1.2. Thermo gravimetric analysis (TGA):

Presence of coordinated water in the complex was identified by a loss of mass above 120⁰C.⁴¹⁻⁴³ 10% mass loss occurred upto 120⁰C which corresponds to loss of two molecules of coordinated water from the complex (Figure 4).

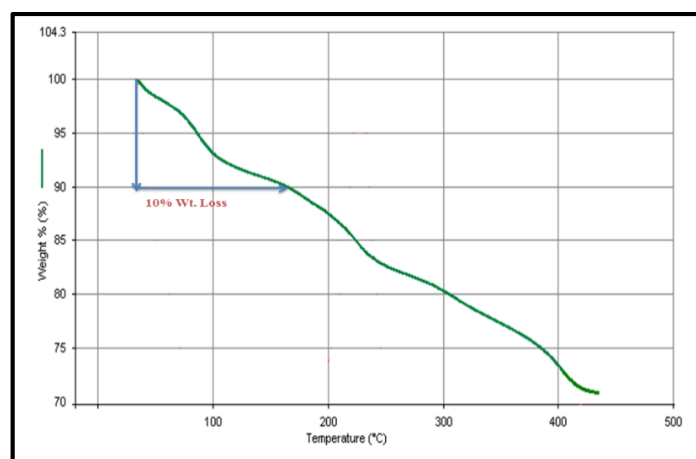


Figure 4: TGA of Complex

4.1.3. Mass spectrometric analysis:

Molecular formula and structural information could be obtained from ESI-MS analysis. The molecular formula of the complex $[\text{Mn}(\text{sal-oxime})_2(\text{H}_2\text{O})_2]$ obtained from analytical techniques is $\text{C}_{14}\text{H}_{16}\text{MnN}_2\text{O}_6$ (Mol. Wt. 363.04), which is supported by the observed ESI-mass spectrum of the complex. The mass spectrum exhibits a peak at 363.04 (molecular weight), corresponding to the molecular ion (M^+). Additionally, a peak at 386.03, with the highest abundance, represents the molecular ion (M^+) combined with Na^+ (Figure 5).

Synthesis, characterisation, theoretical simulation and DNA nuclease activity of a newly synthesized Mn-based chemotherapeutic agent

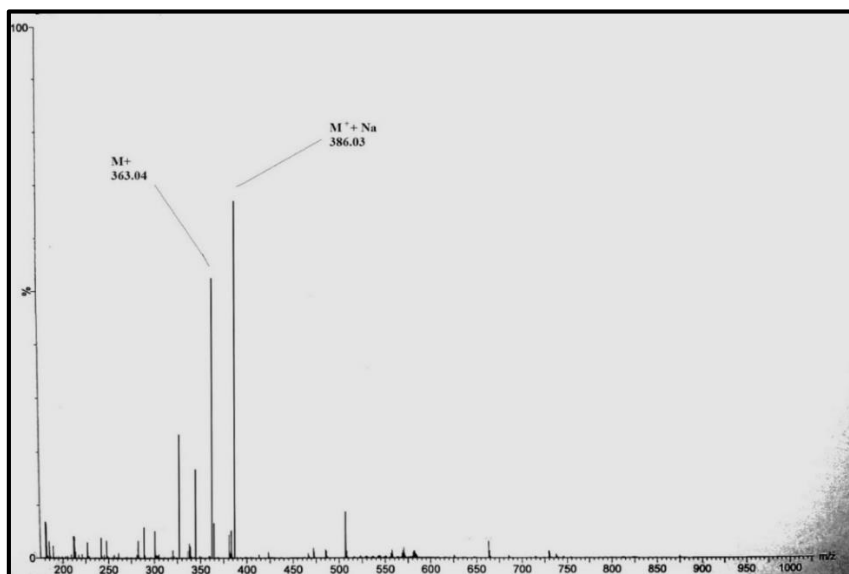


Figure 5: ESI-MS of Complex

4.1.4. Magnetic Moment:

Room temperature (298 K) magnetic moment of the complex was found to be 5.89 B.M. which indicates the presence of a high spin Mn(II) centre having octahedral geometry.⁴⁴

4.1.5. EPR spectra:

The EPR spectrum of the complex $[\text{Mn}^{\text{II}}(\text{sal-oxime})_2(\text{H}_2\text{O})_2]$ was recorded in solid state at room temperature. A single EPR line was observed (Figure 6) which revealed the presence of a strong signal at $g = 1.97$. Such single line spectrum suggests unambiguously a mononuclear nature for the complex.⁴¹⁻⁴³ From the low value of 'g', it can be said there can be an important contribution of ligand spin-orbit coupling that indicates covalency.^{45,46}

Synthesis, characterisation, theoretical simulation and DNA nuclease activity of a newly synthesized Mn-based chemotherapeutic agent

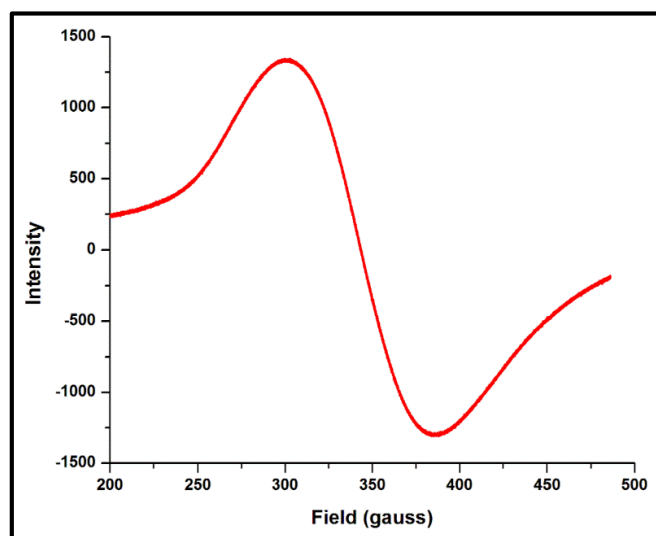


Figure 6: EPR spectra of complex $(\text{Mn}[\text{sal-oxime}]_2[\text{H}_2\text{O}]_2)$ at 298 K. ($g = 1.97$; freq. = 9445.141 MHz, power = 0.9908 mW, sweep time = 4.00 min.)

4.1.6. Optimization of molecular geometry and electronic structure:

By employing Density Functional Theory (DFT)^{47–50}, the geometry of both the ligand and the metal complex has been optimized. The ground state optimized geometry of the ligand and its Mn^{2+} complex is shown in Figure. 7 a and b respectively where both the ligand and Mn^{2+} complex had a C1 point group. The main optimized geometrical parameters of the complex are listed in Table 1. The modelled geometry possesses a distorted octahedral arrangement around the Mn(II) centre.

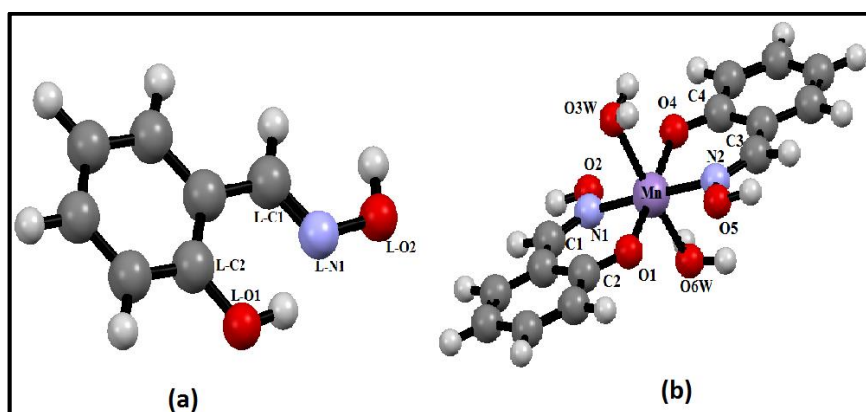


Figure 7: Optimized Geometry of (a) ligand and (b) complex

Synthesis, characterisation, theoretical simulation and DNA nuclease activity of a newly synthesized Mn-based chemotherapeutic agent

Table 1: Selected optimized geometrical parameters for the complex in the ground state calculated at LANL2DZ levels

Bond Length (Å)

Mn-N1	1.996
Mn-O1	1.928
Mn-O3W	2.162
Mn-O4	1.976
Mn-N2	2.022
Mn-O6W	2.158

Bond angles (°)

O1-Mn-N1	88.25
N1-Mn-O3W	92.42
O3W-Mn-O4	90.84
O4-Mn-N2	90.06
N2-Mn-O6W	88.09
O6W-Mn-O1	86.71
N1-Mn-O4	91.92
O4-Mn-N2	88.25
N2-Mn-O1	89.91
O1-Mn-N1	90.06
N1-Mn-N2	178.20
O1-Mn-O4	175.28
O3W-Mn-O6W	171.14

Synthesis, characterisation, theoretical simulation and DNA nuclease activity of a newly synthesized Mn-based chemotherapeutic agent

All calculated Mn–N distances occur in the range 1.996–2.022 Å and Mn–O distances in the range 1.928–2.162 Å. The calculated IR stretching frequencies of the complex were compared with experimental findings (Table 2) (Figure 8a) and values were found to be in good agreement. Hence, all DFT calculations confirm and establish the structure of the Mn compound as depicted in Figure 7b. For the ligand (sal-oxime) at ground state, electron density at HOMO-1, HOMO, LUMO, and LUMO+1 orbitals mainly reside on the benzene moiety. Energy difference between HOMO and LUMO (Figure 9) is 4.68 eV in case of the ligand. This assignment was supported by TD-DFT calculations. For the complex all LUMO, LUMO+1, LUMO+2, HOMO and HOMO-1 mainly originate from the ligand π and π^* orbitals while LUMO+2, HOMO, LUMO, and HOMO-1 arise from contribution of metal d orbitals along with ligand p orbitals. The energy difference between HOMO and LUMO is 3.38 eV in the complex while for the ligand it is 4.68 eV.

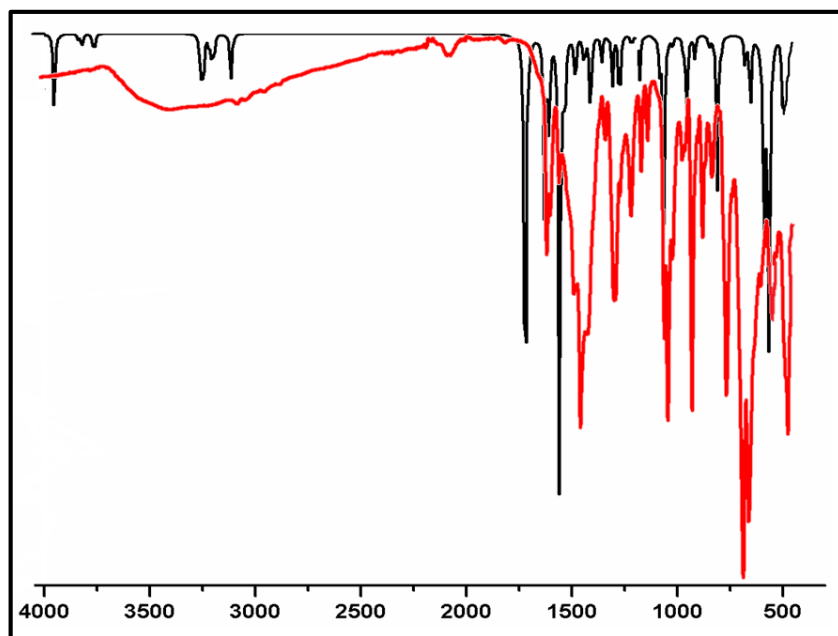


Figure 8a: Calculated (black) and experimental (red) Infrared spectra of **complex**

Synthesis, characterisation, theoretical simulation and DNA nuclease activity of a newly synthesized Mn-based chemotherapeutic agent

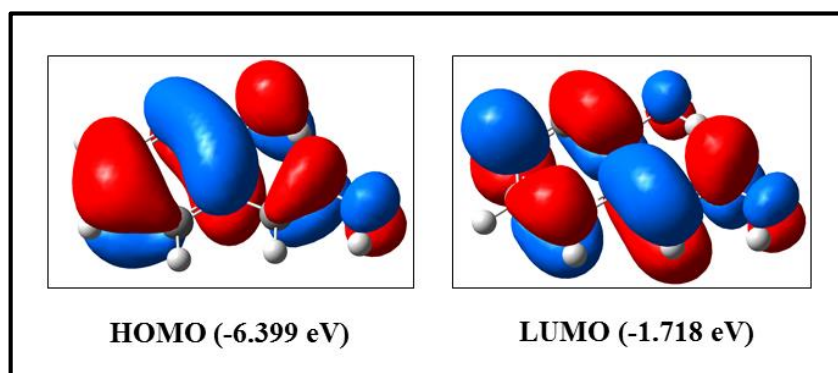


Figure 9: HOMO and LUMO of sal-oxime Ligand

Table 2: Comparisons of experimental and theoretical stretching frequency of complex

Frequency	Theoretical values (cm^{-1})	Experimental Values (cm^{-1})	% of Deviation
$\nu\text{Mn-N1}$ and $\nu\text{Mn-N2}$	501	463	8.2
$\nu\text{Mn-O1}$ and $\nu\text{Mn-O4}$	560	539	3.8

The complex shows two absorption bands at 216 nm and 253 nm in aqueous solution at room temperature. Absorptions calculated from TD-DFT show bands at 239 nm and 255 nm for the complex. The calculated value is in good agreement with experimental results (Table 3) (Figure 8b).⁵¹

Synthesis, characterisation, theoretical simulation and DNA nuclease activity of a newly synthesized Mn-based chemotherapeutic agent

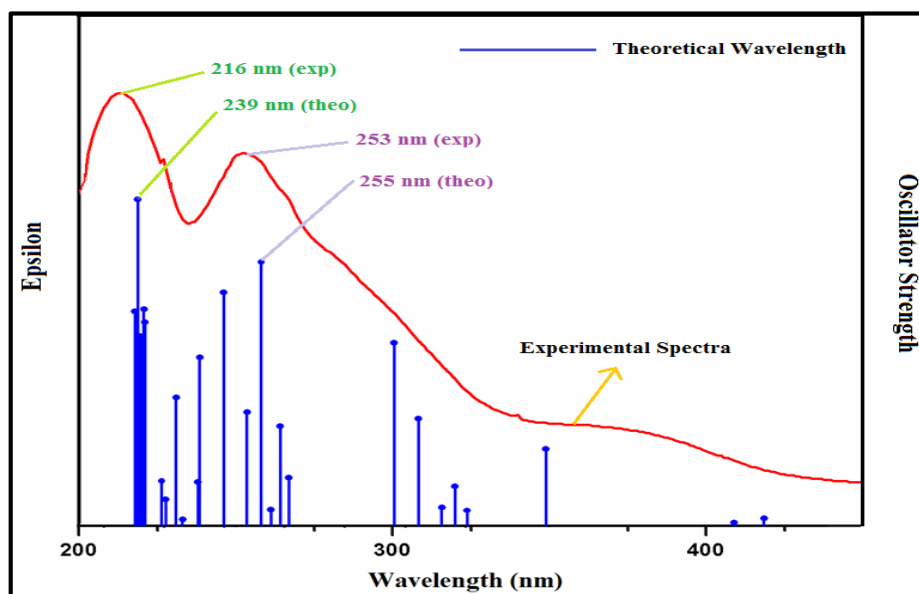


Figure 8b: Comparison of Theoretical and Experimental electronic spectra of **complex**

Table 3: Selected UV–vis energy transitions at B3LYP level for **complex** in aqueous medium

λ_{cal} (nm)	Oscillator strength (f)	λ_{expt} (nm)	Key transitions
239	0.0252	216	HOMO \rightarrow L+2, H-1 \rightarrow L+1
255	0.0117	253	H-1 \rightarrow L+1, HOMO \rightarrow L+1, H-1 \rightarrow LUMO

HOMO–LUMO energy

In chemistry, energy difference between molecular orbitals, HOMO (highest occupied molecular orbital) and LUMO (lowest unoccupied molecular orbital) is called HOMO–LUMO gap. These molecular orbitals are known as “frontier orbitals” as these are the farthest boundary of the electrons in molecule (Figure 10).⁵² The HOMO–LUMO gap determines the rate of excitation of the molecule in which the rate increases with a decrease in the gap.

Synthesis, characterisation, theoretical simulation and DNA nuclease activity of a newly synthesized Mn-based chemotherapeutic agent

HOMO and LUMO orbitals with corresponding energies are shown in Figure 11 and the HOMO-LUMO E_{diff} is 3.379 eV. Here, HOMO is distributed to a large extent in the aromatic part of the molecule and metal atom. Electron density is greater on one of the aromatic rings of the ligand over the other ligand attached to the metal ion. In case of LUMO, the above mentioned electron density (found in HOMO) is reversed on the aromatic part of another ligand attached to metal centre. An intriguing observation is that the electron density on the metal ion disappears in the LUMO, whereas it is present in sufficient quantities in the HOMO. The highest occupied molecular orbital (HOMO) primarily exhibits π -bonding character, while the lowest unoccupied molecular orbital (LUMO) predominantly displays π anti-bonding character. The significant energy gap between the HOMO and LUMO indicates that the complex possesses high stability, as the molecule necessitates higher energy levels for excitation.

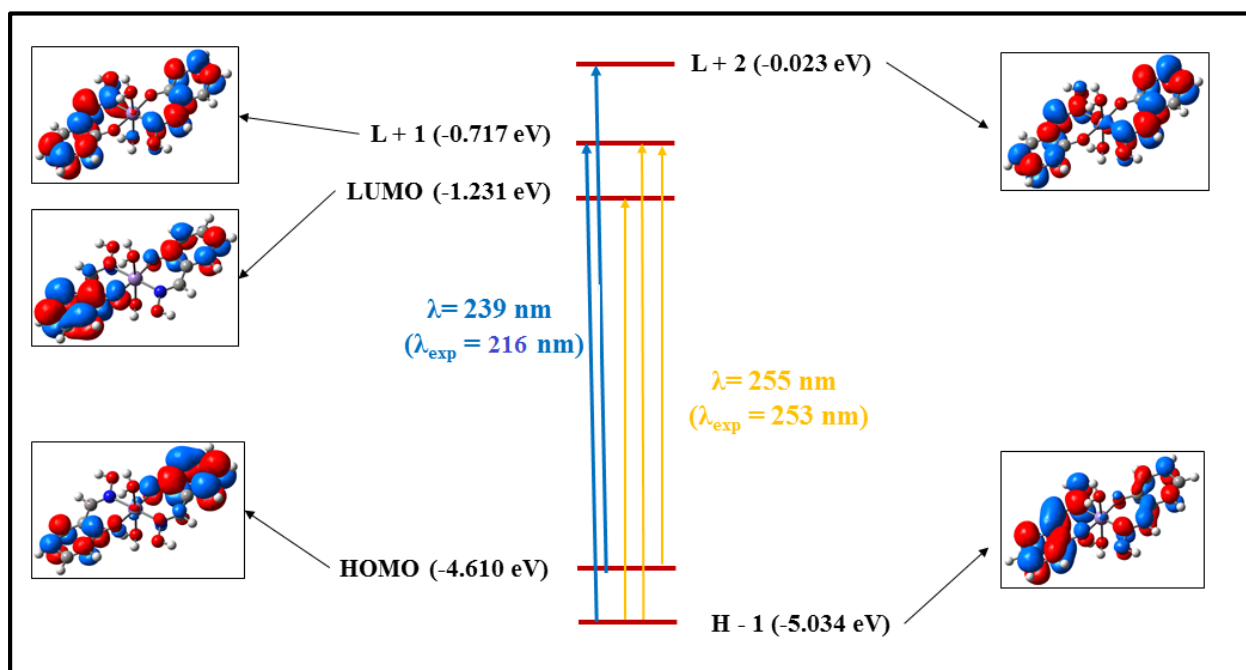


Figure 10: Frontier molecular orbitals involved in the UV-vis absorption of metal complex

Synthesis, characterisation, theoretical simulation and DNA nuclease activity of a newly synthesized Mn-based chemotherapeutic agent

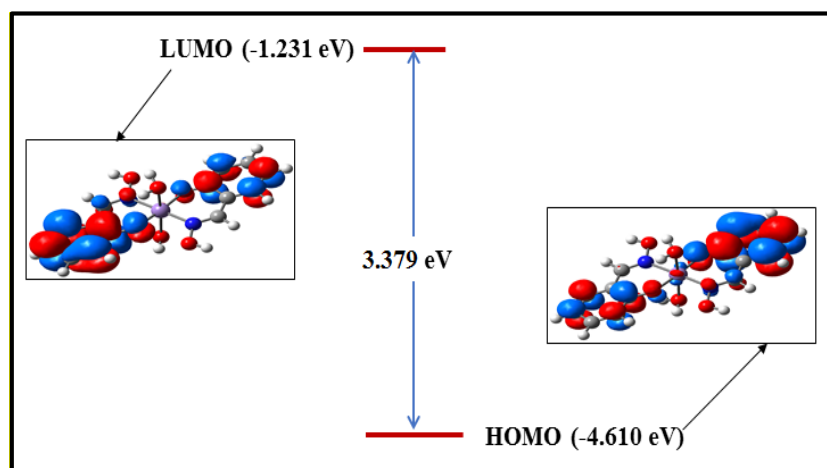


Figure 11: Frontier orbitals (HOMO-LUMO) of the **complex**

4.2. DNA binding studies:

The study is directed towards development of a synthetic DNA nuclease. It therefore demands a thorough study on the ability of the compound to bind to double-stranded DNA. Hence, binding to DNA by the molecule was studied and the results are presented herein.

4.2.1. Electronic absorption spectral studies:

Monitoring changes in the absorption profile of metal complexes upon the addition of increasing amounts of DNA has emerged as a widely employed method for comprehending the intricate interactions between the complex and DNA.⁵³ To investigate this interaction, the electronic spectra of the complex were diligently observed both in the absence and presence of DNA. Specifically, the absorption spectrum of the complex was scrutinized by modulating the concentration of calf thymus DNA. Notably, with the gradual addition of DNA, a remarkable augmentation in the intensity of the spectra was observed in the complex (Figure 12). This conspicuous hyperchromic effect primarily arises due to the electrostatic attraction between the complex and DNA, resulting in potential damage to the secondary structure of DNA. Consequently, the helical structure of DNA may experience partial untwisting, leading

Synthesis, characterisation, theoretical simulation and DNA nuclease activity of a newly synthesized Mn-based chemotherapeutic agent

to the exposure of additional DNA bases.^{54,55} These distinctive spectroscopic characteristics strongly imply a discernible interaction between the complex and DNA.^{54,55}

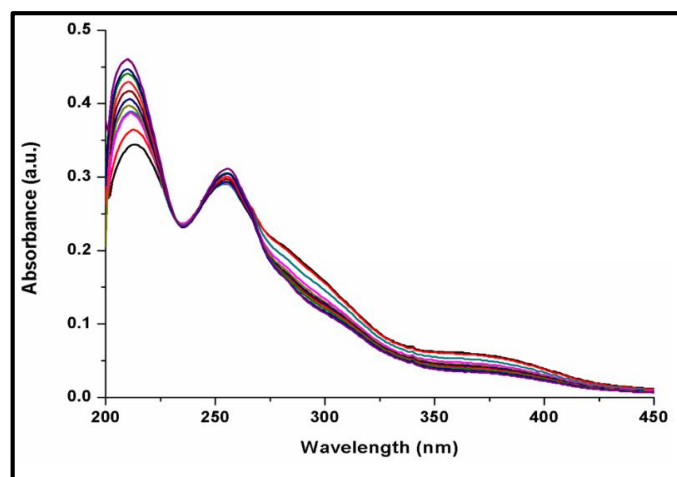


Figure 12: Absorption spectra of the complex in the presence of increasing amounts of calf thymus DNA

4.2.2. Viscometric studies:

To further investigate the mode of binding between the complex and DNA, a viscosity measurement was carried out. The spectroscopic technique is useful but not sufficient to understand the mode of binding of the complex with DNA.⁵⁶ Hydrodynamic measurements which are sensitive to change in DNA length are used to confirm spectral data. Hence, viscosity is used to be a sensitive technique to understand mode of DNA binding.^{57–61} Relative viscosity of the calf thymus DNA solution is known to increase on intercalative binding to substrates because insertion of intercalators causes base pairs of the DNA to get apart and causing lengthening of the DNA helix and leading to increase in viscosity. While molecules bound to DNA through groove do not alter their relative viscosity.^{62,63} Values of relative specific viscosities of DNA in the absence and presence of the complex are plotted against $[\text{complex}]/[\text{DNA}]$ (Figure 13). It is observed addition of the complex to calf thymus DNA does not show a significant increase in viscosity of calf thymus DNA. Hence, the

Synthesis, characterisation, theoretical simulation and DNA nuclease activity of a newly synthesized Mn-based chemotherapeutic agent

possibility of the complex to be an intercalator is ruled out. There may be some electrostatic interactions of the complex with the DNA. The complex can also participate in hydrogen bond formation with DNA base pairs, that may lead to better binding affinity between the complex and DNA base pairs, thereby suggesting involvement of complex as a DNA groove binder.

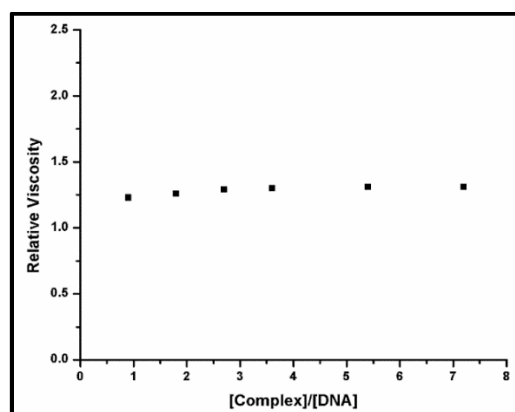


Figure 13: Effect of increasing amount of the complex on specific viscosity of calf thymus DNA

4.2.3. Gel electrophoresis study for nuclease activity:

Double-stranded plasmid pUC19 DNA exists in a compact supercoiled (SC) form. Upon introduction of nuclease, the naturally occurring supercoiled (SC) form, gives rise to the nicked circular (NC) form. A relatively fast migration is observed for supercoiled (SC) form than the nicked circular (NC) form when the plasmid DNA is subjected to electrophoresis. Hence, DNA strand breaks were quantified by measuring the transformation of the supercoiled form into the nicked circular form.^{62,63} The ability of the manganese complex to induce DNA cleavage was studied by gel electrophoresis using supercoiled pUC19 DNA in Tris-HCl/NaCl buffer (pH 7.2) which was treated with increasing amounts of metal complex alone (over a range of 18–36 μM) or with addition of H_2O_2 (16 μM) (Figure 14) (Table 4).^{62–66} In the control pUC19 DNA sample where no complex or H_2O_2 were added, the percentage of

Synthesis, characterisation, theoretical simulation and DNA nuclease activity of a newly synthesized Mn-based chemotherapeutic agent

the NC form was only 10% (lane 1). Upon the addition of the compound at concentrations of 18 μ M (lane 3) and 36 μ M (lane 5), the percentage of the NC form increased to 31% and 42% respectively. However, when different concentrations of the compound (18 μ M in lane 4 and 36 μ M in lane 5) were added together with a fixed concentration of H₂O₂ (16 μ M), the DNA was cleaved significantly. This was evident from the increased percentage of the NC form, which reached 40% (lane 4) and 48% (lane 6) respectively. This clearly indicates that the compound alone can show moderate nuclease activity but can exhibit greater nuclease activity when used in combination with H₂O₂.^{38,39,62–66}

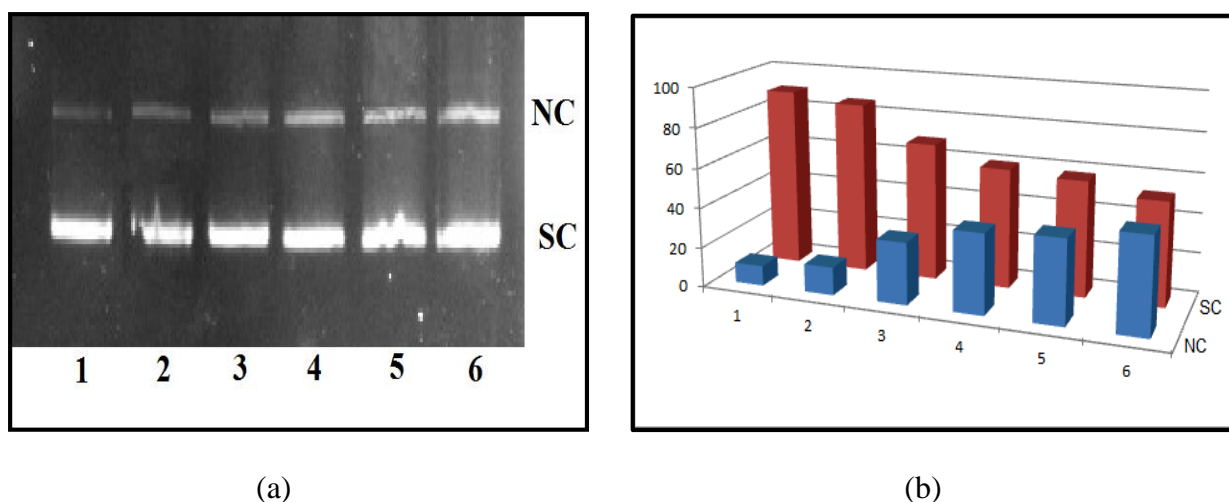


Figure 14: (a) Agarose gel (0.9%) electrophoregram of supercoiled DNA (0.5 μ g) incubated for 45 min at 37°C in PBS buffer (0.15 M, pH 7.2) at 37°C. Lane1: DNA control; Lane 2: DNA + H₂O₂; Lane 3: DNA + complex (18 μ M); Lane 4: DNA + complex (18 μ M) + H₂O₂; Lane 5: DNA + complex (36 μ M); Lane 6: DNA + complex (36 μ M) + H₂O₂; (b) Graphical representation of % cleavage in different lanes.

Synthesis, characterisation, theoretical simulation and DNA nuclease activity of a newly synthesized Mn-based chemotherapeutic agent

Table 4: Results of the cleavage of pUC19 DNA determined by gel electrophoresis study.

Lane no.	Reaction Condition	Form I (% SC)	Form II (% NC)
1	Control DNA	90	10
2	DNA + H ₂ O ₂ (16 μ M)	86	14
3	DNA + complex (18 μ M)	69	31
4	DNA + complex (18 μ M) + (16 μ M) H ₂ O ₂	60	40
5	DNA + complex (36 μ M)	58	42
6	DNA + complex (36 μ M) + (16 μ M) H ₂ O ₂	52	48

4.2.4. Theoretical simulation for the interaction of DNA with the complex:

Theoretical simulation in the form of molecular docking was used to realize binding of the complex with DNA (PDB access code 2BNA).⁶⁷ Docking simulation showed the complex has an aromatic ring-containing ligand system having electronegative atoms like nitrogen and two water molecules. Therefore, there is a balance between hydrophobic and hydrophilic parts in the molecule. The investigating molecule is capable of interacting with DNA residues through hydrogen bonding and other weak electrostatic interactions. Docking study shows the molecule interacts with DNA through its minor groove (Figure 15), the energy minimized conformation of the complex inside DNA and change in free energy for the interaction is – 6.21 kcal/mol. There are four hydrogen bonding interactions between DNA and complex. They are found at NH₂ group of G10 and G14 residue with oxime OH and water molecule of the complex respectively. In addition to that the sugar oxygen, G16 residue and C=O of C11 residues separately interact with two water molecules present in the complex through H-

Synthesis, characterisation, theoretical simulation and DNA nuclease activity of a newly synthesized Mn-based chemotherapeutic agent

bonding as shown in Figure 16. So, the theoretical simulations support the proposition of groove binding which was suggested from other experimental findings also.

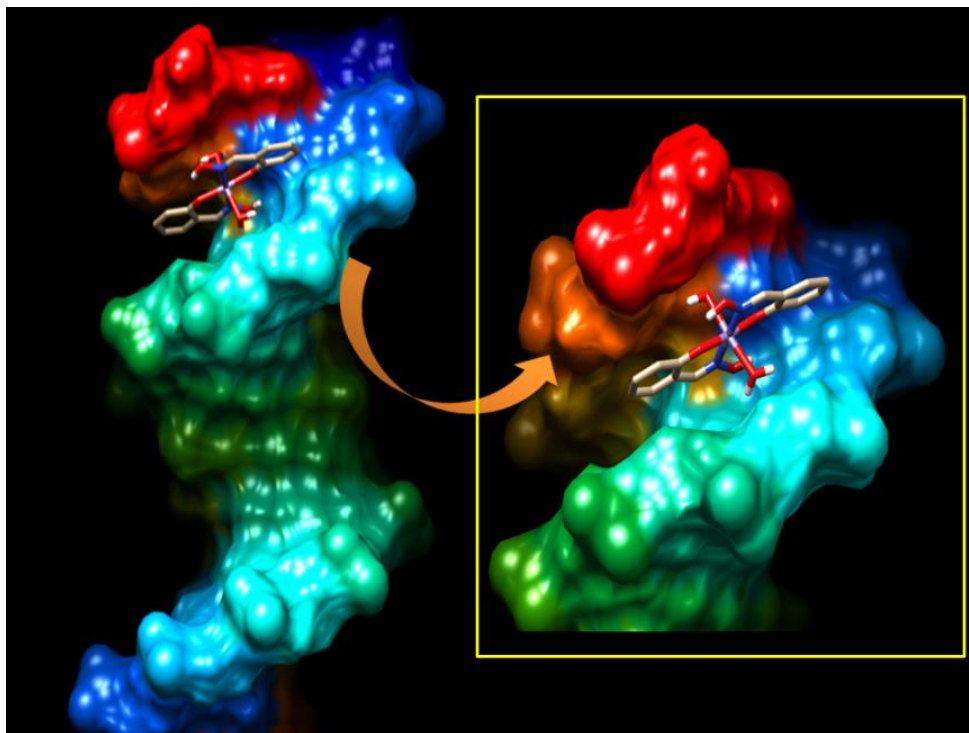


Figure 15: Docked pose of complex showing interaction with base pairs; inset: Enlarged view of the docked pose

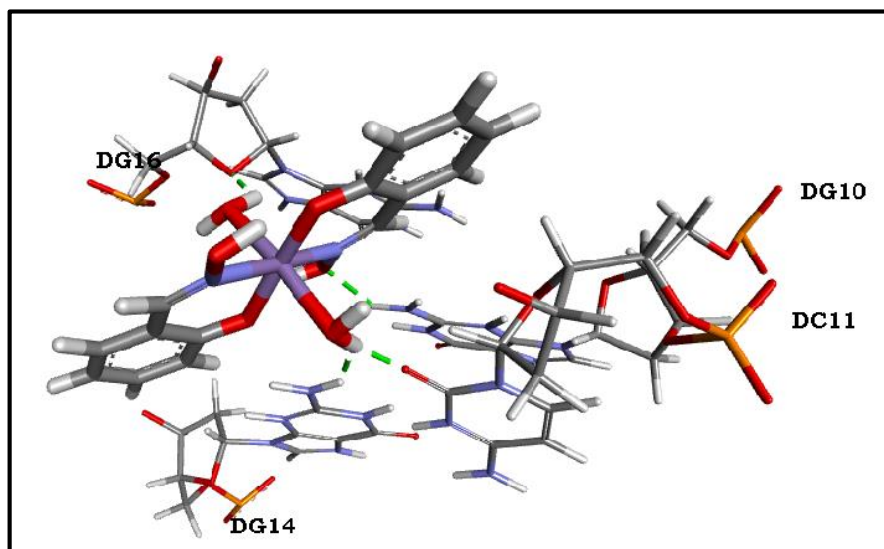


Figure 16: Hydrogen bonding interactions of the complex with DNA base pairs

5. Conclusion:

The Mn complex was characterized by different physico-analytical techniques and its geometry was optimized by DFT calculations. The TD-DFT study clearly supports the optimized structure of the complex and is in good agreement with experimental findings. In the present study interaction of the complex with calf thymus DNA was examined by absorbance and viscometric methods. Results of DNA binding experiment suggest that the complex binds in the groove of calf thymus DNA that is supported by molecular docking. The complex exhibits effective concentration-dependent nuclease activity in presence of H_2O_2 by cleaving supercoiled plasmid (pUC19) DNA to NC. Therefore, the present study provides evidence for a non- platinum-based Manganese-based new class of nuclease as a potential artificial nuclease.

Synthesis, characterisation, theoretical simulation and DNA nuclease activity of a newly synthesized Mn-based chemotherapeutic agent

References:

- (1) Khandekar, M. J.; Banks, A. S.; Laznik-Bogoslavski, D.; White, J. P.; Choi, J. H.; Kazak, L.; Lo, J. C.; Cohen, P.; Wong, K. K.; Kamenecka, T. M.; Griffin, P. R.; Spiegelman, B. M. Noncanonical Agonist PPAR γ Ligands Modulate the Response to DNA Damage and Sensitize Cancer Cells to Cytotoxic Chemotherapy. *Proc. Natl. Acad. Sci. United States Am.* **2018**, *115* (3), 561–566.
- (2) Brabec, V.; Malina, J.; Margiotta, N.; Natile, G.; Kasparkova, J. Thermodynamic and Mechanistic Insights into Translesion DNA Synthesis Catalyzed by Y-Family DNA Polymerase Across a Bulky Double-Base Lesion of an Antitumor Platinum Drug. *Chem. – A Eur. J.* **2012**, *18* (48), 15439–15448.
- (3) Wang, B.; Tan, J.; Zhu, L. Selective Binding of Small Molecules to DNA: Application and Perspectives. *Colloids Surfaces B Biointerfaces* **2010**, *79* (1), 1–4.
- (4) Wang, X. L.; Chao, H.; Li, H.; Hong, X. L.; Ji, L. N.; Li, X. Y. Synthesis, Crystal Structure and DNA Cleavage Activities of Copper(II) Complexes with Asymmetric Tridentate Ligands. *J. Inorg. Biochem.* **2004**, *98* (3), 423–429.
- (5) Baraldi, P. G.; Bovero, A.; Fruttarolo, F.; Preti, D.; Tabrizi, M. A.; Pavani, M. G.; Romagnoli, R. DNA Minor Groove Binders as Potential Antitumor and Antimicrobial Agents. *Med. Res. Rev.* **2004**, *24* (4), 475–528.
- (6) Tullius, T. D.; Greenbaum, J. A. Mapping Nucleic Acid Structure by Hydroxyl Radical Cleavage. *Curr. Opin. Chem. Biol.* **2005**, *9* (2), 127–134.
- (7) West, J. D.; Marnett, L. J. Endogenous Reactive Intermediates as Modulators of Cell Signaling and Cell Death. *Chem. Res. Toxicol.* **2006**, *19* (2), 173–194.
- (8) Stubbe, J.; Kozarich, J. W. Mechanisms of Bleomycin-Induced DNA Degradation. *Chem. Rev.* **1987**, *87* (5), 1107–1136.

Synthesis, characterisation, theoretical simulation and DNA nuclease activity of a newly synthesized Mn-based chemotherapeutic agent

- (9) Kang, J.; Zhuo, L.; Lu, X.; Liu, H.; Zhang, M.; Wu, H. Electrochemical Investigation on Interaction between DNA with Quercetin and Eu–Qu₃ Complex. *J. Inorg. Biochem.* **2004**, *98* (1), 79–86.
- (10) Opaliński, Ł.; Szymczyk, J.; Szczepara, M.; Kucińska, M.; Krowarsch, D.; Zakrzewska, M.; Otlewski, J. High Affinity Promotes Internalization of Engineered Antibodies Targeting FGFR1. *Int. J. Mol. Sci.* **2018**, *19* (5), 1435.
- (11) Becco, L.; Rodríguez, A.; Bravo, M. E.; Prieto, M. J.; Ruiz-Azuara, L.; Garat, B.; Moreno, V.; Gambino, D. New Achievements on Biological Aspects of Copper Complexes Casiopeínas®: Interaction with DNA and Proteins and Anti-Trypanosoma Cruzi Activity. *J. Inorg. Biochem.* **2012**, *109*, 49–56.
- (12) Correia, I.; Roy, S.; Matos, C. P.; Borovic, S.; Butenko, N.; Cavaco, I.; Marques, F.; Lorenzo, J.; Rodríguez, A.; Moreno, V.; Pessoa, J. C. Vanadium(IV) and Copper(II) Complexes of Salicylaldimines and Aromatic Heterocycles: Cytotoxicity, DNA Binding and DNA Cleavage Properties. *J. Inorg. Biochem.* **2015**, *147*, 134–146.
- (13) Ghosh, A.; Mandoli, A.; Kumar, D. K.; Yadav, N. S.; Ghosh, T.; Jha, B.; Thomas, J. A.; Das, A. DNA Binding and Cleavage Properties of a Newly Synthesised Ru(II)-Polypyridyl Complex. *Dalt. Trans.* **2009**, No. 42, 9312–9321.
- (14) Costas, M.; Mehn, M. P.; Jensen, M. P.; Que, L. Dioxygen Activation at Mononuclear Nonheme Iron Active Sites: Enzymes, Models, and Intermediates. *Chem. Rev.* **2004**, *104* (2), 939–986.
- (15) Parkin, G. Synthetic Analogues Relevant to the Structure and Function of Zinc Enzymes. *Chem. Rev.* **2004**, *104* (2), 699–767.
- (16) Bortolini, O.; Conte, V. Vanadium (V) Peroxocomplexes: Structure, Chemistry and Biological Implications. *J. Inorg. Biochem.* **2005**, *99* (8), 1549–1557.

Synthesis, characterisation, theoretical simulation and DNA nuclease activity of a newly synthesized Mn-based chemotherapeutic agent

- (17) Wu, A. J.; Penner-Hahn, J. E.; Pecoraro, V. L. Structural, Spectroscopic, and Reactivity Models for the Manganese Catalases. *Chem. Rev.* **2004**, *104* (2), 903–938.
- (18) Crans, D. C.; Smee, J. J.; Gaidamauskas, E.; Yang, L. The Chemistry and Biochemistry of Vanadium and the Biological Activities Exerted by Vanadium Compounds. *Chem. Rev.* **2004**, *104* (2), 849–902.
- (19) Mirica, L. M.; Ottenwaelder, X.; Stack, T. D. P. Structure and Spectroscopy of Copper-Dioxygen Complexes. *Chem. Rev.* **2004**, *104* (2), 1013–1045.
- (20) Pogozelski, W. K.; Tullius, T. D. Oxidative Strand Scission of Nucleic Acids: Routes Initiated by Hydrogen Abstraction from the Sugar Moiety. *Chem. Rev.* **1998**, *98* (3), 1089–1107.
- (21) Burrows, C. J.; Muller, J. G. Oxidative Nucleobase Modifications Leading to Strand Scission. *Chem. Rev.* **1998**, *98* (3), 1109–1151.
- (22) Kedarnath, G.; Jain, V. K. Pyridyl and Pyrimidyl Chalcogen (Se and Te) Compounds: A Family of Multi Utility Molecules. *Coord. Chem. Rev.* **2013**, *257* (7–8), 1409–1435.
- (23) Jeffery, G. H.; Bassett, J.; Mendham, J.; Denney, R. C. *Vogel's Text Book of Quantitative Chemical Analysis.*, Wesley Longman Limited, United Kingdom, 5th Ed, (1989).
- (24) Bühl, M.; Ashbrook, S. E.; Dawson, D. M.; Doyle, R. A.; Hrobárik, P.; Kaupp, M.; Smellie, I. A. Paramagnetic NMR of Phenolic Oxime Copper Complexes: A Joint Experimental and Density Functional Study. *Chem. – A Eur. J.* **2016**, *22* (43), 15328–15339.
- (25) Munde, A. S.; Jagdale, A. N.; Jadhav, S. M.; Chondhekar, T. K. Synthesis and Characterization of Some Transition Metal Complexes of Unsymmetrical Tetradentate Schiff Base Ligand. *J. Korean Chem. Soc.* **2009**, *53* (4), 407–414.

Synthesis, characterisation, theoretical simulation and DNA nuclease activity of a newly synthesized Mn-based chemotherapeutic agent

- (26) Nakamoto, K. *Infrared and Raman Spectra of Inorganic and Coordination Compounds Part B: Applications in Coordination, Organometallic, and Bioinorganic Chemistry Sixth Edition*.
- (27) Becke, A. D. Density-Functional Exchange-Energy Approximation with Correct Asymptotic Behavior. *Phys. Rev. A* **1988**, 38 (6), 3098.
- (28) Leung, K.; Rempe, S. B.; Schultz, P. A.; Sproviero, E. M.; Batista, V. S.; Chandross, M. E.; Medforth, C. J. Density Functional Theory and DFT+U Study of Transition Metal Porphines Adsorbed on Au(111) Surfaces and Effects of Applied Electric Fields. *J. Am. Chem. Soc.* **2006**, 128 (11), 3659–3668.
- (29) Lee, C.; Yang, W.; Parr, R. G. Development of the Colle-Salvetti Correlation-Energy Formula into a Functional of the Electron Density. *Phys. Rev. B* **1988**, 37 (2), 785.
- (30) Hay, P. J.; Wadt, W. R. Ab Initio Effective Core Potentials for Molecular Calculations. Potentials for K to Au Including the Outermost Core Orbitals. *J. Chem. Phys.* **1985**, 82 (1), 299–310.
- (31) Handy, N. C.; Henry, ; Schaefer, F.; Schaefer, H. F. On the Evaluation of Analytic Energy Derivatives for Correlated Wave Functions. *J. Chem. Phys.* **1984**, 81 (11), 5031–5033.
- (32) Nicklass, A.; Dolg, M.; Stoll, H.; Preuss, H. Ab Initio Energy-adjusted Pseudopotentials for the Noble Gases Ne through Xe: Calculation of Atomic Dipole and Quadrupole Polarizabilities. *J. Chem. Phys.* **1995**, 102 (22), 8942–8952.
- (33) Gaussian 09, (Revision A.1), Gaussian, Inc., Wallingford, CT, 2009.
- (34) Yanai, T.; Tew, D. P.; Handy, N. C. A New Hybrid Exchange–Correlation Functional Using the Coulomb-Attenuating Method (CAM-B3LYP). *Chem. Phys. Lett.* **2004**, 393 (1–3), 51–57.

Synthesis, characterisation, theoretical simulation and DNA nuclease activity of a newly synthesized Mn-based chemotherapeutic agent

- (35) Barone, V.; Cossi, M. Quantum Calculation of Molecular Energies and Energy Gradients in Solution by a Conductor Solvent Model. *J. Phys. Chem. A* **1998**, *102* (11), 1995–2001.
- (36) O’Boyle, N. M.; Tenderholt, A. L.; Langner, K. M. Cclib: A Library for Package-Independent Computational Chemistry Algorithms. *J. Comput. Chem.* **2008**, *29* (5), 839–845.
- (37) Chaires, J. B.; Dattagupta, N.; Crothers, D. M. Studies on Interaction of Anthracycline Antibiotics and Deoxyribonucleic Acid: Equilibrium Binding Studies on Interaction of Daunomycin with Deoxyribonucleic Acid. *Biochemistry* **1982**, *21* (17), 3933–3940.
- (38) Saha, U.; Mukherjea, K. K. DNA Binding and Nuclease Activity of an Oxovanadium Valinato-Schiff Base Complex. *Int. J. Biol. Macromol.* **2014**, *66*, 166–171.
- (39) Selim, M.; Mukherjea, K. K. The Nuclease Activity of an Oxo-Peroxo Molybdenum Complex. *J. Biomol. Struct. Dyn.* **2009**, *26* (5), 561–566.
- (40) Pradeep, C. P.; Zacharias, P. S.; Das, S. K. A Chiral Mn(IV) Complex and Its Supramolecular Assembly: Synthesis, Characterization and Properties. *J. Chem. Sci.* **2006**, *118* (4), 311–317.
- (41) Mabad, B.; Cassoux, P.; Tuchagues, J. P.; Hendrickson, D. N. Manganese(II) Complexes of Polydentate Schiff Bases. 1. Synthesis, Characterization, Magnetic Properties, and Molecular Structure. *Inorg. Chem.* **1986**, *25* (9), 1420–1431.
- (42) A.H. Manikshete, M.M.Awatade, S. K. Sarsamkar, M. R. A. No Title. *Int. J. Eng. Sci. Inven.* **2015**, *4*, 22.
- (43) A.Earnshaw. “*Magnetochemistry Academic Press*”, Newyork (1968).
- (44) Ghosh, D.; Saha, U.; Mukherjea, K. K. A Light Harvesting Mononuclear Manganese(II) Complex: Synthesis, Characterization, DFT and TDDFT Calculations and

Synthesis, characterisation, theoretical simulation and DNA nuclease activity of a newly synthesized Mn-based chemotherapeutic agent

- Photophysical Profile. *RSC Adv.* **2014**, 4 (30), 15558–15568.
- (45) Kandel, L. D.; Passeggi, M. C. G.; Buch, T. Gyromagnetic Factors and Covalency in Tetrahedral D₅— Complexes. *J. Phys. Chem. Solids* **1969**, 30 (2), 321–328.
- (46) Weil, J. A.; Bolton, J. R. *Electron Paramagnetic Resonance: Elementary Theory and Practical Applications, Second Edition, John Wiley & Sons, Inc, (2007).*; John Wiley & Sons, Inc.: Hoboken, NJ, USA, 2006.
- (47) Liu, T.; Zhang, H. X.; Xia, B. H. Theoretical Studies on Structures and Spectroscopic Properties of a Series of Novel Cationic [Trans-(CAN)₂Ir(PH₃)₂]⁺ (CAN = Ppy, Bzq, Ppz, Dfppy). *J. Phys. Chem. A* **2007**, 111 (35), 8724–8730.
- (48) Zhou, X.; Zhang, H. X.; Pan, Q. J.; Xia, B. H.; Tang, A. C. Theoretical Studies of the Spectroscopic Properties of [Pt(Trpy)C≡CR] + (Trpy = 2,2',6',2''-Terpyridine; R = H, CH₂OH, and C₆H₅). *J. Phys. Chem. A* **2005**, 109 (39), 8809–8818.
- (49) Zhou, X.; Ren, A. M.; Feng, J. K. Theoretical Studies on the Ground States in M(Terpyridine)₂²⁺ and M(n-Butyl-Phenylterpyridine)₂²⁺ (M = Fe, Ru, Os) and Excited States in Ru(Terpyridine)₂²⁺ Using Density Functional Theory. *J. Organomet. Chem.* **2005**, 690 (2), 338–347.
- (50) Albertino, A.; Garino, C.; Ghiani, S.; Gobetto, R.; Nervi, C.; Salassa, L.; Rosenberg, E.; Sharmin, A.; Viscardi, G.; Buscaino, R.; Croce, G.; Milanesio, M. Photophysical Properties and Computational Investigations of Tricarbonylrhenium(I)[2-(4-Methylpyridin-2-Yl)Benzo[d]-X-Azole]L and Tricarbonylrhenium(I)[2-(Benzo[d]-X-Azol-2-Yl)-4-Methylquinoline]L Derivatives (X = N-CH₃, O, or S; L = Cl⁻, Pyridine). *J. Organomet. Chem.* **2007**, 692 (6), 1377–1391.
- (51) Fu, X.-X.; Li, J.-F.; Zhang, R.-Q. Strong Orbital Interaction in Pi-Pi Stacking System. *doi arXiv1601.01150* **2016**.

Synthesis, characterisation, theoretical simulation and DNA nuclease activity of a newly synthesized Mn-based chemotherapeutic agent

- (52) Asadi, Z.; Mosallaei, H.; Sedaghat, M.; Yousefi, R. Competitive Binding Affinity of Two Lanthanum(III) Macrocyclic Complexes toward DNA and Bovine Serum Albumin in Water. *J. Iran. Chem. Soc.* **2017**, *14* (11), 2367–2385.
- (53) Li, H.; Le, X. Y.; Pang, D. W.; Deng, H.; Xu, Z. H.; Lin, Z. H. DNA-Binding and Cleavage Studies of Novel Copper(II) Complex with L-Phenylalaninate and 1,4,8,9-Tetra-Aza-Triphenylene Ligands. *J. Inorg. Biochem.* **2005**, *99* (11), 2240–2247.
- (54) Mandegani, Z.; Asadi, Z.; Asadi, M.; Karbalaeei-Heidari, H. R.; Rastegari, B. Synthesis, Characterization, DNA Binding, Cleavage Activity, Cytotoxicity and Molecular Docking of New Nano Water-Soluble $[M(5-CH_2PPh_3-3,4-Salpyr)](ClO_4)_2$ (M = Ni, Zn) Complexes. *Dalt. Trans.* **2016**, *45* (15), 6592–6611.
- (55) Shahabadi, N.; Kashanian, S.; Khosravi, M.; Mahdavi, M. Multispectroscopic DNA Interaction Studies of a Water-Soluble Nickel(II) Complex Containing Different Dinitrogen Aromatic Ligands. *Transit. Met. Chem.* **2010**, *35* (6), 699–705.
- (56) Asadi, Z.; Nasrollahi, N.; Karbalaeei-Heidari, H.; Eigner, V.; Dusek, M.; Mobaraki, N.; Pournajati, R. Investigation of the Complex Structure, Comparative DNA-Binding and DNA Cleavage of Two Water-Soluble Mono-Nuclear Lanthanum(III) Complexes and Cytotoxic Activity of Chitosan-Coated Magnetic Nanoparticles as Drug Delivery for the Complexes. *Spectrochim. Acta Part A Mol. Biomol. Spectrosc.* **2017**, *178*, 125–135.
- (57) Liu, Y. chun; Yang, Z. yin. Crystal Structures, Antioxidation and DNA Binding Properties of Dy(III) Complexes with Schiff-Base Ligands Derived from 8-Hydroxyquinoline-2-Carboxaldehyde and Four Aroylhydrazines. *Eur. J. Med. Chem.* **2009**, *44* (12), 5080–5089.
- (58) Satyanarayana, S.; Dabrowiak, J. C.; Chaires, J. B. Tris(Phenanthroline)Ruthenium(II)

Synthesis, characterisation, theoretical simulation and DNA nuclease activity of a newly synthesized Mn-based chemotherapeutic agent

- Enantiomer Interactions with DNA: Mode and Specificity of Binding. *Biochemistry* **1993**, 32 (10), 2573–2584.
- (59) Sigman, D. S.; Mazumder, A.; Perrin, D. M. Chemical Nucleases. *Chem. Rev.* **1993**, 93 (6), 2295–2316.
- (60) Wang, Y.; Yang, Z. Y.; Wang, Q.; Cai, Q. K.; Yu, K. B. Crystal Structure, Antitumor Activities and DNA-Binding Properties of the La(III) Complex with Phthalazin-1(2H)-One Prepared by a Novel Route. *J. Organomet. Chem.* **2005**, 690 (21–22), 4557–4563.
- (61) Satyanarayana, S.; Dabrowiak, J. C.; Chaires, J. B. Neither Δ -nor Δ -Tris(Phenanthroline)Ruthenium(II) Binds to DNA by Classical Intercalation. *Biochemistry* **1992**, 31 (39), 9319–9324.
- (62) Patra, S.; Chatterjee, S.; Si, T. K.; Mukherjea, K. K. Synthesis, Structural Characterization, VHPO Mimicking Peroxidative Bromination and DNA Nuclease Activity of Oxovanadium(V) Complexes. *Dalt. Trans.* **2013**, 42 (37), 13425–13435.
- (63) Palmajumder, E.; Sepay, N.; Mukherjea, K. K. Development of Oxidovanadium and Oxido-Peroxido Vanadium-Based Artificial DNA Nucleases via Multi Spectroscopic Investigations and Theoretical Simulation of DNA Binding. *J. Biomol. Struct. Dyn.* **2017**, 36 (4), 919–927.
- (64) Naskar, S.; Palmajumder, E.; Patra, S.; Mitra, J.; Mukherjea, K. K. Biomimicking Oxidative Bromination and DNA Nuclease Activities of a New Structurally Characterised Oxido-Diperoxidomolybdenum(VI) Complex. *ChemistrySelect* **2017**, 2 (31), 10199–10205.
- (65) Chowdhury, S. R.; Selim, M.; Chatterjee, S.; Igarashi, S.; Yukawa, Y.; Mukherjea, K. K. Synthesis, Structure, DNA-Binding, and Nuclease Activity of a 3d–4f Mixed Metal Nitrosyl Complex, $[\text{Pr}(\text{Phen})_2(\text{MeOH})(\text{H}_2\text{O})_2][\text{Fe}(\text{CN})_5(\text{NO})]$.

Synthesis, characterisation, theoretical simulation and DNA nuclease activity of a newly synthesized Mn-based chemotherapeutic agent

- (Phen)(DMF)(MeOH)(H₂O). *J. Coord. Chem.* **2012**, 65 (19), 3469–3480.
- (66) Saha, U.; Mukherjea, K. K. Development of a Multifunctional Biomimicking 1 - Cysteine Based Oxovanadium(Iv) Complex: Synthesis, DFT Calculations, Bromo-Peroxidation and Nuclease Activity. *RSC Adv.* **2015**, 5 (114), 94462–94473.
- (67) Tabassum, S.; Al-Asbahy, W. M.; Afzal, M.; Arjmand, F.; Bagchi, V. Molecular Drug Design, Synthesis and Structure Elucidation of a New Specific Target Peptide Based Metallo Drug for Cancer Chemotherapy as Topoisomerase I Inhibitor. *Dalt. Trans.* **2012**, 41 (16), 4955–4964.

Chapter 9

Synthesis and Characterization

of a Dioxomolybdenum Complex [*cis*-MoO₂(BHAN)₂]

Using β -hydroxy- α -naphthaldehyde (BHAN) as Ligand

**Synthesis and characterization of a Dioxomolybdenum complex [*cis*-MoO₂(BHAN)₂]
using β -hydroxy- α -naphthaldehyde (BHAN) as ligand**

1. Introduction:

In the realm of coordination chemistry, the synthesis and characterization of transition metal complexes play a pivotal role in expanding our understanding of their structural diversity, reactivity, and potential applications. Among these complexes, Molybdenum, a 4d transition element, plays a vital role in various biological functions necessary for life on Earth. The physiologically active oxidation states of molybdenum include +4, +5, and +6, and it is commonly found coordinated to proteins.^{1,2} Molybdenum-based compounds have garnered significant attention due to their unique properties and catalytic capabilities in various chemical transformations. In this context, the utilization of novel ligands can impart enhanced coordination abilities and tailor the reactivity of the resulting complexes. In recent years, the development of new ligands derived from aromatic aldehydes has emerged as a fascinating area of research in coordination chemistry. β -Hydroxy- α -naphthaldehyde (BHAN), a readily available compound, serves as a valuable starting material for the synthesis of diverse metal complexes. This compound features a salicylic functional group, which is highly sought after in nucleophilic addition reactions. The activation of its carbonyl group is facilitated by the presence of phenolic hydrogen, leading to the formation of an intramolecular hydrogen bond. Such interactions contribute to the reactivity and selectivity of this compound as a good ligand making it an excellent candidate for the development of novel metal complexes.³

Within this context, this thesis focuses on the synthesis of a molybdenum *cis*-dioxo complex utilizing BHAN as a ligand. The incorporation of BHAN into the coordination sphere of molybdenum allows for the exploration of its electronic and steric effects on the resulting complex, and subsequently, the investigation of its reactivity in various catalytic and biological applications.

Synthesis and characterization of a Dioxomolybdenum complex [*cis*-MoO₂(BHAN)₂]

using β -hydroxy- α -naphthaldehyde (BHAN) as ligand

2. Experimental Procedures:

2.1. Materials and methods:

Ammonium molybdate tetrahydrate of extra-pure quality were obtained from E. Merck, India. β -Hydroxy- α -naphthaldehyde (BHAN) was obtained from Sigma Aldrich and was used as obtained. All other reagents used, were purchased from E. Merck (India) and was used as obtained. Solvents used for physico-chemical studies were of analytical reagent grade and were further purified as suggested in the literature whenever necessary.⁴

2.2. Physical Measurements:

IR spectra were run on KBr discs at room temperature on a Perkin Elmer RFX-I IR spectrophotometer. Perkin-Elmer 2400 series II CHNS analyser was used for elemental analyses. UV-vis spectra (200–800 nm) were recorded against appropriate reagent blanks on a Shimadzu U-1800 spectrophotometer using 1 cm quartz cell. Mass spectrum was recorded on Micromass Q-T of microTM, Waters Corporation.

2.3. Preparation of the complex:

To a methanolic solution of β -Hydroxy- α -naphthaldehyde (BHAN) (0.018 mol), an aqueous solution of [(NH₄)₆Mo₇O₂₄, 4H₂O] (1.23 g) was added with constant stirring.⁵ To this mixture, concentrated HCl (12M, 1ml) was added dropwise. A yellow precipitate appeared. The mixture was stirred at room temperature for 4 h to achieve complete precipitation. The solid was collected by filtration, washed with cold water and methanol and dried under vacuum. It was purified by recrystallization. The yield was 80%. Despite multiple attempts, diffractable grade suitable single crystals were not obtained. Hence, an attempt was made to characterize the complex in solid state as well as in solution. IR (KBr, cm⁻¹); complex [*cis*-MoO₂(BHAN)₂] (C₂₂H₁₄MoO₆):911 and 935 [ν (Mo=O)]. ESI-MS (+ve) in MeOH: m/z (relative intensity): 471.98 [M⁺]. UV-Vis (λ_{\max} /nm) for complex: 220, 255, 290, 317. Elemental analysis, calc. C, 56.18%; H, 3.00%; Found: C, 56.08%; H, 2.90%.

2.4. Structural optimization of the complex by DFT calculations:

The ground state molecular geometry of the complex was optimized using the B3LYP function, a widely used method known for providing reliable and accurate results for geometrical parameters. To calculate optical properties, time-dependent density functional method was used with CAM-B3LYP functional (TD-CAM-B3LYP). All calculations were performed using Gaussian 09 program package.⁶ Ground state geometry was fully optimized using B3LYP method with conductor-like polarization continuum model (CPCM) of solvent in an aqueous medium. The B3LYP method includes exchange and correlation effects by incorporating a hybrid exchange-correlation functional (Becke + Slater + HF exchange and LYP + VWN5 correlations).⁷⁻⁹ The CPCM solvent model accounts for polarized solute-solvent interaction, including geometry relaxation of the solute in equilibrium with solvent reaction field.¹⁰ The basis set used included 6-311++G(d,p) for C, H, and O atoms and 3-21G(d) for Mo. The calculated vibrational frequencies were all found to be real, indicating a true minimum in the potential hypersurface. To determine solvent-modified transition energy and spectroscopic properties associated with the vertical excitations of the complex, TD-DFT method was used with CAM-B3LYP functional (TD-CAM-B3LYP) in the CPCM solvent model, with the same basis set as was used for optimization calculation. Excited state calculations were carried out for the forty lowest-lying singlet states.

3. Results & Discussions:

3.1. Synthetic aspects of the complex:

The complex was synthesized following scheme 1 (Figure 1). The isolated complex from the reaction mixture was washed thoroughly with cold water and methanol several times and dried under vacuum. It was then purified by recrystallization. The complex was found to be stable in air. It was a yellow colored material. The compound was found to be soluble in organic solvents like methanol, ethanol and acetonitrile behaving as a non-electrolyte.

Synthesis and characterization of a Dioxomolybdenum complex [*cis*-MoO₂(BHAN)₂]
using β -hydroxy- α -naphthaldehyde (BHAN) as ligand

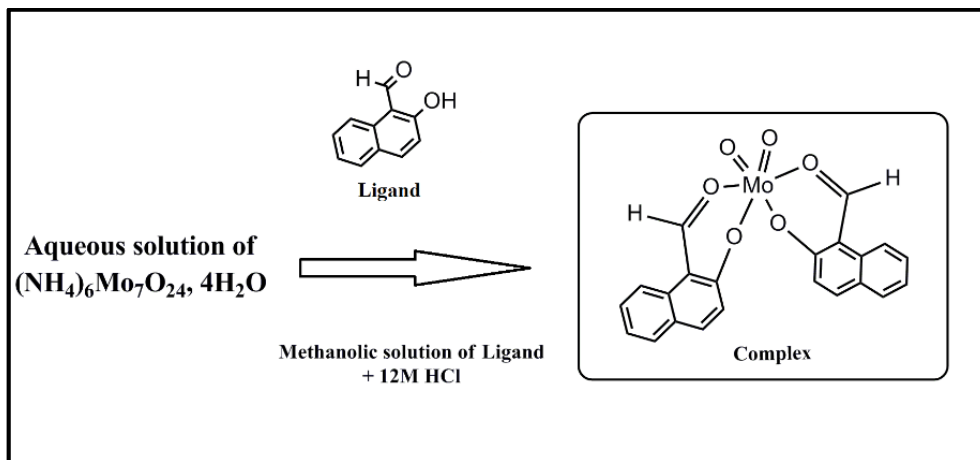


Figure 1: Scheme 1- Synthetic scheme of complex [*cis*-MoO₂(BHAN)₂]

3.2. Spectral characterisations:

3.2.1. IR and UV-Vis spectral analysis:

The IR spectrum shows strong stretching vibrations $\nu_{\text{Mo}=\text{O}}$ at 911, 935 cm^{-1} for two oxo groups that are mutually *cis* to each other (Figure 2). The electronic spectral bands at 220 nm could be assigned to intra ligand $\pi \rightarrow \pi^*$ transitions of the aromatic ring. Additional two bands around 255 nm and 290 nm for complex were assigned to $n \rightarrow \pi^*$ of C=O of the two coordinated ligands¹¹. The experimental values of spectroscopic techniques (IR and UV) were further supported by DFT studies to an extent of reasonable agreement. Molar conductivity values in methanol clearly indicates that the *cis*-MoO₂(BHAN)₂ is a non-electrolyte.

Synthesis and characterization of a Dioxomolybdenum complex [*cis*-MoO₂(BHAN)₂]

using β -hydroxy- α -naphthaldehyde (BHAN) as ligand

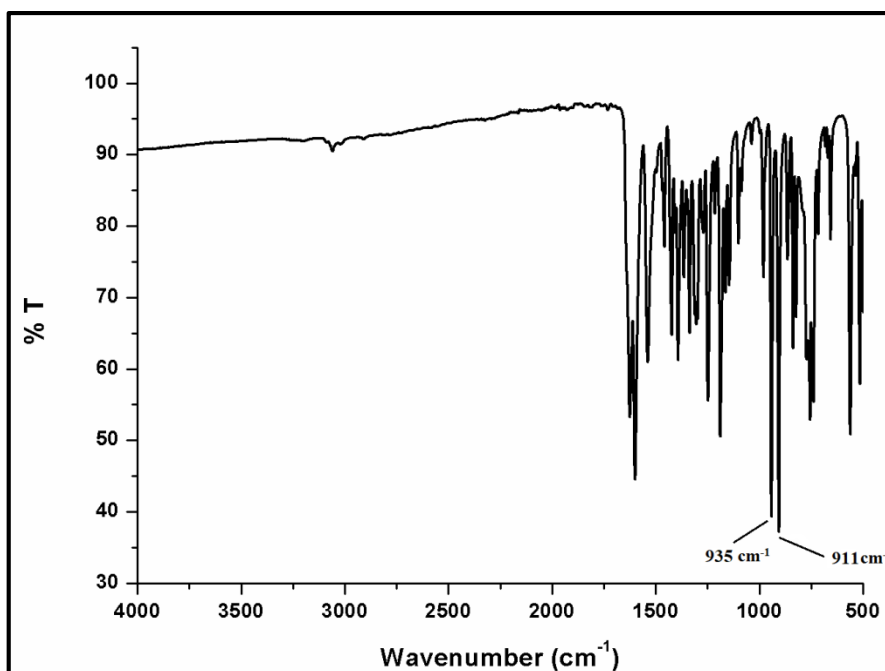


Figure 2: IR spectra of the *cis*-MoO₂(BHAN)₂

3.2.2. NMR spectral analysis:

¹H NMR confirmed that the *cis*-MoO₂(BHAN)₂ as well as ligand (BHAN) was stable in solution phase. In case of the complex, phenolic –OH was deprotonated characterized by a disappearance of the proton signal at δ 12 (Figure 3).

Synthesis and characterization of a Dioxomolybdenum complex [*cis*-MoO₂(BHAN)₂]
using β -hydroxy- α -naphthaldehyde (BHAN) as ligand

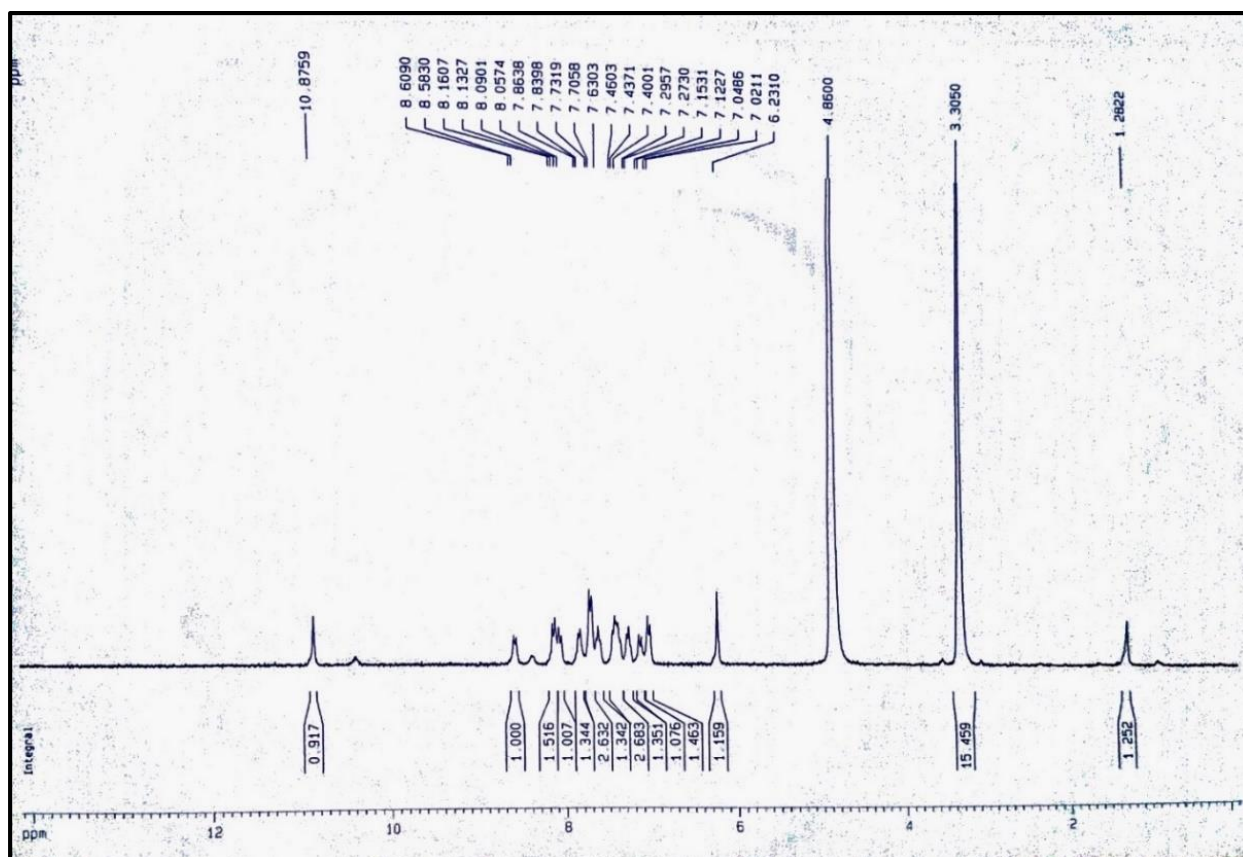


Figure 3: NMR spectra of the *cis*-MoO₂(BHAN)₂

This suggests the ligand (BHAN) behaves as a mono anionic O, O donor. Aromatic protons in case of the free ligand appears at 8.9-7.2 ppm (Figure 4), while these were found at 7.01-8.6 ppm in the complex (Figure 3). From the shift of aromatic proton signals it could be concluded that the ligand was coordinated to the metal in the complex. Moreover, the presence of aromatic proton signals in the *cis*-MoO₂(BHAN)₂ are a clear indication that ligands are present in the zone of coordination.

Synthesis and characterization of a Dioxomolybdenum complex [*cis*-MoO₂(BHAN)₂]
using β -hydroxy- α -naphthaldehyde (BHAN) as ligand

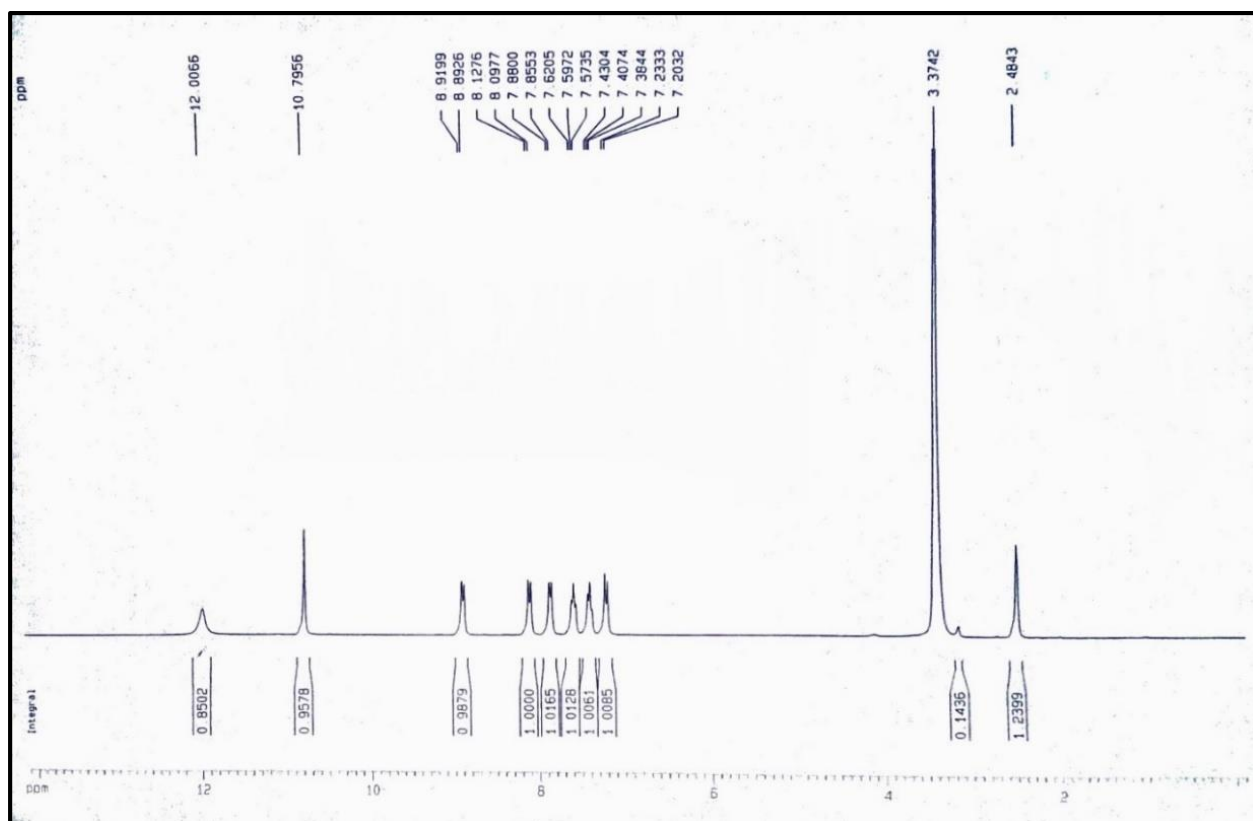


Figure 4: NMR spectra of the **ligand (BHAN)**

4. Optimization of Molecular geometry and electronic structure:

DFT study is an important tool to obtain better insight into the geometry, electronic structure, and optical properties of coordinated systems. Geometry of both ligand and complex [*cis*-MoO₂(BHAN)₂] were optimized by Density Functional Theory (DFT). The ground state optimized geometry of the complex is shown in Figure 5. Important optimized geometrical parameters of the complex are listed in Table 2.

Synthesis and characterization of a Dioxomolybdenum complex [*cis*-MoO₂(BHAN)₂]
using β -hydroxy- α -naphthaldehyde (BHAN) as ligand

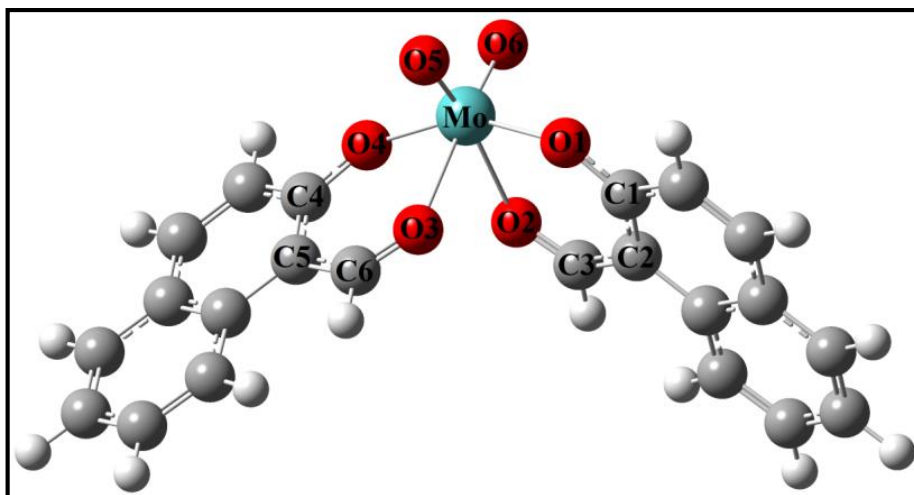


Figure 5: The B3LYP optimized ground state electronic structure of *cis*-MoO₂(BHAN)₂ in water

Table 2: Selected optimized geometrical parameters for *cis*-MoO₂(BHAN)₂ in the ground state calculated at B3LYP levels

Type of bonds	Bond Lengths (Å)
Mo-O1	2.02
Mo-O2	2.23
Mo-O3	2.34
Mo-O4	1.97
Mo-O5	1.71
Mo-O6	1.70
Type of bonds	Bond Angles (°)
<O1-Mo-O2	78.25
<O2-Mo-O3	75.31
<O3-Mo-O4	77.40

Synthesis and characterization of a Dioxomolybdenum complex [*cis*-MoO₂(BHAN)₂]

using β -hydroxy- α -naphthaldehyde (BHAN) as ligand

<O3-Mo-O4	100.57
<O5-Mo-O6	104.14

The calculated IR frequencies of the investigated molecule were found to be in good agreement with experimental results (see **Table 3**).

Table 3: B3LYP/6-311++G(d,p) [6-311++G(d,p) for C, H, O and 3-21G(d) for Mo]

Calculated IR frequencies ($\bar{\nu}$, cm⁻¹) and intensities obtained for *cis*-MoO₂(BHAN)₂ using CPCM Model.

Frequency	Theoretical values (cm ⁻¹)	Experimental Values (cm ⁻¹)
Mo-Complex		
ν Mo=O (cis)	912.8	935.4
	844.8	911.1

The solvent modified transition energy and spectroscopic properties associated with vertical excitations of the chosen complex [*cis*-MoO₂(BHAN)₂] was calculated at the solvent-modified geometry using the time-dependent density functional method for CAM-B3LYP functional (TD-CAM-B3LYP) in the framework of the CPCM solvent model for the same set of basis set as employed in the optimization calculation. The excited state calculations were carried out for forty lowest lying singlet states. The TD-DFT approach has been demonstrated to be reliable for calculating spectral properties of many transition metal complexes.¹²⁻¹⁴ The calculated results obtained for important electronic transitions are presented in Table 4. Calculated results for the λ_{max} obtained for complex was in good agreement with the

Synthesis and characterization of a Dioxomolybdenum complex [*cis*-MoO₂(BHAN)₂]

using β -hydroxy- α -naphthaldehyde (BHAN) as ligand

corresponding experimental results. The frontier molecular orbital diagrams (Figure 6) involved in electronic transitions indicate significant reorganization of charge distribution around the symmetric structure leading to shift in electron density either from ligand to the molybdenum-oxygen moiety or vice versa.

Table 4: TD-CAM-B3LYP/6-311++G(d,p) Calculated Transition Wavelength (λ_{max} , nm), Oscillator Strength (f_0) and Transition MOs Involved in the Crucial Transition obtained for *cis*-MoO₂(BHAN)₂ in Water Solvent Using CPCM Model

λ_{max} (Cal.)	λ_{max} (Exp.)	% of deviation	Oscillator strength (f_0)	Major transition
233.0	220.0	5.6	0.18	H-11→L+2
255.7	255.0	0.27	0.06	H-2→L+2
284.9	290.0	1.79	0.09	H-4→L+1
321.8	317.0	1.49	0.35	H-3→L
400.0	385.0	3.75	0.06	H→L

Synthesis and characterization of a Dioxomolybdenum complex [*cis*-MoO₂(BHAN)₂]
using β -hydroxy- α -naphthaldehyde (BHAN) as ligand

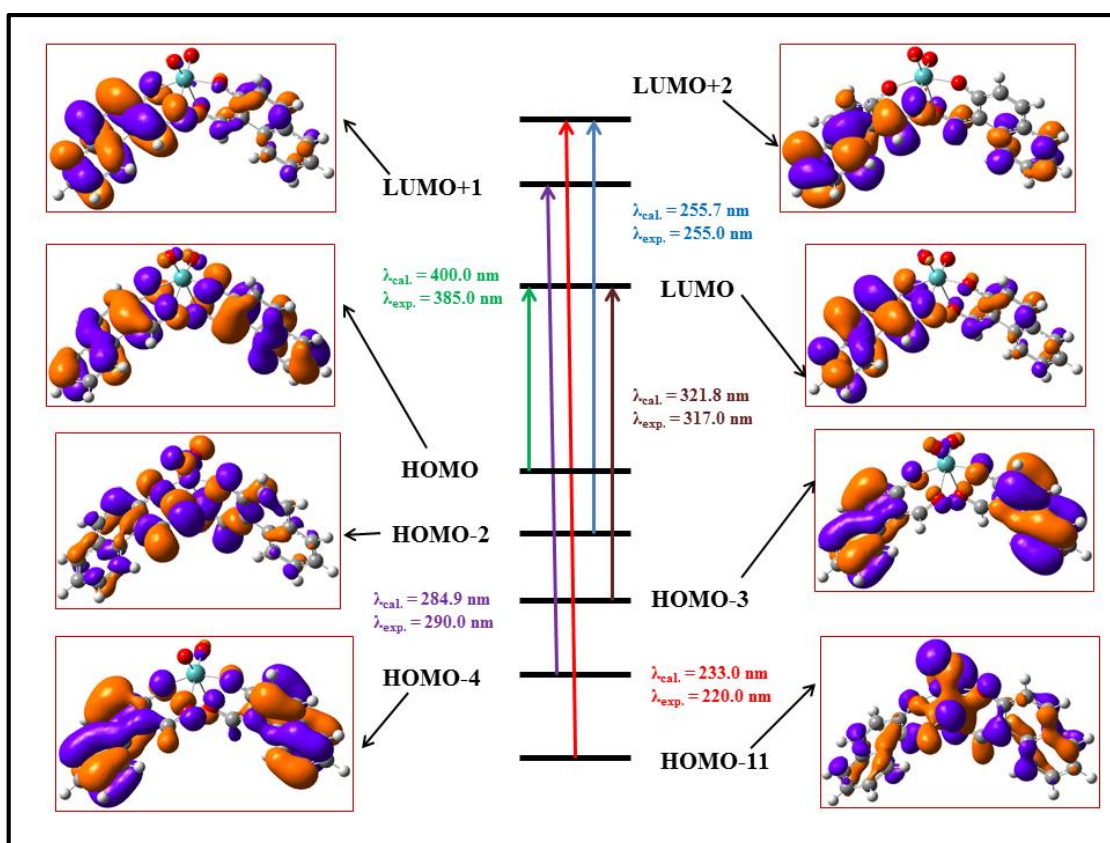


Figure 6: Frontier molecular orbitals involved in the UV-vis absorption of *cis*-MoO₂(BHAN)₂ in aqueous solution at room temperature

5. Conclusion:

The present chapter describes the synthesis and characterization of a Molybdenum based complex, *cis*-MoO₂(BHAN)₂ that was characterized using various spectroscopic methods like IR, ESI-MS, UV-VIS, NMR etc. The structure of the complex was also arrived at using DFT showing very good agreement with experimental findings so that it may be concluded that the *cis*-MoO₂(BHAN)₂ was synthesized successfully and isolated in very pure form

Synthesis and characterization of a Dioxomolybdenum complex [*cis*-MoO₂(BHAN)₂]
using β -hydroxy- α -naphthaldehyde (BHAN) as ligand

References:

- (1) Moula, G.; Bose, M.; Sarkar, S. Replica of a Fishy Enzyme: Structure-Function Analogue of Trimethylamine-n-Oxide Reductase. *Inorg. Chem.* **2013**, 52 (9), 5316–5327.
- (2) Mitra, J.; Sarkar, S. Modelling the Reduced Xanthine Oxidase in Active Sulfo and Inactive Desulfo Forms. *Dalt. Trans.* **2013**, 42 (9), 3050–3058.
- (3) Das, A. K.; Goswami, S. 2-Hydroxy-1-Naphthaldehyde: A Versatile Building Block for the Development of Sensors in Supramolecular Chemistry and Molecular Recognition. *Sensors Actuators, B Chem.* **2017**, 245, 1062–1125.
- (4) G.H. Jeffery, J. Bassett, J. Mendham, R. C. D. A. *Vogel's Text Book of Quantitative Chemical Analysis, 5th Ed., Wesley Longman Limited, United Kingdom, 1989.*
- (5) Yamanouchi, K.; Yamada, S. Oxomolybdenum Complexes with Schiff Bases Obtained from Salicylaldehyde Derivatives and Alkyl- and Aryl-Amines. *Inorganica Chim. Acta* **1974**, 9, 83–86.
- (6) Gaussian 09, (Revision A.1), Gaussian, Inc., Wallingford, CT, 2009.
- (7) Becke, A. D. Density-functional Thermochemistry. III. The Role of Exact Exchange. *J. Chem. Phys.* **1993**, 98, 5648–5652.
- (8) Stephens, P. J.; Devlin, F. J.; Chabalowski, C. F.; Frisch, M. J. Ab Initio Calculation of Vibrational Absorption and Circular Dichroism Spectra Using Density Functional Force Fields. *J. Phys. Chem.* **1994**, 98 (45), 11623–11627.
- (9) Hertwig, R. H.; Koch, W. On the Parameterization of the Local Correlation Functional. What Is Becke-3-LYP? *Chem. Phys. Lett.* **1997**, 268 (5–6), 345–351.

**Synthesis and characterization of a Dioxomolybdenum complex [*cis*-MoO₂(BHAN)₂]
using β -hydroxy- α -naphthaldehyde (BHAN) as ligand**

- (10) Cossi, M.; Rega, N.; Scalmani, G.; Barone, V. Energies, Structures, and Electronic Properties of Molecules in Solution with the C-PCM Solvation Model. *J. Comput. Chem.* **2003**, *24* (6), 669–681.
- (11) Paul, S. S.; Selim, M.; Mukherjea, K. K. Synthesis, Characterization and DNA Nuclease Activity of Oxo-Peroxomolybdenum(VI) Complexes. *J. Coord. Chem.* **2017**, *70* (10), 1739–1760.
- (12) Zhou, X.; Ren, A. M.; Feng, J. K. Theoretical Studies on the Ground States in M(Terpyridine)₂²⁺ and M(n-Butyl-Phenylterpyridine)₂²⁺ (M = Fe, Ru, Os) and Excited States in Ru(Terpyridine)₂²⁺ Using Density Functional Theory. *J. Organomet. Chem.* **2005**, *690* (2), 338–347.
- (13) Zhou, X.; Zhang, H. X.; Pan, Q. J.; Xia, B. H.; Tang, A. C. Theoretical Studies of the Spectroscopic Properties of [Pt(Trpy)C≡CR] + (Trpy = 2,2',6',2''-Terpyridine; R = H, CH₂OH, and C₆H₅). *J. Phys. Chem. A* **2005**, *109* (39), 8809–8818.
- (14) Liu, T.; Zhang, H. X.; Xia, B. H. Theoretical Studies on Structures and Spectroscopic Properties of a Series of Novel Cationic [Trans-(CAN)₂Ir(PH₃)₂]⁺ (CAN = Ppy, Bzq, Ppz, Dfppy). *J. Phys. Chem. A* **2007**, *111* (35), 8724–8730.

Chapter 10

***cis*-MoO₂(BHAN)₂ Complex: its Role in the Protection of Radiation-Induced DNA Damage**

1. Introduction:

Radiation therapy is an essential treatment for many types of cancer, but it can also damage healthy tissue. This damage is mainly caused by reactive oxygen species (ROS) generated during radiolysis¹, which can attack and modify DNA molecules. One potential strategy to mitigate this damage is to use antioxidants that scavenge ROS and prevent their harmful effects.² Dioxomolybdenum complexes have shown promise in this regard due to their ability to act as efficient radical scavengers.³ These complexes consist of a molybdenum atom surrounded by two oxo-bonds in a *cis* configuration, with additional ligands that can influence their reactivity and selectivity. By interacting with ROS and converting them into less harmful species, dioxomolybdenum complexes could potentially protect DNA from radiation-induced damage. Recent studies have investigated the interactions between the Dioxomolybdenum complex and DNA and their ability to protect DNA from radiation damage.⁴ In this chapter, the ability of the synthesized Dioxomolybdenum complex to protect DNA from gamma radiation is explored and demonstrated. It has been found that the complex was able to scavenge radicals generated during radiolysis which was examined by Electron paramagnetic resonance (EPR) and thus can prevent DNA damage. The protective effects of Dioxomolybdenum complex has also been investigated *in vitro*. Overall, the Dioxomolybdenum complex shows promise as an efficient scavenger of ROS generated during radiation therapy. Thus, their ability to protect DNA from damage suggests that they could be used as radioprotectors for normal tissue during radiotherapy. Further studies are needed to optimize their selectivity and efficacy and investigate potential side effects or toxicity.

2. Experimental Procedures:

2.1. Materials and physical methods:

calf thymus DNA and supercoiled plasmid pUC19 DNA were obtained from Sigma Chemical Company, USA, and Genei, India, respectively. All DNA solutions were prepared in Tris-HCl buffer; at pH 7.4. Concentration of calf thymus DNA was determined considering molar extinction coefficient at 260 nm to be 6600 M⁻¹ cm⁻¹. Absorbance at 260 nm and 280 nm were noted for calculating A₂₆₀/A₂₈₀. Values being greater than 1.8 but less than 1.9 indicate the DNA was sufficiently free of protein. Quality of calf thymus DNA was also checked by its characteristic circular dichroism band at 260 nm recorded on a J815 Spectropolarimeter. The investigation was conducted using Millipore water.

2.2. Physical Measurements:

Gamma radiation was passed through DNA solution with the help of a GC-900 Gama Chamber. Emission intensity were measured with a Perkin Elmer LS-55 spectrofluorimeter. Electron paramagnetic resonance (EPR) measurements were performed in Jeol JES-FA 200 ESR spectrometer equipped with a Jeol microwave bridge. The gel electrophoresis study was carried out with UVP Bio Doc-It Imaging System and nicking was assayed by UVP DOC-ItLS software.

3. DNA binding Studies:

3.1. Emission studies for DNA interaction:

the Complex [*cis*-MoO₂(BHAN)₂] was also subjected to titration with increasing concentrations of DNA, by the emission spectroscopy technique. In this experiment, the excitation of the methanolic solution of *cis*-MoO₂(BHAN)₂ at 317 nm shows emission with λ_{\max} at 353 nm. The experimental data obtained from fluorescence quenching were further

analyzed using the Stern-Volmer equation (1)^{3,5}, a widely used equation to quantify the quenching of fluorescence.

$$I_0/I = 1 + K_{SV}[\text{DNA}] \quad (1)$$

Where I_0 and I are the fluorescence intensities in the absence and presence of DNA, respectively; and K_{SV} is the Stern–Volmer quenching constant, which is a measure of the efficiency of quenching by DNA, providing valuable insights into the nature and strength of the binding interaction between the *cis*-MoO₂(BHAN)₂ and calf thymus DNA. These results contribute significantly to our understanding of the binding behavior and potential applications of the *cis*-MoO₂(BHAN)₂ in DNA-related studies.

3.2. Viscometric study:

Viscosity measurement data were presented as $(\eta/\eta_0)^{1/3}$ versus the ratio of the concentration of either of the ligand or the complex to that of the calf thymus DNA, where η_0 is the viscosity of calf thymus DNA solution alone and η is the viscosities of calf thymus DNA solution in the presence of the *cis*-MoO₂(BHAN)₂.⁶ The values were calculated from the observed flow time of calf thymus DNA by the relation; $\eta = t - t_0$, where t and t_0 are the values of flow times for the solution and the buffer respectively.

4. DNA damage and protection:

4.1. Irradiation by gamma-ray:

The calf thymus DNA and DNA-complex samples were incubated at 37 °C for 30 min and then irradiated in a ⁶⁰Co γ -chamber at a dose rate of 1.88 kGyhr⁻¹ for a total dose of 35 Gy. The irradiation doses for plasmid DNA samples were either 20 or 25 Gy. Our experimental design entailed administering a radiation dose that significantly surpassed the standard therapeutic dosage employed in normal radiotherapy to treat cancer patients. This deliberate augmentation of radiation dosage aimed to induce a comprehensive disruption of DNA,

enabling us to evaluate the potential of the synthesized compounds in protecting DNA against such extensive damage. Notably, all experiments were meticulously conducted in well-controlled *in-vitro* settings, providing us with a suitable platform to explore the effects of higher radiation doses. This line of investigation holds promise for the clinical application of these compounds as a good radioprotectors during radiotherapy.

4.2. Assessment of DNA damage followed by irradiation:

4.2.1. Estimation of radiation induced damage in calf thymus DNA by fluorescence

spectroscopy:

Here, calf thymus DNA solution was irradiated by a ⁶⁰Co-γ source as described earlier. Then the radiation induced calf thymus DNA damage was assessed by fluorescence spectroscopy using ethidium bromide (EB) as probe. Thereafter, the emissions were recorded at 591 nm after excitation at 500 nm. This was compared with the fluorescence of the non-irradiated DNA-EB system under identical experimental set-up. The dose–response relation is obtained from the plot of $(I-I_a)/(I_0-I_a)$ versus dose^{3,7}, where I_a is the fluorescence intensity of EB, I_0 , the fluorescence intensity of EB-DNA control and I , the fluorescence intensity of EB-DNA irradiated sample.

4.2.2. Protection of plasmid pUC19 DNA from radiation induced damage by the complexes and the ligand against different doses of gamma-radiation:

Supercoiled pUC19 DNA solutions were pre-incubated for 30 min with different concentrations of complex or the ligand (0–2 mM) were exposed to different doses of 20 or 25 Gy gamma radiation. The agarose gel electrophoresis technique monitored the DNA damage protective ability of *cis*-MoO₂(BHAN)₂ and the ligand (BHAN). The samples were run on a 0.9% agarose in 1 X TAE buffer for 3 h at 80 mV, then it was treated with EB

solution and the bands were visualized by UV light and photographed with UVP Bio Doc-It Imaging System.

4.2.3. Mechanism of protection from radiation induced DNA damage by the ligands and the complexes; DPPH radical scavenging activity by EPR spectroscopy:

Electron paramagnetic resonance (EPR) measurements were performed at room temperature (298 K). Spectroscopic parameters were 9.44 GHz (frequency), 100 mT (field sweep), 0.998 mW (microwave power) and a modulation amplitude of 3000 mT. The stability of freshly prepared DCM solution of DPPH was confirmed by monitoring^{8,9} the solution for 30 min, where no significant loss of signal was observed. In 100 μM DPPH solution, different concentrations (0–40 μM) of either *cis*-MoO₂(BHAN)₂ or the ligand (BHAN) were added and mixed thoroughly. The EPR signal was recorded after 2 minutes of mixing of either the complex or the ligand in appropriate cases with the DPPH solution under identical instrumental conditions.

5. Results & discussions:

5.1. DNA binding studies:

The emission intensity of the complex *cis*-MoO₂(BHAN)₂ exhibited a gradual decrease as calf thymus DNA was progressively added (Figure.1), which further supported the binding between the complex and DNA. The fluorescence intensity eventually reached a plateau at a relatively higher concentration of DNA, indicating that the binding reached saturation. This saturation point implies that the binding sites on DNA were fully occupied by the complex, resulting in a constant fluorescence intensity. To quantify the degree of fluorescence quenching, the Stern-Volmer equation was utilized, and the fluorescence quenching constant (K_{SV}) was determined to be $1.6 \times 10^4 \text{ M}^{-1}$ complex *cis*-MoO₂(BHAN)₂ at 25 °C. This value provides additional evidence for the binding of the complex to calf thymus DNA and

highlights the efficacy of the complex in quenching the fluorescence emission. These compelling findings contribute to a comprehensive understanding of the complex's interaction with DNA and its potential as a valuable tool in DNA-related applications.

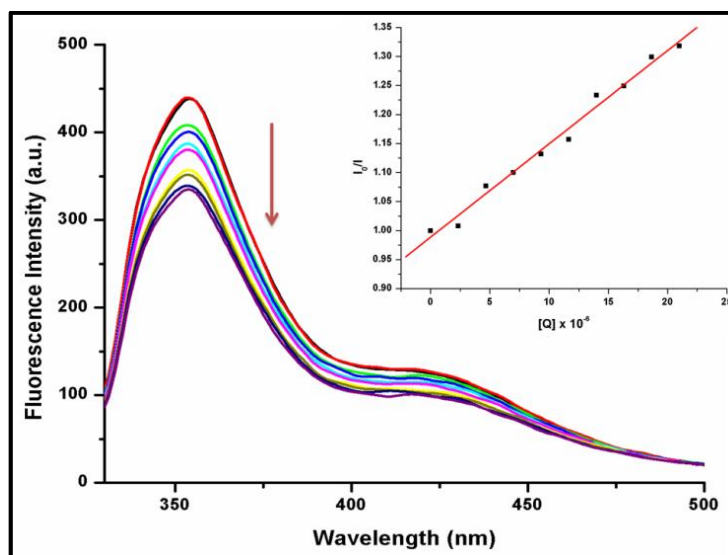


Figure 1: Emission spectra of *cis*-MoO₂(BHAN)₂ in the presence of increasing amounts of DNA [Inset: Stern–Volmer plot]

Viscosity analysis, a highly sensitive technique, was then employed to gain insights into the mode of interaction between the complex and DNA. This method provides a deep understanding of the intricate nature of DNA binding.^{10–13} The values of relative specific viscosities of DNA in the absence and presence of complex are plotted against [complex]/[DNA] (Figure.2). It is observed that the addition of *cis*-MoO₂(BHAN)₂ to the calf thymus DNA solution does not show any significant increase in the viscosity of calf thymus DNA, which clearly rules out the possibility of intercalation. If any small molecules bind to DNA through groove, that do not alter the relative viscosity value. Hence, in this case, the viscosity measurement results clearly hint at the groove binding of calf thymus DNA by *cis*-MoO₂(BHAN)₂.

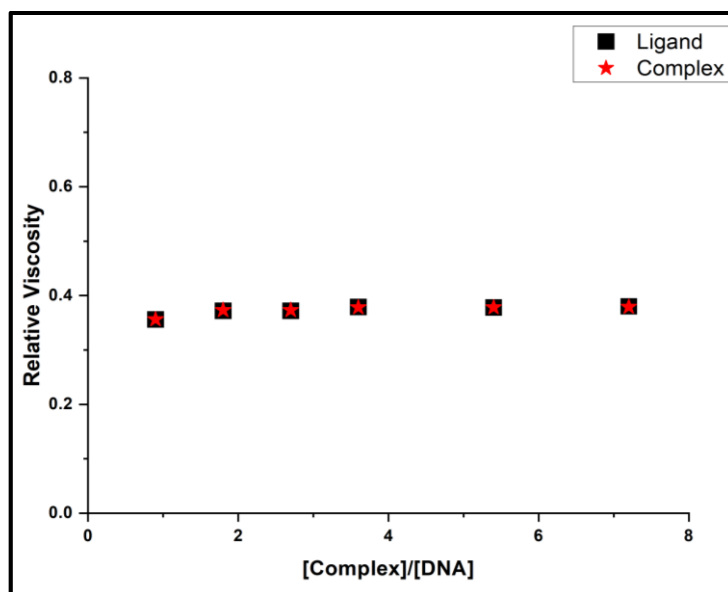


Figure 2: Effect of increasing amount of the *cis*-MoO₂(BHAN)₂ and the ligand (BHAN) on the specific Viscosity of calf thymus DNA

5.2. Radiation induced DNA damage and protection:

The assessment of DNA damage caused by radiation was conducted using a fluorometric technique that employed ethidium bromide (EB) as a probe.¹⁴⁻¹⁶ EB has a weak emission in an aqueous solution, but when it binds with DNA, its emission intensity increases significantly due to its strong intercalation between adjacent DNA base pairs. If gamma irradiation causes damage to the DNA double helix then EB can't intercalate with DNA, and this resulting damage of DNA due to irradiation, will cause relatively more EB to remain in the aqueous solution, which will be indicated by a reduction in fluorescence intensity. Therefore, this model was used to estimate radiation-induced DNA damage and evaluate methods for its protection.¹⁷

5.2.1. Estimation of the protection of DNA damage by fluorometric technique:

In order to evaluate the protective effects of a ligand or complex against radiation-induced DNA damage, DNA was pretreated with increasing concentrations of the ligand (BHAN) or *cis*-MoO₂(BHAN)₂ before exposure to radiation, after that EB was added to the solution.

Then the resulting fluorescence intensity of EB-DNA solutions was measured, and the data is presented in Figure 3 (i)-(ii). The data showed that the fluorescence intensity of EB bound to irradiated DNA increased gradually with an increase in the concentration of the BHAN or *cis*-MoO₂(BHAN)₂, indicating that both the ligand and complex provide protection to the DNA against radiation-induced damage.

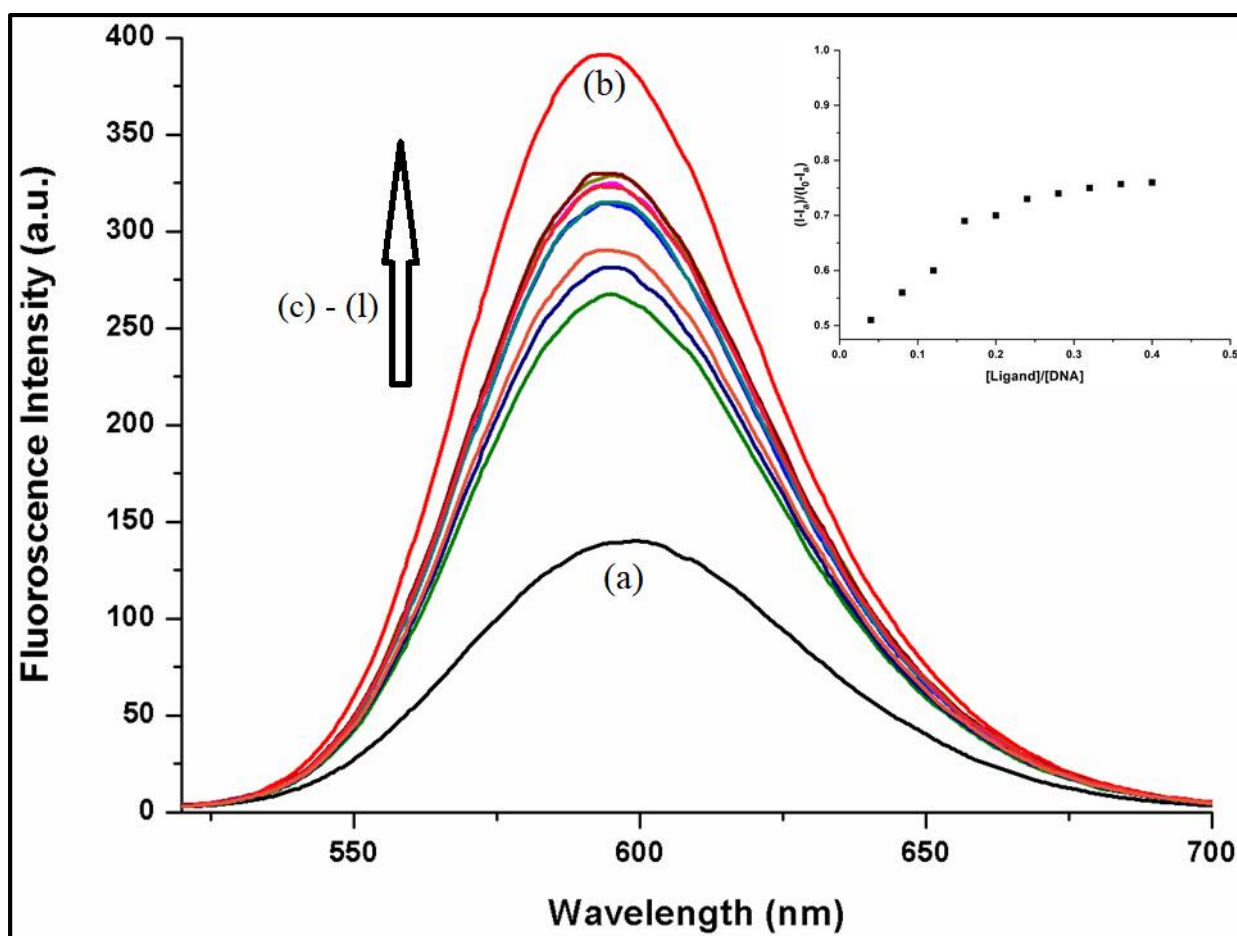


Figure 3 (i): Fluorescence emission spectra of EB-DNA obtained after treatment of calf thymus DNA with EB following irradiation provided to DNA solutions either in absence or the presence of increasing amounts of **ligand (BHAN)**; (a) = EB 900 μ M, (b) = DNA 60 μ M (unirradiated) + EB 900 μ M (maintained 15 folds higher), (c)-(l) = DNA 60 μ M (irradiated) + increasing concentration of the

ligand (BHAN) (0-24 μ M) + EB 900 μ M {Inset: Plot of $(I - I_a)/(I_0 - I_a)$ versus [ligand]/[calf thymus DNA]}

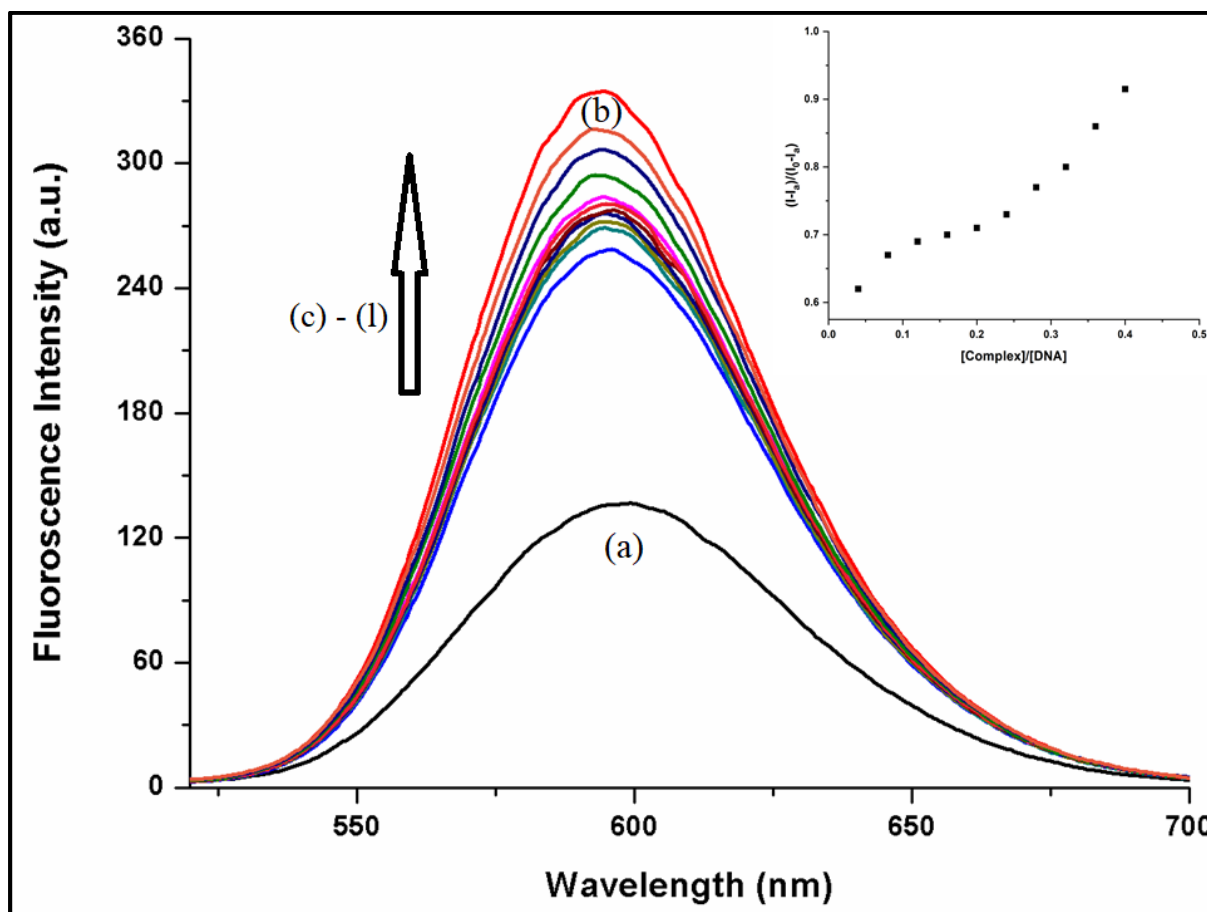


Figure 3 (ii): Fluorescence emission spectra of EB-DNA obtained after treatment of calf thymus DNA with EB following irradiation provided to DNA solutions either in absence or the presence of increasing amounts of *cis*-MoO₂(BHAN)₂; (a) = EB 900 μ M, (b) = DNA 60 μ M (unirradiated) + EB 900 μ M (maintained 15 folds higher) (c)-(l) = DNA 60 μ M (irradiated) + increasing concentration of the complex (0-24 μ M) + EB 900 μ M {Inset: Plot of $(I - I_a)/(I_0 - I_a)$ versus [complex]/[calf thymus DNA]}

Further a plot of $(I - I_a)/(I_0 - I_a)$ versus [radioprotector]/[calf thymus DNA] was generated to calculate the percentage of protection exerted by either the complex or the ligand (shown in the inset of Figure 3 i & ii). The results indicated that as the concentration of the ligand (BHAN) or complex [*cis*-MoO₂(BHAN)₂] increased, the damage caused by radiation to DNA was inhibited. Specifically, the percentage of protection provided by the ligand (BHAN) was calculated to be 76%, while the complex [*cis*-MoO₂(BHAN)₂] can provide a much higher level of protection at 92%. The results indicate that the *cis*-MoO₂(BHAN)₂ is highly effective in shielding the DNA from radiation induced damage. These findings have significant implications for the advancement of new approaches to minimize radiation-induced DNA damage in the future.

5.2.2. The role of the ligand and complex in the protection from gamma-radiation induced strand breaks in plasmid pUC19 DNA:

To further examine the protective capabilities of ligands and complexes against damage caused by gamma radiation on circular DNA, supercoiled pUC19 DNA was employed in a Tris-HCl/NaCl buffer (pH 7.2). The activity of the compounds was assessed using gel electrophoresis technique. Exposure of the plasmid DNA to gamma radiation at different doses (25 Gy and 20 Gy) resulted in strand breaks, leading to the relaxation of the plasmid DNA from a supercoiled (SC) form to a nicked coil (NC) form^{3,14-16}, as seen in figures 4-5. However, when radiation-induced damaged pUC19 DNA was treated with varying concentrations of either the complex [*cis*-MoO₂(BHAN)₂] or the ligand (BHAN), significant protection from the damage was observed. The results of these experiments are presented in Table 1 (Figure.6 & 7).

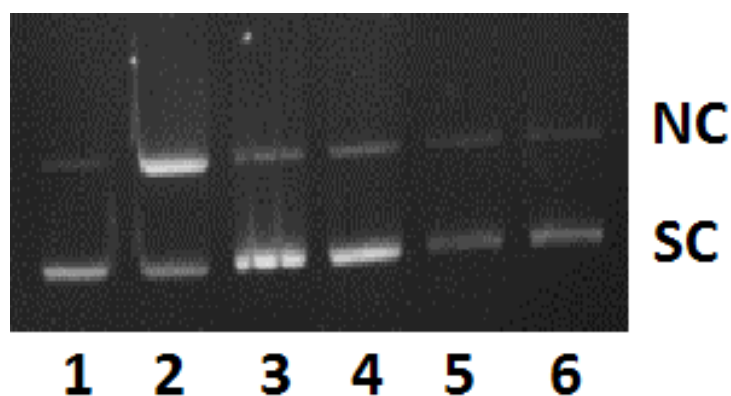


Figure 4: Protection of plasmid pUC19 DNA at 25 Gy with different concentrations of ligand (BHAN) and *cis*-MoO₂(BHAN)₂ on gamma-radiation induced strand breaks. *Lane 1:* DNA control (No irradiation); *Lane 2:* DNA irradiated; *Lane 3:* DNA + 1 mM BHAN; *Lane 4:* DNA + 1 mM *cis*-MoO₂(BHAN)₂; *Lane 5:* DNA + 2 mM BHAN; *Lane 6:* DNA + 2 mM *cis*-MoO₂(BHAN)₂

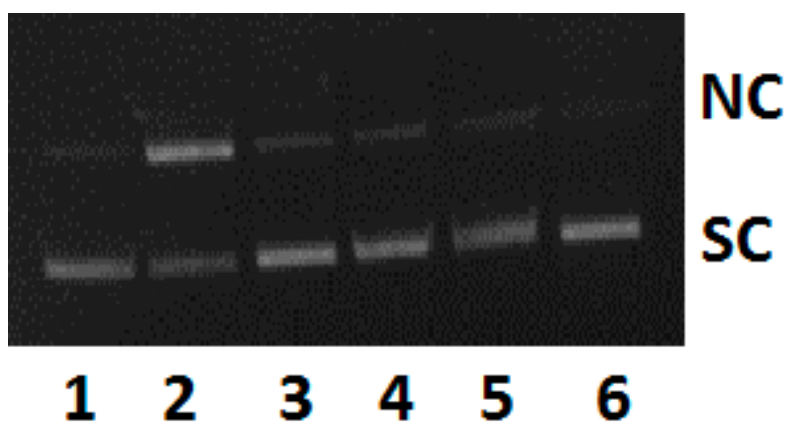


Figure 5: Protection of plasmid (pUC19) DNA at 20 Gy with different concentrations of ligand (BHAN) and *cis*-MoO₂(BHAN)₂ on gamma-radiation induced strand breaks. *Lane 1:* DNA control (No irradiation); *Lane 2:* DNA irradiated; *Lane 3:* DNA + 1 mM BHAN; *Lane 4:* DNA + 1 mM *cis*-MoO₂(BHAN)₂; *Lane 5:* DNA + 2 mM BHAN; *Lane 6:* DNA + 2 mM *cis*-MoO₂(BHAN)₂

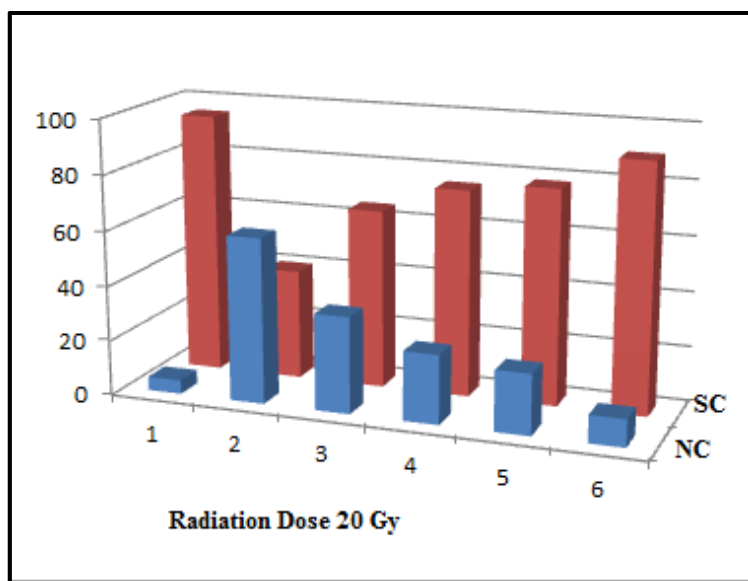


Figure 6: Graphical representation of protection by the **ligand (BHAN)** and the *cis*-MoO₂(BHAN)₂ at radiation dose of 20 Gy

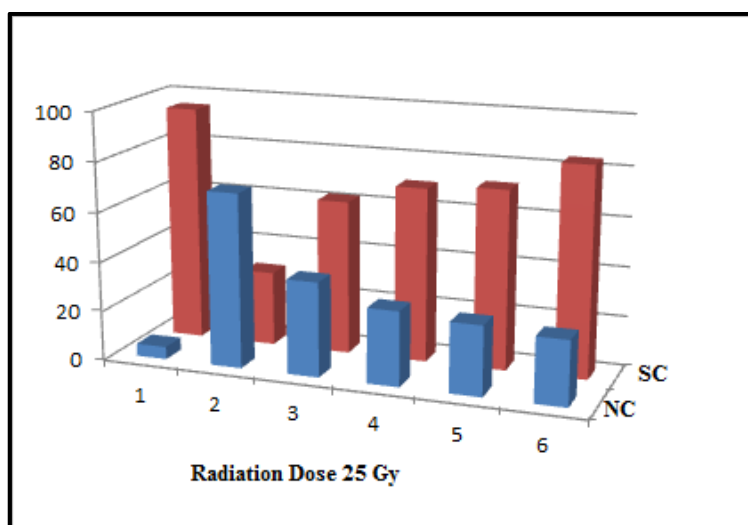


Figure 7: Graphical representation of protection by the **ligand (BHAN)** and the *cis*-MoO₂(BHAN)₂ at radiation dose of 25 Gy

Table 1: Extent of DNA SC pUC19 protection by the **ligand (BHAN)** and the *cis*-MoO₂(BHAN)₂

Lane no.	Reaction condition	<i>Form I</i> (% SC)		<i>Form II</i> (% NC)	
1	DNA Control (No radiation)	95		5	
Lane no.	Radiation dose	20 Gy		25 Gy	
	Reaction condition	<i>Form I</i> (% SC)	<i>Form II</i> (% NC)	<i>Form I</i> (% SC)	<i>Form II</i> (% NC)
2	DNA irradiated	40	60	30	70
3	DNA + 1 mM <i>ligand</i>	65	35	62	38
4	DNA + 1 mM <i>Complex</i>	75	25	70	30
5	DNA + 2 mM <i>ligand</i>	78	22	72	28
6	DNA + 2 mM <i>Complex</i>	90	10	84	26

The table provided displays the results of an experiment examining the effects of different treatments on the protection of DNA from radiation-induced damage. In Lane 1, the control group (without addition of any complex or ligand or any exposure to radiation) shows the percentages of Form I (supercoiled) and Form II (nicked circular) DNA, with 95% of the DNA remaining in the supercoiled form and only 5% in the nicked circular form.

In Lane 2 there is only plasmid DNA without addition of any complex or ligand and exposed to radiation doses of 20 Gy and 25 Gy. In this lane, the percentage of supercoiled DNA decreases while the percentage of nicked circular DNA increases which indicated the DNA damage due to radiation. Lane 2 shows 40% supercoiled DNA and 60% nicked circular DNA, with a radiation dose of 20 Gy, while with a radiation dose of 25 Gy, exhibits 30% supercoiled DNA and 70% nicked circular DNA.

To assess the protective effects of the ligand and complex, additional treatments were applied in Lanes 4 to 6. In Lane 4, the DNA was treated with a 1 mM concentration of the ligand, resulting in an increase in the percentage of supercoiled DNA to 75% and a decrease in nicked circular DNA to 25% only. Similarly, in Lane 5, the DNA was treated with a 1 mM concentration of the complex, resulting in 78% supercoiled DNA and only 22% of nicked circular DNA. Increasing the concentration to 2 mM for both the ligand and complex in Lanes 5 and 6 respectively, further enhanced the protective effects, with the complex demonstrating the highest level of protection. In Lane 6, the DNA treated with 2 mM complex exhibited 90% supercoiled DNA whereas nicked circular form is only 10%.

These results suggest that both the ligand (BHAN) and complex [*cis*-MoO₂(BHAN)₂] have a protective effect on DNA, with the complex demonstrating a greater ability to shield the DNA from radiation-induced damage. The findings highlight the potential of these compounds for mitigating radiation-induced DNA damage and provide valuable insights for future studies and the development of novel strategies in this field. The *cis*-MoO₂(BHAN)₂ can provide upto 90% and 84% protection against radiation doses of 20 and 25 Gy, respectively. The gel electrophoresis results clearly indicate that both the complex and ligand can offer significant protection to DNA against gamma radiation-induced damage in vitro by reducing the formation of NC form.

5.3. Mechanism of protection from radiation induced DNA damage; Assessment of the scavenging of DPPH by EPR spectroscopy:

Radiation exposure in solutions can give rise to harmful radicals that pose a risk to biomolecules, including DNA. In order to mitigate this damage, it becomes crucial to eliminate the radicals generated during radiolysis. One effective strategy to protect molecules from radiation-induced harm involves the introduction of a compound with radical scavenging abilities into the solution during radiolysis. By doing so, this compound can effectively intercept and neutralize the harmful radicals. To evaluate the radical scavenging activity of both the ligand and the complex, electron paramagnetic resonance (EPR) spectroscopy was employed. EPR spectroscopy is a powerful technique widely used to investigate the behavior of radicals and their interactions with various compounds. In this study, the EPR signal of DPPH, a stable radical commonly utilized to assess the antioxidant capacities of natural and synthetic substances, was closely monitored²¹. This allowed for the accurate evaluation of the ligand and complex's ability to scavenge radicals and protect against radiation-induced damage. The EPR spectra of DPPH in solutions of dichloromethane (DCM) were carefully observed during the titration process with incremental amounts of either the ligand (BHAN) or the *cis*-MoO₂(BHAN)₂. Remarkably, the intensity decrease observed in the spectra indicates that both the complex and the ligand possess the ability to effectively scavenge free radicals of DPPH (Figure.8). However, the impact appears to be more pronounced in the case of the complex. These compelling findings further reinforce the outcomes obtained from the experiments conducted to assess the protection against DNA damage.

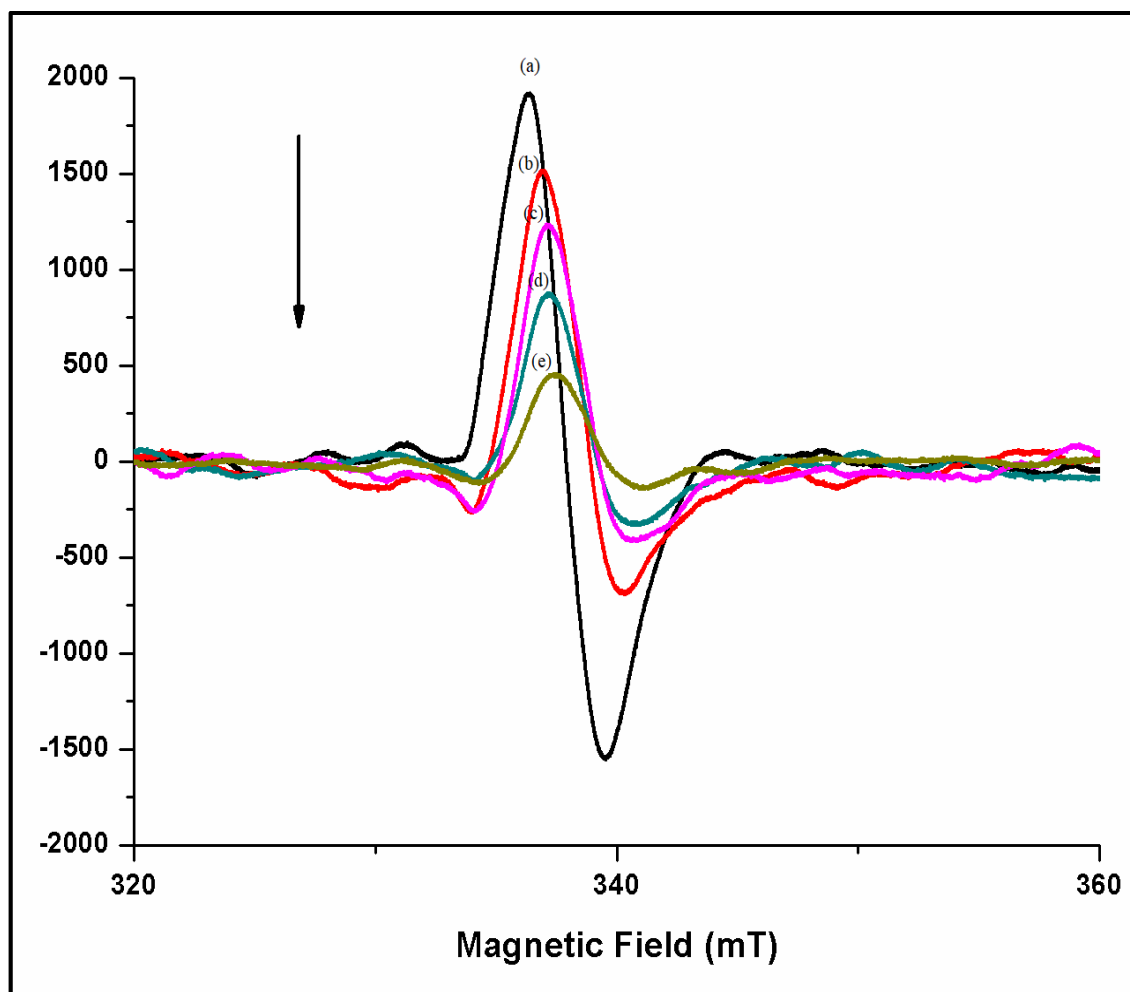


Figure 8 (i): EPR spectra of DPPH (*a*:100 μM DPPH) with different concentrations of *cis*-MoO₂(BHAN)₂ in DCM solution (*b*:10μM; *c*:20μM; *d*: 30μM; *e*: 40μM)

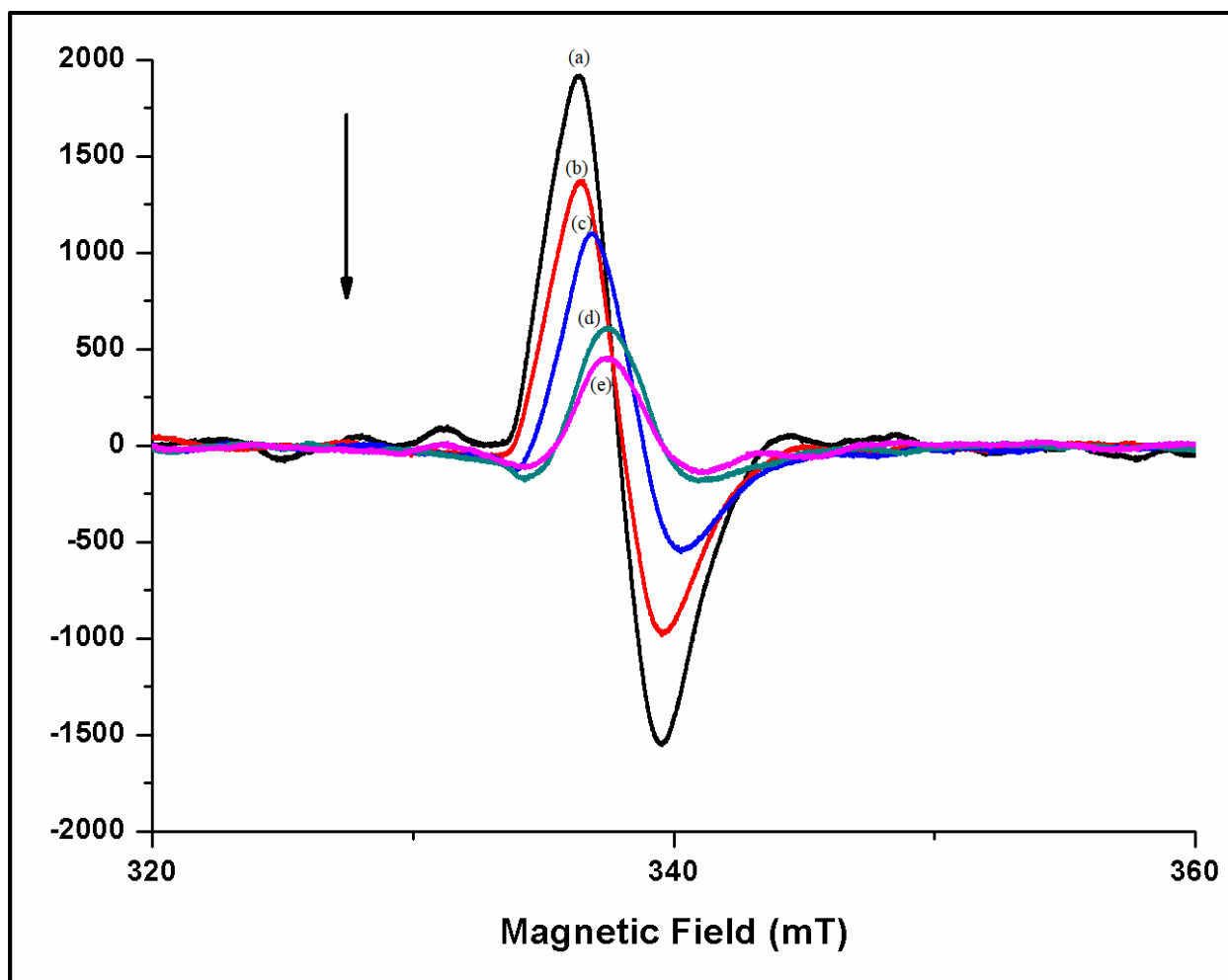


Figure 8 (ii): EPR spectra of DPPH (*a*:100 μ M DPPH) with different concentrations of ligand (BHAN) in DCM solution (*b*:10 μ M; *c*:20 μ M; *d*: 30 μ M; *e*: 40 μ M)

6. Conclusion:

The molybdenum complex [*cis*-MoO₂(BHAN)₂] synthesized in this project has demonstrated a remarkable ability to protect DNA from radiation-induced damage. It was found that the *cis*-MoO₂(BHAN)₂ provided a higher degree of protection to radiolysed DNA than the ligand (BHAN). In fact, at a concentration of 2 mM, the complex was able to protect 90% of damaged plasmid DNA from radiation at exposure of radiation dosage of 20Gy. Furthermore, the complex was able to protect approximately 92% of radiation-induced damage to CTDNA from gamma rays. These findings suggest that the *cis*-MoO₂(BHAN)₂ has tremendous

potential as an efficient radioprotector for normal tissues in radiotherapy. The ability of this complex to protect DNA from radiation-induced damage is particularly noteworthy, and the results of this study could have significant implications for the development of new therapies for a range of medical conditions. Overall, the complex's ability to protect DNA from radiation-induced damage is a promising development in the field of radioprotection and could lead to important advances in the years to come.

References:

- (1) Nilsson, R.; Liu, N. A. Nuclear DNA Damages Generated by Reactive Oxygen Molecules (ROS) under Oxidative Stress and Their Relevance to Human Cancers, Including Ionizing Radiation-Induced Neoplasia Part I: Physical, Chemical and Molecular Biology Aspects. *Radiat. Med. Prot.* **2020**, *1* (3), 140–152.
- (2) Poljsak, B. Strategies for Reducing or Preventing the Generation of Oxidative Stress. *Oxid. Med. Cell. Longev.* **2011**.
- (3) Paul, S. S.; Selim, M.; Saha, A.; Mukherjea, K. K. Synthesis and Structural Characterization of Dioxomolybdenum and Dioxotungsten Hydroxamato Complexes and Their Function in the Protection of Radiation Induced DNA Damage. *Dalt. Trans.* **2014**, *43* (7), 2835–2848.
- (4) Paul, S. S.; Selim, M.; Saha, A.; Mukherjea, K. K. Synthesis and Structural Characterization of Dioxomolybdenum and Dioxotungsten Hydroxamato Complexes and Their Function in the Protection of Radiation Induced DNA Damage. *Dalt. Trans.* **2014**, *43* (7), 2835–2848.
- (5) Wolfe, A.; Shimer, G. H.; Meehan, T. Polycyclic Aromatic Hydrocarbons Physically Intercalate into Duplex Regions of Denatured DNA. *Biochemistry* **1987**, *26* (20),

- 6392–6396.
- (6) Chaires, J. B.; Dattagupta, N.; Crothers, D. M. Studies on Interaction of Anthracycline Antibiotics and Deoxyribonucleic Acid: Equilibrium Binding Studies on Interaction of Daunomycin with Deoxyribonucleic Acid. *Biochemistry* **1982**, *21* (17), 3933–3940.
- (7) Selim, M.; Saha, A.; Mukherjea, K. K. Protection of Radiation Induced DNA Damage by a Newly Developed Molybdenum Complex. *J. Radioanal. Nucl. Chem.* **2017**, *311* (1), 189–193.
- (8) Hatano, T.; Kagawa, H.; Yasuhara, T.; Okuda, T. Two New Flavonoids and Other Constituents in Licorice Root : Their Relative Astringency and Radical Scavenging Effects. *Chem. Pharm. Bull.* **1988**, *36* (6), 2090–2097.
- (9) J. A. Weil, J. R. Bolton and J. E. Wertz. *Electron Paramagnetic Resonance: Elementary Theory and Applications*, New York, John Wiley & Sons, 1994.
- (10) Liu, Y. chun; Yang, Z. yin. Crystal Structures, Antioxidation and DNA Binding Properties of Dy(III) Complexes with Schiff-Base Ligands Derived from 8-Hydroxyquinoline-2-Carboxaldehyde and Four Aroylhydrazines. *Eur. J. Med. Chem.* **2009**, *44* (12), 5080–5089.
- (11) Satyanarayana, S.; Dabrowiak, J. C.; Chaires, J. B. Tris(Phenanthroline)Ruthenium(II) Enantiomer Interactions with DNA: Mode and Specificity of Binding. *Biochemistry* **1993**, *32* (10), 2573–2584.
- (12) Sigman, D. S.; Mazumder, A.; Perrin, D. M. Chemical Nucleases. *Chem. Rev.* **1993**, *93* (6), 2295–2316.
- (13) Deb, P.; Ghose, M.; Sepay, N.; Maiti, S.; Mukherjea, K. K. Synthesis, Characterization, Theoretical Simulation, and DNA-Nuclease Activity of a Newly Synthesized Mn–Oximato Complex. *J. Coord. Chem.* **2018**, *71* (20), 3250–3265.

- (14) Richard Morgan, A.; Pulleyblank, D. E. Native and Denatured DNA, Cross-Linked and Palindromic DNA and Circular Covalently-Closed DNA Analysed by a Sensitive Fluorometric Procedure. *Biochem. Biophys. Res. Commun.* **1974**, *61* (2), 396–403.
- (15) Prütz, W. A. Inhibition of DNA-Ethidium Bromide Intercalation Due to Free Radical Attack upon DNA. *Radiat. Environ. Biophys.* *1984* **231** **1984**, *23* (1), 1–6.
- (16) Prütz, W. A. Measurement of Copper-Dependent Oxidative DNA Damage by HOCl and H₂O₂ with the Ethidium-Binding Assay. *J. Biochem. Biophys. Methods* **1996**, *32* (2), 125–135.
- (17) Ganguly, D.; Santra, R. C.; Mazumdar, S.; Saha, A.; Karmakar, P.; Das, S. Radioprotection of Thymine and Calf Thymus DNA by an Azo Compound: Mechanism of Action Followed by DPPH Radical Quenching & ROS Depletion in WI 38 Lung Fibroblast Cells. **2020**.
- (18) Froehlich, E.; Mandeville, J. S.; Weinert, C. M.; Kreplak, L.; Tajmir-Riahi, H. A. Bundling and Aggregation of DNA by Cationic Dendrimers. *Biomacromolecules* **2011**, *12* (2), 511–517.
- (19) Rogers, K. R.; Apostol, A.; Madsen, S. J.; Spencer, C. W. Detection of Low Dose Radiation Induced DNA Damage Using Temperature Differential Fluorescence Assay. *Anal. Chem.* **1999**, *71* (19), 4423–4426.
- (20) Banerjee, S.; Selim, M.; Saha, A.; Mukherjea, K. K. Radiation Induced DNA Damage and Its Protection by a Gadolinium(III) Complex: Spectroscopic, Molecular Docking and Gel Electrophoretic Studies. *Int. J. Biol. Macromol.* **2019**, *127*, 520–528. <https://doi.org/10.1016/J.IJBIOMAC.2019.01.031>.
- (21) Gao, Z.; Huang, K.; Yang, X.; Xu, H. Free Radical Scavenging and Antioxidant Activities of Flavonoids Extracted from the Radix of *Scutellaria Baicalensis* Georgi.

cis-MoO₂(BHAN)₂ complex: its role in the protection of radiation- induced DNA
damage

Biochim. Biophys. Acta - Gen. Subj. **1999**, 1472 (3), 643–650.

Chapter 11

The Role of *cis*-MoO₂(BHAN)₂ Complex in Haloperoxidase Mimicking Oxidative Bromination

1. Introduction:

Biomimetic vanadium haloperoxidase (VHPO) catalysts are synthetic catalysts designed to mimic the structure and function of naturally occurring VHPO enzymes. These biomimetic catalysts have the potential to catalyze a range of useful reactions in a more efficient and environmentally friendly manner compared to traditional chemical catalysts. The development of biomimetic VHPO catalysts has been the subject of extensive research in recent years.¹ One approach to developing these catalysts is to synthesize new molecules that mimic the active site of VHPO enzymes. Overall, the development of biomimetic VHPO catalysts is a promising area of research that has the potential to lead to development of new and more efficient catalysts for a range of applications. However, further research is needed to fully understand the structure and function of VHPO enzymes and to develop more efficient biomimetic catalysts based on such understanding. Discovery of vanadium haloperoxidases (VHPOs) has generated considerable interest in understanding their active site structure and mode of action. As part of this effort, researchers have identified numerous vanadium complexes that can serve as structural and/or functional models for VHPOs. One noteworthy development in this area is the work of A. Butler et al. who were the first to develop haloperoxidase mimics.² This led to discovery of in vitro bromoperoxidase activity by molybdenum complexes. Specifically, oxidoperoxidomolybdenum (VI) complexes were found to catalyze two-electron oxidation of Br⁻ to Br⁺ in presence of H₂O₂ and considered functional mimics of vanadium bromoperoxidases.²⁻⁴

In this chapter, *cis*-MoO₂(BHAN)₂ is the subject of investigation to determine its ability to mimic biological catalysis using VHPO. Results of the study show that the compound exhibits a favorable response, suggesting it may have potential applications as a VHPO

mimic. These findings represent an important contribution to ongoing efforts to develop new and more effective catalysts for a range of applications.

2. Experimental Procedures:

2.1. Materials and physical methods:

Hydrogen peroxide (30% w/v), phenol red and all other reagents were products of E. Merck (India) and were used directly. All solvents for physico-chemical studies were of analytical grade and were further purified by literature method wherever necessary.⁵ Millipore water was used throughout the course of the investigation.

2.2. Physical Measurements:

UV-vis spectra (200–800 nm) were recorded against appropriate reagent blanks on a Shimadzu U-1800 spectrophotometer using 1 cm quartz cell. pH measurements were made with an Elico (India) digital pH meter.

2.3. Assessment of bromination:

Bromination was conducted in an aqueous solution at a constant temperature ($30 \pm 0.5^\circ\text{C}$). Reactions involving bromide ions were carried out under constant temperature. The solutions used for kinetic measurements were maintained at constant H⁺ concentration (pH = 5.0) by adding NaH₂PO₄-Na₂HPO₄.⁶ The rate of the reaction was determined by the rate equation: $dc/dt = k c_1^x c_2^y c_3^z$, from which " $\log (dc/dt) = \log k + x \log c_1 + y \log c_2 + z \log c_3$ " was derived. This equation can be rearranged as

$$-\log (dc/dt) = -x \log c_1 - b \text{ (where } b = \log k + y \log c_2 + z \log c_3 \text{)}.$$

The measurable absorbance of the resultant solution was denoted by A, and thus, the equation " $-\log (dA/dt) = -x \log c_1 - b$ " was obtained. By plotting absorbance data at 592 nm against time, a straight line was obtained. The slope of this line was used to calculate the reaction rate (dA/dt) of the dioxomolybdenum complex. By varying concentration of the complex, a series

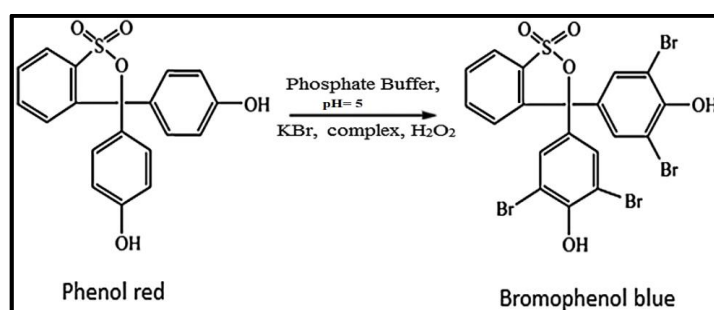
of dA/dt data were obtained and from a plot of $-\log (dA/dt)$ versus $-\log c_1$, reaction rate constant (k) was calculated.

3. Results and discussions:

The primary objective of the study was to create a mimic of bromoperoxidase, which is an area of great interest in the field of biochemistry. Many oxidovanadium complexes were found to imitate the reaction catalyzed by bromoperoxidases that involves bromination of organic substrates in presence of H₂O₂ and KBr. One of the widely used methods to investigate catalytic ability of metal complexes as haloperoxidases is by studying the model catalytic bromination reaction of phenol red to bromophenol blue.⁷ The bromoperoxidase activity of oxido-peroxidomolybdenum complexes has also been reported in other studies.^{2,8} In this study, catalytic activity of dioxomolybdenum complex was monitored by UV-vis spectrophotometry (Figure 1) using phenol red as substrate.

3.1. Bromination activity of the *cis*-MoO₂(BHAN)₂ for mimicking VHPO:

In this study, we examined the catalytic bromination capabilities of *cis*-MoO₂(BHAN)₂ by utilizing phenol red as substrate. The reaction involves transformation of phenol red to bromophenol blue and occurs quickly and in a stoichiometric manner. **Scheme 1** illustrates the reaction pathway.



Scheme 1. The reactive process of bromination reaction for the complex [*cis*-MoO₂(BHAN)₂].

When a solution of *cis*-MoO₂(BHAN)₂ was added to a standard bromide reaction in a phosphate buffer containing phenol red as a means of trapping oxidized bromine, color of the solution changed from yellow to blue. During catalytic conversion, a gradual decrease in absorption at 443 nm was observed due to loss of phenol red. At the same time, a new peak emerged at 592 nm as a result of the production of bromophenol blue, as shown in Figure 1.

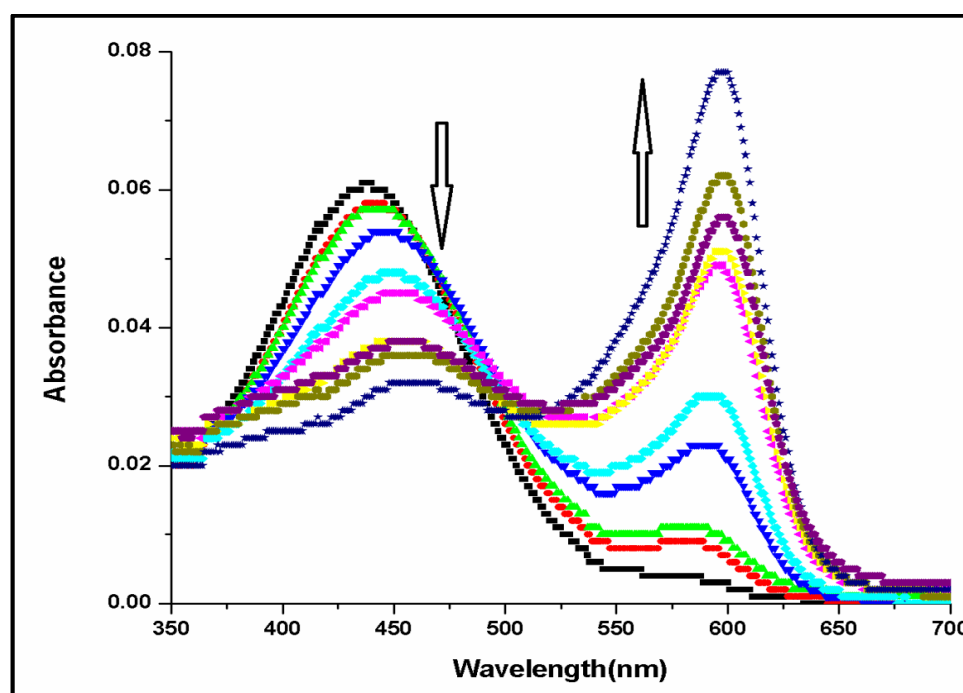


Figure 1: Oxidative bromination of phenol red catalyzed by the *cis*-MoO₂(BHAN)₂ (0.02 mmol). Spectral changes at 10 min intervals. Spectral data taken of aliquots in pH = 5.0 aqueous phosphate buffer, $c(\text{phosphate buffer}) = 50 \text{ mmol L}^{-1}$, $c(\text{KBr}) = 0.4 \text{ mol L}^{-1}$, $c(\text{phenol red}) = 0.1 \text{ mmol L}^{-1}$.

3.2. Kinetic studies of bromination:

Rate of bromination can be expressed by the equation: $dc/dt = k c_1^x c_2^y c_3^z$. Using Lambert-Beer's law, we can relate the measurable absorbance of bromophenol blue (A) to concentration (c) of the solution. By differentiating this equation, we obtain $dA/dt = \epsilon d(c/dt)$, where ϵ represents molar absorption coefficient of bromophenol blue ($\epsilon = 14,500$

The role of *cis*-MoO₂(BHAN)₂ complex in the Haloperoxidase mimicking oxidative

bromination

M⁻¹cm⁻¹ at 592 nm) and d represents the path length of light in the sample cell (d = 1 cm). By substituting these values in the equation $-\log (dA/dt) = -x\log c_1 - b$ (where $b = \log k + y\log c_2 + z\log c_3$), we determined the reaction rate constant (k) and the order of the reaction with respect to concentrations of Mo-complex (c₁), KBr (c₂) and phenol red (c₃) as x, y, and z, respectively.

To obtain reaction rates for various concentrations of *cis*-MoO₂(BHAN)₂ we plotted absorbance data at 592 nm against time. Resulting straight lines enabled us to calculate a series of reaction rates for the complex (dA/dt) (Figure 2). The reaction rate constant (k) could be determined from a plot of $-\log(dc/dt)$ against $-\log c_1$. The experiment for bromination used previously established data from literature^{9,10} to determine reaction orders of KBr and phenol red (y and z), both of which were considered as 1. Concentrations of c₂ and c₃ were known i. e. 0.4 and 10⁻⁴ mol L⁻¹, respectively. Using the equation " $b = \log k + y \log c_2 + z \log c_3$," we solved for the reaction rate constant (k). Plotting $-\log(dc/dt)$ against $-\log c$ (Figure 3) yielded straight lines with a slope of 0.85 and an intercept of 2.56 respectively for *cis*-MoO₂(BHAN)₂. Using these values, we could calculate the reaction rate constant for catalytic conversion using *cis*-MoO₂(BHAN)₂ as catalyst, which was found to be 0.7 x 10² (ML⁻¹)⁻²s⁻¹.

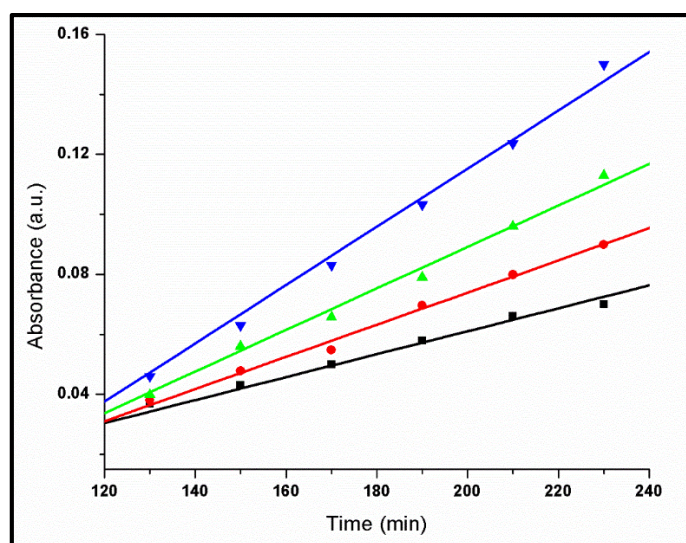


Figure 2: A series of linear calibration plots of the absorbance at 592 nm dependence of time for different concentrations of *cis*-MoO₂(BHAN)₂. Conditions used: pH 5, c(KBr) = 0.4 M L⁻¹, c(H₂O₂) = 0.02 M L⁻¹, c (phenol red) = 10⁻⁴ M L⁻¹. c (complex/M L⁻¹) = a: 1x10⁻⁶ (black square); b: 2x10⁻⁶ (red circle); c: 3x10⁻⁶ (green triangle); d: 4x10⁻⁶ (blue triangle).

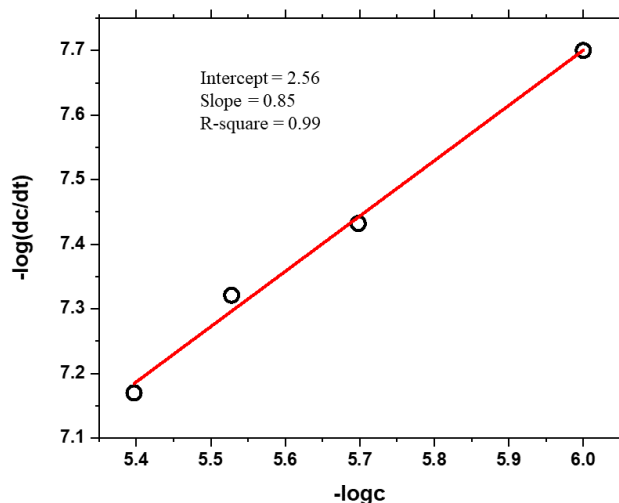


Figure 3: $-\log(dc/dt)$ vs. $-\log c$ (c is the concentration of the complex) for *cis*-MoO₂(BHAN)₂; conditions used: c (phosphate buffer) = 50 mM L⁻¹, pH = 5, c(KBr) = 0.4 mol L⁻¹, c(phenol red) = 10⁻⁴ M L⁻¹.

The role of *cis*-MoO₂(BHAN)₂ complex in the Haloperoxidase mimicking oxidative bromination

The obtained result indicates that the order of the reaction with respect to *cis*-MoO₂(BHAN)₂ in bromination is approximately 1, which confirms first-order dependence on the molybdenum species. Overall, this approach provides a clear and quantitative means of determining rate constant and reaction orders of the bromination reaction, paving the way for further research into the mechanism and optimization of an important chemical process.

4. Conclusion:

The *cis*-MoO₂(BHAN)₂ has shown promising potential as a biomimetic catalyst for VHPO (vanadium haloperoxidase) activity. In particular, it has demonstrated effective catalytic activity in the bromination of organic substrates such as phenol red producing the corresponding brominated product, bromo phenol blue. This reaction closely mimics bromoperoxidase activity, highlighting the potential of the synthesized complex as a bio-inspired catalyst. Overall, these findings open exciting avenues for development of novel Mo-based VHPO biomimetic catalysts with potential applications in diverse fields like organic synthesis, catalysis and pharmaceuticals.

References:

- (1) Everett, R. R.; Kanofsky, J. R.; Butler, A. A Functional Mimic of Vanadium Bromoperoxidase. *J. Am. Chem. SOC* **1992**, *114* (4), 265.
- (2) Meister, G. E.; Butler, A. Molybdenum(VI)- and Tungsten(VI)-Mediated Biomimetic Chemistry of Vanadium Bromoperoxidase. *Inorg. Chem.* **1994**, *33* (15), 3269–3275.
- (3) Boruah, J. J.; Das, S. P.; Borah, R.; Gogoi, S. R.; Islam, N. S. Polymer-Anchored Peroxo Compounds of Molybdenum and Tungsten as Efficient and Versatile Catalysts for Mild Oxidative Bromination. *Polyhedron* **2013**, *52*, 246–254.

The role of *cis*-MoO₂(BHAN)₂ complex in the Haloperoxidase mimicking oxidative bromination

- (4) Reynolds, M. S.; Morandi, S. J.; Raebiger, J. W.; Melican, S. P.; Smith, S. P. E. Kinetics of Bromide Oxidation by (Oxalato)Oxodiperoxomolybdate(VI). *Inorg. Chem.* **1994**, 33 (22), 4977–4984.
- (5) G.H. Jeffery, J. Bassett, J. Mendham, R. C. D. A. *Vogel's Text Book of Quantitative Chemical Analysis, 5th Ed., Wesley Longman Limited, United Kingdom, 1989.*
- (6) Verhaeghe, E.; Buisson, D.; Zekri, E.; Leblanc, C.; Potin, P.; Ambroise, Y. A Colorimetric Assay for Steady-State Analyses of Iodo- and Bromoperoxidase Activities. *Anal. Biochem.* **2008**, 379 (1), 60–65.
- (7) Saha, U.; Mukherjea, K. K. Development of a Multifunctional Biomimicking 1 - Cysteine Based Oxovanadium(IV) Complex: Synthesis, DFT Calculations, Bromo-Peroxidation and Nuclease Activity. *RSC Adv.* **2015**, 5 (114), 94462–94473.
- (8) Naskar, S.; Palmajumder, E.; Patra, S.; Mitra, J.; Mukherjea, K. K. Biomimicking Oxidative Bromination and DNA Nuclease Activities of a New Structurally Characterised Oxido-Diperoxidomolybdenum(VI) Complex. *ChemistrySelect* **2017**, 2 (31), 10199–10205.
- (9) Colpas, G. J.; Hamstra, B. J.; Kampf, J. W.; Pecoraro, V. L. Functional Models for Vanadium Haloperoxidase: Reactivity and Mechanism of Halide Oxidation. *J. Am. Chem. Soc.* **1996**, 118 (14), 3469–3478.
- (10) Adhikari, H.; Mukherjea, K. K. Mononuclear Oxidodiperoxido Vanadium(V) Complex: Synthesis, Structure, VHPO Mimicking Oxidative Bromination, and Potential Detection of Hydrogen Peroxide. *J. Coord. Chem.* **2018**, 71 (4), 542–555.

Chapter 12

**Synthesis and Characterization of a Dioxomolybdenum
Complex [*cis*-MoO₂(OV)₂] Using Ortho-Vanilline (OV) as
a Ligand**

Synthesis and characterization of a dioxomolybdenum complex [*cis*-MoO₂(OV)₂] using ortho-vanilline (OV) as a ligand

1. Introduction:

In the realm of modern chemistry, design and synthesis of novel coordination complexes have always captivated the scientific community due to their profound applications in catalysis, material science, and medicine.^{1,2} Among the intriguing complexes, molybdenum dioxo complexes have emerged as particularly fascinating species, exhibiting exceptional reactivity and versatility in various catalytic transformations.³ In this vein, the synthesis and characterization of a molybdenum dioxo complex employing ortho-vanillin as the ligand represents a pivotal milestone in this field. Ortho-vanillin possesses a unique molecular structure that combines the functional groups of a phenolic moiety and an aldehyde. This exceptional combination endows ortho-vanillin with a rich array of coordination possibilities, making it a promising candidate for constructing complex metal-ligand architectures.⁴⁻⁷ Additionally, its availability, low cost, and non-toxic nature make it an attractive choice for sustainable and practical use.⁶ Furthermore, synthesis of the molybdenum dioxo complex utilizing ortho-vanillin as a ligand involves a systematic and rigorous methodology. Precise control over reaction parameters and meticulous purification techniques ensure the isolation of a pure, well-defined coordination compound. Comprehensive characterization techniques, like nuclear magnetic resonance (NMR), infrared spectroscopy (IR) and X-ray crystallography provide valuable insights into the structural features that confirm the successful coordination of ortho-vanillin with molybdenum.

In summary, the synthesis of a molybdenum dioxo complex employing ortho-vanillin as a ligand represents a significant advancement in the field of coordination chemistry. By harnessing the distinctive properties of ortho-vanillin, this complex showcases remarkable stability, enhanced catalytic pathways, and an expansive scope of biological applications.

Synthesis and characterization of a dioxomolybdenum complex [*cis*-MoO₂(OV)₂] using ortho-vanilline (OV) as a ligand

2. Experimental Procedures:

2.1. Materials and physical methods:

We obtained high-quality ammonium molybdatetetrahydrate from Merck, India. Orthovanillin (OV) was obtained from Sigma Aldrich and used without further purification. All other reagents were purchased from Merck, India and used directly. For physico-chemical studies, we used analytical grade solvents that were further purified using established methods whenever necessary.⁸ Throughout investigations we used Millipore water.

2.2. Physical Measurements:

A KBr disc IR spectrum was obtained using a Perkin Elmer RFX-I IR spectrophotometer at room temperature. Elemental analyses were conducted using a Perkin-Elmer 2400 series II CHNS analyzer. UV-vis spectra ranging from 200 to 800 nm were measured against suitable reagent blanks with a Shimadzu U-1800 spectrophotometer using a 1 cm quartz cell. Mass spectrum was recorded on Micromass Q-T of microTM, Waters Corporation.

2.3. Synthesis of the complex:

Synthesis of a complex of Mo(VI) with orthovanillin (OV) was carried out according to Scheme 1 (Figure 1). An aqueous solution of [(NH₄)₆Mo₇O₂₄, 4H₂O] (1.23 g) was added to a methanolic solution of orthovanillin (OV) (2.7 g) under constant stirring.⁹ 12M HCl (total volume of ~ 1 ml) was added dropwise to the mixture resulting in the formation of a yellow precipitate. Stirring was continued for 4 hours at room temperature to ensure complete precipitation. The solid was collected by filtration and washed with cold water followed by methanol. Finally, the product was dried under vacuum and purified by recrystallization. Literature¹⁰ contains a report on the synthesis of a *cis* Mo compound using a similar ligand. However, there is no information available regarding its characterization (spectroscopic and structural). Therefore, an effort was made to thoroughly characterize our prepared complex,

Synthesis and characterization of a dioxomolybdenum complex [*cis*-MoO₂(OV)₂] using ortho-vanilline (OV) as a ligand

both physicochemically and structurally. Single crystals of the compound suitable for X-ray diffraction analysis were obtained by slow evaporation of the solvent containing methanol and acetonitrile in a 1:1 ratio. The compound is soluble in organic solvents like methanol, ethanol and acetonitrile.

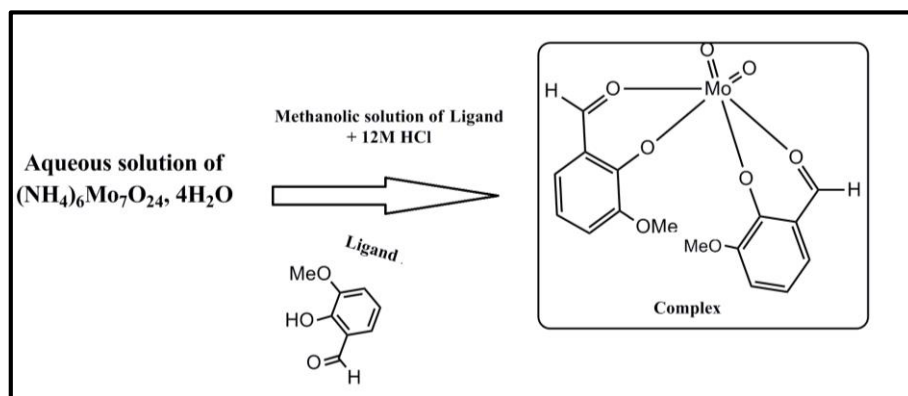


Figure 1: Preparation scheme for the **complex**

2.4. X-Ray crystal structure determination for complex:

X-ray diffraction data for the complex was collected at 296K on a Bruker AXS SMART APEX II diffractometer. The diffractometer was equipped with a CCD detector¹¹ with a fine focus of 1.75 kW sealed tube using Mo K α radiation ($\lambda=0.71073\text{\AA}$). The data was processed using SAINT and absorption corrections were made using SADABS.¹² Structure was solved by the direct method and refined by full matrix least-squares on the basis of F^2 using the WINGX software and SHELX suites.¹³ Non-hydrogen atoms were refined anisotropically, while hydrogen atoms were placed with fixed thermal parameters at idealized positions. Perspective views of the molecule were obtained by Mercury.

2.5. Structural optimization of the complex by DFT calculations:

DFT study is an important tool to obtain better insights into the geometry, electronic structure, and optical properties of coordination systems. The ground state molecular geometry of the complex was optimized by using B3LYP function, since this method can

Synthesis and characterization of a dioxomolybdenum complex [*cis*-MoO₂(OV)₂] using ortho-vanilline (OV) as a ligand

provide reliable and accurate results for geometrical parameters. Optical properties of the being investigated metal complex were calculated using time-dependent density functional method for CAM-B3LYP functional (TD-CAM-B3LYP). All DFT calculations were performed using Gaussian 09 program package.¹⁴ The ground state geometry of [*cis*-MoO₂(OV)₂] in aqueous medium were fully optimized at the B3LYP level using conductor like polarization continuum model (CPCM) of solvent. The B3LYP method accounts for the exchange and correlation effects by incorporating hybrid exchange-correlation functional (Becke + Slater + HF exchange and LYP + VWN5 correlations).¹⁵⁻¹⁷ Detailed procedure describing CPCM solvent model are provided in the literature.¹⁸ The polarized solute-solvent interaction within CPCM considers geometry relaxation of the solute in equilibrium with the solvent reaction field. The basis set employed in the present calculation includes 6-311++G(d,p) for C, H and O atoms and 3-21G(d) for Mo. The calculated vibrational frequencies obtained for the molecule were all found to be real which indicates a true minimum in the potential hypersurface. The solvent modified transition energy and spectroscopic properties associated with vertical excitations of the chosen metal complex were calculated by using time-dependent density functional (TD-DFT) method for the CAM-B3LYP functional (TD-CAM-B3LYP) in the framework of CPCM solvent model for the same basis set as employed in the optimization calculation. Excited state calculations were carried out for forty lowest lying singlet states.

3. Results & discussions:

3.1. Spectral characterization of the complex:

3.1.1. IR and UV-VIS spectral analysis of the complex:

IR (in KBr pellets) of the complex (C₁₆H₁₄MoO₈) (Figure 2) recorded two peaks at 905 and 941 respectively [$\nu_{(\text{Mo}=\text{O})}$] confirming two oxo-bonds are *cis* to each other. UV-Vis ($\lambda_{\text{max}}/\text{nm}$)

Synthesis and characterization of a dioxomolybdenum complex [*cis*-MoO₂(OV)₂] using ortho-vanilline (OV) as a ligand

for complex: 202, 220 and 277. The electronic spectral bands at 202 nm for *cis*-MoO₂(OV)₂, is assigned to intra ligand $\pi \rightarrow \pi^*$ transitions of the aromatic ring. Additional two bands around 220 nm and 277 nm for the complex can be assigned as $n \rightarrow \pi^*$ of C=O functional group of both coordinated ligands.¹⁹

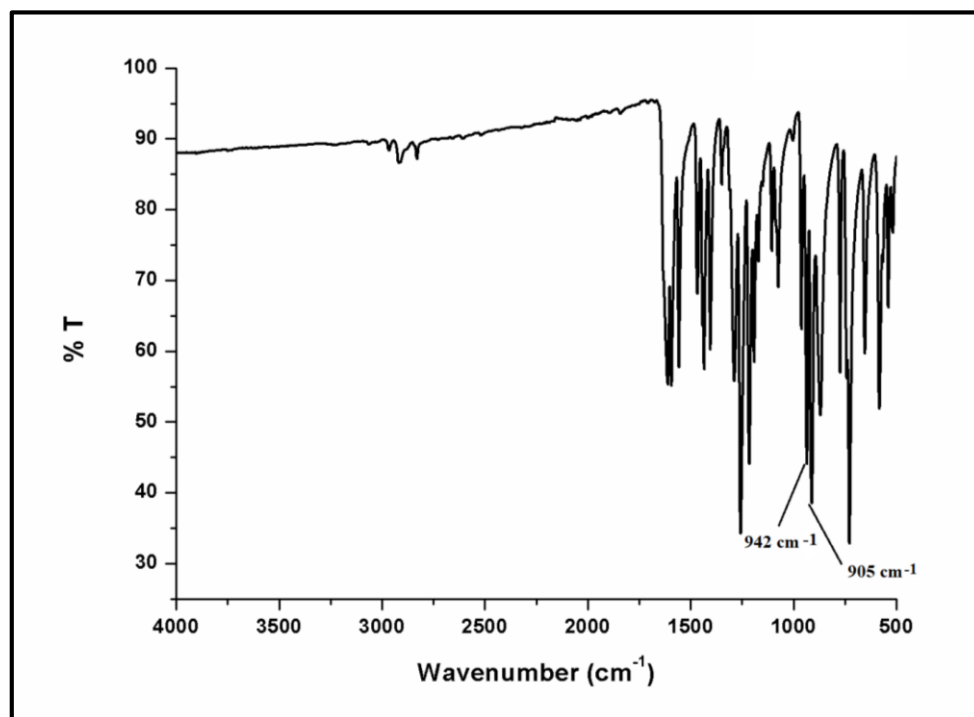


Figure 2: IR spectrum of *cis*-MoO₂(OV)₂

3.1.2. Mass and elemental analysis of the complex:

ESI-MS(+ve) in MeOH: m/z (relative intensity) complex: 431.97 [M⁺]. Elemental analysis of the complex: Calc. C, 44.67%; H, 3.28%; found: C, 44.59%; H, 3.20%.

3.1.3. NMR spectral analysis of the complex:

¹H NMR confirmed that *cis*-MoO₂(OV)₂ as well as the ligand (OV) are stable in solution phase. In the complex, phenolic -OH is deprotonated characterized by the disappearance of the -OH proton signal at δ 10 (Figure 3 & 4). This suggests that the ligand (OV) behaves as a mono anionic O, O donor centre. Moreover, presence of aromatic proton signals in the complex [*cis*-MoO₂(OV)₂] clearly indicate involvement of the ligand in coordination.

Synthesis and characterization of a dioxomolybdenum complex [*cis*-MoO₂(OV)₂] using
ortho-vanilline (OV) as a ligand

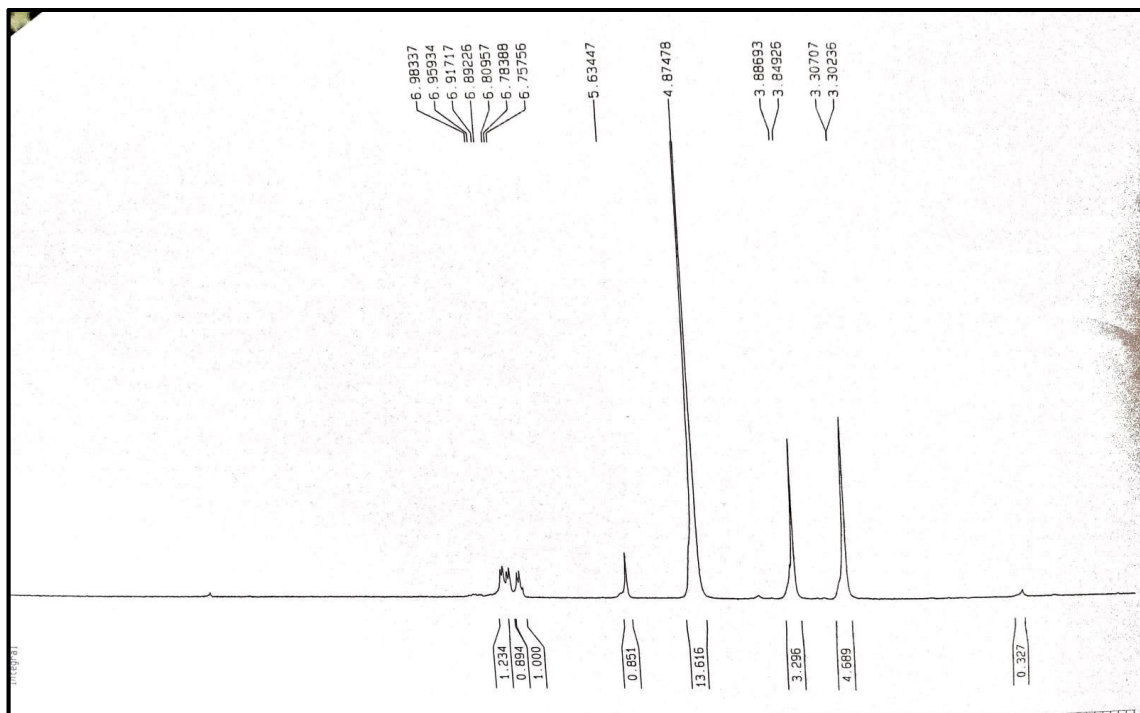


Figure 3: NMR spectra of *cis*-MoO₂(OV)₂

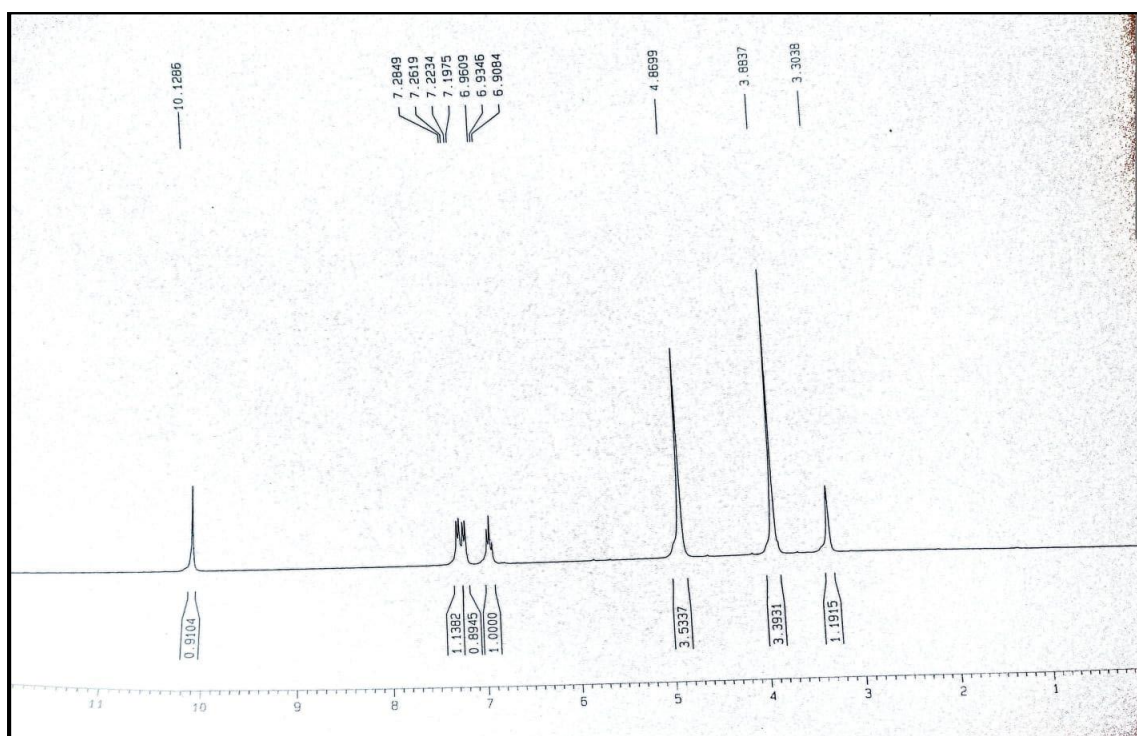


Figure 4: NMR spectra of Ligand (OV)

**Synthesis and characterization of a dioxomolybdenum complex [*cis*-MoO₂(OV)₂] using
ortho-vanilline (OV) as a ligand**

Experimental values of various spectroscopic techniques like IR and UV for the complex was supported by DFT studies and there was good agreement. Molar conductivity values of the complex in methanol indicates it is non-electrolytic in nature.

3.2. Structural characterization of the complex:

3.2.1. Crystal structure of complex:

Crystals that were obtained for the compound were of very good quality and suitable for diffraction. The molecular structure was established with the help of single crystal X-ray diffraction and found to have a *cis* conformation with respect to the two oxo bonds around Mo of [*cis*-MoO₂(OV)₂]. Crystallographic data and details regarding the structure of the prepared compound are summarized in Table 1. Some selected bond lengths and bond angles are presented in Table 2.

Table 1. Crystal data and structure refinement parameters of the *cis*-MoO₂(OV)₂

CCDC no: 1834954

Parameters	
Moiety formula	C16 H14 Mo O8
Mr	215.11
T/K	296(2)
$\lambda/\text{\AA}$	0.71073
Crystal system	Monoclinic
Space group	P 2/n
Unit cell dimensions	
$a/\text{\AA}$	9.6886(5)
$b/\text{\AA}$	6.5198(3)
$c/\text{\AA}$	13.0911(6)
$\alpha/^\circ$	90.00
$\beta/^\circ$	103.985(3)
$\gamma/^\circ$	90.00

Synthesis and characterization of a dioxomolybdenum complex [*cis*-MoO₂(OV)₂] using
ortho-vanilline (OV) as a ligand

V/Å ³	802.42(7)
Z ,Dx/g cm ⁻³	4, 1.781
F(000)	432.0
h,k,lmax	12,8,16
Nref	1842
Data completeness	0.995
Theta(max)	27.518
Theta(min)	2.363
R(reflections)	0.0455(1397)
wR2(reflections)	0.1734(1842)

Table 2. Selected ground state optimized geometrical parameters for *cis*-MoO₂(OV)₂ obtained at the B3LYP level.

Type of bonds	Bond Lengths (Å)	
	Calculated (DFT)	Experimental (SC-XRD)
Mo-O1	1.95	1.94
Mo-O2	2.34	2.27
Mo-O3	2.34	2.27
Mo-O4	1.95	1.94
Mo-O5	1.71	1.68
Mo-O6	1.71	1.68
O1-C1	1.32	1.32
O2-C3	1.24	1.23

Synthesis and characterization of a dioxomolybdenum complex [*cis*-MoO₂(OV)₂] using
ortho-vanilline (OV) as a ligand

O3-C6	1.24	1.23
O4-C4	1.32	1.32
Type of bonds	Bond Angles (°)	
<O1-Mo-O2	78.81	80.20
<O2-Mo-O3	74.93	73.79
<O3-Mo-O4	78.81	80.23
<O5-Mo-O6	105.32	105.48
<C1-C2-C3	121.21	121.19
<C4-C5-C6	121.21	121.17

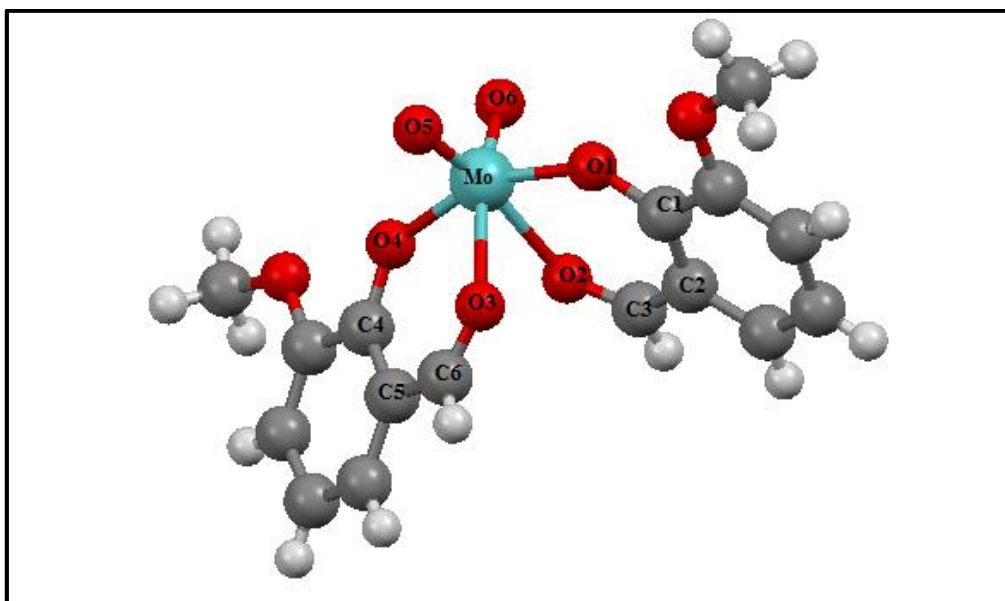


Figure 5: ORTEP view of the crystal structure of the *cis*-MoO₂(OV)₂

The ORTEP view of the crystal is shown in Figure 5. The compound crystallizes in monoclinic P2/n space group with the two-fold symmetry clearly passing through the central metal atom. The central Mo(VI) is coordinated to two oxido ligands while the other two O

Synthesis and characterization of a dioxomolybdenum complex [*cis*-MoO₂(OV)₂] using ortho-vanilline (OV) as a ligand

atoms from each ortho-valinato ligand results in a six coordinated environment having a distorted octahedral geometry around the metal centre. Oxido ligands are coordinated in the *cisoid* position with respect to the metal. The Mo=O bond lengths (Mo1=O5 and Mo1=O6) are 1.68 Å each, that are typical of such molybdenum-oxido double bond linkages^{20,21}. Coordination of the O atom from the phenolic -OH moiety of OV to the central Mo(VI) has a bond length of 1.94 Å and coordination of the carbonyl oxygen with the metal centre shows a length of 2.27 Å. Increased bond length in case of phenolate oxygens and carbonyl oxygens with Mo with respect to that of the Mo-oxido bonds indicates single bond character of these oxygens to the metal centre. The methoxy O of either ligand does not participate in bonding. The ligand forms two six membered rings with bond angles 80.20° (O1-Mo-O2) and 73.79° (O2-Mo-O3). The axial positions of the octahedral structure are occupied by one oxido group and one carbonyl O atom while equatorial positions that are roughly planar with three valinato O atoms and a remaining oxido group, thereby creating an octahedron but slightly distorted. The phase purity of *cis*-MoO₂(OV)₂ was confirmed by comparing a simulation, based on the single-crystal structure with that of a powder X-ray diffraction (PXRD) pattern (Figure. 6)²². Peaks obtained from simulated PXRD, based on single crystal XRD data, and the experimentally obtained PXRD indicates a high degree of matching.

Synthesis and characterization of a dioxomolybdenum complex [*cis*-MoO₂(OV)₂] using
ortho-vanilline (OV) as a ligand

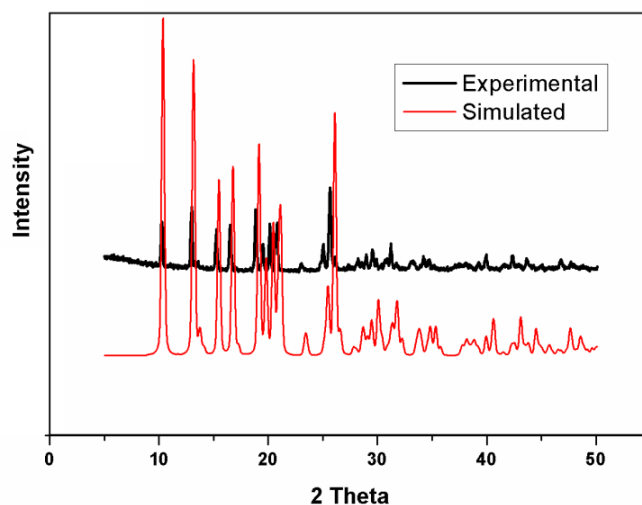


Figure 6: Experimental and simulated (from single crystal X-ray data) PXRD patterns of *cis*-MoO₂(OV)₂

3.2.2. Optimization of structure of the complex:

Geometry of both ligand and metal complex were optimized by Density Functional Theory (DFT). The ground state optimized geometry of the complex is shown in Figure 7. Important optimized geometrical parameters are listed in Table 2 for a comparison with experimental results obtained from single crystal X-ray diffraction of relevant structural parameters obtained for the complex.

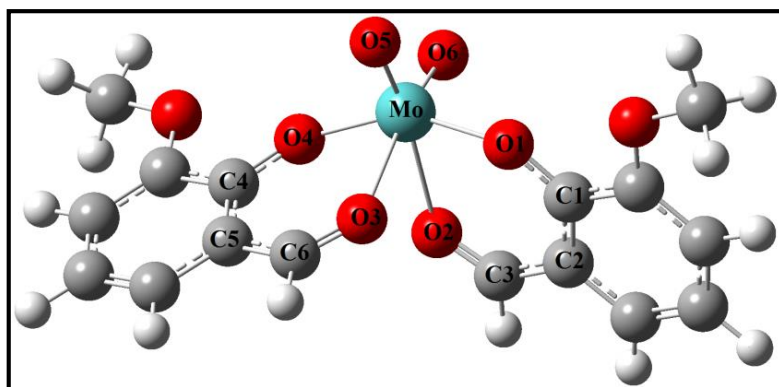


Figure 7: The B3LYP optimized ground state electronic structure of *cis*-MoO₂(OV)₂

**Synthesis and characterization of a dioxomolybdenum complex [*cis*-MoO₂(OV)₂] using
ortho-vanilline (OV) as a ligand**

As can be seen from **Table 2**, B3LYP calculated bond lengths and bond angles show good agreement with experimental values. Calculated IR frequencies of the prepared compound under investigation was found to be in good agreement with experimental results (**Table 3**).

Table 3. B3LYP/6-311++G(d,p) [6-311++G(d,p) for C, H, O and 3-21G(d) for Mo] Calculated IR frequencies ($\bar{\nu}$, cm⁻¹) and intensities obtained for *cis*-MoO₂(OV)₂ using CPCM Model.

Frequency	Theoretical values (cm ⁻¹)	Experimental Values (cm ⁻¹)
Complex		
ν Mo=O (<i>cis</i>)	972.1	942
	913.3	905

Solvent modified transition energy and spectroscopic properties associated with vertical excitations of the complex were calculated at solvent-modified geometry of each compound by time-dependent density functional method for CAM-B3LYP functional (TD-CAM-B3LYP) in the framework of the CPCM solvent model for the same basis set as employed in the optimization calculation. The excited state calculations are carried out for forty lowest lying singlet states. The TD-DFT approach is demonstrated to be reliable for calculating spectral properties of many transition metal complexes.²³⁻²⁶ The calculated results for important electronic transitions are presented in Table 4. The calculated results for λ_{max} of *cis*-MoO₂(OV)₂ are in good agreement with corresponding experimental results. The frontier molecular orbital diagrams (Figure 8) involved in electronic transitions indicate significant

Synthesis and characterization of a dioxomolybdenum complex [*cis*-MoO₂(OV)₂] using
ortho-vanilline (OV) as a ligand

reorganization of charge distribution around symmetric structure leading to a shift in electron density either from the ligand to molybdenum-oxygen moiety or vice versa.

Table 4. TD-CAM-B3LYP/6-311++G(d,p) Calculated Transition Wavelength (λ_{max} , nm), Oscillator Strength (f_0) and Transition MOs Involved in the Crucial Transition obtained for *cis*-MoO₂(OV)₂ in Water Solvent Using CPCM Model

λ_{max} (Cal.)	λ_{max} (Exp.)	% of deviation	Oscillator strength (f_0)	Major transition
216	202	6.48	0.75	H→L+7
218	220	0.92	0.38	H-6→L+2
283	277	2.12	0.13	H-2→L

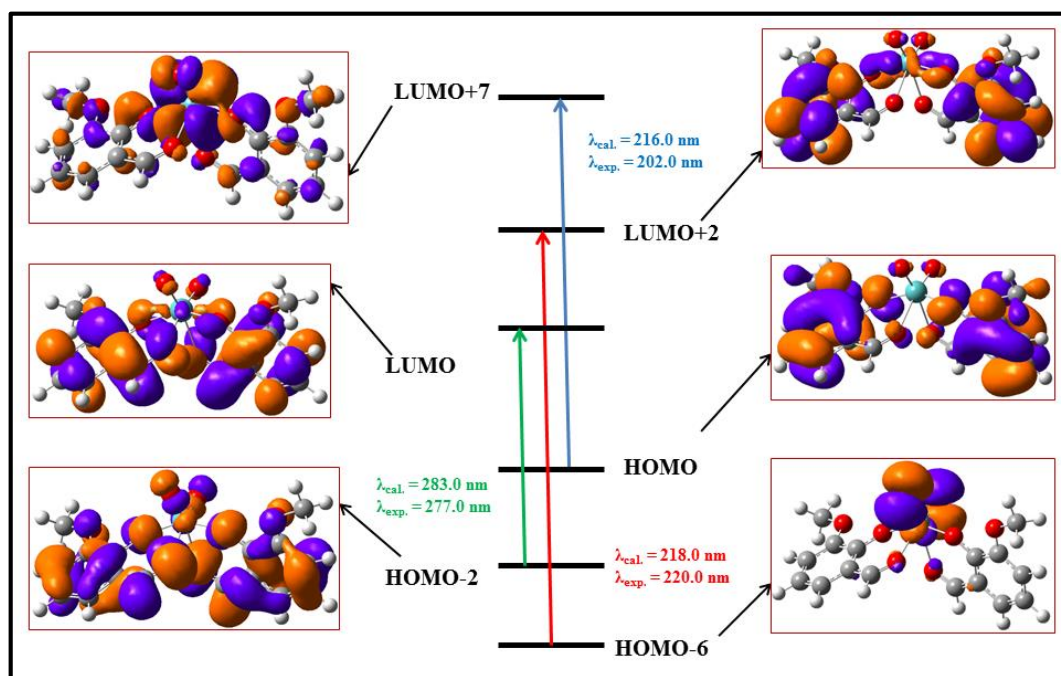


Figure 8: Frontier molecular orbitals involved in the UV-vis absorption of *cis*-MoO₂(OV)₂ in aqueous solution at room temperature.

**Synthesis and characterization of a dioxomolybdenum complex [*cis*-MoO₂(OV)₂] using
ortho-vanilline (OV) as a ligand**

4. Conclusion:

This chapter provides details regarding the synthesis and experimental characterization of *cis*-MoO₂(OV)₂. DFT analysis was also performed that confirms accuracy of experimental results and demonstrates that the Mo-complex was synthesized in a highly pure form.

References:

- (1) Abu-Dief, A. M.; Mohamed, I. M. A. A Review on Versatile Applications of Transition Metal Complexes Incorporating Schiff Bases. *Beni-Suef Univ. J. Basic Appl. Sci.* **2015**, *4* (2), 119–133.
- (2) Annibale, V. T.; Song, D. Coordination Chemistry and Applications of Versatile 4,5-Diazafluorene Derivatives. *Dalt. Trans.* **2015**, *45* (1), 32–49.
- (3) Meister, G. E.; Butler, A. Molybdenum(VI)- and Tungsten(VI)-Mediated Biomimetic Chemistry of Vanadium Bromoperoxidase. *Inorg. Chem.* **1994**, *33* (15), 3269–3275.
- (4) Das, A. K.; Goswami, S. 2-Hydroxy-1-Naphthaldehyde: A Versatile Building Block for the Development of Sensors in Supramolecular Chemistry and Molecular Recognition. *Sensors Actuators, B Chem.* **2017**, *245*, 1062–1125.
- (5) De, A.; Ray, H. P.; Jain, P.; Kaur, H.; Singh, N. Synthesis, Characterization, Molecular Docking and DNA Cleavage Study of Transition Metal Complexes of o-Vanillin and Glycine Derived Schiff Base Ligand. *J. Mol. Struct.* **2020**, *1199*, 126901.
- (6) Das, G. C.; Kumar Das, A.; Das, D.; Raj Maity, T.; Samanta, A.; Ali Alasmary, F.; Salem Almalki, A.; Iqbal, A.; Dolai, M. Ortho-Vanillin Based Multifunctional Scaffold for Selective Detection of Al³⁺ and Zn²⁺ Employing Molecular Logic with DFT Study and Cell Imaging with Live Grass Pea. *J. Photochem. Photobiol. A Chem.* **2023**, *440*, 114663.

**Synthesis and characterization of a dioxomolybdenum complex [*cis*-MoO₂(OV)₂] using
ortho-vanilline (OV) as a ligand**

- (7) Muche, S.; Harms, K.; Biernasiuk, A.; Malm, A.; Popiołek, Ł.; Hordyjewska, A.; Olszewska, A.; Hołyńska, M. New Pd(II) Schiff Base Complexes Derived from Ortho-Vanillin and l-Tyrosine or l-Glutamic Acid: Synthesis, Characterization, Crystal Structures and Biological Properties. *Polyhedron* **2018**, *151*, 465–477.
- (8) G.H. Jeffery, J. Bassett, J. Mendham, R. C. D. A. *Vogel's Text Book of Quantitative Chemical Analysis, 5th Ed., Wesley Longman Limited, United Kingdom, 1989.*
- (9) Yamanouchi, K.; Yamada, S. Oxomolybdenum Complexes with Schiff Bases Obtained from Salicylaldehyde Derivatives and Alkyl- and Aryl-Amines. *Inorganica Chim. Acta* **1974**, *9*, 83–86.
- (10) Maruta, Y.; Abiko, A. Bis(Salicylaldehydato)Dioxomolybdenum Complexes: Catalysis for Ring-Opening Polymerization. *Polym. Bull.* **2014**, *71* (6), 1433–1440.
- (11) Bruker, APEX 2, SAINT, XPREP, Bruker AXS Inc., Madison, Wisconsin, USA, 2007.
- (12) Bruker, SADABS, Bruker AXS Inc., Madison, Wisconsin, USA, 2001.
- (13) SHELXS 97 and SHELXL 97: G. M. Sheldrick. *Acta Crystallogr., S. A. F.*; *Crystallogr.* **64**, 112 (2008).
- (14) Gaussian 09, (Revision A.1), Gaussian, Inc., Wallingford, CT, 2009.
- (15) Becke, A. D. Density-functional Thermochemistry. III. The Role of Exact Exchange. *J. Chem. Phys.* **1993**, *98* (7), 5648–5652.
- (16) Stephens, P. J.; Devlin, F. J.; Chabalowski, C. F.; Frisch, M. J. Ab Initio Calculation of Vibrational Absorption and Circular Dichroism Spectra Using Density Functional Force Fields. *J. Phys. Chem.* **1994**, *98* (45), 11623–11627.
- (17) Hertwig, R. H.; Koch, W. On the Parameterization of the Local Correlation Functional. What Is Becke-3-LYP? *Chem. Phys. Lett.* **1997**, *268* (5–6), 345–351.

**Synthesis and characterization of a dioxomolybdenum complex [*cis*-MoO₂(OV)₂] using
ortho-vanilline (OV) as a ligand**

- (18) Cossi, M.; Rega, N.; Scalmani, G.; Barone, V. Energies, Structures, and Electronic Properties of Molecules in Solution with the C-PCM Solvation Model. *J. Comput. Chem.* **2003**, *24* (6), 669–681.
- (19) Paul, S. S.; Selim, M.; Mukherjea, K. K. Synthesis, Characterization and DNA Nuclease Activity of Oxo-Peroxomolybdenum(VI) Complexes. *J. Coord. Chem.* **2017**, *70* (10), 1739–1760.
- (20) Paul, S. S.; Selim, M.; Saha, A.; Mukherjea, K. K. Synthesis and Structural Characterization of Dioxomolybdenum and Dioxotungsten Hydroxamato Complexes and Their Function in the Protection of Radiation Induced DNA Damage. *Dalt. Trans.* **2014**, *43* (7), 2835–2848.
- (21) Selim, M.; Saha, A.; Mukherjea, K. K. Protection of Radiation Induced DNA Damage by a Newly Developed Molybdenum Complex. *J. Radioanal. Nucl. Chem.* **2017**, *311* (1), 189–193.
- (22) Saha, U.; Palmajumder, E.; Mukherjea, K. K. Synthesis, Structure, DNA Binding Studies and Nuclease Activities of Two Luminescent Neodymium Complexes. *J. Coord. Chem.* **2016**, *69* (19), 2920–2941.
- (23) Liu, T.; Zhang, H. X.; Xia, B. H. Theoretical Studies on Structures and Spectroscopic Properties of a Series of Novel Cationic [Trans-(CAN)₂Ir(PH₃)₂]⁺ (CAN = Ppy, Bzq, Ppz, Dfppy). *J. Phys. Chem. A* **2007**, *111* (35), 8724–8730.
- (24) Zhou, X.; Zhang, H. X.; Pan, Q. J.; Xia, B. H.; Tang, A. C. Theoretical Studies of the Spectroscopic Properties of [Pt(Trpy)C≡CR] + (Trpy = 2,2',6',2''-Terpyridine; R = H, CH₂OH, and C₆H₅). *J. Phys. Chem. A* **2005**, *109* (39), 8809–8818.
- (25) Zhou, X.; Ren, A. M.; Feng, J. K. Theoretical Studies on the Ground States in M(Terpyridine)₂²⁺ and M(n-Butyl-Phenylterpyridine)₂²⁺ (M = Fe, Ru, Os) and

Synthesis and characterization of a dioxomolybdenum complex [*cis*-MoO₂(OV)₂] using
ortho-vanilline (OV) as a ligand

- Excited States in Ru(Terpyridine)₂²⁺ Using Density Functional Theory. *J. Organomet. Chem.* **2005**, 690 (2), 338–347.
- (26) Albertino, A.; Garino, C.; Ghiani, S.; Gobetto, R.; Nervi, C.; Salassa, L.; Rosenberg, E.; Sharmin, A.; Viscardi, G.; Buscaino, R.; Croce, G.; Milanesio, M. Photophysical Properties and Computational Investigations of Tricarbonylrhenium(I)[2-(4-Methylpyridin-2-Yl)Benzo[d]-X-Azole]L and Tricarbonylrhenium(I)[2-(Benzo[d]-X-Azol-2-Yl)-4-Methylquinoline]L Derivatives (X = N-CH₃, O, or S; L = Cl⁻, Pyridine). *J. Organomet. Chem.* **2007**, 692 (6), 1377–1391.

Chapter 13

Application of *cis*-MoO₂(OV)₂ in Protection of Radiation- Induced DNA Damage

1. Introduction:

Radiation therapy is a powerful technique in the fight against cancer. However, it comes with several drawbacks. While it effectively destroys cancer cells, it could simultaneously cause harm to healthy tissues that are present in the immediate vicinity of a radiation exposure. Reactive oxygen species (ROS) being the main culprit here, that initiates the damage that occurs as a consequence of incident radiation, capable of causing immense havoc on DNA.¹ To combat and control such situations scientists have explored the possibility of using antioxidants that can neutralize harmful ROS thus preventing harm that could have been caused to patients.² Dioxomolybdenum complexes that contain a molybdenum atom surrounded by two oxygen atoms in a dioxo configuration have shown promise as efficient scavengers of radicals. These complexes can interact with ROS and convert them to less harmful species, and in the process protect DNA from radiation-induced damage. Recent studies have investigated interactions between dioxomolybdenum complexes and DNA demonstrating an ability to scavenge radicals generated during radiolysis.³

This chapter focuses on a study that used a dioxomolybdenum complex of a bidentate ligand that protects plasmid DNA from gamma radiation. The protective effect of the dioxomolybdenum complex was examined *in vitro*, suggesting they could be used as radioprotectors for normal tissue during radiotherapy. However, further research is required to optimize their selectivity and efficacy to completely assess their potential both with regard to efficacy and toxic side effects.

2. Experimental Procedures:

2.1. Materials and physical methods:

Calf thymus DNA was procured from Sigma Chemical Company, USA while supercoiled plasmid pUC19 DNA was obtained from Genei, India. Tris-HCl buffer (pH ~ 7.4) was used to

Application of *cis*-MoO₂(OV)₂ in protection of radiation-induced DNA damage

prepare DNA solutions. Concentration of calf thymus DNA was determined considering molar extinction coefficient at 260 nm to be 6600 M⁻¹ cm⁻¹. Absorbance at 260 nm and 280 nm were noted for calculating A₂₆₀/A₂₈₀. Values being greater than 1.8 but less than 1.9 indicate the DNA was sufficiently free of protein. Quality of calf thymus DNA was also checked by its characteristic circular dichroism band at 260 nm recorded on a J815 Spectropolarimeter. The investigation was conducted using Millipore water.

2.2. Physical Measurements:

The thus prepared solution of calf thymus DNA was exposed to gamma radiation using a GC-900 Gamma Chamber. Any form of damage caused to calf thymus DNA was subsequently detected from the generated fluorescence obtained due to addition of ethidium bromide on to an irradiated solution of DNA used for investigation using a Perkin Elmer LS-55 spectrofluorimeter. To study the effects of radiation on DNA gel electrophoresis was performed using a UVP Bio Doc-It imaging system. Nicked DNA was evaluated using UVP DOC-ItLS software.

3. DNA binding Studies:

3.1. Fluorescence emission spectral studies for DNA interaction:

An attempt to realize binding was also made by maintaining *cis*-MoO₂(OV)₂ constant and adding increasing amount of DNA which was followed by fluorescence spectroscopy. In this case solutions were excited at 275 nm (going by the λ_{max} of *cis*-MoO₂(OV)₂ in methanol = 275 nm); emission was recorded at 315 nm. The experimental data obtained from fluorescence quenching was analyzed by the Stern-Volmer equation (Eq. 1)^{4,5}, a widely used technique to quantify quenching of fluorescence.

$$I_0/I = 1 + K_{SV}[DNA] \quad (1)$$

where I₀ and I are fluorescence intensities in the absence and presence of calf thymus DNA respectively; K_{SV} is Stern–Volmer quenching constant, which is a measure of the efficiency of

quenching by DNA that provides valuable insights into the nature and strength of the binding interaction between *cis*-MoO₂(OV)₂ and DNA. The results contribute significantly to our understanding of binding and potential application of *cis*-MoO₂(OV)₂ in DNA-related studies.

3.2. Viscometric study:

Viscosity measurements are presented as $(\eta/\eta_0)^{1/3}$ versus ratio of concentration of either ligand or complex to that of calf thymus DNA; η_0 denotes the viscosity of a solution of calf thymus DNA alone while η denotes viscosities of solutions of calf thymus DNA in the presence of compounds.⁶ Values were calculated from observed flow time of calf thymus DNA using the relation; $\eta = t - t_0$, where t and t_0 are values for flow times for the solution and buffer respectively.

4. DNA damage and protection:

4.1. Irradiation by gamma ray:

Incubation of calf thymus DNA and calf thymus DNA with complex was done at a temperature of 37°C for a duration of 30 minutes followed by irradiation using ⁶⁰Co γ rays. The irradiation process was performed under a dose rate of 1.88 kGyhr⁻¹ and a dose of 35 Gy was provided. For plasmid DNA samples, two different irradiation doses were employed i. e. 20 Gy and 25 Gy.

Our experiments were designed to intentionally exceed the standard therapeutic radiation dose employed during any routine cancer radiotherapy, in order to understand for ourselves the extent to which our prepared complex was performing as a suitable radioprotector. The deliberate increase in radiation dose was to induce extensive disruption of a DNA structure and in the presence of our prepared complex, to see that the same is prevented from occurring in order to clearly demonstrate the prepared compound acts as a radioprotector. In the process, it would enable an evaluation of the efficacy of the synthesized compound to protect DNA against what should otherwise be severe damage. All experiments were meticulously

Application of *cis*-MoO₂(OV)₂ in protection of radiation-induced DNA damage

conducted within well-controlled *in vitro* environments, providing a foundation to investigate effects of higher radiation dose. Such an investigation holds significant promise for clinical applications of the compound as an effective radioprotector during radiotherapy. The research aims to contribute to the development of improved therapeutic strategies for cancer treatment that enhance efficacy and safety of radiotherapy protocols.

4.2. Assessment of DNA damage followed by irradiation:

4.2.1. Estimation of radiation induced damage in calf thymus DNA by fluorescence spectroscopy:

To assess damage caused by radiation to calf thymus DNA, a ⁶⁰Co- γ ray source was used. Evaluation of the extent of damage was done with the help of fluorescence spectroscopy where ethidium bromide (EB) was used as the probe whose interaction with DNA shows a strong fluorescence. Emission of irradiated DNA that was treated with EB, following irradiation, was recorded at 591 nm (excitation at 500 nm). This was compared with the fluorescence of non-irradiated DNA-EB under identical experimental conditions. The dose-response relation was obtained by plotting $(I-I_a)/(I_0-I_a)$ versus dose^{3,7}, where I_a denotes fluorescence intensity of EB, I_0 denotes fluorescence intensity of unirradiated DNA treated with EB (the control), and I the fluorescence intensity of irradiated DNA that was subsequently treated with EB.

4.2.2. Protection of plasmid pUC19 DNA from radiation induced damage by the complexes and the ligand against different doses of gamma-radiation:

To evaluate the ability of *cis*-MoO₂(OV)₂ and the ligand (OV) to protect supercoiled pUC19 DNA subjected to gamma irradiation, solutions were pre-incubated having different concentrations of compounds (ranging from 0-2 mM) in Tris-HCl (buffer). Samples were exposed to gamma irradiation at doses of 20 Gy and 25 Gy. Protective effects of *cis*-MoO₂(OV)₂ and the ligand (OV) were assessed using agarose gel electrophoresis. Specifically, DNA samples were run on 0.9% agarose gel in 1 X TAE buffer for 3 hours at 80 mV, then

Application of *cis*-MoO₂(OV)₂ in protection of radiation-induced DNA damage

stained with EB solution and subjected to UV light. Images were captured using UVP Bio Doc-It Imaging System.

4.2.3. Mechanism of protection from radiation induced DNA damage by the ligands and the complexes; DPPH radical scavenging activity by EPR spectroscopy:

Electron paramagnetic resonance (EPR) measurements were carried out at room temperature (298 K) on a Jeol JES-FA 200 ESR spectrometer equipped with Jeol microwave bridge. Spectroscopic parameters were 9.44 GHz (frequency), 100 mT (field sweep), 0.998 mW (microwave power) and a modulation amplitude of 3000 mT. Stability of freshly prepared solution of DPPH in dichloromethane was assessed by monitoring the solution for 30 minutes, during which no significant loss of signal was detected.^{8,9} Subsequently, different concentrations (ranging from 0-40 μM) of *cis*-MoO₂(OV)₂ or the ligand (OV) were added to a 100 μM DPPH solution and mixed thoroughly. An EPR signal was recorded after 2 minutes of mixing of the compounds to the DPPH solution under identical instrumental conditions.

5. Results & discussions:

5.1. DNA binding studies:

Interaction between *cis*-MoO₂(OV)₂ and calf thymus DNA was realized by gradually adding calf thymus DNA to *cis*-MoO₂(OV)₂ and recording fluorescence at 315 nm. Excitation was made at 275 nm (Figure.1). A gradual decrease in fluorescence intensity was observed following increase in calf thymus DNA that provides evidence in favour of interaction between the complex and calf thymus DNA. Eventually, fluorescence intensity reached a plateau at a relatively high DNA concentration indicating a possible saturation of the binding sites in the DNA. Saturation suggests that binding sites on the DNA were occupied by the complex resulting in a constant intensity. To quantitatively assess the extent of fluorescence quenching, Stern-Volmer equation was employed that allows the determination of the fluorescence quenching constant (K_{SV}). This was found to be $1.4 \times 10^4 \text{ M}^{-1}$ for *cis*-MoO₂(OV)₂ at 25 °C. The

Application of *cis*-MoO₂(OV)₂ in protection of radiation-induced DNA damage

calculated value also provides evidence in favour of binding between *cis*-MoO₂(OV)₂ and calf thymus DNA guided by the quenching of fluorescence emission. These findings significantly contribute to a comprehensive understanding of interaction between *cis*-MoO₂(OV)₂ and the DNA used paving the way for potential applications of *cis*-MoO₂(OV)₂ in various aspects of biology.

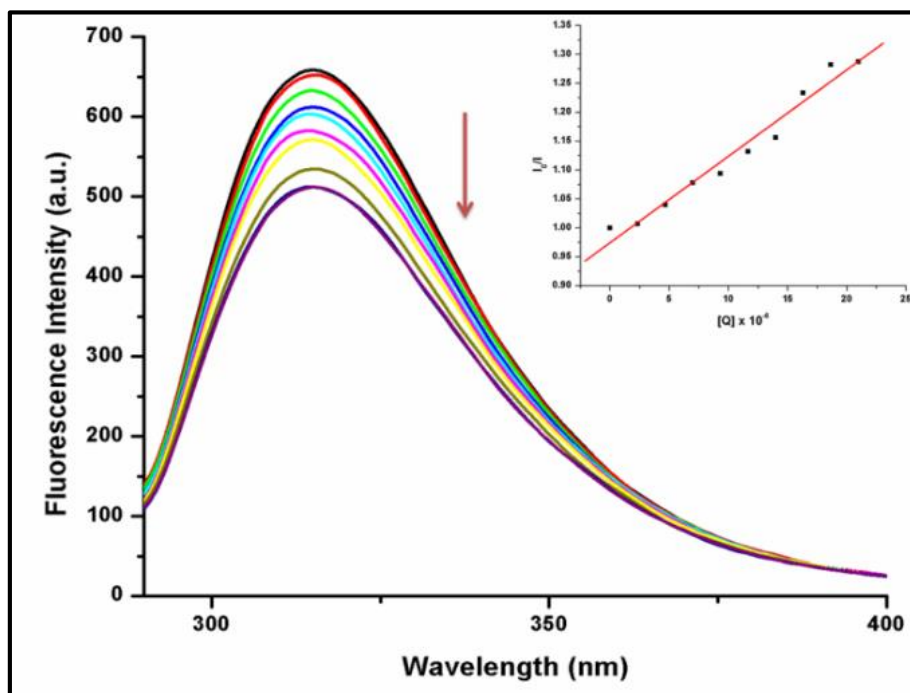


Figure 1: Emission spectra *cis*-MoO₂(OV)₂ in the presence of increasing amounts of DNA
[Inset: Stern–Volmer plot]

To gain an insight into the mode of binding of the complex with calf thymus DNA, viscosity measurements were made; being a sensitive technique^{10–13} in this regard. The relative specific viscosities of DNA in the presence and absence of *cis*-MoO₂(OV)₂ or the ligand (OV) were plotted against [complex]/[DNA] (Figure.2). Results show addition of both compounds solutions of calf thymus DNA does not cause any significant increase in viscosity that rules out the possibility of intercalation. Small molecules binding to DNA at grooves do not alter relative viscosity. Thus viscosity measurements strongly suggest that *cis*-MoO₂(OV)₂ and the ligand bind to the groove at the groove.

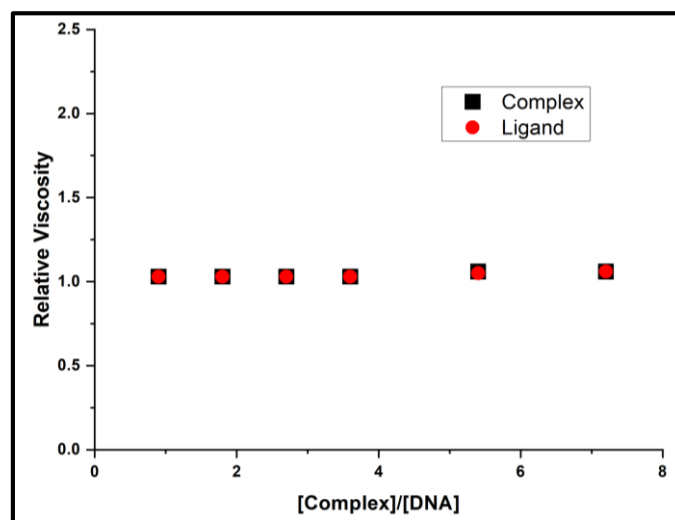


Figure 2: Effect of increasing amount of *cis*-MoO₂(OV)₂ and **ligand (OV)** on the specific viscosity of calf thymus DNA.

5.2. Possible protection to attempted radiation induced damage to DNA

Radiation-induced damage or modification caused to DNA may be determined by measuring the fluorescence response of the DNA being treated with ethidium bromide (EB).¹⁴⁻¹⁶ In aqueous solution EB has weak emission. However, its emission intensity increases significantly when bound to DNA owing to its ability to intercalate between the adjacent strands of DNA. When a DNA double helix sustains damage owing to any form of stimuli (here it being gamma rays), then the interaction of EB with DNA gets affected which is manifested almost quantitatively in the fluorescence response of the DNA-EB adduct. Hence, decrease in fluorescence intensity following DNA being subjected to external stimuli and treated with EB against that of interaction of EB with the same DNA that was not subjected to such stimuli, serves as a measure of a possible damage or modification caused to the DNA by the external stimuli. This model is therefore useful as a probe to estimate radiation-induced DNA damage.^{5,17} Hence, if there is either no change observed with regard to fluorescence for DNA subjected to irradiation in the presence of any compound or that the change observed is negligible in comparison to the same DNA unirradiated and treated with EB then it may be said that the compound maintained alongside the DNA during irradiation, provides some sort

Application of *cis*-MoO₂(OV)₂ in protection of radiation-induced DNA damage

of protection as a consequence of which irradiation (the external stimuli, in this case) that was unable to inflict any damage on to the DNA. Such compounds that provide protection to an attempted radiation-induced damage owing to their presence in close vicinity of a target on which a damage was intended are termed as radio-protectors and a method such as this one helps to qualitatively ascertain, to some extent evaluate the protection afforded by that compound.

5.2.1. Estimation of the protection of DNA damage by fluorometric technique:

To have a clear idea on possible protection from radiation induced damage, the DNA was pretreated with different concentrations of either the ligand (OV) or *cis*-MoO₂(OV)₂. Irradiated samples as well as those that received no irradiation were subsequently treated with EB and emission was measured. It was observed that fluorescence intensity of the EB-DNA solutions increased with an increase in concentration of either ligand or complex, and approaching to the intensity of EB with non-irradiated DNA, which clearly indicates that both the complex and the ligand are actually able to protect the DNA from radiation induced damage Figure 3 (i) & (ii). Concentration of the ligand or of the complex was maintained in the range 0- 24 μM. It was observed that with an increase in the concentration of the ligand (OV) or of *cis*-MoO₂(OV)₂, the complex, there was a gradual increase in fluorescence intensity of EB bound to irradiated DNA. This indicates that the complex as well as ligand imparts protection to calf thymus DNA from damage induced by radiation.

A plot of $(I - I_a)/(I_0 - I_a)$ versus [radioprotector]/[calf thymus DNA] is shown as inset in Figure 3 (i) & (ii). It is found that with increase in concentration of either the ligand (OV) *cis*-MoO₂(OV)₂, the damage that could have been caused to calf thymus DNA due to irradiation are actually inhibited. Precisely, percentage of protection imparted either by the ligand was evaluated to be 79%, whereas that due to *cis*-MoO₂(OV)₂ was calculated to be ~ 89%. Hence,

it may be concluded that both *cis*-MoO₂(OV)₂ and the ligand OV provide reasonably good protection to calf thymus DNA from radiation induced damage.

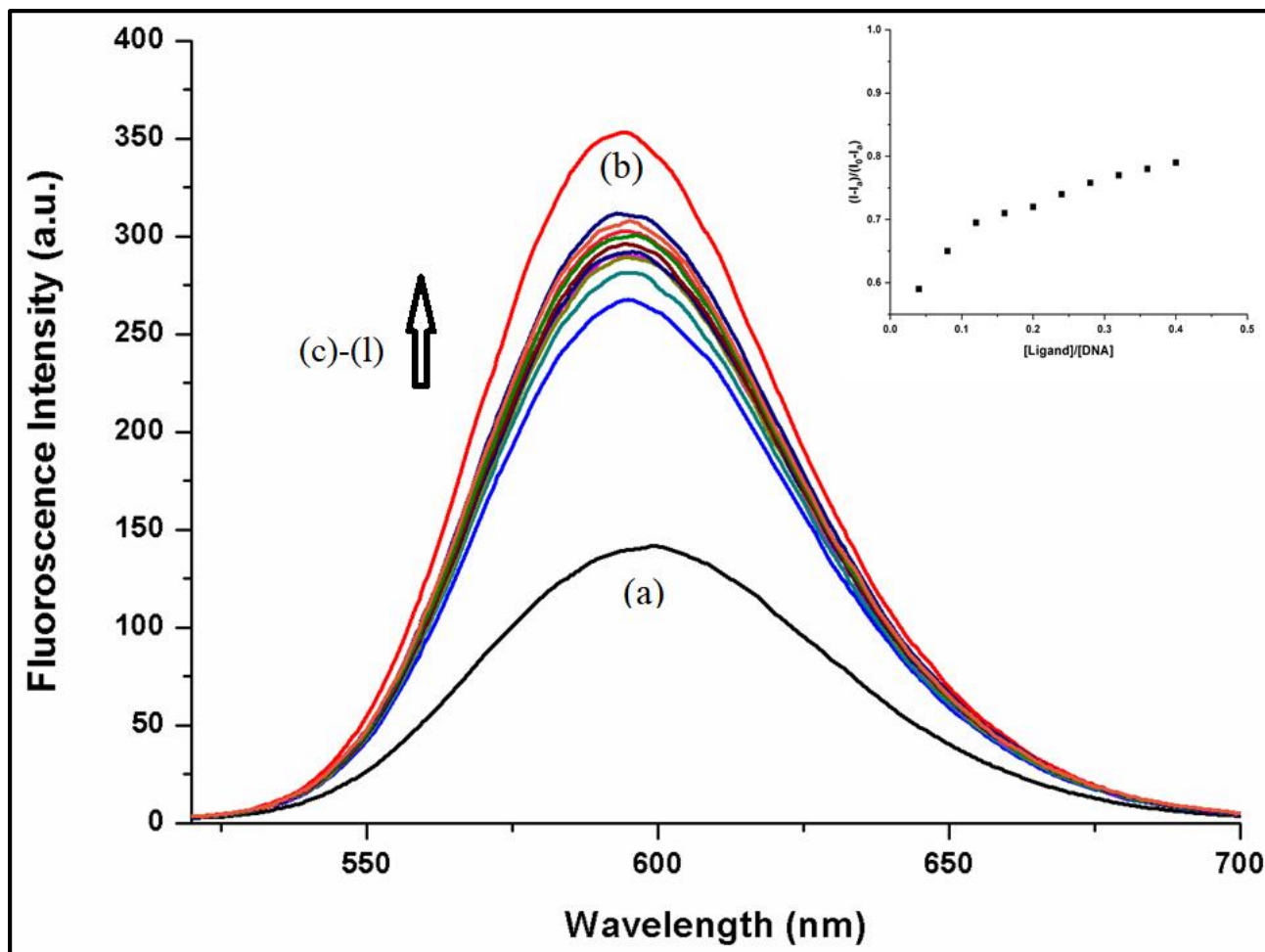


Figure 3 (i): Fluorescence emission spectra of EB-DNA obtained after treatment of calf thymus DNA with EB following irradiation provided to DNA solutions either in absence or the presence of increasing amounts of **ligand (OV)**; (a) = EB 900 μ M, (b) = DNA 60 μ M (unirradiated) + EB 900 μ M (maintained 15 folds higher), (c)-(l) = DNA 60 μ M (irradiated) + increasing concentration of the ligand (0-24 μ M) + EB 900 μ M {Inset: Plot of $(I - I_a)/(I_0 - I_a)$ versus $[\text{ligand}]/[\text{calf thymus DNA}]$ }

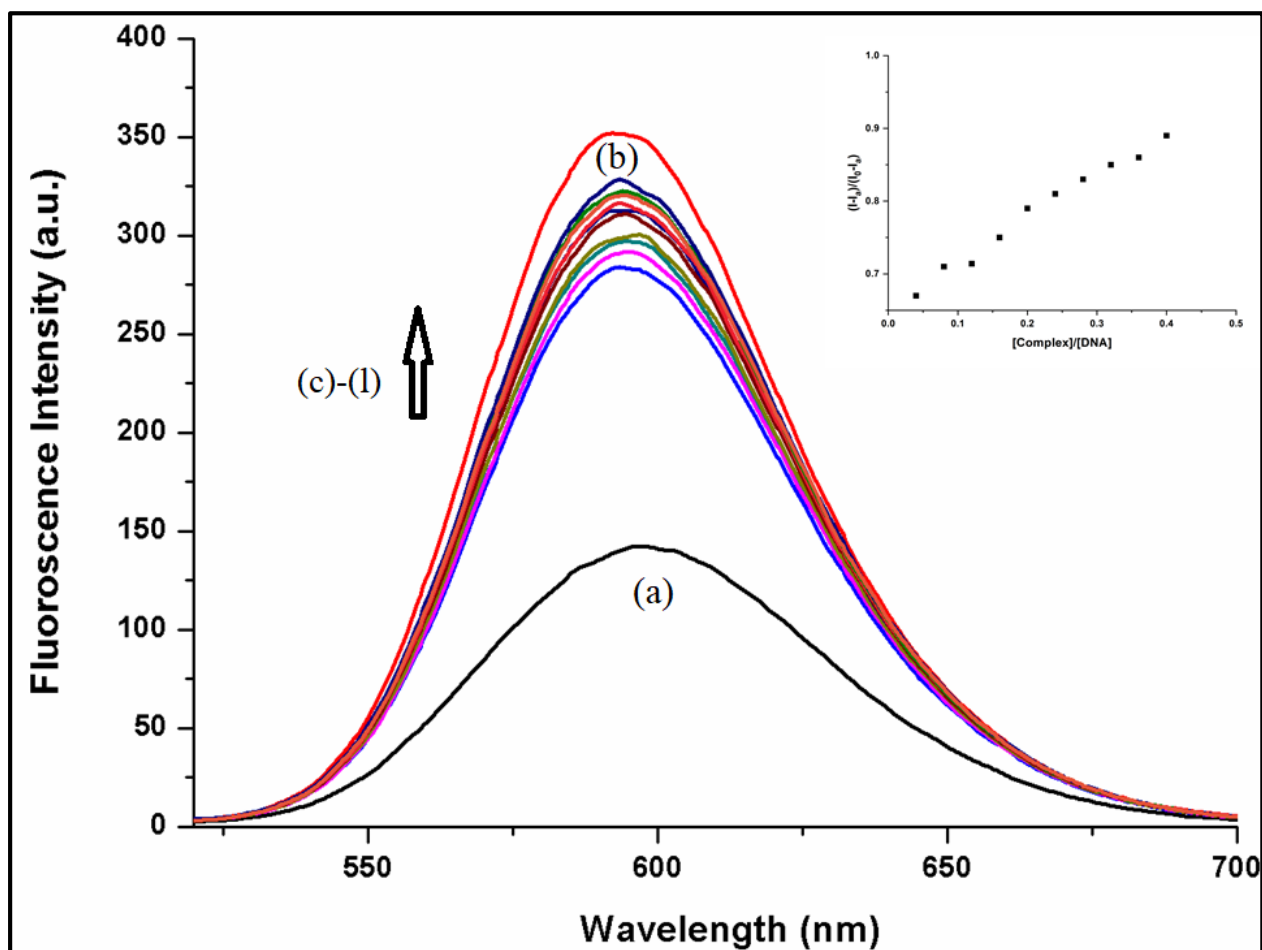


Figure 3 (ii): Fluorescence emission spectra of EB-DNA obtained after treatment of calf thymus DNA with EB following irradiation provided to DNA solutions either in absence or the presence of increasing amounts of *cis*-MoO₂(OV)₂; (a) = EB 900 μ M, (b) = DNA 60 μ M (unirradiated) + EB 900 μ M (maintained 15 folds higher) (c)-(I) = DNA 60 μ M (irradiated) + increasing concentration of the complex (0-24 μ M) + EB 900 μ M {Inset: Plot of $(I - I_a)/(I_0 - I_a)$ versus $[\text{complex}]/[\text{calf thymus DNA}]$ }

5.2.2. Discussion the contribution of the ligand (OV) and *cis*-MoO₂(OV)₂ in protection of plasmid pUC19 DNA from damage induced by gamma radiation:

To investigate the protective abilities of the ligand OV and *cis*-MoO₂(OV)₂ on plasmid DNA against gamma-radiation-induced damage, gel electrophoresis was conducted using supercoiled pUC19 DNA in Tris-HCl/NaCl (buffer) at pH 7.2. When plasmid DNA was

Application of *cis*-MoO₂(OV)₂ in protection of radiation-induced DNA damage

exposed to different dose of gamma radiation (25 Gy and 20 Gy), it resulted in strand breaks causing the DNA to transition from a supercoiled (SC) form to a nicked coil (NC) form.^{3,18,19} This transition was clearly observed through experiments performed and is shown in figures (Figure 4 & 5). The extent of protection provided by *cis*-MoO₂(OV)₂ and the ligand OV can be quantified by assessing the difference in DNA strand conversion from supercoiled (SC) to nicked coil (NC) form upon exposure to radiation. By comparing gel electrophoresis results, it is evident that *cis*-MoO₂(OV)₂ and ligand significantly reduce the conversion of DNA strands from SC to NC, indicating their ability to protect the DNA from radiation-induced damage. To evaluate such protective effects of the ligand (OV) and *cis*-MoO₂(OV)₂ against radiation-induced damage, on pUC19 DNA, the DNA was pre-treated with various concentrations of either *cis*-MoO₂(OV)₂ or ligand and exposed to irradiation. The results that are presented in Table 1 (Figure 6 & 7), demonstrate a significant level of protection to the DNA from radiation due to ⁶⁰Co γ rays. Quantification of protection is further supported by calculation, indicating the extent to which the complex or the ligand shield pUC19 DNA from a probable radiation induced damage. Notably, the *cis*-MoO₂(OV)₂ offers a remarkable level of protection, with approximately 85% to 80% preservation of the SC form at radiation dose of 20 Gy and 25 Gy respectively. The ligand (OV) exhibits a protective effect of ~ 72% and ~ 70% of the SC form from radiation-induced damage at the same respective radiation dose (20 Gy and 25 Gy). These quantitative measurements provide compelling evidence that both *cis*-MoO₂(OV)₂ (the complex) and the ligand possess substantial protective capabilities against gamma-radiation-induced DNA damage. Reduced conversions of DNA strands from the SC form to the NC form coupled with quantified percentages of protection confirm the effectiveness of the compounds in mitigating detrimental effects of radiation on the integrity of the DNA that was used as the target.

Application of *cis*-MoO₂(OV)₂ in protection of radiation-induced DNA damage

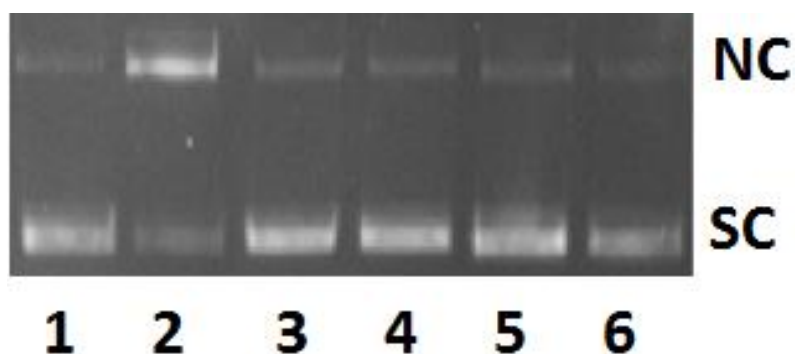


Figure 4: Protection of plasmid pUC19 DNA at **25 Gy** with different concentrations of **ligand (OV)** and *cis*-MoO₂(OV)₂ on gamma-radiation induced strand breaks. *Lane 1*: DNA control (No irradiation); *Lane 2*: DNA irradiated; *Lane 3*: DNA + 1 mM OV; *Lane 4*: DNA + 1 mM *cis*-MoO₂(OV)₂; *Lane 5*: DNA + 2 mM OV; *Lane 6*: DNA + 2 mM *cis*-MoO₂(OV)₂

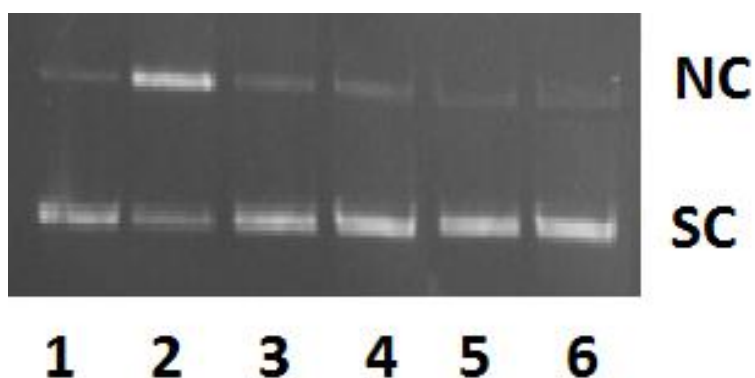


Figure 5: Protection of plasmid (pUC19) DNA at **20 Gy** with different concentrations of **ligand (OV)** and *cis*-MoO₂(OV)₂ on gamma-radiation induced strand breaks. *Lane 1*: DNA control (No irradiation); *Lane 2*: DNA irradiated; *Lane 3*: DNA + 1 mM OV; *Lane 4*: DNA + 1 mM *cis*-MoO₂(OV)₂; *Lane 5*: DNA + 2 mM OV; *Lane 6*: DNA + 2 mM *cis*-MoO₂(OV)₂

Application of *cis*-MoO₂(OV)₂ in protection of radiation-induced DNA damage

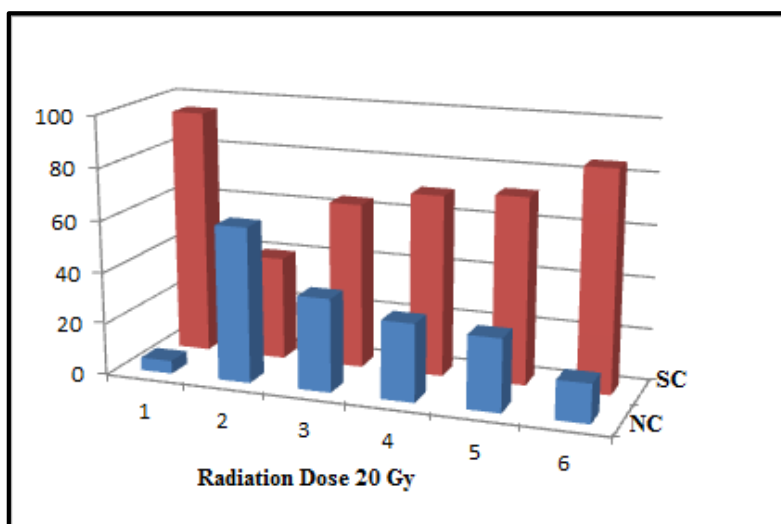


Figure 6: A graphical representation of the protection provided by the ligand (OV) and *cis*-MoO₂(OV)₂ under a radiation dose of 20 Gy.

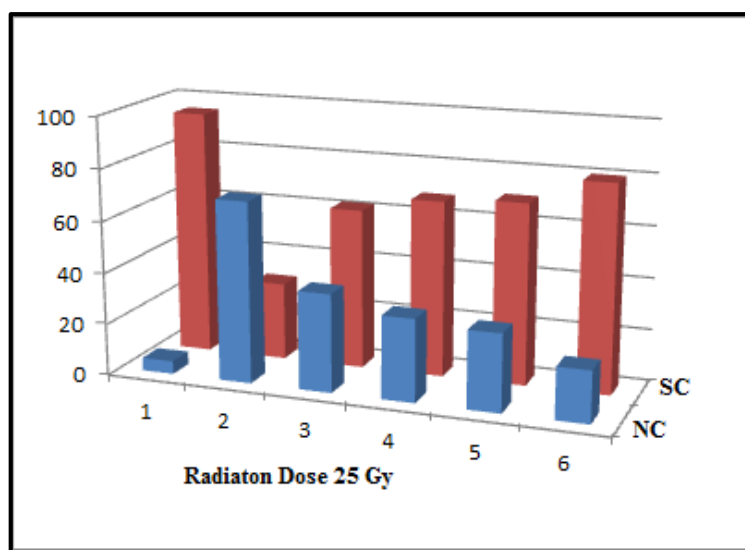


Figure 7: A graphical representation of protection by the ligand (OV) and *cis*-MoO₂(OV)₂ under radiation dose of 25 Gy.

Table 1: Extent of protection provided to SC form of pUC19 DNA by OV and *cis*-MoO₂(OV)₂

Lane no.	Reaction condition	<i>Form I</i> (% SC)		<i>Form II</i> (% NC)	
1	DNA Control (No irradiation)	95		5	
Lane no.	Radiation dose	20 Gy		25 Gy	
	Reaction condition	<i>Form I</i> (% SC)	<i>Form II</i> (% NC)	<i>Form I</i> (% SC)	<i>Form II</i> (% NC)
2	DNA irradiated	40	60	30	70
3	DNA + 1 mM OV	64	36	62	38
4	DNA + 1 mM <i>cis</i> -MoO ₂ (OV) ₂	70	30	68	32
5	DNA + 2 mM OV	72	28	70	30
6	DNA + 2 mM <i>cis</i> -MoO ₂ (OV) ₂	85	15	80	20

5.2.3. Mechanism of protection from radiation induced DNA damage: An assessment of scavenging of DPPH by EPR spectroscopy:

Generation of radicals during and subsequent to irradiation of an aqueous solution by ⁶⁰Co γ rays is capable of inducing damage to biomolecules. In our experiments, DNA was used as the target. Under normal circumstances, these radicals that are generated would interact with the DNA and induce modifications on it that in common terms referred to as damage. Hence,

Application of *cis*-MoO₂(OV)₂ in protection of radiation-induced DNA damage

elimination of such radicals from the solution should be able to protect the molecules (here DNA) present in the solution from any damage induced by the incident radiation. Therefore, if any entity, capable of scavenging such produced free radicals be present in solution during the radiolysis of water, it should protect other molecules present (here DNA) in the same solution from any possible damage. Hence, to examine the radical scavenging ability of the compounds we were studying, EPR spectroscopy was used. DPPH is a widely known substance that is used in case of such studies to evaluate antioxidant capabilities of natural and synthetic products, being a stable radical itself.²⁰ We used it and monitored the EPR signal of DPPH to establish the free radical scavenging activity of *cis*-MoO₂(OV)₂ and OV (the ligand). EPR spectrum of DPPH (100 μM) in DCM was taken. Subsequently, the same DPPH was titrated with incremental amounts of either OV or *cis*-MoO₂(OV)₂ (0–40 μM) (Figure.8) and EPR spectra were recorded under identical conditions. Although, both *cis*-MoO₂(OV)₂ and OV could induce scavenging of free radicals present on DPPH, the effect was more pronounced in case of the complex. This strongly supports our experimental findings pertaining to damage caused to DNA and protection provided by compounds in this regard.

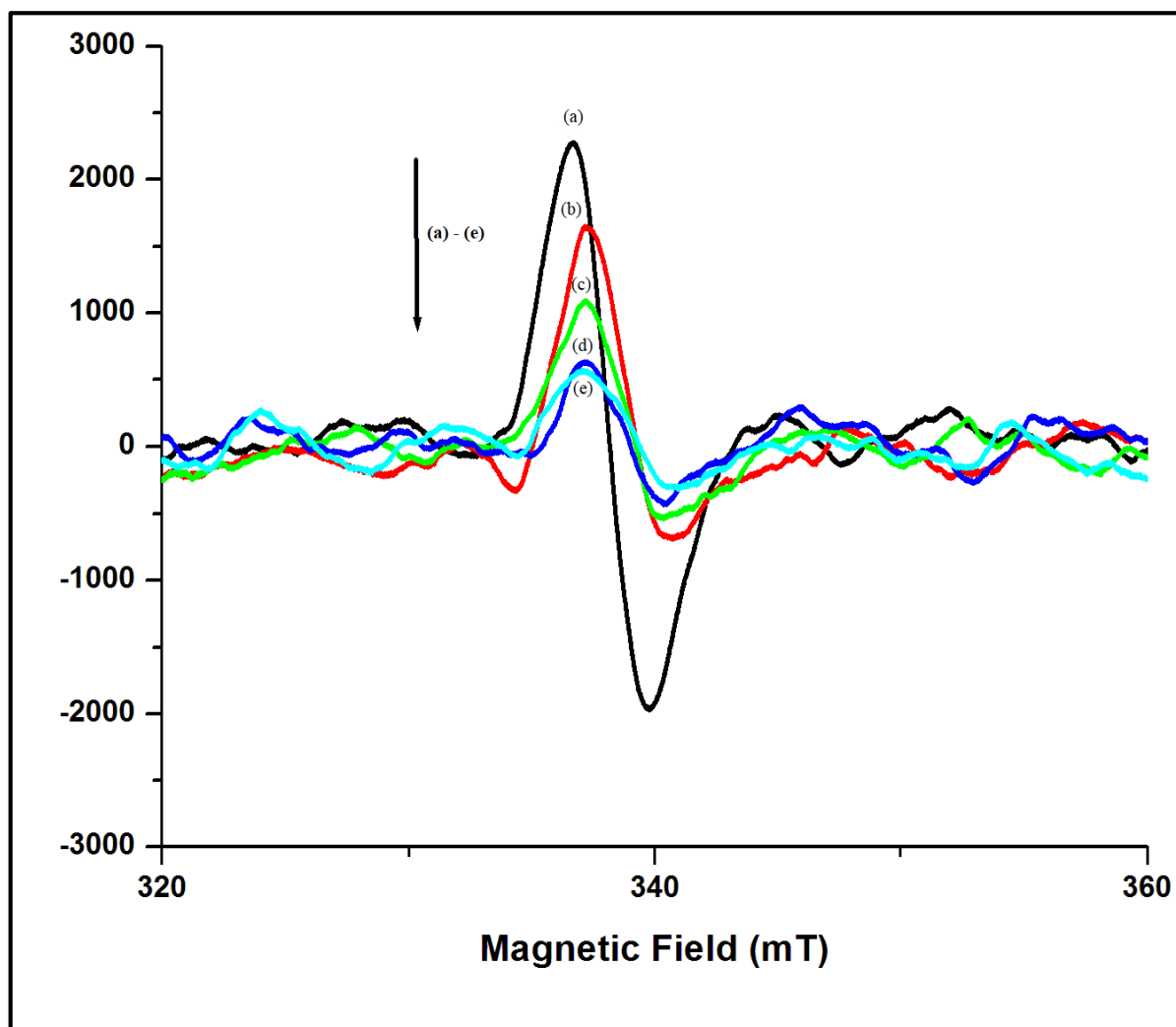


Figure 8 (i): EPR spectra of DPPH (*a*:100 μM DPPH) with different concentrations of *cis*-MoO₂(OV)₂ in DCM solution (*b*:10μM; *c*:20μM; *d*: 30μM; *e*: 40μM)

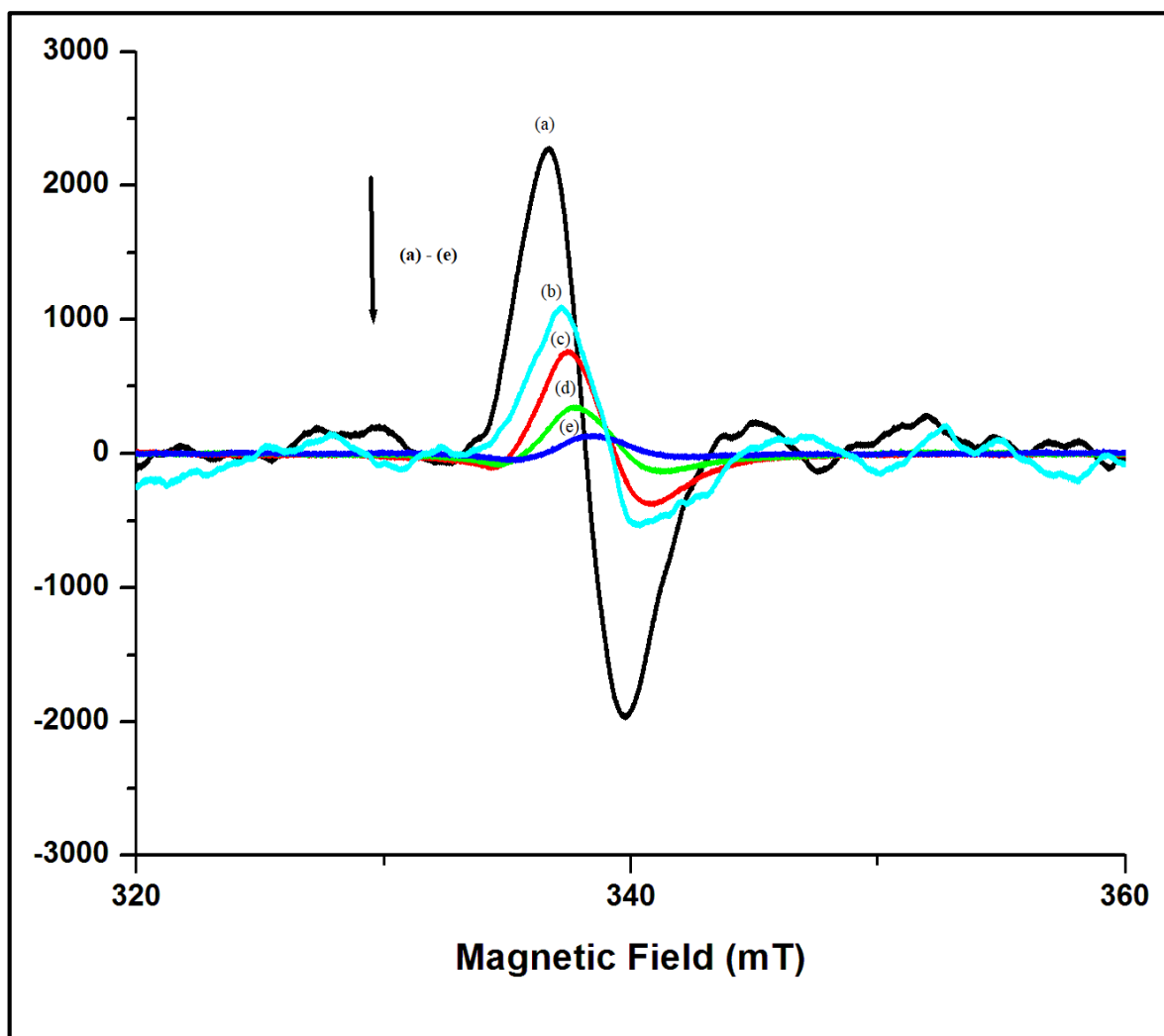


Figure 8 (ii): EPR spectra of DPPH (*a*: 100 μ M DPPH) with different concentrations of **ligand (OV)** in DCM solution (*b*: 10 μ M; *c*: 20 μ M; *d*: 30 μ M; *e*: 40 μ M)

6. Conclusion:

In this study, a molybdenum complex was synthesized and found to have a remarkable ability to protect DNA from radiation-induced damage. Compared to the ligand (OV), the complex [*cis*-MoO₂(OV)₂] demonstrated a higher degree of radioprotective effect, protecting 89% of damaged plasmid DNA. At a dosage of 20Gy, at a concentration of 2 mM the *cis*-MoO₂(OV)₂ was able to protect approximately 85% of radiation-induced damage to plasmid (pUC19) DNA from gamma rays. These findings suggest that *cis*-MoO₂(OV)₂ has tremendous potential as an efficient radioprotector for normal tissues in radiotherapy. The ability of the complex to protect

Application of *cis*-MoO₂(OV)₂ in protection of radiation-induced DNA damage

DNA from radiation-induced damage is particularly noteworthy, and the results of this study could have significant implications for the development of new therapies for a range of medical conditions. This exciting discovery could pave the way for significant advances in the field of radioprotection.

References:

- (1) Nilsson, R.; Liu, N. A. Nuclear DNA Damages Generated by Reactive Oxygen Molecules (ROS) under Oxidative Stress and Their Relevance to Human Cancers, Including Ionizing Radiation-Induced Neoplasia Part I: Physical, Chemical and Molecular Biology Aspects. *Radiat. Med. Prot.* **2020**, *1* (3), 140–152.
- (2) Poljsak, B. Strategies for Reducing or Preventing the Generation of Oxidative Stress. *Oxid. Med. Cell. Longev.* **2011**.
- (3) Paul, S. S.; Selim, M.; Saha, A.; Mukherjea, K. K. Synthesis and Structural Characterization of Dioxomolybdenum and Dioxotungsten Hydroxamato Complexes and Their Function in the Protection of Radiation Induced DNA Damage. *Dalt. Trans.* **2014**, *43* (7), 2835–2848.
- (4) Wolfe, A.; Shimer, G. H.; Meehan, T. Polycyclic Aromatic Hydrocarbons Physically Intercalate into Duplex Regions of Denatured DNA. *Biochemistry* **1987**, *26* (20), 6392–6396.
- (5) Paul, S. S.; Selim, M.; Saha, A.; Mukherjea, K. K. Synthesis and Structural Characterization of Dioxomolybdenum and Dioxotungsten Hydroxamato Complexes and Their Function in the Protection of Radiation Induced DNA Damage. *Dalt. Trans.* **2014**, *43* (7), 2835–2848.

Application of *cis*-MoO₂(OV)₂ in protection of radiation-induced DNA damage

- (6) Chaires, J. B.; Dattagupta, N.; Crothers, D. M. Studies on Interaction of Anthracycline Antibiotics and Deoxyribonucleic Acid: Equilibrium Binding Studies on Interaction of Daunomycin with Deoxyribonucleic Acid. *Biochemistry* **1982**, *21* (17), 3933–3940.
- (7) Selim, M.; Saha, A.; Mukherjea, K. K. Protection of Radiation Induced DNA Damage by a Newly Developed Molybdenum Complex. *J. Radioanal. Nucl. Chem.* **2017**, *311* (1), 189–193.
- (8) Hatano, T.; Kagawa, H.; Yasuhara, T.; Okuda, T. Two New Flavonoids and Other Constituents in Licorice Root: Their Relative Astringency and Radical Scavenging Effects. *Chem. Pharm. Bull.* **1988**, *36* (6), 2090–2097.
- (9) J. A. Weil, J. R. B. J. E. W. *Electron Paramagnetic Resonance: Elementary Theory and Applications*, New York, John Wiley & Sons, 1994.
- (10) Liu, Y. chun; Yang, Z. yin. Crystal Structures, Antioxidation and DNA Binding Properties of Dy(III) Complexes with Schiff-Base Ligands Derived from 8-Hydroxyquinoline-2-Carboxaldehyde and Four Aroylhydrazines. *Eur. J. Med. Chem.* **2009**, *44* (12), 5080–5089.
- (11) Satyanarayana, S.; Dabrowiak, J. C.; Chaires, J. B. Tris(Phenanthroline)Ruthenium(II) Enantiomer Interactions with DNA: Mode and Specificity of Binding. *Biochemistry* **1993**, *32* (10), 2573–2584.
- (12) Sigman, D. S.; Mazumder, A.; Perrin, D. M. Chemical Nucleases. *Chem. Rev.* **1993**, *93* (6), 2295–2316.
- (13) Deb, P.; Ghose, M.; Sepay, N.; Maiti, S.; Mukherjea, K. K. Synthesis, Characterization, Theoretical Simulation, and DNA-Nuclease Activity of a Newly Synthesized Mn–Oximato Complex. *J. Coord. Chem.* **2018**, *71* (20), 3250–3265.

Application of *cis*-MoO₂(OV)₂ in protection of radiation-induced DNA damage

- (14) Richard Morgan, A.; Pulleyblank, D. E. Native and Denatured DNA, Cross-Linked and Palindromic DNA and Circular Covalently-Closed DNA Analysed by a Sensitive Fluorometric Procedure. *Biochem. Biophys. Res. Commun.* **1974**, *61* (2), 396–403.
- (15) Prütz, W. A. Inhibition of DNA-Ethidium Bromide Intercalation Due to Free Radical Attack upon DNA. *Radiat. Environ. Biophys.* *1984* **1984**, *23* (1), 1–6.
- (16) Prütz, W. A. Measurement of Copper-Dependent Oxidative DNA Damage by HOCl and H₂O₂ with the Ethidium-Binding Assay. *J. Biochem. Biophys. Methods* **1996**, *32* (2), 125–135.
- (17) Ganguly, D.; Santra, R. C.; Mazumdar, S.; Saha, A.; Karmakar, P.; Das, S. Radioprotection of Thymine and Calf Thymus DNA by an Azo Compound: Mechanism of Action Followed by DPPH Radical Quenching & ROS Depletion in WI 38 Lung Fibroblast Cells. **2020**.
- (18) Froehlich, E.; Mandeville, J. S.; Weinert, C. M.; Kreplak, L.; Tajmir-Riahi, H. A. Bundling and Aggregation of DNA by Cationic Dendrimers. *Biomacromolecules* **2011**, *12* (2), 511–517.
- (19) Rogers, K. R.; Apostol, A.; Madsen, S. J.; Spencer, C. W. Detection of Low Dose Radiation Induced DNA Damage Using Temperature Differential Fluorescence Assay. *Anal. Chem.* **1999**, *71* (19), 4423–4426.
- (20) Gao, Z.; Huang, K.; Yang, X.; Xu, H. Free Radical Scavenging and Antioxidant Activities of Flavonoids Extracted from the Radix of *Scutellaria Baicalensis* Georgi. *Biochim. Biophys. Acta - Gen. Subj.* **1999**, *1472* (3), 643–650.

Chapter 14

Application of *cis*-MoO₂(OV)₂ in Haloperoxidase

Mimicking Oxidative Bromination

1. Introduction:

Synthetic biomimetic haloperoxidase (HPO) catalysts were designed to imitate the structure and functions of natural HPO enzymes. These biomimetic catalysts have the potential to catalyze useful reactions in an efficient and environmentally friendly way compared to traditional catalysts. Recent years have witnessed an extensive research towards development of biomimetic HPO catalysts.¹ One approach to achieving this was to synthesize new molecules that mimic the active site of HPO.² The field of biomimetic HPO catalysts is promising and has the potential to lead to development of novel and more efficient catalysts for diverse applications. However, further research is necessary to fully comprehend structures and functions of HPO and develop more efficient biomimetic catalysts based on their understanding. The discovery of vanadium haloperoxidases (VHPOs) has created substantial interest in understanding their active site structure and mode of action. Researchers have identified numerous vanadium complexes that could serve as structural and/or functional models for VHPOs. One significant development in this area was a pioneering work of A. Butler et al., who was the first to create haloperoxidase mimics.³ This led to the discovery of *in vitro* bromoperoxidase activity by some molybdenum complexes. Specifically, oxidoperoxidomolybdenum(VI) complexes were identified as functional mimics of vanadium bromoperoxidases capable of catalyzing two-electron oxidation of Br⁻ to Br⁺ in the presence of H₂O₂.³⁻⁵

In this chapter, the work performed with a dioxomolybdenum complex aimed at determining its ability to mimic biological catalysts using VHPO is reported. Findings indicate that the compound showed a favorable response, highlighting its potential application as a VHPO mimic. The findings represent a crucial step toward developing new effective catalysts for diverse applications.

2. Experimental Procedures:

2.1. Materials and physical methods:

Hydrogen peroxide (30% w/v), phenol red and other reagents required for the study were purchased from Merck (India) and utilized as received. Analytical grade solvents were used for physico-chemical studies and were further purified utilizing literature methods.⁶ Throughout the investigation, Millipore water was used.

2.2. Physical Measurements:

UV-vis spectra in the range 200 nm to 800 nm were obtained using a Shimadzu U-1800 spectrophotometer. All spectra were recorded against their corresponding reagent blanks using a 1 cm quartz cell. pH measurements were conducted on a digital pH meter Elico (India).

2.3. Evaluation of Bromination Capability:

The bromination reaction was carried out in an aqueous medium at 30 ± 0.5 °C. Reactions involving bromide were performed under constant temperature. Solutions used for kinetic measurements were maintained at a constant concentration of H⁺ (pH = 5.0) by addition of NaH₂PO₄-Na₂HPO₄.⁷

Rate of the reaction studied may be described by the rate equation: $dc/dt = k c_1^x c_2^y c_3^z$, from which “ $\log (dc/dt) = \log k + x \log c_1 + y \log c_2 + z \log c_3$ ” was obtained, corresponding to “ $-\log (dc/dt) = -x \log c_1 - b$ ($b = \log k + y \log c_2 + z \log c_3$)”, where k is the reaction rate constant. c_1 , c_2 , c_3 are concentrations of *cis*-MoO₂(OV)₂, KBr and phenol red respectively; while x , y and z are the corresponding reaction orders. This therefore corresponds to $-\log (dA/dt) = -x \log c_1 - b$ ($b = \log k + y \log c_2 + z \log c_3$), where A is the measurable absorbance of the resultant solution; k the reaction rate constant; c_1 , c_2 , c_3 concentrations of *cis*-MoO₂(OV)₂, KBr and phenol red respectively; while x , y and z are the corresponding reaction orders. A plot of the absorbance data at 592 nm *versus* time provides a straight line whose slope gives

Application of *cis*-MoO₂(OV)₂ in Haloperoxidase Mimicking Oxidative Bromination

the reaction rate of the complex (dA/dt). Changing the concentration of the complex, a series of dA/dt data were obtained and from a plot of $-\log(dA/dt)$ versus $-\log c_1$ the reaction rate constant (k) was calculated.

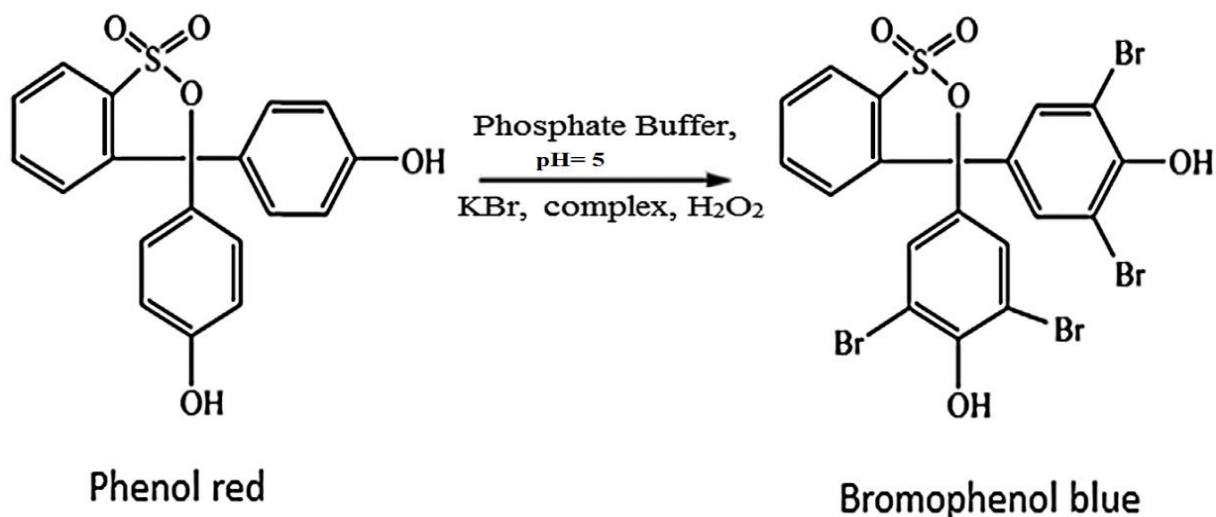
3. Results and discussions:

The purpose of the work was to develop a bromoperoxidase mimic, which is currently an area of significant interest in the field of biochemistry. Previous studies have identified oxidovanadium complexes as potential mimics of catalytic reactions performed by bromoperoxidases. This reaction involves bromination of organic substrates in presence of H₂O₂ and KBr. To assess the catalytic ability of metal complexes to act as haloperoxidases, one commonly used method is to examine the model catalytic bromination reaction of phenol red to bromophenol blue.^{8,9} This reaction has been used in numerous studies. Various research work also found oxidoperoxidomolybdenum complexes to possess bromoperoxidase activity.^{9,10} In this investigation, a dioxomolybdenum *cis*-MoO₂(OV)₂ showed catalytic activity which was monitored by UV-vis spectrophotometry, as in Figure 1; phenol red serving as the substrate.

3.1. Bromination activity of the complex for mimicking VHPO:

The aim of this study was to evaluate the catalytic potential of *cis*-MoO₂(OV)₂ for bromination using phenol red as the substrate. The reaction involves conversion of phenol red to bromophenol blue in a stoichiometric manner; the reaction being pretty fast (as shown in Scheme 1).

Application of *cis*-MoO₂(OV)₂ in Haloperoxidase Mimicking Oxidative Bromination



Scheme 1. The reactive process of bromination reaction for the complex [*cis*-MoO₂(OV)₂].

Upon addition of *cis*-MoO₂(OV)₂ solution to a standard bromide reaction in phosphate buffer containing phenol red as the trapping agent for oxidized bromine, the color of the solution changed from yellow to blue. UV-vis spectrophotometry revealed gradual decrease in absorption at 443 nm, corresponding to loss of phenol red during catalytic conversion. Simultaneously, a new peak appeared at 592 nm due to formation of bromophenol blue (Figure 1).

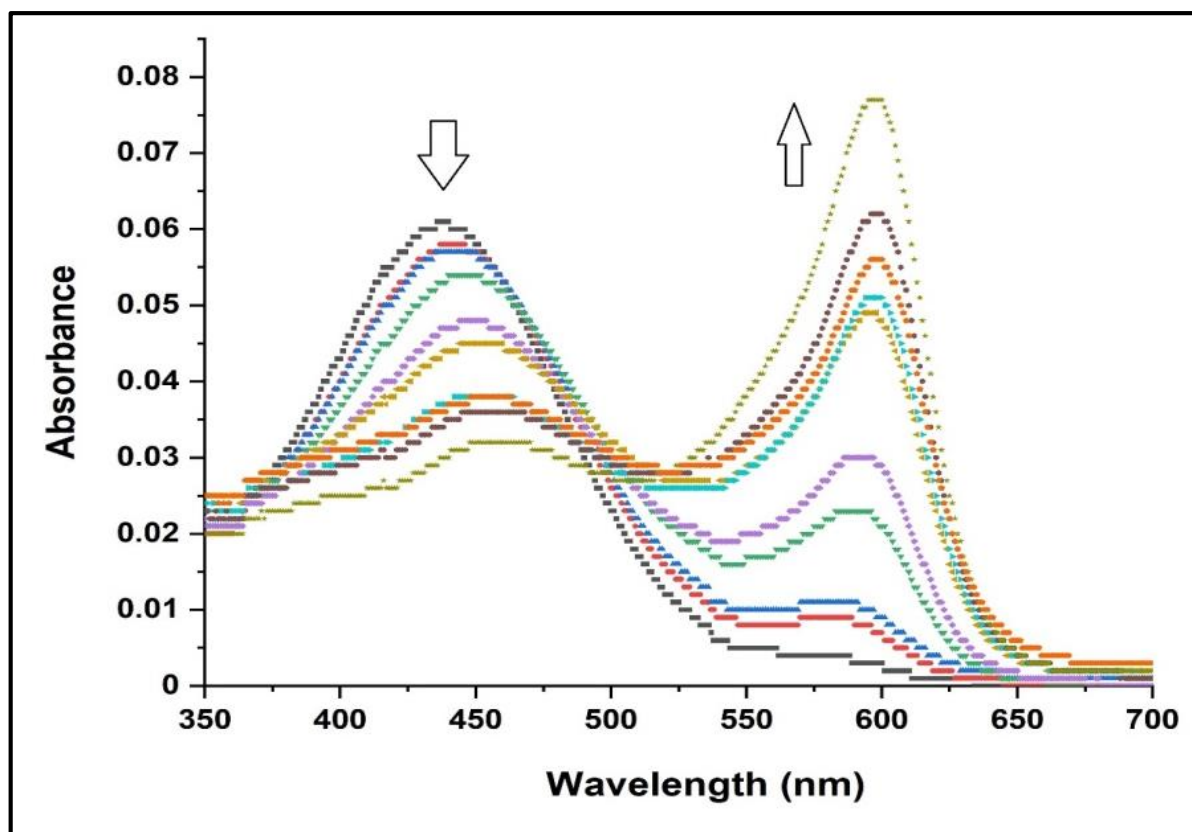


Figure 1: Oxidative bromination of phenol red catalyzed by the *cis*-MoO₂(OV)₂ (0.02 mmol). Spectral changes at 10 min intervals. Spectral data taken of aliquots in pH = 5.0 aqueous phosphate buffer, $c(\text{phosphate buffer}) = 50 \text{ mmol L}^{-1}$, $c(\text{KBr}) = 0.4 \text{ mol L}^{-1}$, $c(\text{phenol red}) = 0.1 \text{ mmol L}^{-1}$.

3.2. Kinetic studies of bromination:

Rate of this reaction may expressed as $dc/dt = k c_1^x c_2^y c_3^z$. According to Lambert–Beer’s law, $A = \epsilon dc$, which on differentiation gives $dA/dt = \epsilon d(dc/dt)$, where ‘A’ is the measurable absorbance of bromophenol blue at 592 nm; ‘ ϵ ’ is the molar extinction coefficient (for bromophenol blue $\epsilon = 14\,500 \text{ M}^{-1} \text{ cm}^{-1}$ at 592 nm) and ‘d’ the path length of light passing through the sample cell ($d=1$). Plots of absorbance data at 592 nm *versus* time for various concentrations of the complexes gave straight lines and from the slopes of these lines a series of reaction rates of the complex (dA/dt) were obtained (Figure.2).

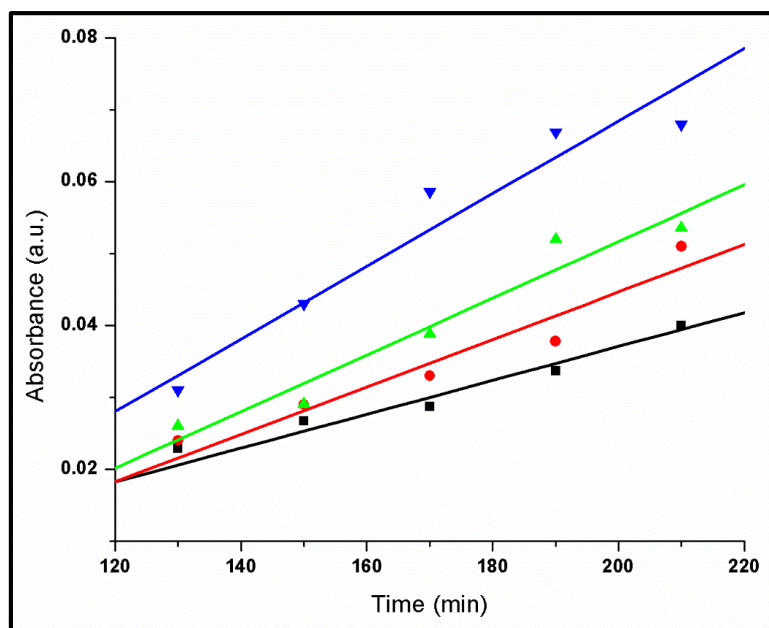


Figure 2: A series of linear calibration plots of the absorbance at 592 nm dependence of time for different concentrations of *cis*-MoO₂(OV)₂. Conditions used: pH 5, c(KBr) = 0.4 M L⁻¹, c(H₂O₂) = 0.02 M L⁻¹, c (phenol red) = 10⁻⁴ M L⁻¹. c(complex/M L⁻¹) = a: 1x10⁻⁶(black square); b: 2x10⁻⁶(red circle); c: 3x10⁻⁶(green triangle); d: 4x10⁻⁶(blue triangle).

The reaction rate constant (k) was obtained from the plot of $-\log (dc/dt)$ versus $-\log c_1$. In this bromination experiment, the reaction orders of KBr and phenol red (y and z) were taken as 1 according to the literature¹¹, c_2 and c_3 are known as 0.4 and 10⁻⁴ mol L⁻¹, respectively. By using the equation “ $b = \log k + y \log c_2 + z \log c_3$ ”, the reaction rate constant (k) can be obtained. The plot of $-\log (dc/dt)$ versus $-\log c$ (Figure. 3) gives a straight line with a slope of 0.84 and an intercept of 2.94 respectively for the complex [*cis*-MoO₂(OV)₂]. The rate constant for this catalytic conversion using the dioxomolybdenum complex [*cis*-MoO₂(OV)₂] as catalyst were calculated to be 0.3×10^2 (M L⁻¹)⁻² s⁻¹ for complex.

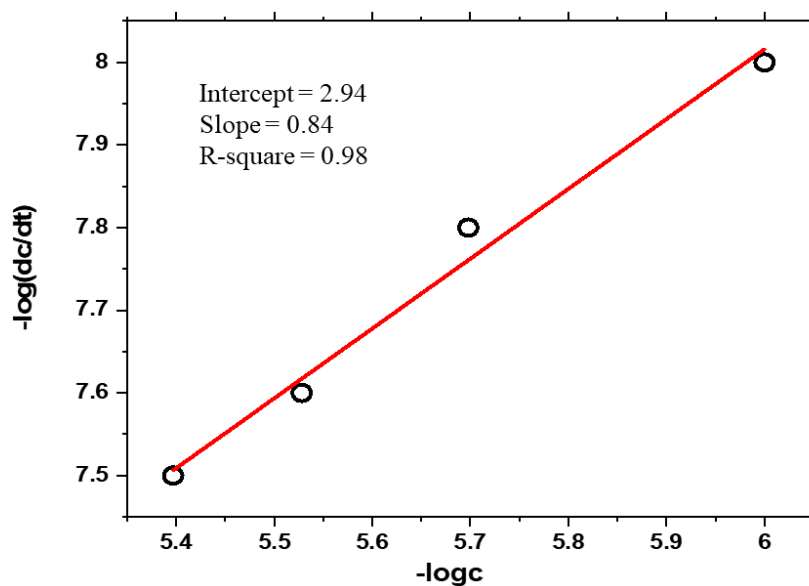


Figure 3: $-\log(dc/dt)$ vs. $-\log c$ (c is the concentration of the complex) for *cis*-MoO₂(OV)₂; conditions used: c (phosphate buffer) = 50 mM L⁻¹, pH = 5, c (KBr) = 0.4 mol L⁻¹, c (phenol red) = 10⁻⁴ M L⁻¹.

Based on the results obtained, it may be concluded that bromination is approximately first-order with respect to *cis*-MoO₂(OV)₂. The method used in the study provides a reliable and quantitative way to determine reaction order and rate constants for bromination reactions. These findings have significant implications for research that would investigate the mechanism and optimization of this very crucial process.

4. Conclusions:

In conclusion, synthesized *cis*-MoO₂(OV)₂ shows a promise as a biomimetic catalyst for VHPO activity, particularly for the bromination of organic substrates. Its effective catalytic activity in this reaction indicates its ability to very closely mimic bromoperoxidase activity, highlighting its potential as a bio-inspired catalyst. Findings suggest exciting possibilities for development of novel Mo-based VHPO biomimetic catalysts having potential application in diverse fields like organic synthesis, catalysis and pharmaceuticals. Further research into the

Application of *cis*-MoO₂(OV)₂ in Haloperoxidase Mimicking Oxidative Bromination

mechanism and optimization of an important chemical process may lead to more significant advances in this area.

References:

- (1) Schneider, C. J.; Zampella, G.; DeGioia, L.; Pecoraro, V. L. Understanding the Mechanism of Vanadiumdependent Haloperoxidases and Related Biomimetic Catalysis. *ACS Symp. Ser.* **2007**, *974*, 148–162.
- (2) Kravitz, J. Y.; Pecoraro, V. L. Synthetic and Computational Modeling of the Vanadium-Dependent Haloperoxidases. *Pure Appl. Chem.* **2005**, *77* (9), 1595–1605.
- (3) Meister, G. E.; Butler, A. Molybdenum(VI)- and Tungsten(VI)-Mediated Biomimetic Chemistry of Vanadium Bromoperoxidase. *Inorg. Chem.* **1994**, *33* (15), 3269–3275.
- (4) Boruah, J. J.; Das, S. P.; Borah, R.; Gogoi, S. R.; Islam, N. S. Polymer-Anchored Peroxo Compounds of Molybdenum and Tungsten as Efficient and Versatile Catalysts for Mild Oxidative Bromination. *Polyhedron* **2013**, *52*, 246–254.
- (5) Reynolds, M. S.; Morandi, S. J.; Raebiger, J. W.; Melican, S. P.; Smith, S. P. E. Kinetics of Bromide Oxidation by (Oxalato)Oxodiperoxomolybdate(VI). *Inorg. Chem.* **1994**, *33* (22), 4977–4984.
- (6) G.H. Jeffery, J. Bassett, J. Mendham, R. C. D. A. *Vogel's Text Book of Quantitative Chemical Analysis, 5th Ed., Wesley Longman Limited, United Kingdom, 1989.*
- (7) Verhaeghe, E.; Buisson, D.; Zekri, E.; Leblanc, C.; Potin, P.; Ambroise, Y. A Colorimetric Assay for Steady-State Analyses of Iodo- and Bromoperoxidase Activities. *Anal. Biochem.* **2008**, *379* (1), 60–65.

Application of *cis*-MoO₂(OV)₂ in Haloperoxidase Mimicking Oxidative Bromination

- (8) Saha, U.; Mukherjea, K. K. Development of a Multifunctional Biomimicking L-Cysteine Based Oxovanadium(IV) Complex: Synthesis, DFT Calculations, Bromo-Peroxidation and Nuclease Activity. *RSC Adv.* **2015**, 5 (114), 94462–94473.
- (9) Naskar, S.; Palmajumder, E.; Patra, S.; Mitra, J.; Mukherjea, K. K. Biomimicking Oxidative Bromination and DNA Nuclease Activities of a New Structurally Characterised Oxido-Diperoxidomolybdenum(VI) Complex. *ChemistrySelect* **2017**, 2 (31), 10199–10205.
- (10) Patra, S.; Mukherjea, K. K. Rare Examples of Biomimicking Molybdenum(VI) Catalysed Peroxidative Bromination of the Organic Substrates That Coordinate to the Oxido-Diperoxido Mo(VI) Centre. *ChemistrySelect* **2017**, 2 (1), 521–526.
- (11) Colpas, G. J.; Hamstra, B. J.; Kampf, J. W.; Pecoraro, V. L. Functional Models for Vanadium Haloperoxidase: Reactivity and Mechanism of Halide Oxidation. *J. Am. Chem. Soc.* **1996**, 118 (14), 3469–3478.

Summary and Conclusions

This thesis focuses on the design and synthesis of multifunctional biomimetic metal complexes with immense potential as chemotherapeutic and radio-protective agents. Amongst the complexes prepared, some exhibit anticancer properties while others possess an unique ability to safeguard DNA against radiation-induced damage. To establish and highlight such multifunctionality experiments were performed to evaluate their ability to mimic the haloperoxidase enzymes, further enhancing their versatility. The overall conclusions are portrayed herewith systematically.

In **Chapter 8**, the synthesized $\text{Mn}^{\text{II}}(\text{sal-oxime})_2(\text{H}_2\text{O})_2$ complex was shown to be successfully prepared and extensively characterized as a novel artificial nuclease. Interaction of the complex with calf thymus DNA was investigated using absorbance and viscometric methods, revealing that it binds effectively at the grooves of DNA. These were further supported by theoretical molecular docking studies. The complex also exhibits significant concentration-dependent nuclease activity demonstrated by an analysis performed with the help of gel electrophoresis. In the presence of H_2O_2 , the compound displayed a remarkable ability to cleave almost 48% supercoiled (SC) plasmid (pUC19) DNA converting them to the nick-circular (NC) form against its standalone activity of 42% cleavage. This indicates that the complex possesses promising artificial nuclease properties suggesting its potential use as an effective chemotherapeutic agent. Findings of the study shed light on the potential of non-platinum-based manganese-oxime complexes as candidates for DNA cleavage during cancer treatment.

Chapter 9 and **Chapter 12** focused on two synthesized Molybdenum dioxocomplexes, namely *cis*- $\text{MoO}_2(\text{BHAN})_2$ and *cis*- $\text{MoO}_2(\text{OV})_2$ respectively. The primary emphasis in both chapters was on successful synthesis and characterization of molybdenum-based *cis*-dioxo complexes by multiple spectroscopic techniques and single crystal analysis for *cis*- $\text{MoO}_2(\text{OV})_2$. It could be concluded from experimental results that the ligands, β -hydroxy- α -naphthaldehyde (BHAN) and ortho-vanilline (OV) are attached to molybdenum resulting in

the formation of a *cis*-dioxo *cis*-MoO₂(BHAN)₂ and *cis*-MoO₂(OV)₂ complexes respectively. Moreover, strong agreement between experimental and theoretical (DFT) studies further validates a successful synthesis and isolation of both complexes in a highly pure form.

Chapter 10 and **Chapter 13** focus on the application of two synthesized molybdenum complexes *cis*-MoO₂(BHAN)₂ and *cis*-MoO₂(OV)₂ respectively as potential radioprotectors, specifically safeguarding DNA from radiation-induced damage. The complexes *cis*-MoO₂(BHAN)₂ and *cis*-MoO₂(OV)₂ provide protection against radiation-induced damage more efficiently compared to their corresponding ligands BHAN and OV. Interestingly, at a concentration of 2 mM, *cis*-MoO₂(BHAN)₂ provide a protection to the extent of 90% to plasmid DNA from radiation induced damage at a dosage of 20 Gy while *cis*-MoO₂(OV)₂ was able to protect it to an extent of approximately 85%, confirmed by results of the gel electrophoresis technique. Moreover, *cis*-MoO₂(BHAN)₂ protected approximately 92% of calf thymus DNA from radiation-induced damage and *cis*-MoO₂(OV)₂ about 89%, as realized from fluorimetric studies using ethidium bromide. From the experimental data, it could be concluded that protective capability of *cis*-MoO₂(BHAN)₂ against radiation-induced DNA damage was better than *cis*-MoO₂(OV)₂. EPR titration using DPPH proves both complexes show good radical scavenging activity making them promising radioprotectors. This work on molybdenum-based radioprotectors therefore contributes to an expanding knowledge on radioprotection paving the way for improved strategies to protect healthy tissues during treatment of cancer by radiotherapy.

Another important objective of the thesis was to realize biomimetic vanadium haloperoxidase (VHPO) functions of *cis*-MoO₂(BHAN)₂ and *cis*-MoO₂(OV)₂ that has been discussed in **Chapter 11** and **Chapter 14** respectively. Ability of both *cis*-MoO₂(BHAN)₂ and *cis*-MoO₂(OV)₂ to catalyze single-pot bromination of phenol red to bromophenol blue was evaluated and show a positive response. The results demonstrate that both complexes are

potential biomimetic catalysts for VHPO activity particularly in the bromination of organic substrates. Their effective catalytic activity closely mimics bromoperoxidase activity highlighting their potential as bio-inspired catalysts.

Appendix – I

List of Publications and Manuscripts Under Preparation

List of publications

“Synthesis, characterization, theoretical simulation, and DNA-nuclease activity of a newly synthesized Mn–oximate complex”. Journal of Coordination Chemistry, 3250-3265, 71 (20), 2018. **Priyanga Deb**, Madhulika Ghose, Nayim Sepay, Satyabrata Maiti & Kalyan K. Mukherjea.

Manuscripts under preparation

1. Synthesis and Characterization of a Highly Active Dioxomolybdenum Complex [*cis*-MoO₂(BHAN)₂] with β -Hydroxy- α -Naphthaldehyde (BHAN) Ligand: Insights into Structural Features and Promising Catalytic Performance in Haloperoxidase mimicking oxidative bromination.
2. Unveiling the Protective Role of *cis*-MoO₂(BHAN)₂ Complex against Radiation-Induced DNA Damage: Insights into Mechanisms and Potential Therapeutic Applications.
3. Ortho-Vanillin Derived *cis*-MoO₂(OV)₂ Complex: Synthesis, Characterization, and Remarkable Haloperoxidase Activity for Oxidative Bromination Reactions.
4. Harnessing the Potency of *cis*-MoO₂(OV)₂ Complex for Safeguarding against Radiation-Induced DNA Damage: Insights and Implications for Radioprotective Strategies.

Appendix – II

Reprint of Publication



Synthesis, characterization, theoretical simulation, and DNA-nuclease activity of a newly synthesized Mn-oximate complex

Priyanga Deb, Madhulika Ghose, Nayim Sepay, Satyabrata Maiti & Kalyan K. Mukherjea

To cite this article: Priyanga Deb, Madhulika Ghose, Nayim Sepay, Satyabrata Maiti & Kalyan K. Mukherjea (2018) Synthesis, characterization, theoretical simulation, and DNA-nuclease activity of a newly synthesized Mn-oximate complex, Journal of Coordination Chemistry, 71:20, 3250-3265, DOI: [10.1080/00958972.2018.1508662](https://doi.org/10.1080/00958972.2018.1508662)

To link to this article: <https://doi.org/10.1080/00958972.2018.1508662>




View supplementary material 



Accepted author version posted online: 14 Aug 2018.
Published online: 09 Nov 2018.



Submit your article to this journal 



Article views: 34



View Crossmark data 



Synthesis, characterization, theoretical simulation, and DNA-nuclease activity of a newly synthesized Mn–oximato complex

Priyanga Deb^a, Madhulika Ghose^a, Nayim Sepay^a, Satyabrata Maiti^b and Kalyan K. Mukherjea^a

^aDepartment of Chemistry, Jadavpur University, Kolkata, India; ^bSaha Institute of Nuclear Physics, Kolkata, India

ABSTRACT

A new $[\text{Mn}^{\text{II}}(\text{sal-oxime})_2(\text{H}_2\text{O})_2]$ complex has been synthesized and characterized by various spectroscopic techniques (IR, UV–vis, ESI-MS, and EPR studies). The molecular geometry of the complex was further established by DFT study. TD-DFT calculations also showed a good agreement with the experimental results of the complex. The DNA-binding activity of the complex has been studied by various physicochemical tools such as UV–vis spectroscopy and viscosity measurements. The intrinsic binding constant (K_b) of the complex with CT-DNA was calculated to be $(2.40 \pm 0.2) \times 10^3 \text{ M}^{-1}$. The results of the DNA-binding experiments were also supported by molecular docking. The compound showed a good nuclease activity which was assessed by gel electrophoresis technique.

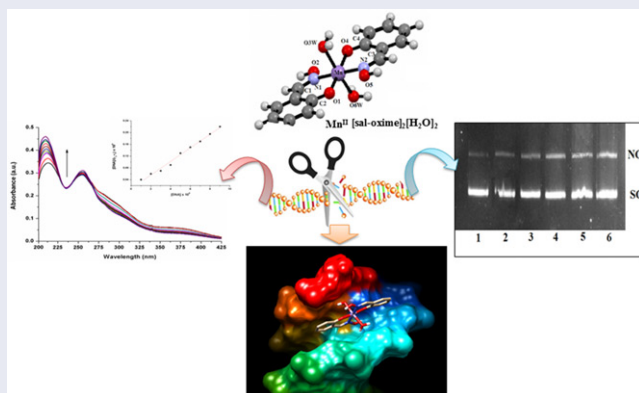
ARTICLE HISTORY

Received 26 April 2018
Accepted 6 July 2018

KEYWORDS

Mn–Oximato complex; DFT; DNA-binding study; DNA-nuclease activity; molecular docking

GRAPHICAL ABSTRACT



CONTACT Prof. Kalyan K. Mukherjea  k_mukherjea@yahoo.com  Department of Chemistry, Jadavpur University, Kolkata-700032, India

 Supplemental data for this article can be accessed <https://doi.org/10.1080/00958972.2018.1508662>

© 2018 Informa UK Limited, trading as Taylor & Francis Group

1. Introduction

DNA is the commonly known primary intracellular target of anti-cancer drugs as well as many chemotherapeutic agents. Interaction between small molecules and DNA may cause DNA-damage in cancer cells; this damage inhibits the proliferation [1]. Over the past few decades, studies on the activity of small molecules showing DNA-binding and DNA-cleavage have generated much interest [2, 3] due to their potential applications as DNA-probes and anti-cancer drugs. Like natural enzymes, artificial nucleases can also hydrolyze DNA, and therefore these cleaving agents have found extensive applications as potential chemotherapeutic agents [4]. Natural nucleases such as restriction endonucleases and topoisomerases can efficiently catalyze DNA hydrolysis, wherein their activity is attributed to the involvement of active metallic centers [5]. Although numerous naturally occurring nucleases are known [6], the development of synthetic nucleases would be of great utility and importance to monitor or manipulate desired biological reactions at the molecular level. Recently, interactions of transition metal complexes with DNA have attracted major attention due to the role of these complexes as the original cancer therapeutic agents and their functions as potential probes of DNA structure and conformation [7]. Transition metal complexes of Fe, Cu, Ni, Pt, Ru, Rh, V, Cr, Co, Os, and Pd have been reported to mediate DNA-cleavage in the presence of oxidants, reductants or without any assisting agents [8]. However, the detailed investigation on the DNA-interaction and nuclease activity exhibited by manganese complexes is scanty. To the best of our knowledge, the field of DNA-binding studies of oxime-based Mn complexes has not been explored yet. In the present work, we discuss the DNA-binding properties and the nuclease activity of the newly developed oxime-based Mn complex, which could prove to be of biochemical significance.

2. Materials and methods

2.1. Materials and physical methods

Manganese chloride tetrahydrate, salicylaldehyde, and hydroxylamine hydrochloride of extra-pure quality were obtained from Merck (India) and used as obtained. All other reagents used were of G.R. grade and were obtained from Merck (India). Analytical grade solvents used for physicochemical studies were further purified by literature method before use [9], wherever necessary. CT-DNA and supercoiled plasmid pUC19 DNA were obtained from Sigma Chemical Company, USA, and Genei Bangalore, India, respectively. All DNA solutions were prepared in Tris-HCl buffer at pH 7.4. Other stock solutions were prepared in Tris-HCl buffer. Millipore water was used throughout the course of the investigation.

2.2. Physical measurements

IR spectra were taken as KBr disks at room temperature on a Perkin Elmer RFX-I IR spectrophotometer. PXRD data were collected on a Bruker D8 Advance X-ray diffractometer using Cu K α radiation ($\lambda = 1.548 \text{ \AA}$) generated at 40 kV and 40 mA. Elemental analyses were carried out using a Perkin-Elmer 2400 series II CHNS analyzer. UV-vis

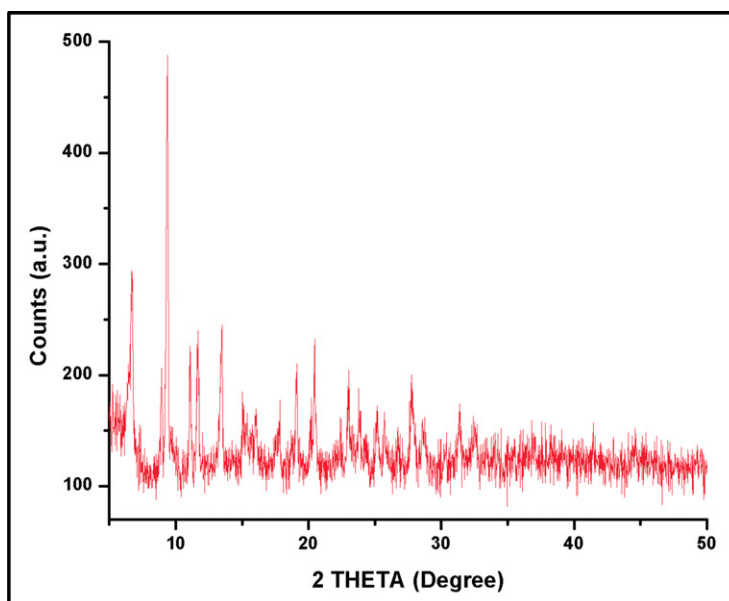


Figure 1. PXRD pattern of the complex.

spectra (200–800 nm) were recorded against appropriate reagent blank at room temperature with a Shimadzu U-1800 spectrophotometer using 1 cm quartz cell. EPR spectra were obtained on a JEOL-JES FA200 ESR spectrometer at room temperature. The mass spectral analyses were done by a Waters mass spectrometer (model: XEVO-G2QTOF#YCA351). The gel electrophoresis study was carried out with UVP Bio Doc-It Imaging System and nicking was analyzed by UVP DOC-ItLS software.

3. Experimental

3.1. Preparation of the complex

The ligand salicylaldehyde-oxime (sal-oxime) was prepared by literature method [10]. Methanolic solution (5 mL) of manganese chloride tetrahydrate (2 mmol) was mixed with the methanolic solution (10 mL) of salicylaldehyde-oxime (sal-oxime) (4 mmol) dropwise with constant stirring. Then 20 mL of water was added and stirring was continued for another 12 h, which on standing produced a light green solid. The solid was collected by filtration, washed with cold water, dried under vacuum and purified by recrystallization. Yield was 75%. Despite multiple attempts, diffractable grade suitable single-crystals could not be obtained. IR (KBr, cm^{-1}): 463 [$\nu(\text{Mn-N})$], 539 [$\nu(\text{Mn-O})$] [11]. ESI-MS (+ve) in MeOH: m/z (relative intensity) 363.04 [M^+], 386.03 [$\text{M}^+ + \text{Na}$]. UV-Vis ($\lambda_{\text{max}}/\text{nm}$): 216 and 253. Elemental analysis: found% (calc.%) C, 46.12 (C, 46.29); H, 3.99 (H, 4.44); N, 7.51 (N, 7.71). The nature of the PXRD results (Figure 1) indicates that the complex is crystalline in nature. The compound is soluble in organic solvents like methanol, acetonitrile, chloroform, acetone, *N,N*-dimethylformamide (DMF), dimethylsulfoxide (DMSO) and tetrahydrofuran (THF) and behaves like a non-electrolyte (molar conductance $2 \text{ Ohm}^{-1} \cdot \text{cm}^2 \cdot \text{mole}^{-1}$). Therefore, the molecular

formula of the compound is $[\text{Mn}^{\text{II}}(\text{sal-oxime})_2(\text{H}_2\text{O})_2]$, which was further supported by DFT study.

3.2. DFT Calculations

The molecular geometry of the complex has been optimized by density functional theory (DFT) study because it has proved to be an important tool to obtain better insights into the geometry, electronic structure, and optical properties of systems. The geometry of both the ligand and the metal complex has been optimized using DFT. All DFT calculations were performed using Gaussian09 package. Ligand geometry was optimized with Becke three parameter hybrid exchange functional and the Lee–Yang–Parr correlation functional (B3LYP) [12] with 6–31+g(d,p) basis set. Optimization of the complex molecule was done using unrestricted hybrid DFT by Becke's 3 parameter exchange functional [12, 13] with nonlocal Lee–Yang–Parr electron correlation (UB3LYP model) [12, 14] functional and basis set has been augmented to LANL2DZ (ECP) [15] for Mn atom jointly with 6-31G(d,p) basis set for other atoms (C,O,N and H) using Gaussian09 [16]. The TD-DFT was performed considering optimized geometry using CAM-B3LYP [12, 14, 17] function in combination with LANL2DZ (ECP) [15] for Mn atom and 6–31G(d,p) for other atoms (C, H, N and O) for the calculation of spectral feature of the complex. In order to include solvation effect in TD-DFT calculation, we included continuum model (CPCM) [18] (polarizable conductor calculation model along with united-atom topological model having $\epsilon = 78.39$). The geometry of the ligand and complex was fully optimized without any symmetry constraints. GaussSum 2.1 program [19] was used to calculate the molecular orbital contributions from groups or atoms.

3.3. DNA-Binding studies

3.3.1. UV–vis spectral study

The solution of CT-DNA in Tris–HCl/NaCl (50 mM Tris–HCl and 50 mM NaCl, pH7.2) was made and stock solutions were stored at 4 °C and used within 4 days. The electronic spectrum of the complex was monitored in the presence and absence of CT-DNA. In this absorption titration experiment, a fixed concentration of the complex was titrated with increasing amounts of DNA over a range of 0–10 μM . To eliminate the absorbance of DNA, equal amounts of DNA were added to the reference solution as well. The intrinsic binding constant is determined as follows [20]:

$$[\text{DNA}]/(\epsilon_a - \epsilon_f) = [\text{DNA}]/(\epsilon_b - \epsilon_f) + 1/[K_b(\epsilon_b - \epsilon_f)] \quad (1)$$

where [DNA] is the concentration of DNA in base pairs, the apparent absorption coefficients ϵ_a , ϵ_f and ϵ_b corresponds to $A_{\text{obsd}}/[\text{complex}]$, the extinction coefficient for the free complex, and the extinction coefficient for the complex in the fully bound form, respectively. Plots of $[\text{DNA}]/(\epsilon_a - \epsilon_f)$ versus [DNA] gave a slope $1/(\epsilon_b - \epsilon_f)$ with Y-intercept $1/[K_b(\epsilon_b - \epsilon_f)]$. The intrinsic binding constant K_b was obtained from the ratio of the slope to the intercept.

3.3.2. Viscometric study

Viscosity of sonicated DNA [21] (average molecular weight of ~ 200 base pairs was made by using a Labsonic 2000 sonicator) was measured by a fabricated microviscometer, maintained at $28 \pm 0.5^\circ\text{C}$ in a thermostatic water bath. Data were presented as $(\eta/\eta_0)^{1/3}$ versus the ratio of the concentration of either of the ligand or the complex to that of the CT-DNA, where η_0 is the viscosity of CT-DNA solution alone and η is the viscosity of CT-DNA solution in the presence of the complex. Viscosity values were calculated from the observed flow time of CT-DNA by the relation $\eta = t - t_0$, where t and t_0 are the values of flow times for the solution and the buffer, respectively.

3.3.3. Gel electrophoresis study

DNA-cleavage activity of the complex was monitored with the help of a gel electrophoresis Model No. 2101, Genei, Bangalore. The super coiled pUC19 DNA (0.5 mg per reaction) in Tris-HCl/NaCl buffer (pH 7.2) was treated with increasing amounts of metal complex over a range of 18–36 μM along with H_2O_2 (16 μM) [22]. After incubation for 45 min at 37°C , it was mixed with a sample loading dye. The samples were run on a 0.9% agarose in 1 X TAE buffer for 3 h at 80 mV; then it was treated with EB solution and the bands were visualized by UV light and photographed with UVP Bio Doc-It Imaging System. The percentage of cleavage of supercoiled (SC) pUC19 DNA-cleavage induced by the complex was determined by using UVP BIODOC-ItLS software.

3.3.4. Molecular docking study

The molecular docking study of the Mn complex with CT-DNA was carried out using Auto Dock 4.2.0 software package. The energy minimized conformation of the complex obtained from DFT calculations were used for docking studies. The docking study was performed with Lamarckian Genetic Algorithm (LGA) inside the $126 \times 126 \times 126$ grid box. For visualization of the results, Discovery studio visualizer 2016 and Chimera 1.10.2 were used.

4. Results and discussions

4.1. Characterization of the complex

4.1.1. IR and UV-vis studies of the complex

Some important infrared absorption frequencies of the metal complex are analyzed. The azomethine group frequencies of free Schiff base shifts toward the lower frequency region in the complex from around 1618 cm^{-1} to 1587 cm^{-1} due to involvement of the N atom of the $-\text{C}=\text{N}-$ group in coordination with the metal center [23]. Bands at 463 and 539 cm^{-1} are due to $\nu(\text{Mn}-\text{N}1)$, $\nu(\text{Mn}-\text{N}2)$ and $\nu(\text{Mn}-\text{O}1)$, $\nu(\text{Mn}-\text{O}4)$ vibrations, respectively, of the coordinated sal-oxime ligand. The complex shows a broad absorbance throughout the visible region; this may be due to the d-d transition of the metal Mn(II) in the complex. The complex shows broad peaks at 253 nm and

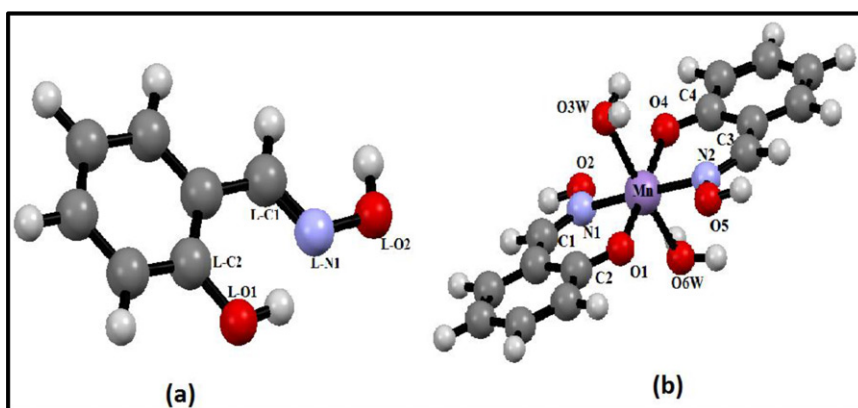


Figure 2. Optimized geometry of (a) ligand and (b) complex.

216 nm which can be assigned as the $n-\pi^*$ and $\pi-\pi^*$ of intra-ligand electronic transitions.

4.1.2. Thermo gravimetric analysis

The presence of the coordinated water in the complex is characterized by a mass loss above 120 °C [24]. The 10% mass loss occurred at this temperature, which corresponds to the loss of two molecules of coordinated water in the complex (Figure S1).

4.1.3. Mass spectrometric analysis

The molecular formulation and some structural information can be obtained from ESI-MS analysis. The molecular formula of the complex $[\text{Mn}(\text{sal-oxime})_2(\text{H}_2\text{O})_2]$ obtained from the analytical techniques is $\text{C}_{14}\text{H}_{16}\text{MnN}_2\text{O}_6$ (MW = 363.04), which is also supported by the observed ESI-mass spectra of the complex which show the mass of the complex (M) at 363.04 m/z added with a sodium at 386.03 m/z with maximum abundance (Figure S2).

4.1.4. Magnetic moment

The room temperature (298 K) magnetic moment of the complex is 5.89 BM, which indicates the presence of high-spin Mn(II) center in the octahedral geometry of the complex [25].

4.1.5. EPR spectra

The EPR spectrum of $[\text{Mn}^{\text{II}}(\text{sal-oxime})_2(\text{H}_2\text{O})_2]$ was recorded in solid state at room temperature. A single EPR line is observed (Figure S3), which revealed the presence of a strong signal in the $g = 1.97$ region. Such single-line spectrum suggests unambiguously the mononuclear nature of the complex [24]. From the low value of g , it can be said that there can be important contribution of ligand spin-orbit coupling, which actually indicates the presence of covalency [26].

Table 1. Selected optimized geometrical parameters for the complex in the ground state calculated at LANL2DZ levels.

Bond lengths (Å)	
Mn–N1	1.996
Mn–O1	1.928
Mn–O3W	2.162
Mn–O4	1.976
Mn–N2	2.022
Mn–O6W	2.158
Bond angles (°)	
O1–Mn–N1	88.25
N1–Mn–O3W	92.42
O3W–Mn–O4	90.84
O4–Mn–N2	90.06
N2–Mn–O6W	88.09
O6W–Mn–O1	86.71
N1–Mn–O4	91.92
O4–Mn–N2	88.25
N2–Mn–O1	89.91
O1–Mn–N1	90.06
N1–Mn–N2	178.20
O1–Mn–O4	175.28
O3W–Mn–O6W	171.14

Table 2. Comparisons of experimental and theoretical stretching frequency of complex.

Frequency	Theoretical values (cm ⁻¹)	Experimental values (cm ⁻¹)	% of Deviation
$\nu(\text{Mn-N1})$ and $\nu(\text{Mn-N2})$	501	463	8.2
$\nu(\text{Mn-O1})$ and $\nu(\text{Mn-O4})$	560	539	3.8

4.1.6. Optimization of molecular geometry and electronic structure

DFT study has proved to be an important tool to obtain better insights into the geometry, electronic structure, and optical properties of these systems. The TD-DFT approach has been demonstrated to be reliable for calculating spectral properties of many transition metal complexes [27]. The geometry of both the ligand and the metal complex has been optimized by using DFT. The ground-state optimized geometry of ligand and its Mn²⁺ complex is shown in Figure 2, where both the ligand and the Mn²⁺ complex have C1 point group. Main optimized geometrical parameters of the complex are listed in Table 1. The modeled geometry possesses a distorted octahedral arrangement around the Mn(II) center.

In the complex, all calculated Mn–N distances occur in the range 1.996–2.022 Å and Mn–O distances are in the range 1.928–2.162 Å. Hence, all the DFT calculations unequivocally support the structure of the Mn compound. The calculated IR stretching frequencies of the complex are compared with experimental findings (Table 2 and Figure 3(a)) and the values are found to be in good agreement. In the case of ligand (sal-oxime) at ground state, the electron density at HOMO–1, HOMO, LUMO, and LUMO +1 orbitals mainly resides on the benzene moiety. The energy difference between HOMO (highest occupied molecular orbital) and LUMO (lowest unoccupied molecular orbital) of the ligand (Figure S4) is 4.68 eV. This assignment was supported by TD-DFT calculations. In the case of the complex, all the LUMO, LUMO +1, LUMO +2, HOMO, and HOMO–1 mainly originate from ligand π and π^* orbital contributions while the LUMO +2, HOMO, LUMO, and HOMO–1 arise from the contribution of Mn d

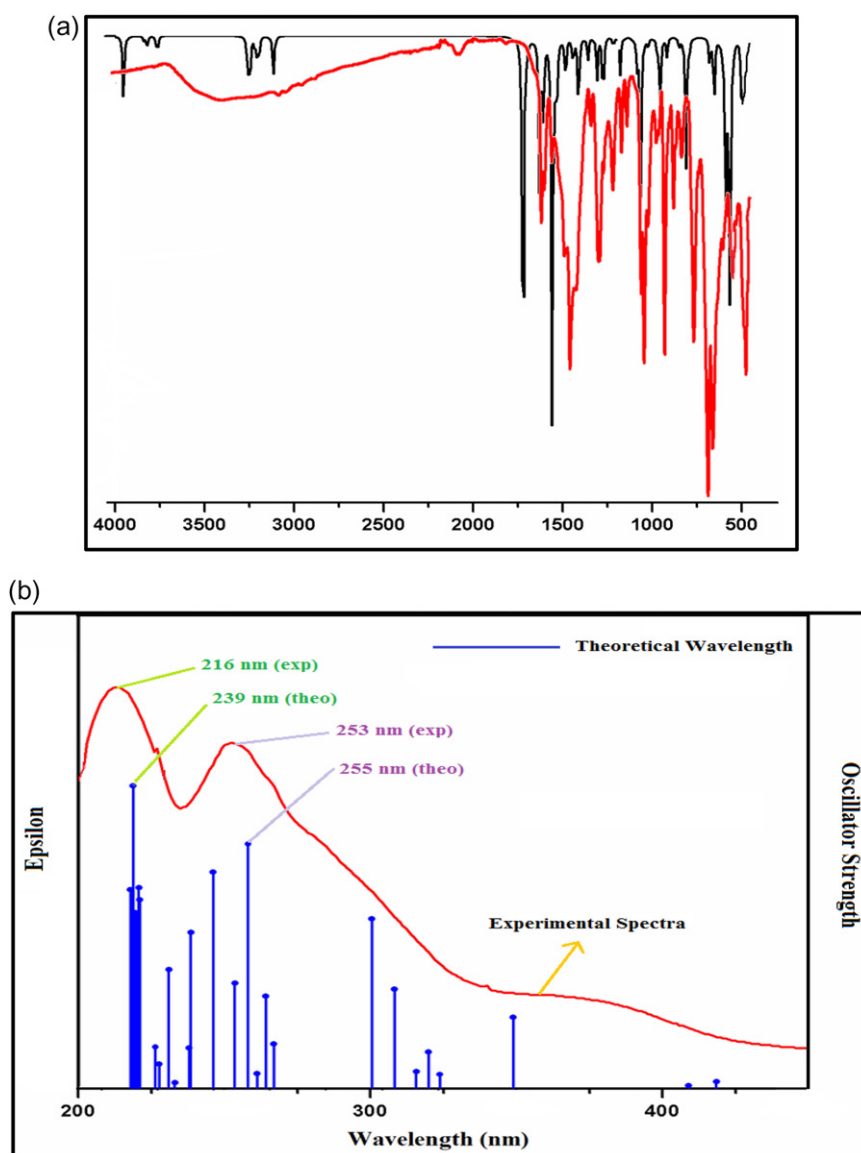


Figure 3. (a) Calculated (black) and experimental (red) IR spectra of the complex. (b) Comparison of theoretical and experimental electronic spectra of the complex.

Table 3. Selected UV–vis energy transitions at the B3LYP level for complex in aqueous medium.

λ_{cal} (nm)	Oscillator strength (f)	λ_{expt} (nm)	Key transitions
239	0.0252	216	HOMO \rightarrow L + 2, H-1 \rightarrow L + 1
255	0.0117	253	H-1 \rightarrow L + 1, HOMO \rightarrow L + 1, H-1 \rightarrow LUMO

orbitals along with ligand p orbital. The energy difference between HOMO and LUMO in the complex is 3.38 eV while for the ligand it is 4.68 eV.

The complex shows two absorption bands at 216 and 253 nm in aqueous solution at room temperature. The spectra calculated from TD-DFT show bands at 239 and

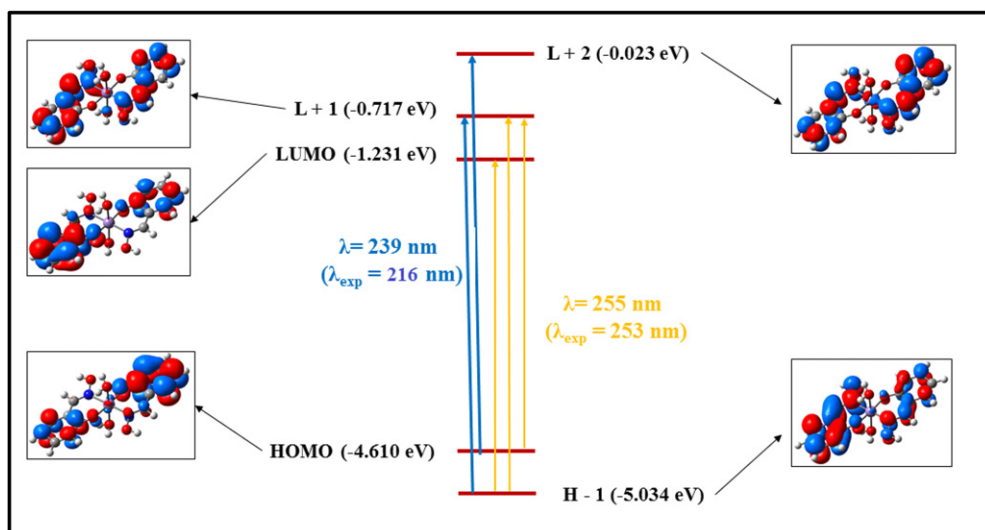


Figure 4. Frontier molecular orbitals involved in the UV-vis absorption of metal complex.

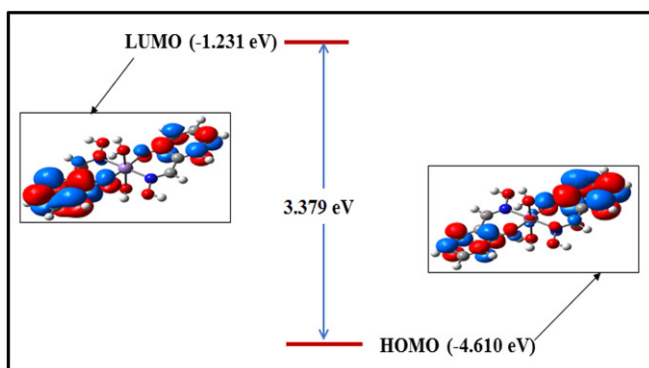


Figure 5. Frontier orbitals (HOMO-LUMO) of the complex.

255 nm for the complex (Figure 3). This calculated value is in good agreement with the experimental results (Table 3 and Figure 3(b)) [28].

4.1.7. HOMO-LUMO energy

In chemistry, the energy difference between HOMO and LUMO is called the HOMO-LUMO gap and these molecular orbitals are well known as “frontier orbitals” as these kinds of orbitals are farthest boundary of the electrons of the molecule (Figure 4) [29]. The HOMO-LUMO gap determines the rate of excitation of the molecule in which the rate increases with decreasing the gap. The HOMO and LUMO orbitals with corresponding energies are shown diagrammatically in Figure 5 and the HOMO-LUMO E_{diff} is 3.379 eV. Here, HOMO is distributed to the large extent of the aromatic part of the molecule and the metal atom. The electron density is greater on one of the aromatic parts of the ligand over another between two ligands attached to the metal ion. In the case of LUMO, the above mentioned electron density (found in HOMO) is

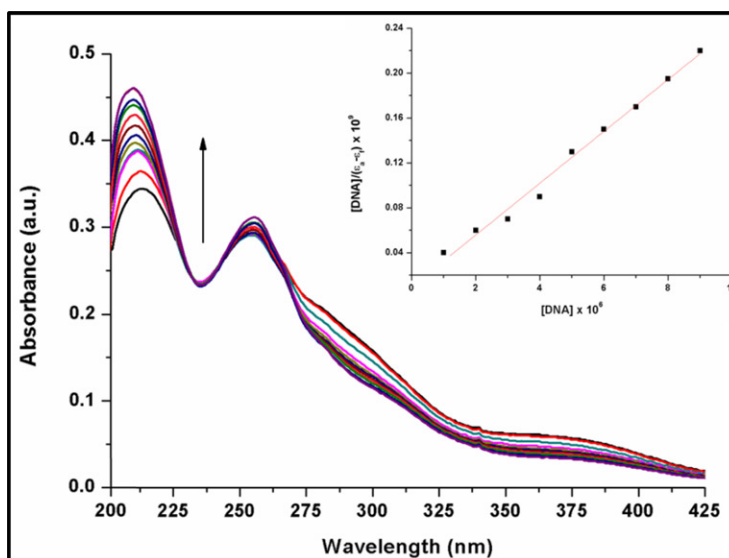


Figure 6. Absorption spectra of the complex (10 μM) in the presence of increasing amounts of CT-DNA, $[\text{DNA}]/[\text{complex}] = (a - l)$: 0–10 μM . (inset: plot of $[\text{DNA}]/(\epsilon_a - \epsilon_f) \times 10^9$ (M^2cm) versus $[\text{DNA}] \times 10^6$ (M) for calculating K_b , monitoring 216-nm wavelength).

inversed on the aromatic part of another ligand attached with metal center. It is also interesting to note that the electron density on the metal ion vanished in LUMO where it was sufficient in HOMO. The π -bonding character of HOMO, π -anti-bonding character of LUMO and high HOMO–LUMO gap indicate high stability for the complexes as the molecule requires high energies for excitation.

4.2. DNA-Binding studies

The present project is directed toward the development of synthetic DNA-nuclease, so it demands a thorough study on the ability of the molecule to bind the double-stranded DNA. Hence, the binding of DNA by the complex has been studied, results of which are being presented herein.

4.2.1. Electronic absorption spectral studies

Monitoring the changes in absorption profile of the metal complexes upon addition of increasing amounts of DNA is one of the most widely used methods for determining overall binding constants [30]. The electronic spectra of the complex in the presence and absence of DNA were monitored. The absorption spectrum of the complex is monitored by varying the concentration of CT-DNA. Upon addition of incremental amounts of DNA, the intensity of the bands of the complex at 216 nm and 253 nm increases (Figure 6). The hyperchromic effect is caused mainly because of electrostatic attraction with the DNA and hence causing damage to the secondary structure of DNA which may cause partial untwisting of the helical structure of DNA, exposing more bases of the DNA [31]. These spectroscopic characteristics suggest that the complexes had some interaction with DNA [31]. The basic binding constant (K_b) is a useful

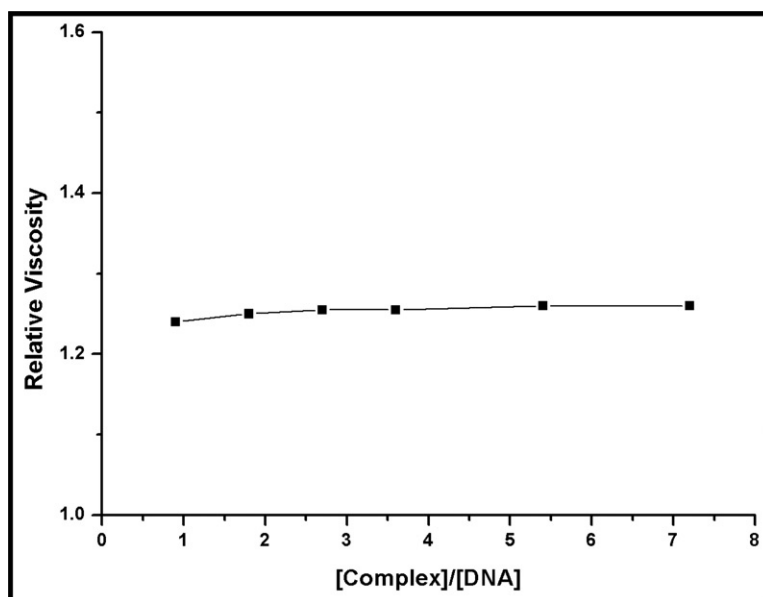
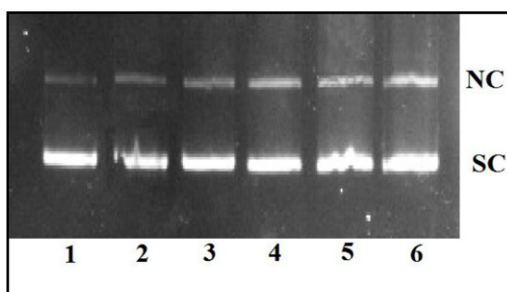


Figure 7. Effect of increasing the amount of the complex on the specific viscosity of CT-DNA.

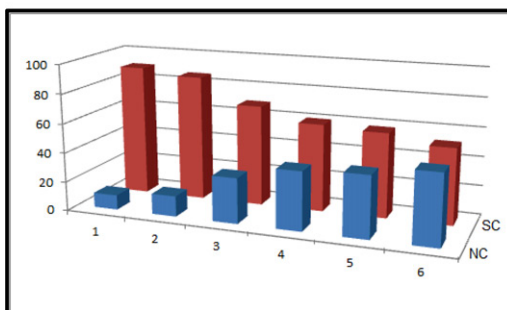
tool to define the magnitude of the binding strength of compounds with DNA, which is calculated to be $(2.40 \pm 0.2) \times 10^3 \text{ M}^{-1}$ monitoring the wavelength of compound at 216 nm. However, this observed binding constant is smaller than the classical intercalators and metallointercalators where the binding constant was reported to be in the order of 10^7 M^{-1} [29]. Hence, the possibility of the complex to be an intercalator is completely ruled out. The K_b value indicates that the complex is moderately bound to CT-DNA and electrostatic interactions cannot be ruled out. Again, the complex can participate in hydrogen bond formation with DNA base pairs, which may lead to better binding affinity between the complex and DNA base pairs, thereby suggesting the involvement of the complex as a DNA groove-binder.

4.2.2. Viscometric studies

To further investigate the mode of binding between the complexes and DNA, viscosity measurements were carried out. The spectroscopic technique is very useful but not sufficient to understand the mode of binding of the complex with DNA [32]. Hydrodynamic measurements which are sensitive to the change in DNA length are used to confirm the spectral data. So, viscosity is used to be a sensitive technique to understand the mode of DNA-binding [33]. The relative viscosity of CT-DNA solution is known to increase on intercalative binding of substrates, because the insertion of intercalators causes the base pairs of the DNA to pull apart and thus causes lengthening of the DNA helix, leading to an increase in the viscosity of DNA. While molecules bound to DNA through groove do not alter the relative viscosity of DNA [34]. The values of relative specific viscosities of DNA in the absence and presence of complex are plotted against [complex]/[DNA] (Figure 7). It is observed that the addition of the complex into the CT-DNA solution does not show significant increase in the viscosity of



(a)



(b)

Figure 8. (a) Agarose gel (0.9%) electrophoresis of supercoiled DNA (0.5 μg) incubated for 45 min at 37 °C, in PBS buffer (0.15 M, pH 7.2) at 37 °C. Lane 1: DNA control; Lane 2: DNA + H_2O_2 ; Lane 3: DNA + complex (18 μM); Lane 4: DNA + complex (18 μM) + H_2O_2 ; Lane 5: DNA + complex (36 μM); Lane 6: DNA + complex (36 μM) + H_2O_2 . (b) Graphical representation of % of cleavage in different lanes.

Table 4. Results of the cleavage of pUC19 DNA determined by gel electrophoresis study.

Lane no.	Reaction condition	Form I (% SC)	Form II (% NC)
1	Control DNA	90	10
2	DNA + H_2O_2 (16 μM)	86	14
3	DNA + complex (18 μM)	69	31
4	DNA + complex (18 μM) + (16 μM) H_2O_2	60	40
5	DNA + complex (36 μM)	58	42
6	DNA + complex (36 μM) + (16 μM) H_2O_2	52	48

CT-DNA, which clearly rules out intercalative binding and hints at the groove binding of CT-DNA by the present complex.

4.2.3. Gel electrophoresis study for nuclease activity

The double-stranded plasmid pUC19 DNA exists in a compact supercoiled (SC) form. Upon introduction of nuclease, the naturally occurring supercoiled (SC) form may give rise to nicked circular (NC) form. Relatively fast migration is observed for supercoiled (SC) form than the NC form when the plasmid DNA is subjected to electrophoresis. Hence, DNA-strand breaks were quantified by measuring the transformation of the supercoiled (SC) form into NC form [34]. The ability of the manganese complex to induce DNA-cleavage was studied by gel electrophoresis using supercoiled pUC19

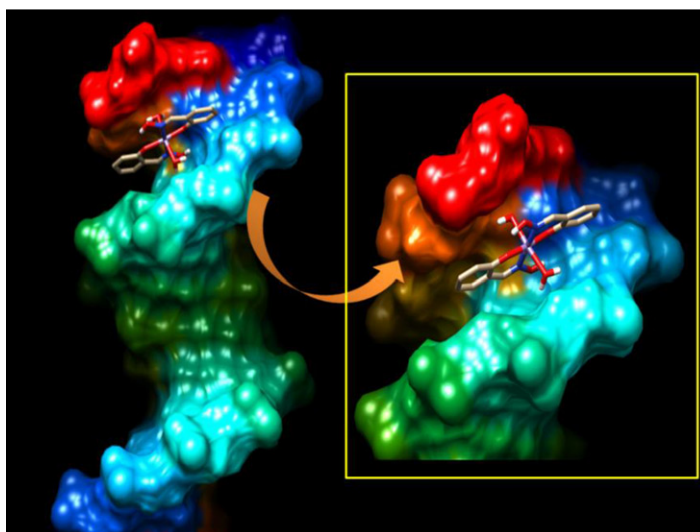


Figure 9. Docked pose of complex showing interaction with base pairs; inset: enlarged view of the docked pose.

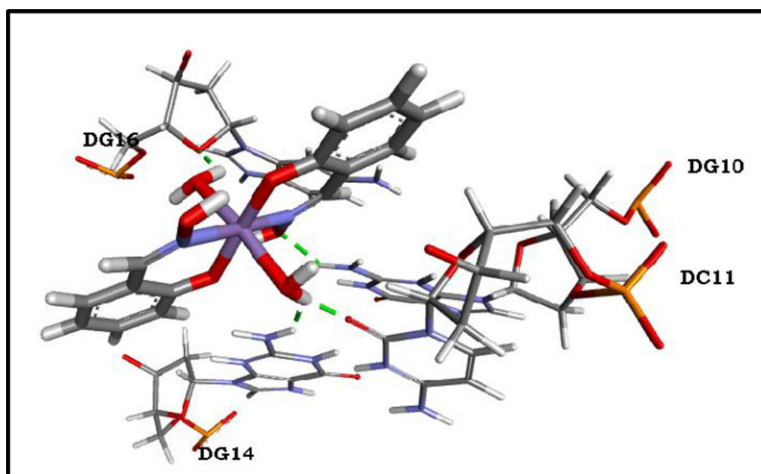


Figure 10. Hydrogen-bonding interactions of the complex with DNA base pairs.

DNA in Tris-HCl/NaCl buffer (pH 7.2) which was treated with increasing amounts of metal complex over a range of 18–36 μM along with H_2O_2 (16 μM) (Figure 8 and Table 4) [34, 35]. On addition of fixed concentration of H_2O_2 (16 μM), the percentage of NC form increases to 14% (lane 2), while on addition of the compound (18–36 μM), the percentage of NC form increases through 31% to 42% in lanes 3 and 5, respectively. Whereas, on addition of different concentrations of compound and H_2O_2 together (16 μM H_2O_2 + 18 μM complex) and (16 μM H_2O_2 + 36 μM complex) the percentage of NC form of DNA increases to 40% (lane 4) and 48% (lane 6), respectively. This clearly indicates that the compound alone shows moderate nuclease activity but exhibits higher nuclease activity when used in combination with H_2O_2 [22, 35].

4.2.4. Theoretical simulation for the interaction of DNA with complex

In the present communication, theoretical simulation in the form of molecular docking is used to realize the binding of complex with DNA (PDB access code 2BNA) [36]. The docking simulation showed that the complex molecule has aromatic ring containing ligand system having electronegative atom like nitrogen as well as two water molecules. Therefore, there is a balance between hydrophobic and hydrophilic parts in the molecule. The investigating molecule is capable of interacting with DNA residues through hydrogen bonding and other weak electrostatic interactions. The docking study shows that the molecule interacts with DNA through its minor groove (Figure 9), the energy minimized conformation of the complex inside the DNA, and the change of free energy for the interaction is -6.21 kcal/mol. There are four hydrogen-bonding interactions between DNA and the complex. They are found between NH_2 group of G10 and G14 residue with oxime OH and water molecule of complex, respectively. In addition, the sugar oxygen of G16 residue and $\text{C}=\text{O}$ of C11 residues separately interact with two water molecules present in the complex through H-bonding as shown in Figure 10. Therefore, the theoretical simulations support the proposition of groove binding, which has been suggested from other experimental findings.

5. Conclusion

The newly developed Mn complex is characterized by a different physicoanalytical technique and its geometry has been optimized by DFT calculations. The TD-DFT study clearly supports the optimized structure of complex, which is in good agreement with the experimental findings. In the present study, the interaction of complex with CT-DNA is examined by absorbance and viscometric methods. The results of the DNA-binding experiments suggest that the complex binds in the groove of CT-DNA, which is also supported by molecular docking. The complex exhibits effective concentration-dependent nuclease activity in the presence of H_2O_2 by cleaving the supercoiled plasmid (pUC19) DNA to NC form. Therefore, the present study provides non-platinum-based manganese based on a new class of nuclease, as a potential artificial nuclease.

Acknowledgments

The authors thank the "Department of Higher Education, Science and Technology and Biotechnology, Govt. of West Bengal" for financial support in the form of a Major Research Project [Sanction no. 849(Sanc.)/ST/P/S&T/9G-31/2013] sanctioned to KKM, where PD is a "Junior Research Fellow." The authors also thank UGC, New Delhi for funding UVP Bio Doc-IT GEL Imaging system in the form of a major research project to KKM [39-706/2010(SR)]. A word of thanks also goes to Jadavpur University for providing the necessary facilities.

References

- [1] (a) V. Brabec, J. Malina, N. Margiotta, G. Natile, J. Kasparkova. *Chem. Eur. J.*, **18**, 15439 (2012); (b) B. Wang, J. Tan, L. Zhu. *Colloids Surf. B*, **79**, 1 (2010); (c) M.J. Khandekar, A.S.

- Banks, D. Laznik-Bogoslavski, J.P. White, J.H. Choi, L. Kazak, J.C. Lo, P. Cohen, K.K. Wong, T.M. Kamenecka, P.R. Griffin, B.M. Spiegelman. *PNAS*, **115**, 561 (2018).
- [2] P.G. Baraldi, A. Bovero, F. Frutterolo, D. Preti, M.A. Tabrizi, M.G. Pavani, R. Romagnoli. *Med. Res. Rev.*, **24**, 475 (2004).
- [3] X.L. Wang, H. Chao, H. Li, X.L. Hong, L.N. Ji, X.Y. Li. *J. Inorg. Biochem.*, **98**, 423 (2004).
- [4] (a) T.D. Tullius, J.A. Greenbaum. *Curr. Opin. Chem. Biol.*, **9**, 127 (2005); (b) J.D. West, L.J. Marnett. *Chem. Res. Toxicol.*, **19**, 173 (2006).
- [5] (a) M.E. Nunez, J.K. Barton. *Curr. Opin. Chem. Biol.*, **4**, 199 (2000); (b) S.E. Wolkenberg, D.L. Boger. *Chem. Rev.*, **102**, 2477 (2002).
- [6] J. Stubbe, J.W. Kozavich. *Chem. Rev.*, **87**, 1107 (1987). [CrossRef][10.1021/cr00081a011]
- [7] (a) J. Kang, L. Zhuo, X. Lu, H. Liu, M. Zhang, H. Wu. *J. Inorg. Biochem.*, **98**, 79 (2004); (b) Ł. Opalinski, J. Szymczyki, M. Szczepara, M. Kucinska, D. Krowarsch, M. Zakrzewska, J. Otlewski. *Int. J. Mol. Sci.*, **19**, 1435 (2018).
- [8] (a) L. Becco, A. Rodriguez, M.E. Bravo, M.J. Prieto, L.R. Azuara, B. Garat, D. Gambino. *J. Inorg. Biochem.*, **109**, 49 (2012); (b) I. Correia, S. Roy, C.P. Matos, S. Borovic, N. Butenko, I. Cavaco, F. Marques, J. Lorenzo, A. Rodríguez, V. Moreno, J. Costa Pessoa. *J. Inorg. Biochem.*, **147**, 134 (2015); (c) A. Ghosh, A. Mandoli, D.K. Kumar, N.S. Yadav, T. Ghosh, B. Jha, J.A. Thomas, A. Das. *Dalton Trans.*, 9312 (2009); (d) M. Costas, M.P. Mehn, M.P. Jensen, L. Que, Jr. *Chem. Rev.*, **104**, 939 (2004); (e) G. Parkin. *Chem. Rev.*, **104**, 699 (2004); (f) O. Bortolini, V. Conte. *J. Inorg. Biochem.*, **99**, 1549 (2005); (g) A.J. Wu, J.E. Penner-Hahn, V.L. Pecoraro. *Chem. Rev.*, **104**, 903 (2004); (h) D.C. Crans, J.J. Smee, E. Gaidamauskas, L. Yang. *Chem. Rev.*, **104**, 849 (2004). (i) L.M. Mirica, X. Ottenwaelder, T.D.P. Stack. *Chem. Rev.*, **104**, 1013 (2004); (j) W.K. Pogozelski, T.D. Tullius. *Chem. Rev.*, **98**, 1089 (1998); (k) C.J. Burrows, J.G. Muller. *Chem. Rev.*, **98**, 1109 (1998); (l) G. Kedarnath, V.K. Jain. *Coord. Chem. Rev.*, **257**, 1409 (2003).
- [9] G.H. Jeffery, J. Bassett, J. Mendham, R.C.D. Addison, *Vogel's Text Book of Quantitative Chemical Analysis*, Wesley Longman Limited, United Kingdom, 5th Edn. (1989).
- [10] M. Behl, S.E. Ashbrook, D.M. Dawson, R.A. Doyle, P. Hrobarik, M. Kaupp, I.A. Smellie. *Chem. Eur. J.*, **22**, 15328 (2016). [CrossRef][10.1002/chem.201602567]
- [11] (a) A.S. Munde, A.N. Jagadale, S.M. Jadhav, T.K. Chondhekar. *J. Korean. Chem. Soc.*, **53**, 407 (2009); (b) N. Nakamoto. *Infrared Spectra and Raman Spectra of Inorganic and Coordination Compounds*, 5th Edn., Vol. **93**, John Wiley & Sons, New York (1997).
- [12] A.D. Becke. *Phys. Rev. A Gen. Phys.*, **38**, 3098 (1988).
- [13] K. Leung, S.B. Rempe, P.A. Schultz, E.M. Sproviero, V.S. Batista, M.E. Chandross, C.J. Medforth. *J. Am. Chem. Soc.*, **128**, 3659 (2006).
- [14] C. Lee, W. Yang, R.G. Parr. *Phys. Rev. B*, **37**, 785 (1988). [CrossRef][10.1103/PhysRevB.37.785]
- [15] (a) P.J. Hay, W.R. Wadt. *J. Chem. Phys.*, **82**, 299 (1985); (b) N.C. Handy, H.F. Schaefer. *J. Chem. Phys.*, **81**, 5031 (1984); (c) A. Nicklass, M. Dolg, H. Stoll, H. Preuss. *J. Chem. Phys.*, **102**, 8942 (1995).
- [16] Gaussian 09, (Revision A.1), Gaussian, Inc., Wallingford, CT (2009).
- [17] T. Yanai, D.P. Tew, N.C. Handy. *Chem. Phys. Lett.*, **393**, 51 (2004).
- [18] V. Barone, M. Cossi. *J. Phys. Chem. A*, **102**, 1995 (1998). [CrossRef][10.1021/jp9716997]
- [19] N.M. O'Boyle, A.L. Tenderholt, K.M. Langner. *J. Comput. Chem.*, **29**, 839 (2008).
- [20] A. Wolfe, G.H. Shimer, T. Meehan. *Biochemistry*, **26**, 6392 (1987).
- [21] J.B. Chaires, N. Dattagupta, D.M. Crothers. *Biochemistry*, **21**, 3933 (1982).
- [22] (a) U. Saha, K.K. Mukherjea. *Int. J. Biol. Macromol.*, **66**, 166 (2014); (b) M. Selim, K.K. Mukherjea. *J. Biomol. Struct. Dyn.*, **26**, 561 (2009); (c) M. Selim, S.R. Chowdhury, K.K. Mukherjea. *Int. J. Biol. Macromol.*, **41**, 579 (2007).
- [23] C.P. Pradeep, P.S. Zacharias, S.K. Das. *J. Chem. Sci.*, **118**, 311 (2006).
- [24] (a) B. Mabad, P. Cassoux, J.P. Tuchagues, D.N. Hendrickson. *Inorg. Chem.*, **25**, 1420 (1986); (b) A.H. Manikshete, M.M. Awatade, S.K. Sarsamkar, M.R. Asabe. *Int. J. Eng. Sci. Inven.*, **4**, 22 (2015); (c) A. Earnshaw. *Introduction to Magnetochemistry*, Academic Press, New York (1968).

- [25] D. Ghosh, U. Saha, K.K. Mukherjea. *RSC Adv.*, **4**, 15558 (2014). [CrossRef][10.1039/C4RA00729H]
- [26] (a) L.D. Kandel, M.C.G. Passecgi, T. Buch. *J. Phys. Chem. Solids*, **30**, 321 (1969); (b) *Electron Paramagnetic Resonance: Elementary Theory and Practical Applications*, 2nd Edn, John Wiley & Sons, Inc. (2007).
- [27] (a) T. Liu, H.X. Zhang, B.H. Xia. *J. Phys. Chem. A*, **111**, 8724 (2007); (b) X.P. Zhou, H.X. Zhang, Q.J. Pan, B.H. Xia, A.C. Tang. *J. Phys. Chem. A*, **109**, 8809 (2005); (c) X.P. Zhou, A.M. Ren, J.K. Feng. *J. Organomet. Chem.*, **690**, 338 (2005); (d) A. Albertino, C. Garino, S. Ghiani, R. Gobetto, C. Nervi, L. Salassa, E. Rosenverg, A. Sharmin, G. Viscardi, R. Buscaino, G. Cross, M. Milanesio. *J. Organomet. Chem.*, **692**, 1377 (2007).
- [28] X.-X. Fu, J.-F. Li, R.-Q. Zhang., doi: [arXiv:1601.01150](https://arxiv.org/abs/1601.01150) (2016).
- [29] Z. Asadi, H. Mosallaei, M. Sedaghat, R. Yousefi. *J. Iran. Chem. Soc.*, **14**, 2367 (2017).
- [30] H. Li, X.Y. Le, D.W. Pang, H. Deng, Z.H. Xu, Z.H. Lin. *J. Inorg. Biochem.*, **99**, 2240 (2005).
- [31] (a) Z. Mandegani, Z. Asadi, M. Asadi, H.R. K.Heidari, B. Rastegari. *Dalton Trans.*, **45**, 6592 (2016). (b) N. Shahabadi, S. Kashanian, M. Khosravi, M. Mahdavi. *Transit. Met. Chem.*, **35**, 699 (2010).
- [32] Z. Asadi, N. Nasrollahi, H.K. Heidari, V. Eigner, M. Dusek, N. Mobaraki, R. Pournajati. *Spectrochim. Acta A Mol. Biomol. Spectrosc.*, **178**, 125 (2017).
- [33] (a) Y.C. Liu, Z.Y. Yang. *Eur. J. Med. Chem.*, **44**, 5080 (2009); (b) S. Satyanarayana, J.C. Dabrowiak, J.B. Chaires. *Biochemistry*, **32**, 2573 (1993); (c) D.S. Sigman, A. Mazumder, D.M. Perrin. *Chem. Rev.*, **93**, 2295 (1993); (d) Y. Wang, Z.Y. Yang, Q. Wang, Q.K. Cai, K.B. Yu. *J. Organomet. Chem.*, **690**, 4557 (2005); (e) S. Satyanarayana, J.C. Dabrowiak, J.B. Chaires. *Biochemistry*, **31**, 9319 (1992).
- [34] (a) T.K. Si, S.S. Paul, M.G.B. Drew, K.K. Mukherjea. *Dalton Trans.*, **41**, 5805 (2012); (b) S. Patra, S. Chatterjee, T.K. Si, K.K. Mukherjea. *Dalton Trans.*, **42**, 13425 (2013); (c) E. Palmajumder, N. Sepay, K.K. Mukherjea. *J. Biomol. Struct. Dyn.*, **36**, 919 (2017).
- [35] (a) S. Naskar, E. Palmajumdar, S. Patra, J. Mitra, K.K. Mukherjea. *Chem. Select.*, **2**, 10199 (2017); (b) S.R. Chowdhury, M. Selim, S. Chatterjee, S. Igarashi, Y. Yukawa, K.K. Mukherjea. *J. Coord. Chem.*, **65**, 3469 (2012); (c) U. Saha, K.K. Mukherjea. *RSC Adv.*, **5**, 94462 (2015).
- [36] S. Tabassum, W.M. Al-Asbahy, M. Afzal, F. Arjmand, V. Bagchi. *Dalton Trans.*, **41**, 4955 (2012).